50272-101

REPORT DOCUMENTATION PAGE	1. REPORT NO. UILU-ENG-84-2004	2.	3. Recipient's Accession No. PB84 224377
4. Title and Subtitle: COMPUTED NONLINEAR SEISMIC RESPONSE OF R/C WALL-FRAME STRUCTURES			5. Report Date: MAY 1984
			6.
7. Author(s): Mehran Keshavarzian and William C. Schnobrich			8. Performing Organization Rept. No.: SRS. No. 515
9. Performing Organization Name and Address: Department of Civil Engineering, University of Illinois, 208 N. Romine Street, Urbana, IL 61801			10. Project/Task/Work Unit No.
			11. Contract(C) or Grant(G) No. (C) (G) NSF CEE 83-12041
12. Sponsoring Organization Name and Address: National Science Foundation, Washington, D.C.			13. Type of Report & Period Covered
			14.

15. Supplementary Notes

16. Abstract (Limit: 200 words)

This study presents a method of nonlinear analysis for the response of a R/C coupled shear wall and/or wall-frame structure subjected to strong earthquake motion. The objective is to maintain relative simplicity in the method itself, yet produce reasonable reliability in the computed results. The computed responses of one cantilever column member, two coupled shear wall structures, and one wall-frame system under dynamic loads and static loads are compared with the available test results. The effects of moment-axial force interaction of wall members as well as the effects of pinching action and strength decay of coupling beams on overall computed responses of the coupled shear wall structures are discussed.

17. Document Analysis a. Descriptors

Structural engineering
Dynamic analysis
Analytical model
Reinforced concrete
Wall-frame
Coupled shear wall
Damping
Hysteresis
Equations of motion

b. Identifiers/Open-Ended Terms

c. COSATI Field/Group

18. Availability Statement	19. Security Class (This Report): UNCLASSIFIED	21. No. of Pages: 219
	20. Security Class (This Page): UNCLASSIFIED	22. Price

(See ANSI-Z39.18) See Instructions on Reverse OPTIONAL FORM 272 (4-77) (Formerly NTIS-35) Department of Commerce

ACKNOWLEDGEMENT

This report is based on the doctoral thesis of M. Keshavarzian, submitted in partial fulfillment of the requirements for the Ph.D. in Civil Engineering at the University of Illinois.

The study was supported by the National Science Foundation under Grant No. CEE 83-12041. This support is gratefully acknowledged.

The numerical results presented in this report were obtained with the use of the CDC Cyber 175 computer system; most of the figures were prepared using the GCS-Zeta plotting device. These facilities are supported by the Computing Services Office (CSO) of the University of Illinois.

TABLE OF CONTENTS

Page

LIST OF TABLES

LIST OF FIGURES

Figure Page

Figure Page

CHAPTER 1

INTRODUCTION

1.1 General

It is well recognized that structures subjected to strong ground motion will undergo inelastic deformations at certain critical locations. If the structure is to survive, the individual structural members must be ductile enough to develop these deformations without failing. To ascertain these ductility demands, understanding the nonlinear dynamic response of building structures becomes a reasonable objective.

Dynamic tests of model structures conducted on a shaking table can reveal some general information about the structural responses and inertia forces generated under simulated earthquake motions. However, it is realized that it is very difficult to extract detailed information from dynamic tests due to complex interaction of various parameters. Consequently dynamic tests of either real buildings or model test structures are rather aimed toward obtaining the overall structural responses and also obtaining source data to test mathematical models for use in nonlinear analysis.

1.2 Object and Scope

The main purpose of the study reported herein is to analytically investigate the nonlinear responses of several types of small-scale test structures for which experimental data are available in the literature. This study is performed with the following specific objectives in mind:

1---To develop a new column element with the following aims: a) consideration of the axial force-flexural interaction diagram; b) allowance for the spread of inelastic flexural rigidity along the critical regions of an element rather than having it localized at a section; c) acceptance of almost any form of linear moment distribution along the member; and, d) development of a reliable yet relatively simple element, as compared to a multiple spring model;

2---To extend the standard one-component model to consider axial force-flexural interaction in the calculation of the yield moment as well as for the element stiffness;

3---To discuss significant shortcomings of four element models, namely, the one-component model, the general two-component model, the multiple spring model, and the model which is developed in the course of this study. These element models are used to model wall elements in a multi-story wall-frame test structure;

4---To study the sensitivity of response of a structure to parameters such as damping, P-Delta effect and, axial force-flexural interaction.

In this study, work is done on developing a method of analysis capable of performing an inelastic analysis of plane, rectangular wall-frame and/or coupled shear wall structures. The method uses four different element models with inelastic member behavior, The results form the basis for evaluating inelastic structural response. Such a method (computer program) can then be used to study not only the inelastic response of a structure, but also the effects of different assumed conditions.

The main steps involved in the analysis of a structure are modeling, computation, and interpretation. In the first step a real structure or a test structure and its loading are idealized as a mathematical model. In

the computation step the structural response of the mathematical model is determined from a few well-established routines. In the last step, the results for the mathematical model are applied to the real or test structure. The first and last steps usually require substantial engineering judgement, especially when simple models are used to represent complex structures.

Chapters 2, 3, and 4 are concerned with modeling and the numerical procedures used in the computer program. Chapter 5 studies the effects of using different models of member inelastic behavior and analytical conditions on response. Furthermore, the computed results are discussed by comparison with the test results. Finally, Chapter 6 presents a short summary and the significant conclusions of this study. Also a critical review of this research effort is presented so that the results and conclusions may be perceived in proper scope.

A detailed review of existing anaytical models for general R/C frame structures is given by Keshavarzian and Schnobrich (1983), while a review directed at coupled shear walls can be found in the report by Aktan and Bertero (1981).

CHAPTER 2

FORCE DEFORMATION RELATIONSHIPS FOR STRUCTURAL ELEMENTS

2.1 Introductory Remarks

Computer analysis of a structure requires a proper modeling if reliable results are to be obtained. Because the behavior of each individual element is studied in this investigation, structures are modeled by means of line elements. It is extremely important to specify the properties of these line elements properly so that both the elastic and any inelastic behavior of the members can be simulated accurately. While specification of the force-deformation relationship for the elastic regions is straightforward, representation of inelastic zones in the element requires special attention.

This chapter discribes procedures to evaluate end moment-end rotation relationships of a simply supported element based on four analytical models, a one-component model, a general two-component model, a multiple spring model, and a new proposed model.

2.2 Material Properties

End moment-end rotation characteristics of structural elements for montonically increasing loads are calculated based on established material properties. To simplify such an evaluation a few idealizations, similar to those of several other analytical studies (Otani, 1972; Takayanagi and Schnobrich, 1976; Saiidi and Sozen, 1979), have been made. These are explained in the following section.

2.2.1 Stress-Strain Relationships for Concrete and Steel

A parabola combined with a straight line in the form proposed by Hognestad (1951) and shown in Fig. 2.1 is adopted here to idealize the stress-strain relationship of concrete.

For steel, a piecewise linear stress-strain relationship is assumed. A typical example of the assumed curve is shown in Fig. 2.2. The stress-strain relationship of steel is assumed to be symmetric about its origin.

2.3 Moment-Curvature Relationship

Based on the Bernoulli-Euler assumption of a linear variation of strain through the depth of a section , the primary moment-curvature relationship applicable to a member with a constant axial force and under a progressively increasing moment can be derived. The calculated moment-curvature curve is idealized as a bilinear curve with only one breakpoint, Fig. 2.3. Yielding of the section, which is associated with yielding of the tensile reinforcement, is assumed to occur at that breakpoint on the idealized curve. Thus, the idealized moment-curvature curve is based on properties that are only slightly different from the cracked transformed cross-section, i.e. any initial uncracked section behavior is explicity ignored. In this study, no final limit on the flexural strength of individual members is considered.

2.3.1 Effect of Axial Force on Moment-Curvature Curve

During the response of a structure to static or dynamic loading, there can be continual adjustments in the level of axial forces present in the

columns. Thus, there should be smooth shifts between moment-curvature curves corresponding to these different axial forces. These shifts reflect either a hardening or a softening of the member due to an increase or decrease in the axial force, respectively.

The section's current stiffness of moment-curvature in which the effect of axial force on that moment-curvature relationship is taken into account, is calculated based on a procedure which was initially developed by Takayanagi and Schnobrich (1976). The moment-curvature curve for a section under a changing axial load is developed by introducing appropriate shifts or movements between the family of moment-curvature curves for various constant axial forces.

For the sake of simplicity, while the bending moment is assumed to be a function of both curvature and axial force, the axial force is assumed to be a linear function of only the average axial strain.

$$m = M(\phi, n) \tag{2.1}$$

$$n = EA * \varepsilon \tag{2.2}$$

m : Bending moment of a section;

ϕ : Curvature of a section;

n : Axial force on a section;

M : Bending moment function;

EA : Axial rigidity of a section;

ε : Average axial strain.

The incremental form of moment can be expressed by differentiating that function:

$$\Delta m = \frac{\partial M}{\partial \phi} \Delta\phi + \frac{\partial M}{\partial n} \Delta n \tag{2.3}$$

or

$$\Delta m = [\frac{\partial M}{\partial \phi} + \frac{\partial M}{\partial n} * \frac{\Delta n}{\Delta \phi}] \Delta \phi \tag{2.4}$$

The bracket term can be thought of as a current EI_i,

$$\Delta m = EI_i * \Delta \phi \tag{2.5}$$

where

$$EI_i = \frac{\partial M}{\partial \phi} + \frac{\partial M}{\partial n} * \frac{\Delta n}{\Delta \phi} \tag{2.6}$$

In this expression

Δm : Increment of bending moment;

Δn : Increment of axial force;

$\Delta \phi$: Increment of curvature.

It is worth mentioning that by rearranging Eq. 2.3, the current flexural rigidity which was used by Takayanagi and Schnobrich (1976) under constant axial rigidity can be obtained.

$$EI_i = \frac{\partial M}{\partial \phi} (1 - \frac{\partial M}{\partial n} * \frac{\Delta n}{\Delta m})^{-1} \tag{2.6a}$$

This current section stiffness established from the moment-curvature, Eq. 2.6, contains two terms. The first term, $\frac{\partial M}{\partial \phi}$, is the slope of the moment-curvature relationship under a constant axial force. The second term, $\frac{\partial M}{\partial n} * \frac{\Delta n}{\Delta \phi}$, represents the effect of a change in the axial force on the slope of the moment-curvature. Thus, the flexural rigidity, EI_i, which is the transition slope between two moment-curvature curves with different axial forces (Fig. 2.4), is calculated on the basis of loading history which involves the changes of axial force and bending moment on the section.

The value of $\frac{\partial M}{\partial \phi}$ can be established from the idealized moment-curvature hysteresis loop with the appropriate axial force acting on the section. The

$\frac{\partial M}{\partial n}$ value can be determined from the axial force-moment interaction diagram appropriate to the section. The details of the procedures for evaluating $\frac{\partial M}{\partial \phi}$ and $\frac{\partial M}{\partial n}$ are described in Appendix A.

It should be noted that the basic concept of introducing the effect of changing axial force is only to update the element stiffness for the subsequent loading increment, based on an axial force calculated from the current loading increment.

2.3.2 Axial Force-Moment Interaction

A typical axial force-moment interaction diagram is shown in Fig. 2.5. Points on the interaction diagram below the balance point correspond to yielding of the reinforcement, while points above the balance point correspond to crushing of the concrete. Hence, an increase in the axial force above the balanced load indicates possible crushing of the concrete prior to yielding of the reinforcement. During the response of a structure to static or dynamic loading, axial forces in the columns are expected to have values below that corresponding to the balanced load, and thus the relationship between axial force and moment is assumed to be linear, Fig. 2.5.

Cases where crushing of the concrete in the section occurs before yielding of reinforcement or where the relationship between the axial force and the moment is not linear are not considered in the models that are presented in this study.

During analysis, the yield moment of a section, corresponding to the current axial force, is determined from the moment-axial force interaction diagram for each loading increment. This yield moment is used for calculating both the section stiffness and the inelastic length at each end of the element.

2.4 End Moment-End Rotation Relationship Due to Flexure

The end moment-end rotation relationship of a cantilever element is determined from the idealized moment-curvature characteristics, developed around a constant axial force, as described in Section 2.3. The end rotation can be described in terms of curvature, as follows:

$$\theta_A = \frac{1}{\ell_A} \int_0^{\ell_A} (\phi(x)) \; x \; dx \qquad (2.7)$$

where the symbols refer to Fig. 2.6 and, $\phi(x)$ is the curvature as a function of the distance from the free end.

Because the variation of the moment along the member is assumed to be linear, and furthermore, because the skeleton of the moment-curvature curve is assumed to consist of linear segments, the curvature also varies linearly along the element. Hence, the computation of the end rotation as described by Eq. 2.7 is reduced to the evalution of the first moment of the area of a triangular part in the elastic region and a trapezoidal segment in the yielding portion. Based on the above discussion, the end moment-end rotation relationship can be readily calculated, and then normalized to a unit length cantilever beam.

The primary end moment-end rotation relationship is simplified as a bilinear curve. This means that the primary curve of a typical member consists of two segments, one representing the elastic range and the other the post-yield or inelastic range. In arriving at a bilinear idealization of a particular moment-rotation relationship, a number of approaches can be used. In this study, fitting a bilinear curve for the calculated end moment-end rotation relationship over a reasonable range is used.

This bilinear end moment-end rotation curve is then used for calculation of the member stiffnesses of the one-component model and the general two-component model.

2.5 Derivation of Element Chord Zone Flexibility

This section describes the procedures used to develop the end moment-end rotation relationships for a simply supported member. The 2 by 2 instantaneous flexibility matrix for models such as the one-component model, the general two-component model, the multiple spring model, and the model which is presented in this study, are derived based on the force-deformation relationships of frame elements outlined in Sections 2.3 and 2.4.

A simplified Takeda hysteresis model (Takeda, et al., 1970) is adopted to describe the force-deformation relationships of all four models. The axial force-flexure interaction effects on the element flexibility matrix are included in the multiple spring model and the proposed model as well as with the one-component model.

For the one-component model and general two-component model, the element flexibility matrices are derived directly from the end moment-end rotation relationship, while for the multiple spring model and the proposed model, the element flexibility matrices are calculated based on moment-curvature relationships of several sections along the length of the member.

2.5.1 One-Component Model

Each member's chord zone, i.e. clear span, consists of a linearly elastic element with one equivalent nonlinear rotational spring attached at each end (Giberson, 1967; Suko and Adams, 1971; Otani, 1972), Fig. 2.7. All the member's inelastic deformations are lumped into the rotations of these

two end springs. The flexibilities of the nonlinear rotational springs at the two ends are evaluated based on the assumption that the inflection point occupies a fixed location. Hence, the moment-rotation loading history of these two nonlinear rotational springs can be uniquely and independently specified by hysteresis rules.

The flexibility matrix for the end spring-beam element can be calculated by simply adding the flexibilities of the nonlinear rotational springs to the flexibilities of a linear simply supported beam element. The composite element flexibility matrix is therefore expressed as:

$$[F_1] = \begin{bmatrix} f_{11} & f_{12} \\ f_{12} & f_{22} \end{bmatrix} \tag{2.8}$$

with

$$f_{11} = f_{sh} + f_{A1} \tag{2.8a}$$

$$f_{12} = f_{sh} - \frac{\ell}{6EI} \tag{2.8b}$$

$$f_{22} = f_{sh} + f_{B1} \tag{2.8c}$$

and f_{A1} and f_{B1} are defined as follows:

$$f_{A1} = \frac{\ell}{3EI} + f(M_A) \tag{2.8d}$$

$$f_{B1} = \frac{\ell}{3EI} + f(M_B) \tag{2.8e}$$

where

$f(M_A)$, $f(M_B)$: Flexibilities of the nonlinear rotational springs at ends A and B, respectively. Flexibility of nonlinear rotational spring at end A (B) is evaluated based on the I.P. fixed at a distance ℓ_A (ℓ_B) from end A (B);

$f_{sh} = \frac{1}{GA\ell}$: Flexibility due to shear rigidity.

It can be seen that this model is based on the assumption that ideal plastic hinges with zero length, the nonlinear rotational springs, are formed at the member ends whenever the bending moment exceeds the yield moment. Such idealization of flexural members leads to constant post-yield stiffness coefficients. These coefficients are independent of the previous yield level in the strain-hardening range. Furthermore, the inelastic rotation at one end is determined from the appropriate moment uniquely and independently of the opposite end. This is equivalent to assuming the point of contraflexure remains at its initial position or arbitrarily at midspan of the element instead of being allowed to shift along the member as the current moment distribution would dictate.

It should be noted that the same procedure used to consider fluctuations of axial force on the moment-curvature curve can be applied to the end moment-end rotation relationship. Thus, the stiffness of the nonlinear rotational spring at each end of the element as well as the elastic element stiffness can be modified in the same way to consider the effect of changing axial force.

2.5.2 General Two-Component Model

The concept of the two-component model or the "divided beam" model was introduced by Clough, et al. (1965) and by Aoyama and Sugano (1968) and then extended for general force-deformation relations by Takizawa (1976). While the makeup of the model has no obvious physical basis, it is a mathematical way of arriving at engineering results.

The two-component model, which provides only a form of nondegrading moment resistance for each member, assumes that every member consists of two components: a basic elasto-plastic component which develops a plastic hinge

at either end when the end moment exceeds a specified yield value, and a second component which remains fully elastic, Fig. 2.8. This is equivalent to saying that each element is imaginary divided vertically into two components: an elastic component with moment of inertia, pI, where "I" is total moment of inertia or the second moment of the section, and "p" is strain-hardening ratio, and an elasto-plastic component with moment of inertia (1-p)I.

The general two-component model, which is capable of providing any form of moment resistance for a member, assumes that at each loading stage, the total moment of inertia, $r_A I$, of each member is divided into two components: an elastic component with moment of inertia, $r_B I$, and an elasto-plastic component with moment of inertia, $(r_A - r_B)I$, (when r_A is greater than r_B, change A and B if $r_B > r_A$). Thus, the stiffness matrix for the member can be obtained as the sum of the stiffnesses of its two components.

$$K = r_B K' + (r_A - r_B) K'_B \qquad 1 \geq r_A \geq r_B \qquad (2.9a)$$

$$K = r_A K' + (r_B - r_A) K'_A \qquad 1 \geq r_B \geq r_A \qquad (2.9b)$$

where

K', K'_A, K'_B : Stiffnees matrix for three fundamental cases given in Fig. 2.9.

$$K' = \frac{4EI}{\ell} \begin{bmatrix} 1 & 0.5 \\ 0.5 & 1 \end{bmatrix} \qquad (2.10a)$$

$$K'_A = \frac{3EI}{\ell} \begin{bmatrix} 0 & 0 \\ 0 & 1 \end{bmatrix} \qquad (2.10b)$$

$$K'_B = \frac{3EI}{\ell} \begin{bmatrix} 1 & 0 \\ 0 & 0 \end{bmatrix} \qquad (2.10c)$$

K' : Elastic stiffness matrix for an element with both ends fixed;

K'_A (K'_B) : Elastic stiffness matrix of an element with end A(B) hinged;

K : Element stiffness matrix.

and r_A and r_B are defined as follows:

$$r_A = \frac{k_A}{3EI} \; ; \qquad r_B = \frac{k_B}{3EI} \tag{2.10d,e}$$

where

k_A (k_B) : Instantaneous end moment-end rotation stiffness at end A(B) for a unit length cantilever beam.

It is worth noting the assumption that the total moment of inertia is reduced to $r_A I (r_B I$, when $r_B > r_A)$, when both ends involve inelastic action. This is based on the assumption of the two-component model that the reduction in stiffness applies along the entire length of the element when yielding occurs at both ends.

Evaluation of expressions 2.9 for a bilinear nondegrading hysteresis model, leads to the following values of the stiffness coefficients:

$K=K'$	elastic member, no hinges	$(r_A=r_B=1)$	(2-11a)
$K=pK'+(1-p)K'_B$	hinge at end B	$(r_A=1,\ r_B=p)$	(2-11b)
$K=pK'+(1-p)K'_A$	hinge at end A	$(r_B=1,\ r_A=p)$	(2-11c)
$K=pK'$	hinges at both ends	$(r_A=r_B=p)$	(2-11d)

which are the stiffness coefficients for the two-component model as proposed by Clough and by Aoyama.

Defining f_{A2} and f_{B2} to be $1/k_A$ and $1/k_B$, respectively, the flexural element flexibility matrix can be evaluated from Eqs. 2.12.

$$K^{-1} = \begin{bmatrix} \frac{3}{4} f_{A2} + \frac{1}{4} f_{B2} & -\frac{1}{2} f_{B2} \\ -\frac{1}{2} f_{B2} & f_{B2} \end{bmatrix} \quad f_{B2} \leq f_{A2} \quad (2.12a)$$

$$K^{-1} = \begin{bmatrix} f_{A2} & -\frac{1}{2} f_{A2} \\ -\frac{1}{2} f_{A2} & \frac{3}{4} f_{B2} + \frac{1}{4} f_{A2} \end{bmatrix} \quad f_{B2} \geq f_{A2} \quad (2.12b)$$

Finally, the flexibility matrix, including shear deformation, is expressed as:

$$[F_1] = \begin{bmatrix} f_{11} & f_{12} \\ f_{12} & f_{22} \end{bmatrix} \quad (2.13)$$

$$\left.\begin{aligned} f_{11} &= f_{sh} + \frac{3}{4} f_{A2} + \frac{1}{4} f_{B2} \\ f_{12} &= f_{sh} - \frac{1}{2} f_{B2} \\ f_{22} &= f_{sh} + f_{B2} \end{aligned}\right\} \quad f_{B2} \leq f_{A2} \quad (2.13a)$$

$$\left.\begin{aligned} f_{11} &= f_{sh} + f_{A2} \\ f_{12} &= f_{sh} - \frac{1}{2} f_{A2} \\ f_{22} &= f_{sh} + \frac{3}{4} f_{B2} + \frac{1}{4} f_{A2} \end{aligned}\right\} \quad f_{B2} \geq f_{A2} \quad (2.13b)$$

2.5.2.1 Comparison of the One- and Two-Component Models

Because both the one-component and two-component models are approximations of the actual inelastic member behavior, it is important to compare the results from these two models applied to a single beam element not only to see how closely they match but also to evaluate the strain-hardening ratio of the general two-component model.

In the general two-component model, the change of end rotation of a unit length cantilever beam is related to the change of end moment by the following equation:

$$\Delta\theta_A = (\frac{3}{4} f_{A2} + \frac{1}{4} f) \Delta M_A \tag{2.14a}$$

where

f_{A2} : Instantaneous flexibility of the end moment-end rotation of a unit length cantilever beam for the general two-component model.

$f = 1/3EI$

From comparison of Eq. 2.14a and definition of instantaneous flexibility of an end moment-end rotation curve, the Eq. 2.14b is obtained.

$$f_{A1} = \frac{3}{4} f_{A2} + \frac{1}{4} f \tag{2.14b}$$

where

f_{A1} : Instantaneous flexibility of end moment-end rotation of a unit length cantilever beam defined in section 2.4.

Evaluation of the Eq. 2.14b in the strain-hardening yields to the following expression:

$$p_2 = \frac{3p_1}{4-p_1} \simeq 0.75\ p_1 \tag{2.14c}$$

where p_1 and p_2 are the strain-hardening ratio of the end moment-end rotation relationship of a unit length cantilever beam for one- and two-component models, respectively.

Eq. 2.14c indicates that the strain-hardening ratio of the primary moment-rotation curve for the general two-component model should be approximately 75 % of the strain-hardening ratio of moment-rotation curve

defined in section 2.4 or used for the one-component model.

On the other hand, with the loading according to Fig. 2.10, the following moment-rotation equations under strain-hardening condition are obtained:

A) One-component model, fixed inflection point (I.P.) at point B.

$$\Delta\theta_{A1} = \left[\frac{\ell}{3EI} + \ell \left(\frac{1}{3p_1EI} - \frac{1}{3EI}\right) \right] \Delta M_A = \frac{\ell}{3p_1EI} \Delta M_A \qquad (2.15a)$$

B) Two-component model:

$$\Delta\theta_{A2} = \left[\frac{3}{4} * \frac{\ell}{3p_2EI} + \frac{1}{4} * \frac{\ell}{3EI} \right] \Delta M_A \qquad (2.15b)$$

Substituting for P_2 from Eq. 2.14c in the Eq. 2.15b:

$$\Delta\theta_{A2} = \frac{\ell}{3p_1EI} \Delta M_A \qquad (2.15c)$$

Comparison between Eqs. 2.15a and 2.15c indicates that under this loading condition, the results of the one-component model with fixing I.P. at point B and the general two-component model are identical in the strain-hardening range. Furthermore, Eq. 2.14c evaluates strain-hardening ratio (p_2) of the end moment-end rotation of the general two-component model based on the I.P. at the other end. Thus, the effect of the position of the I.P. can be easily considered in the evaluation of P_2 in the general two-component model when one end remains elastic.

For antisymmetric loading, the value of p_2 can be evaluated by comparing the moment-rotation relations of these two models under strain-hardening range.

A) One-component model, fixed I.P. at midspan:

$$\Delta\theta_{A1} = \frac{\ell}{6p_1EI} \Delta M_A \qquad (2.16a)$$

B) Two-component model:

$$\Delta\theta_{A2} = \frac{\ell}{6p_2EI}\,\Delta M_A \tag{2.16b}$$

By equating Eqs. 2.16a and 2.16b, the following relation between P_1 and p_2 is obtained.

$$p_2 = p_1 \tag{2.16c}$$

It is worth mentioning that Giberson (1967) presented an extensive treatment of the equations describing the one-component model and the two-component model (non-degrading) for a single beam element and concluded that the appropriate condition for matching these two models is by equating the incremental rotations under antisymmetric loading condition.

Table 2.1 compares the flexural flexibility coefficients of the one-component model with those of the general two-component model. These two models are significantly different in nature that an identical results from the two models cannot be expected. In the general two-component model, the reduction of stiffness (based on the minimum reduction of stiffness of moment-rotation hysteresis at either end) is considered over the entire length of the element. On the other hand, in the one-component model, all the reduction of stiffness is assumed to be localized at the two nonlinear rotational springs. This difference in composition is an outgrowth of the fact that the one-component model is based on the assumption of three rotational springs in series. While two rotational springs in parallel is the basis of the general two-component model.

2.5.3 Multiple Spring Model

For this model, each element is divided into several subelements represented in the form of a sequence of nonlinear rotational springs

attached in series, Fig. 2.11. Therefore, each subelement can be subjected to different stages of inelastic action. The moment at the centroid of each of the subelements is used to determine the properties of that subelement. The properties of each segment are then assumed to be constant over the length of that segment. By dividing the element into several segments, the propagation of inelastic deformations as well as the coupling between inelastic rotations at both ends can be taken into account.

The flexibility matrix of the simply supported element can be derived by numerical intergration, over the element length, of the flexibility matrix of a differential slice.

$$[F_1] = \begin{bmatrix} f_{11} & f_{12} \\ f_{12} & f_{22} \end{bmatrix} = \int_0^{\ell} [V]^T [f] [V] \, dx \tag{2.17}$$

$$[f] = \begin{bmatrix} \frac{1}{GA_x^*} & 0 \\ 0 & \frac{1}{EI_x^*} \end{bmatrix} \tag{2.17a}$$

$$[V] = \begin{bmatrix} -\frac{1}{\ell} & -\frac{1}{\ell} \\ \frac{x-\ell}{\ell} & \frac{x}{\ell} \end{bmatrix} \tag{2.17b}$$

$$f_{11} = \int_0^{\ell} \frac{1}{\ell^2} \left(\frac{1}{GA_x^*} + \frac{(x-\ell)^2}{EI_x^*} \right) dx \tag{2.17c}$$

$$f_{12} = \int_0^{\ell} \frac{1}{\ell^2} \left(\frac{1}{GA_x^*} + \frac{x(x-\ell)}{EI_x^*} \right) dx \tag{2.17d}$$

$$f_{22} = \int_0^{\ell} \frac{1}{\ell^2} \left(\frac{1}{GA_x^*} + \frac{x^2}{EI_x^*} \right) dx \tag{2.17e}$$

where

[f] : Flexibility matrix of a slice;

[V] : Transformation matrix;

x : Distance from right support;

EI_x^* , GA_x^* : Current flexural and shear rigidities.

The flexibility coefficients for the multiple spring element can be readily evaluated based on Eqs. 2.17, because the flexural rigidity and the shear rigidity are assumed to be constant over the length of each subelement.

$$f_{11} = \sum_{k=1}^{N} \left\{ \frac{\ell_k}{GA_k^* \ell^2} + \frac{b^3-a^3}{3\ell^2 EI_k^*} \right\} \tag{2.18a}$$

$$f_{12} = \sum_{k=1}^{N} \left\{ \frac{\ell_k}{GA_k^* \ell^2} + \frac{b^3-a^3}{3\ell^2 EI_k^*} - \frac{b^2-a^2}{2\ell EI_k^*} \right\} \tag{2.18b}$$

$$f_{22} = \sum_{k=1}^{N} \left\{ \frac{\ell_k}{GA_k^* \ell^2} + \frac{(b-\ell)^3-(a-\ell)^3}{3\ell^2 EI_k^*} \right\} \tag{2.18c}$$

where

N : Number of subelements;

ℓ_k : Length of the k-th subelement;

EI_k^* , GA_k^* : Current flexural and shear rigidities of the k-th subelement;

a : Distance between right end of the k-th subelement and right end of a simply supported member;

b = ℓ_k +a

2.5.4 The Proposed Model

In the proposed model, the element chord zone or clear span is considered to consist of two types of regions, an elastic central region plus the variable length inelastic zones at each end of the member, as shown in Fig. 2.12. Inelastic actions are confined to these element ends in which the curvature distribution is determined with the aid of idealized moment-curvature hysteresis rules. In order to represent the joint core zones at the member ends, rigid end zone links can also be specified.

The cross sectional stiffness properties of the elastic zone are calculated based on a changing axial force and are therefore not constant. For the inelastic zones the effective section stiffness properties are determined from an appropriate moment-curvature hysteresis idealization which also incorporates the effects of changing axial forces. The effective section stiffness of each inelastic zone is assumed to be constant throughout the length of that zone.

The length of the inelastic zone is considered to depend on the loading history and the axial force. The inelastic zone lengths, which may be different at the two ends of the member, are calculated from the linear moment diagram and the current value of yield moment. The moments at the face of the joints are used to determine the stiffness properties as well as the plastic hinge lengths.

The flexural flexibility of a member chord zone can be readily formulated once the inelastic zone stiffness and inelastic length at each end have been established.

2.5.4.1 Inelastic Zone Length

The inelastic length at each end of the element is determined from Eqs. 2.19.

$$Z_1 = \frac{M_A - M_y * SN_1}{M_A + M_B} * \ell \qquad (2.19a)$$

$$Z_2 = \frac{M_B - M_y * SN_2}{M_A + M_B} * \ell \qquad (2.19b)$$

M_A, M_B : Moments at ends A and B;

M_y : Computed yield moment at current axial force;

ℓ : Clear span of the element;

Z_1, Z_2 : Computed inelastic lengths of the element at ends A and B, respectively.

and $SN_1(SN_2)$ is defined as the sign of $M_A(M_B)$

$$SN_1 = \frac{|M_A|}{M_A}; \qquad SN_2 = \frac{|M_B|}{M_B} \qquad (2.19c,d)$$

These computed inelastic lengths at both ends of the element are based on the following assumptions:

1---No loads are applied within the element, thus; the central element region can be assumed to remain elastic.

2---The inelastic length is zero when the end moment is in the elastic range.

3---Changes in the inelastic length are considered only when the end moment is in the strain-hardening range.

4---The inelastic length is assumed to remain constant and equal to its maximum excursion value when the end moment moves back out of the strain-hardening zone.

It should be emphasized here that this model does not provide any energy dissipation mechanism unless the section yields. Therefore, if the load starts with small amplitude deformations below the yield point, the model considers the element behavior elastic. In reality some nonlinear behavior in a reinforced concrete element can be considered to start immediately after the section cracks.

2.5.4.2 Effective Section Stiffness of an Inelastic Zone

A simplified Takeda hysteresis model is adopted to prescribe the moment-curvature relationship of the critical sections of the element under a constant level of axial force. This critical section stiffness of each inelastic zone is modified based on Eq. 2.6 to obtain the current section stiffness. The current section stiffness of moment-curvature, EI_i, is defined as the slope of the moment-curvature curve at the critical section, while the effective section stiffness, EI^*, is the slope of the moment-curvature curve of all sections in the inelastic zone of the corresponding end. Because inelastic actions are limited to the element ends, the critical sections of an element are defined at the face of the beams or columns.

At the end of each loading step, the member end moments and axial force are determined based on the current member displacements and stiffnesses. These new member end moments and axial force are implemented to evaluate a new member stiffness matrix for the succeeding loading step. For this purpose, it is necessary to distinguish between the various branches of the hysteresis model.

1--- Loading on the Elastic Stage

Loading on the elastic branch produces a response that follows the same stiffness, if the section's axial force remains constant. The effective section stiffness, which is equal to the current section stiffness, is constant along the entire elastic zone of the element

At the end of each loading increment, a new level of axial force and moment are computed. The yield moment corresponding to the current axial force, which is found from the moment-axial force interaction diagram, is compared with the current moment to check if yielding has occurred at a given section. It is important to realize that because of the assumptions made as the basis of the model and mentioned in Appendix A, yielding of a cross section can be also checked on the primary moment-curvature curve.

2--- Loading on the Inelastic Branches, Yielding Stage

When yielding does occur, loading continues along an inelastic branch. In this yielding stage, the current section stiffness of the moment-curvature curve is roughly constant throughout the inelastic zone (not for high strain-hardening ratio of moment-curvature curve). Thus, the effective section stiffness of an inelastic zone is assumed to be equal to the current section stiffness appropriate to the moment-curvature curve at the critical section. For the bilinear moment-curvature relationship, it is apparent that the section stiffness, under constant axial force, is independent of the degree of plasticity present in the yielding stage as shown in Fig. 2.13.

3--- Loading on the Inelastic Branches, Reloading Stage

With a load reversal, the assumption of a bilinear moment-curvature relationship may lead to a nonlinear curvature distribution in the inelastic zone even under a constant axial force. The slope of moment-curvature along the inelastic zone under constant axial force depends on the inelastic curvature, Fig. 2.14.

In order to simplify the procedure for determining the effective section stiffness in the reloading range, the average of the Maximum and Minimum of current section flexibilities (shown as solid line in Fig. 2.14 for constant axial force) is assumed to determine the effective section flexibility of the inelastic zone. This average approximation is:

$$EI^{*} = 2\ (\frac{1}{EI_e} + \frac{1}{EI_i})^{-1} \qquad (2.20)$$

where

EI^{*} : Effective section stiffness of M-ϕ;

EI_i : Current section stiffness of M-ϕ;

EI_e : Elastic section stiffness of M-ϕ at current axial force.

The discrepancy involved with this assumption depends on the loading history and the length of the inelastic zone. The smaller the inelastic length, the more accurate will be the assumption.

A hyperbolic variation of flexural rigidity along the inelastic zone was assumed by Arzoumanidis and Meyer (1981) for the inelastic zone under reloading conditions.

4--- Loading on the Inelastic Branches, Unloading Stage

The same procedure employed for the reloading stage does apply to an unloading stage as well.

An increase or decrease in axial force is reflected by an updating of the section stiffness at the end of each loading increment. At the end of a loading increment, a new level of axial force and moment is obtained. The difference between the axial force at the beginning and that at the end of the current loading increment causes either a softening or a hardening of the element. The current section stiffness of the inelastic zone is given by the slope of the moment-curvature curve as calculated by Eq. 2.6. The section stiffness of the central elastic region is also evaluated from Eq. 2.6 based on the loading history of both ends.

The assumption of constant effective section stiffness of each inelastic zone proceeds from the following logic:

1---It is assumed that all sections of each inelastic zone exhibit a single action, loading, unloading, or reloading, identical to and determined from the action at the corresponding element end. In reality, during the loading history the various sections in the inelastic zone may not be subjected to the same action as shown in Fig. 2.15. To slighty modify this assumption in the yielding stage, the equivalent inelastic length is defined and calculated from the following expression:

$$Z_1^* = Z_1 + \alpha \, (Z_1^{Max} - Z_1) \tag{2.21}$$

where

Z_1 : Length of the inelastic zone which is in the strain-hardening;

$Z_1^{Max} - Z_1$: Length of the inelastic zone which is still in the reloading range;

Z_1^{Max} : Maximum inelastic length at this end;

Z_1^* : Equivalent inelastic length of the member which is

assumed to be in the strain-hardening;

α : Constant value.

2---A single average effective section stiffness is assumed to represent the section stiffness of the entire inelastic zone. This assumption is justified for elements such as columns and beams for which their inelastic lengths are a relatively small portion of the total member length. With a wall element; however, the assumption of a single average effective section stiffness is not realistic, because the inelastic length can be as much as the depth of the wall (Derecho, et al., 1979). However, for a moderate section stiffness of moment-curvature curve during yielding, when the inelastic length is large (larger than 1/3 of the element length) the element stiffness is considerably reduced, compared to an entirely elastic case. Therefore, it is believed that the discrepancy caused by this assumption is small, and that discrepancy is assumed to have no significant contribution on the overall behavior of the element.

2.5.4.3 Element Flexibility Matrix

It can be seen that an element chord zone is divided into three segments. The central element segment is assumed to remain elastic while the two end segments can undergo plastic deformations. The lengths of the plastic segments are determined from Eqs. 2.19 and 2.21 based on the moment diagram and the level of the yield moment at a particular loading step. The unknown section stiffness of each region is evaluated from Eqs. 2.6 and 2.20 based on the loading history of that region. Further details of the procedures for evaluating the section stiffnesses and inelastic lengths are given in Appendix B.

With the model parameters (i.e. inelastic lengths and section stiffnesses) having been evaluated, the flexibility coefficients can be

readily formulated from Eqs. 2.18 by replacing the number of subelements by three:

$$f_{11} = \sum_{k=1}^{3} \left\{ \frac{\ell_k}{GA_k^* \ell^2} + \frac{b^3-a^3}{3\ell^2 EI_k^*} \right\} \tag{2.22a}$$

$$f_{12} = \sum_{k=1}^{3} \left\{ \frac{\ell_k}{GA_k^* \ell^2} + \frac{b^3-a^3}{3\ell^2 EI_k^*} - \frac{b^2-a^2}{2\ell EI_k^*} \right\} \tag{2.22b}$$

$$f_{22} = \sum_{k=1}^{3} \left\{ \frac{\ell_k}{GA_k^* \ell^2} + \frac{(b-\ell)^3-(a-\ell)^3}{3\ell^2 EI_k^*} \right\} \tag{2.22c}$$

By combining the flexibility coefficients of each segment, the composite flexibility coefficients are obtained.

$$f_{11} = f_{sh} + \frac{\ell}{3EI_e}\left[\frac{1}{r_A} + (\eta_A-1)^3\left(\frac{1}{r_A}-1\right) + \eta_B^3\left(\frac{1}{r_B}-1\right)\right] \tag{2.23a}$$

$$f_{12} = f_{sh} - \frac{\ell}{6EI_e}\left[1 + \eta_A^2(3-2\eta_A)\left(\frac{1}{r_A}-1\right) + \eta_B^2(3-2\eta_B)\left(\frac{1}{r_B}-1\right)\right] \tag{2.23b}$$

$$f_{22} = f_{sh} + \frac{\ell}{3EI_e}\left[\frac{1}{r_B} + (\eta_B-1)^3\left(\frac{1}{r_B}-1\right) + \eta_A^3\left(\frac{1}{r_A}-1\right)\right] \tag{2.23c}$$

where

$$f_{sh} = \frac{1}{GA_e \ell}\left[\frac{\eta_A}{r_A} + (1-\eta_A-\eta_B) + \frac{\eta_B}{r_B}\right] \tag{2.23d}$$

$$r_A = \frac{EI_1^*}{EI_e}\ ; \qquad r_B = \frac{EI_2^*}{EI_e} \tag{2.23e}$$

$$r_A = \frac{GA_1^*}{GA_e}\ ; \qquad r_B = \frac{GA_2^*}{GA_e} \qquad \text{(Also see Eq. 2.25)} \tag{2.23f}$$

$$\eta_A = \frac{Z_1}{\ell}\ ; \qquad \eta_B = \frac{Z_2}{\ell} \tag{2.23g}$$

r_A, r_B : Ratio of the inelastic section stiffnesses at both ends to elastic section stiffness;

η_A, η_B : Ratio of inelastic lengths at both ends to clear length of the element;

EI_e : Current elastic flexural rigidity;

GA_e : Current elastic shear rigidity.

Evaluation of these expressions for the elastic case, where $\eta_A = \eta_B = 0.$, and $r_A = r_B = 1.$, leads to the following values of the stiffness coefficients:

$$f_{11} = f_{22} = \frac{\ell}{3EI} \tag{2.24a}$$

$$f_{12} = -\frac{\ell}{6EI} \tag{2.24b}$$

which are the familiar elastic stiffness coefficients for a uniform beam.

In this study after yielding of the critical section, a minimum value for inelastic length ratio is set at 2 %. Such a minimum limitation on the inelastic length is an attempt to prevent any numerical problem in the element stiffness matrix when the strain-hardening ratio is very small.

It should be mentioned here that for constant axial force, the proposed model is similar to the model which was initially developed by Soleimani (1978) and later modified and used by some investigators (Arzoumanidis and Meyer, 1981; Roufaiel and Meyer, 1981; Meyer, et al., 1983; Roufaiel and Meyer, 1983). The main modifications initiated here in the proposed model include the effect of changing axial force on the element stiffness as well as on the yield moment.

2.6 Determination of Shear Rigidity

Calculation of shear rigidity of the section under changing axial force can be done in much the same manner as for flexure. If the shear

force-shear distortion relationship of a member is known, then characteristics of the primary shear force-shear distortion curve for the analytical model can be determined.

To establish the shear rigidity, it is important to specify the loading history of the shear-shear distortion relationship. In determining the total element flexibility, clearly the analytical procedure can be greatly simplified if the assigned hysteretic characteristic of the shear-shear distortion behavior is identical to that of the element moment-curvature relation.

Because axial compression will increase-- or conversely, axial tension will decrease-- the flexural as well as shear capacity of the element, and also because the shear deformation is considered to be of a secondary effect to the entire deformation while the flexural deformation is dominant, the computational effort for the shear is more condensed. Therefore, the inelastic value of shear rigidity is assumed to reduce in direct proportion to the flexural rigidity. The equation stating this assumption can be expressed in the form

$$GA^{*} = GA_{e} * \frac{EI^{*}}{EI_{e}} \tag{2.25}$$

where

EI^{*}, GA^{*}: Inelastic flexural and shear rigidities;

EI_{e}, GA_{e}: Elastic flexural and shear rigidities.

For the multiple spring model as well as for the proposed model, the inelastic shear rigidity is directly used in calculating the element flexibility matrix. For the one-component model and the general two-component model the effect of inelastic shear rigidity is not considered and it is assumed to remain elastic.

2.7 Flexibility Due to Bond Slippage at the Ends of a Member

Due to the significant contribution of the fixed-end rotation resulting from reinforcement slippage at the joint to the total element deformation, a nonlinear rotational spring, as an additional flexibility for an element, is provided at each end to take into account the bond slip of the longitudinal bars at the joint.

Bond stress is assumed to be constant over the development length of the reinforcement. Based on the assumption that the anchorage length of the reinforcement is sufficiently long to provide the maximum tensile stress, the development length is computed from the equilibruim of forces.

$$L_s = \frac{A_s f_s}{\pi D u} \tag{2.26a}$$

where

A_s : Area of the tensile reinforcement;

f_s : Stress in the tensile reinforcement;

D : Diameter of tensile reinforcement bar;

u : Average bond stress.

As the bond stress is constant over the development length, the tensile force from the reinforcement is transmitted into the concrete in such a way that the steel stress varies linearly from a maximum value at the face of joint to zero with one break point at yield stress as shown in Fig. 2.16. Therefore, the elongation of the reinforcement is calculated as:

$$\Delta L_s = \frac{L_s f_s}{2E_s} \qquad f_s \leq f_y \tag{2.26b}$$

$$\Delta L_s = \frac{f_y^2 L_s}{2 f_s E_s} + \left(1 - \frac{f_y}{f_s}\right)\left(\frac{f_y}{E_s} + \frac{f_s - f_y}{2E_y}\right) L_s \qquad f_s \geq f_y \tag{2.26c}$$

where

E_s : Young's modulus of the reinforcement;

E_y : Inelastic modulus of the reinforcement after yielding.

The elongation can be rewritten by subsituting Eqs. 2.26a for L_s in Eqs. 2.26b&c and by replacing A_s by $\frac{\pi D^2}{4}$.

$$\Delta L_s = \frac{1}{8} * \frac{D f_s^2}{E_s u} \qquad f_s \leq f_y \qquad (2.26d)$$

$$\Delta L_s = \frac{D}{4u} \left[\frac{f_y}{E_s} (f_s - \frac{f_y}{2}) + \frac{(f_s - f_y)^2}{2E_y} \right] \qquad f_s \geq f_y \qquad (2.26e)$$

If the compressive reinforcement does not slip and joint concrete is rigid, the rotation, R, due to the slip can be evaluated by the expression:

$$R = \frac{\Delta L_s}{d-d'} \qquad (2.26f)$$

where

d : Depth of the tensile reinforcement;

d' : Depth of the compressive reinforcement.

In order to have a moment-rotation relationship rather than the stress-rotation one, the relation between bending moment and stress is assumed as:

$$\frac{f_s}{f_y} = \frac{M}{M_y} \qquad (2.26g)$$

where

M : Bending moment at the end of a member;

M_y : Yielding moment at the end of a member;

f_y : Yielding stress of the reinforcement.

Then the rotation is related to the moment by the Eqs. 2.26h and 2.26k (Otani, 1972; Takayanagi and Schnobrich, 1976).

$$R = \frac{1}{8} * \frac{D}{E_s u} * \frac{f_y^2}{d-d'} \left(\frac{M}{M_y}\right)^2 \qquad M \leq M_y \qquad (2.26h)$$

$$R = \frac{D f_y^2}{4u} \left[\frac{1}{E_s}\left(\frac{M}{M_y} - \frac{1}{2}\right) + \frac{1}{2E_y}\left(\frac{M}{M_y} - 1\right)^2\right] \frac{1}{d-d'} \qquad M \geq M_y \qquad (2.26k)$$

The end moment-end rotation due to bond slippage of tensile reinforcement is idealized by fitting a bilinear curve on the calculated moment-rotation, rotation due only to bond slip, relationship in the way that the moment at the breakpoint be equal to yield moment determined in sections 2.3, 2.4.

It should be noted here that in the multiple spring model as well as the proposed model, the moment on the primary curve is used to calculate flexibility due to bond slip. Then this flexibility is assumed to change in direct proportion to the flexural rigidity to consider effect of changing axial force.

2.8 Element Flexibility Matrix

The total element incremental end rotations for the clear span are given by adding the fixed-end rotations (rotation due to the bond slip) to the chord end rotations. Therefore, the total flexibility matrix of the element chord zone may be expressed by:

$$[F] = \begin{bmatrix} f_{11} & f_{12} \\ f_{12} & f_{22} \end{bmatrix} + \begin{bmatrix} ff_1 & 0 \\ 0 & ff_2 \end{bmatrix} \qquad (2.27)$$

where

f_{11}, f_{12}, f_{22} : Flexural flexibility coefficients of the element chord zone as determined from Eqs. 2.8, 2.13, 2.18, or 2.23;

ff_1, ff_2 : Flexibility of nonlinear rotational springs due to bond slip.

The 2 by 2 element flexibility matrix then relates the end moments to end rotations of simply supported member with only one rotational degree of freedom at each end.

2.9 Summary

The member chord zone (clear span) flexibility matrix of a line element with only one rotation degree of freedom at each end was derived based on four analytical models. The rotation due to shear deformation as well as fixed-end rotation are taken into account in the element flexibility matrix. The moment-axial force interaction behavior is included in evaluating the flexibility matrices of all analytical models except the general two-component model. The inelastic material behavior of all four models is described by a Takeda type hysteresis model in the form of a moment-curvature curve or an end moment-end rotation relationship.

The primary purpose of this chapter was not to develop a matrix formulation of the flexibility matrix of an element based on these analytical models, but rather to discuss the basic concepts and assumptions of each individual element model. The effect of rigid end zones, and gravity in the element stiffness matrix will be considered in the next chapter.

Before closing this chapter, it is worth mentioning that:

1---the multiple spring model (with sufficiently large number of segments and also under cyclic or dynamic loading) does provide the greatest flexibility and accuracy in calculating the flexural flexibility matrix among the models which were discussed in this chapter. However, this model is very expensive in terms of computing time and computer storage.

2---the one- and the general two-component models have the advantage over the two other models that many different nonlinearities such as fixed-end rotation, strength decay, pinch action can be incorprated in these models very easily and without additional computation and computer storage.

3---when the interaction diagram is considered, none of the models are reliable, if a considerable shifting of I.P. occurs during a loading or a time step, (Fig. 2.17).

CHAPTER 3

ANALYTICAL PROCEDURE

3.1 Introductory Remarks

This chapter describes a method of analysis for a R/C wall-frame and/or coupled shear wall systems subjected to either static load reversals or dynamic base motions. The method is developed to study the behavior of a R/C structure in a post-yielding range in which the flexural behavior dominates.

In order to obtain a solution, the structural system must be suitably idealized as a mathematical model and numerical techniques must be applied. Thus, the computed results are for an idealized model. The degree to which the response of this model represents the response of the test or the actual structure depends on both the way in which the structural system is discretized and on the numerical procedures used in the computations.

3.2 Basic Assumptions

In order to simplify the solution procedure several basic assumptions have to be made with regard to loading, mass, and stiffness of the model. These assumptions are as follows and, unless otherwise noted, are applicable for all the analyses described in this study.

1---Every member in the structure is considered as a massless line member which can be represented by its centroidal axis.

2---The analysis is limited to 2-D structures. Out-of-plane action is ignored. Each nodal point has three degrees of freedom: a horizontal translation, a vertical translation, and a rotation.

3---The mass of the structure is assumed to be lumped at the floor levels, and the effects of rotatory inertia are neglected in the structural system.

4---The idealized structures are assumed to be fixed to infinitely rigid foundations.

5---The inelastic deformation of each constituent member is assumed to follow the Takeda's hysteresis model.

6---Axial deformation of the beams is neglected. Therefore; only one horizontal DOF is considered at each story level.

7---Joint cores at beam-to-column connections are assumed to be infinitely rigid.

8---The possibility of a major geometric nonlinearity is ignored in this analysis. The deformations are assumed to be sufficiently small so that the calculation of inelastic response of the structure can be based on its initial configuration. However, the geometric nonlinearity in the sense of the "P-Delta effect" is considered in the analysis.

9---Base motion is assumed to occur in the plane of the structure in the horizontal direction only. Any vertical component of the base motion is not considered in this study.

10---The frame members are assumed to have infinite ductility; thus, the ultimate strength and the deformation capacity of the members are calculated based on this assumption.

11---Any nonlinearities due to concrete cracking and load cycling prior to yielding are not considered. A constant secant elastic section stiffness is used as the section stiffness before yielding.

Some of these assumptions are discussed in more detailed in the next sections.

3.3 Element Stiffness Matrix

The element stiffness matrix, in terms of end moments-end rotations including the rigid end zones as shown in Fig. 3.1, is obtained by the appropriate transformations of the element clear-span stiffness as expressed in Eq. 3.1.

$$[K'] = [E]^T [F]^{-1} [E] \tag{3.1}$$

where

$$[K'] = \begin{bmatrix} K_{11} & K_{12} \\ K_{12} & K_{22} \end{bmatrix} \tag{3.1a}$$

$$[E] = \begin{bmatrix} 1+\lambda_A & \lambda_B \\ \lambda_A & 1+\lambda_B \end{bmatrix} \tag{3.1b}$$

$$[F] = \begin{bmatrix} f_{11}+ff_1 & f_{12} \\ f_{12} & f_{22}+ff_2 \end{bmatrix} \tag{3.1c}$$

in which

[E] : Transformation matrix;

[F] : Flexibility matrix of an element chord zone;

λ_A, λ_B : Ratio of the rigid length to the clear length at ends A and B, respectively.

Because the change in length of the member due to flexural deformations is ignored, the rotations at both ends of a member have no effect on the axial force component. Thus to account for the axial displacement in the member stiffness matrix, it is only necessary to include one additional term representing the uncoupled axial force-displacement relationship. Incorporating this additional term into the element stiffness matrix leads to the following expanded form of Eq. 3.1.

$$\begin{Bmatrix} \Delta M_i \\ \Delta M_j \\ \Delta n \end{Bmatrix} = [K_1] \begin{Bmatrix} \Delta\theta_i \\ \Delta\theta_j \\ \Delta\delta \end{Bmatrix} \tag{3.2a}$$

$$[K_1] = \begin{bmatrix} K_{11} & K_{12} & 0 \\ K_{12} & K_{22} & 0 \\ 0 & 0 & K_{33} \end{bmatrix} \tag{3.2b}$$

where

ΔM_i, ΔM_j : Incremental moments at ends i and j;

$\Delta\theta_i$, $\Delta\theta_j$: Incremental rotations at ends i and j;

Δn, $\Delta\delta$: Incremental axial force and axial deformation;

K_{33} : Constant axial rigidity, (EA/L).

In the development of the element stiffness matrix, Eq. 3.2b, no shear forces nor the corresponding vertical displacements at the ends of the member have been considered. In order to include any such shear forces at the member ends together with the corresponding lateral displacements in the element stiffness, the transformation matrix, T, is introduced, Fig. 3.2a.

$$\begin{Bmatrix} \Delta\theta_i \\ \Delta\theta_j \\ \Delta\delta \end{Bmatrix} = [T] \begin{Bmatrix} \Delta u_i \\ \Delta v_i \\ \Delta\omega_i \\ \Delta u_j \\ \Delta v_j \\ \Delta\omega_j \end{Bmatrix} \quad ; \quad \begin{Bmatrix} \Delta H_i \\ \Delta V_i \\ \Delta M_i \\ \Delta H_j \\ \Delta V_j \\ \Delta M_j \end{Bmatrix} = [T]^T \begin{Bmatrix} \Delta M_i \\ \Delta M_j \\ \Delta n \end{Bmatrix} \tag{3.3a,b}$$

where

$$[T] = \begin{bmatrix} 0 & \frac{1}{L} & 1 & 0 & -\frac{1}{L} & 0 \\ 0 & \frac{1}{L} & 0 & 0 & -\frac{1}{L} & 1 \\ -1 & 0 & 0 & 1 & 0 & 0 \end{bmatrix} \tag{3.3c}$$

in which

[T] : Transformation matrix of the coordinate systems;

Δu_i, ΔH_i : Incremental horizontal displacements and forces at ends i and j;

Δu_j, ΔH_j

Δv_i, ΔV_i : Incremental vertical displacements and forces at ends i and j;

Δv_j, ΔV_j

$\Delta \omega_i$, ΔM_i : Incremental rotations and moments at ends i and j, respectively.

$\Delta \omega_j$, ΔM_j

By combining Eqs. 3.3, the element stiffness matrix is obtained and symbolically expressed as:

$$[K] = [T]^T [K_1] [T] \tag{3.4}$$

For horizontal elements, the global coordinate system is also adopted as the local coordinate system. Thus the stiffness matrix as given by Eq. 3.4 is directly applicable for beams. For the vertical elements, in order to get the element stiffness into a global coordinate system, the local coordinate system should be rotated. The resulting transformation matrix, T, for vertical element is given by Eq. 3.5, Fig. 3.2b.

$$[T] = \begin{bmatrix} -\frac{1}{L} & 0 & 1 & \frac{1}{L} & 0 & 0 \\ -\frac{1}{L} & 0 & 0 & \frac{1}{L} & 0 & 1 \\ 0 & -1 & 0 & 0 & 1 & 0 \end{bmatrix} \tag{3.5}$$

Finally, Eqs. 3.6 represent an expression of the nodal forces in terms of the nodal displacements of a line element with three degrees of freedom at each end of the member but oriented in the global coordinate system of the structure.

$$\begin{Bmatrix} \Delta H_i \\ \Delta V_i \\ \Delta M_i \\ \Delta H_j \\ \Delta V_j \\ \Delta M_j \end{Bmatrix} = [K] \begin{Bmatrix} \Delta u_i \\ \Delta v_i \\ \Delta \omega_i \\ \Delta u_j \\ \Delta v_j \\ \Delta \omega_j \end{Bmatrix}$$

where

$$[K] = \begin{bmatrix} K_{33} & 0 & 0 & -K_{33} & 0 & 0 \\ & K_1 & K_2 & 0 & -K_1 & K_3 \\ & & K_4 & 0 & -K_2 & K_5 \\ & & & K_{33} & 0 & 0 \\ \text{Sym.} & & & & K_1 & -K_3 \\ & & & & & K_6 \end{bmatrix} \quad \text{(For Horizontal Members)} \qquad (3.6b)$$

$$[K] = \begin{bmatrix} K_1 & 0 & -K_2 & -K_1 & 0 & K_3 \\ & K_{33} & 0 & 0 & -K_{33} & 0 \\ & & K_4 & K_2 & 0 & K_5 \\ & & & K_1 & 0 & K_3 \\ \text{Sym.} & & & & K_{33} & 0 \\ & & & & & K_6 \end{bmatrix} \quad \text{(For Vertical Members)} \qquad (3.6c)$$

in which

$$\begin{aligned} K_1 &= (K_{11}+2K_{12}+K_{22})/L \\ K_2 &= (K_{11}+K_{12})/L \\ K_3 &= (K_{22}+K_{12})/L \\ K_4 &= K_{11}; \qquad K_5 = K_{12} \\ K_6 &= K_{22}; \qquad K_{33} = EA/L \end{aligned} \qquad (3.6d)$$

3.4 Structural Tangent Stiffness Matrix

Since the beam and column or wall element stiffness properties presented in the previous section are formulated in terms of the nodal degrees of freedom shown in Fig. 3.2, the tangent stiffness of an entire structure can be easily formulated by the summing of all the element stiffness matrices at the appropriate locations. The total structure equilibrium equations can thus be expressed as:

$$\begin{Bmatrix} \Delta H \\ \hline \Delta P \\ \Delta M \end{Bmatrix} = \left[\begin{array}{c:c} S_{11} & S_{12} \\ \hline S_{12}^{T} & S_{22} \end{array}\right] \begin{Bmatrix} \Delta U \\ \hline \Delta V \\ \Delta \theta \end{Bmatrix} \tag{3.7}$$

where

S_{11} : Symmetric submatrix of size, N by N;

S_{12} : Submatrix of size, N by 2J;

S_{22} : Symmetric banded submatrix of size, 2J by 2J;

N : Number of stories;

j : Number of joints (excluding supports);

ΔH, ΔU : Incremental story lateral force and displacement vectors, respectively;

ΔP, ΔV : Incremental joint vertical force and displacement vector;

ΔM, $\Delta \theta$: Incremental joint moment and rotation vectors.

In the static loading, all external vertical forces as well as moments at the joints in the structure are assumed to be zero. Only lateral loads are considered for that analysis. For the dynamic loading, it is also assumed that the inertia loads corresponding to the vertical displacements and rotations are negligible and only the lateral modes of vibration are

considered. Thus static condensation can be used for both the static and the dynamic loading cases. The structural stiffness matrix of Eq. 3.7 is condensed to relate the lateral forces directly to just horizontal displacements.

$$\{\Delta H\} = [K]^{*} \{\Delta U\} \tag{3.8a}$$

where

$$[K]^{*} = [S_{11}] - [S_{12}] [S_{22}]^{-1} [S_{12}]^{T} \tag{3.8b}$$

The result of the static condensation is that only one degree of freedom per story is retained explicitly, that being the lateral displacement of the particular story level. However, the effect of all other displacements is retained implicitly. Values of these other displacements can be obtained from a back substitution process.

$$\begin{Bmatrix} \Delta V \\ \Delta \theta \end{Bmatrix} = - [S_{22}]^{-1} [S_{12}]^{T} \{\Delta U\} \tag{3.9}$$

3.5 Column Geometric Stiffness Matrix

The overturning effect of gravity loads acting through the sidesway displacement is commonly called the "P-Delta" effect. In general, for relatively small displacements, the influence of gravity on the response can be disregarded. However, if an excursion into the plastic range occurs during the response, and if the inelastic drift continues to grow, it is obvious that gravity will eventually become the dominant force and make the structure unstable. In this study, the effect of P-Delta on the response of structures is considered.

Because the "geometric stiffness" is believed to be of secondary significance in comparison with the flexural stiffness of the structural members, a linear displacement between the column ends is assumed. The P-Delta forces are balanced by a pair of lateral forces at the column ends as shown in Fig. 3.3 (Clough and Penzien, 1975).

$$V_{i-1}^{j(top)} = \frac{N_{i-1}^{j}}{h_{i-1}} (u_{i-1} - u_i) \tag{3.10a}$$

$$V_{i-1}^{j(bot)} = -V_{i-1}^{j(top)} \tag{3.10b}$$

where

N_{i-1}^{j} : Axial force in column j;

h_{i-1} : Height of columns between DOFs i-1 & i;

u_{i-1}, u_i : Lateral displacements at DOFs i-1 & i;

$V_{i-1}^{j(top)}$, $V_{i-1}^{j(top)}$: A pair of lateral forces at column j caused by P-Delta effect.

For constant axial force, the column geometric stiffness matrix is given by:

$$\begin{Bmatrix} \Delta V_{i-1}^{j(top)} \\ \\ \Delta V_{i-1}^{j(bot)} \end{Bmatrix} = \frac{N_{i-1}^{j}}{h_{i-1}} \begin{bmatrix} +1 & -1 \\ \\ -1 & +1 \end{bmatrix} \begin{Bmatrix} \Delta u_{i-1} \\ \\ \Delta u_i \end{Bmatrix} \tag{3.11}$$

Because at each story only one lateral degree of freedom is permitted, the individual column geometric stiffnesses may be combined into the story geometric stiffness as expressed by:

$$\begin{Bmatrix} \Delta V_{i-1}^{top} \\ \\ \Delta V_{i-1}^{bot} \end{Bmatrix} = \frac{\sum N_{i-1}}{h_{i-1}} \begin{bmatrix} +1 & -1 \\ \\ -1 & +1 \end{bmatrix} \begin{Bmatrix} \Delta u_{i-1} \\ \\ \Delta u_i \end{Bmatrix} \tag{3.12}$$

where

Δu_{i-1}, Δu_i : Top and bottom story incremental lateral displacements, respectively;

ΔV_{i-1}^{top}, ΔV_{i-1}^{bot} : Top and bottom story incremental lateral forces due to gravity effect;

$\sum N_{i-1}$: Story axial force.

It may be noted that in the absence of any gravity load within the element, the beam shears introduce tension in one column and an equal compression in the other. These equal tension and compression forces in the columns produce equal and opposite sidesway shears, with the result that no change occurs in the story shears. Thus, for the purpose of considering the P-Delta effect on the structural stiffness matrix of frames subjected to horizontal ground motions, it is only necessary to consider the static dead loads present in the columns. In other words, the geometric story stiffness matrix is constant regardless of the changing axial forces of the columns. This is because the column geometric stiffness terms, considered in this study, affect only the lateral degrees of freedom, and by equilibrium, the sum of the column axial loads acting in a particular story must remain constant. However, the geometric stiffness of each individual column is dependent on the axial force present in that particular column. The change of shear force in an individual column due to the gravity effect can be evaluated as follows:

$$\Delta V_{i-1}^{j(top)} = \frac{N_{i-1}^{j}}{h_{i-1}} (\Delta u_{i-1} - \Delta u_i) + \frac{\Delta N_{i-1}^{j}}{h_{i-1}} (u_{i-1} - u_i) \qquad (3.13)$$

where

ΔN^{j}_{i-1} : Change of axial force in column j.

In the present study, the member axial forces are considered to remain constant throughout the response, leading to the inclusion of a constant geometric stiffness matrix to approximate the P-Delta effect.

The structure geometric stiffness can be determined by combing Eq. 3.12 of all stories. Symbolically, this may be expressed by:

$$\{\Delta Q\} = [K_G] \{\Delta U\} \tag{3.14}$$

where

ΔQ : Change of shear forces due to P-Delta effect;

K_G : Structural geometric stiffness;

ΔU : Incremental lateral displacements.

It may be mentioned that the structural geometric stiffness is a symmetric banded matrix with contributions from only the two adjacent stories so the band width is equal to three. Because the consequence of gravity effect is to make the structure softer by reducing its lateral stiffness, thus, the modified condensed structural stiffness matrix which relates lateral displacements to lateral forces can be obtained from Eq. 3.15.

$$[K]^{**} = [K]^{*} - [K_G] \tag{3.15}$$

3.6 Mass Matrix

Mass in the structure is assumed to be concentrated at the various floors or framing levels. Mass moment of inertia terms are neglected. This lumped mass idealization can be written as follows:

$$[M] = \begin{bmatrix} m_1 & & O \\ & \ddots & \\ O & & m_n \end{bmatrix} \tag{3.16}$$

M is the diagonal mass matrix, and the elements of the matrix represent story masses. The diagonal form of the mass matrix is very efficient because the equations of motion are then uncoupled in the terms of accelerations.

3.7 Damping Matrix

The damping matrix is assumed to be represented as a linear combination of the mass matrix and the stiffness matrix. This relationship has the form

$$[C] = C_1[M] + C_2[K] \tag{3.17}$$

where C_1 and C_2 are scalar multipliers. Furthermore, the damping ratio, ξ_n, as a percent of critical, can be expressed (Clough and Penzien, 1975) in terms of the scalar multipliers and the modal frequencies, ω_n, as

$$\xi_n = \frac{C_1}{2\omega_n} + \frac{C_2\omega_n}{2} \tag{3.18}$$

From this equation the multipliers C_1 and C_2 can be determined by specifying a predetermined amount of damping in any two modes of vibration. Once C_1 and C_2 are evaluated, the damping in any other mode is defined by Eq. 3.18. It is apparent from Eq. 3.18 that the stiffness proportional damping tends to increase the effect of damping in the higher modes, while the mass proportional damping term has the opposite effect.

Because of the uncertainty in the nature of damping in the inelastic range, it is not clear whether the stiffness proportional term, with its

constant scalar multipliers, should be based on the tangent or the initial elastic stiffness matrix. In studies (Giberson, 1967; Otani, 1972; Soleimani, 1978; Saiidi and Sozen, 1979) the stiffness proportional term of the damping matrix was based on the tangent stiffness. A constant damping matrix based on the initial stiffness has also been used by a few investigators (Emori and Schnobrich, 1978; Takayanagi and Schnobrich). However, if damping is based on the tangent stiffness, there may be a substantial decrease in the effective damping when many members have yielded. This is in contradiction to the hysteretic energy dissipation associated with yielding.

Two types of damping are used in this study. In the first type, a constant damping matrix represented as a linear combination of the mass and the initial elastic stiffness is assumed, Eq. 3.17. The constant scalar multipliers C_1 and C_2 are determined from specified damping ratios for the first two elastic frequencies of the structure. Type II neglects the effects of the mass matrix and evaluates a damping matrix from the current stiffness matrix based on a variable scalar multiplier, C_2. The scalar multiplier, C_2, is calculated from Eqs. 3.19 which are based on the assumption that the first mode shape of the structure does not change throughout the analysis.

$$[C] = C_2 [K] \tag{3.19a}$$

where

$$C_2 = \frac{2\xi_1}{\omega_e} \left(\frac{\phi^T K_e \phi}{\phi^T K \phi} \right)^{1/2} \tag{3.19b}$$

in which

K : Current condensed structural stiffness matrix;

ξ_1 : Damping ratio of the first mode shape;

ω_e : Initial first frequency of the structure;

ϕ : First mode shape;

K_e : Elastic initial condensed structural stiffness matrix.

3.8 Equations of Motion

The equations of motion of a structure are expressed by the equilibrium conditions existing between the inertia forces, damping forces, and resisting forces at each story. The incremental form of these equations can be written in the matrix form as:

$$M\,\Delta\ddot{U} + C\,\Delta\dot{U} + K\,\Delta U = -M\,\Delta\ddot{X}_g \tag{3.20}$$

where M, C, K are, respectively, the structure mass, damping, and stiffness matrices; ΔU , $\Delta\dot{U}$, $\Delta\ddot{U}$ are the incremental nodal horizontal displacement, velocity, and acceleration vectors relative to ground; and $\Delta\ddot{X}_g$ is the incremental ground acceleration. Equation 3.20 indicates that the effect of earthquake ground shaking is equivalent to the effect of an inertia loading $-M\Delta\ddot{X}_g$ applied to a structure fixed at the base.

This system of equations of motion is nonlinear, because the stiffness matrix is dependent on the magnitude of the response.

3.9 Numerical Solution Scheme of Equations of Motion

There are several implicit and explicit numerical integration techniques capable of solving the equations of motion. Among them, Newmark's Beta method is the most efficient and widely used scheme for both linear and nonlinear dynamic response analysis of structures. Although this scheme, when based on average accelerations, (Beta=1/4), is unconditionally stable

for linear systems (Newmark, 1959), it becomes unstable, when large time steps are used for the analysis of nonlinear problems (Adeli, et al., 1978).

In the present study, the equations of motion are solved by using a step-by-step application of Newmark's Beta method. In this method, the incremental velocities and displacements over a short time step are calculated from the following equations.

$$\Delta\dot{U} = \ddot{U}_n \, \Delta t + \frac{1}{2} \Delta\ddot{U} \, \Delta t \tag{3.21a}$$

$$\Delta U = \dot{U}_n \, \Delta t + \frac{1}{2} \ddot{U}_n \, (\Delta t)^2 + \beta \, \Delta\ddot{U} \, (\Delta t)^2 \tag{3.21b}$$

ΔU, $\Delta\dot{U}$, $\Delta\ddot{U}$: Change of horizontal displacement, velocity, and acceleration vectors relative to ground between time step "n" and "n+1";

$\dot{U}$, $\ddot{U}$: Velocity and acceleration vectors relative to ground at the end of step "n".

Eq. 3.21b can be solved to calculate the corresponding incremental acceleration:

$$\Delta\ddot{U} = \frac{1}{\beta(\Delta t)^2} \left[\Delta U - \dot{U}_n \, \Delta t - \frac{1}{2} \ddot{U}_n \, (\Delta t)^2 \right] \tag{3.21c}$$

Substitution of this result into Eq. 3.21a yields:

$$\Delta\dot{U} = \frac{1}{2\beta\Delta t} \left[\Delta U - \dot{U}_n \, \Delta t + (2\beta - \frac{1}{2}) \ddot{U}_n \, (\Delta t)^2 \right] \tag{3.21d}$$

By substituting Eqs. 3.21c and 3.21d into the equations of motion, the incremental displacement vector can be expressed as:

$$\{\Delta U\} = [A]^{-1} \{B\} \tag{3.22}$$

in which

$$A = \frac{M}{\beta(\Delta t)^2} + \frac{C}{2\beta\Delta t} + K \tag{3.22a}$$

and

$$B = M\left(\frac{\dot{U}_n}{\beta\Delta t} + \frac{1}{2\beta}\ddot{U}_n - \Delta\ddot{X}_g\right) + \frac{C}{2\beta}\left(\dot{U}_n - \left(2\beta - \frac{1}{2}\right)\ddot{U}_n\Delta t\right) \tag{3.22b}$$

From Eqs. 3.22, the incremental displacement vector can be obtained. Then the corresponding incremental velocity and acceleration vectors are given by Eq. 3.21d and Eq. 3.21c.

3.10 Residual Forces and Overshoot

The response calculated using this solution method will not satisfy the equilibrium requirement exactly, if the coefficients of the matrices involved in Eq. 3.20 are not constant during a step. In general, nonlinearities such as changes in yield state, column axial force-bending moment interaction, P-Delta effect, etc., may occur at any time during a step. Thus the computed incremental displacements and the element internal forces may not be correct. In this study, all nonlinearities that occur within the time or loading step are disregarded; hence, the equilibrium residual forces are not considered. This simplification can be justified in view of: 1---the relatively short time step or loading step used in the analysis which can minimize the magnitude of these residual forces but can not eliminate them; 2---the reduction in computation effort and computer storage requirements; and, 3---the imprecise nature of the damping forces present during the dynamic response.

The overshooting problem that occurs as a consequence of changes in yield state is one source of the error which results in a violation of the equilibrium conditions at the joints. The overshooting problem in the

force-deformation curve arises whenever the force passes one of the break points, Fig. 3.4. This is mainly because the force-deformation curve consists of linear segments and the fact that the status of the element is checked only at the end of the loading stage or time interval.

In the present study, the incremental nodal displacements computed during a step are assumed to be correct. The resisting forces corresponding to these displacements must however be corrected, if necessary, to satisfy the current force-deformation relationships at each step. Due to this correction, the equilibrium condition is then in turn violated, but no effort is made to adjust this imbalance or to satisfy the current equilibrium condition. These imbalance forces, which are not added to the external load vector for the next step in order to redistribute them to the rest of the structure, are accumulated. Furthermore, these residual forces and deformations do cause slightly different force-deformation characteristics in some members and may somewhat affect the overall structural response. Therefore; these forces must be limited by restricting the time step duration or loading step to ensure the accuracy of the computed incremental nodal displacements and forces.

It should be mentioned that when the interaction diagram is considered, considering residual forces as an external load vector applied during the next step might cause some problems in evaluating the current section stiffness from Eq. 2.6.

3.11 Time Interval

The length of the time step used in the analysis must be sufficiently short so that an accumulation of the errors that have been discussed in the previous section do not override the computed response. The accuracy of the

solution normally would improve as the duration of the time step is reduced. However, computational cost increase correspondingly.

Requirements on the maximum useable time step length depend not only on the dynamic characteristics of the structural system but also on the frequently content of the ground motion. There are at least three criterions which the time interval must satisfy. These three reasons for keeping the time step interval fairly small in this study are as follows:

1---The structure is assumed to remain linearly elastic within each time step interval and the yield conditions of the members are not checked during that time step. This process obviously introduces some errors but it is believed that by providing the step interval sufficiently small these errors would not be significant.

2---The ground motion is usually considered as a piecewise linear function for which the coordinates of the peaks and the relative peaks are given in digital form. Thus the ground acceleration of each time step can be obtained by linear interpolation of the two coordinate points. Hence clearly the time increment must be small compared to the time between coordinate points in order to give adequate representation of the given ground acceleration function.

3---The stability of the numerical integration scheme (Beta=1/6) requires a time step on the order of roughly 1/10 of the smallest period of the structure that has a significant effect on the internal forces.

3.12 Static and Dynamic Analysis

The nonlinear structural response is approximated by the incremental response of a series of linear structures with varying stiffnesses. Within each loading or time step, the structure is assumed to behave in a linear

elastic manner, but the assumed elastic properties of the structure are changed every loading step or every several time increments as dictated by the response. Thus the nonlinear response is obtained as sequence of linear responses of different systems.

The static analysis procedure follows an incremental displacement formulation that assumes linear behavior during a given increment of load. The static load applied to the structure can be either a monotonically increasing load or a cyclic load. However, as mentioned earlier, only lateral loads at the horizontal DOFs are considered as the external loads on the structural system in this analysis. In order to facilitate the tracking of member inelastic formations, the magnitude of lateral loads at each horizontal DOF are given together with the number of times that these lateral loads will be reduced to evaluate the load increments. This results in an incremental lateral load with the same distribution over the height as its total components. The analysis is performed then as many times as prescribed, taking in each case not only the values of the incremental loads but also superimposing the displacements and the forces of each step on the ones accumulated at the end of the preceding loading step.

For each time interval of the dynamic loading, the displacement, velocity, and acceleration increments for each story are computed by integrating the differential equations of motion over the finite time step interval. By superimposing these incremental values on the ones accumulated up to the preceding time step, the total displacements velocities, and accelerations are calculated. These totaled values are then used to calculate the incremental displacement, velocity, and acceleration of each horizotal DOF for the next time step.

Every loading increment or every several time steps, the member forces are computed using the story displacements, and the appropriate element stiffness coefficients. These forces are checked against the capacities of the members and, if yielding has occurred, the stiffness of the member is modified according to the nonlinear material properties selected for the elements. Once all elements have been checked, a new tangent stiffness matrix is assembled which contains information on the state of yield of the entire structure at the exact time step. Thus in every several time steps the constant instantaneous structural stiffness and damping (damping matrix type II) are replaced by an updated one calculated from the updated member stiffnesses. This process is then repeated for the entire loading or time integration.

3.13 Summary

A special purpose computer program for static and dynamic analyses of plane rectangular wall-frame and/or coupled shear wall systems has been developed in this chapter.

Structures are idealized as an assemblage of beams, columns, and rigid joints, all positioned in the same plane. The structural stiffness matrix is formulated by the direct stiffness method, with the nodal displacements as unknowns. The basic source of nonlinearity is considered in the behavior of the elements which are assumed to follow a bilinear force-deformation relationship. The program accounts for inelastic effects by using one of four different element models. The structural elements can be specified to be any of these four models, namely, one-component model, two-component model, multiple spring model, and the proposed model. The influence of geometric nonlinearities (often known as "P-Delta" effect), member thickness

(rigid zone at the end of the member), flexibility due to bond slip, and moment-axial force interaction effects are incorporated in the structural stiffness.

The mass of the structure is assumed to be concentrated at story levels. Two types of damping are available in the program. In the first type, a constant damping matrix as a linear combination of the mass and the elastic initial structural stiffness matrix is assumed. A variable current stiffness proportional damping matrix based on the constant first mode shape of the structure is considered in the second type.

The program performs an inelastic nonlinear analysis of structures by updating the structural stiffness matrix every loading step or every several time steps. The static analysis procedure follows an incremental displacement formulation that assumes linear behavior during a given increment of load. The static load applied to the structure can be either monotonically increasing lateral loads at the horizontal DOFs or cyclic loads. The dynamic inelastic response is evaluated by numerically integrating the equations of motion using the Newmark's Beta method based on the assumption of a defined response acceleration during each time step.

No iterations are carried out on the element states during or subsequent to a load increment or a time step, resulting in an equilibrium imbalance of forces due to the nonlinearities of the structure that develop during the time step.

Two types of hysteresis models which are available in the program will be discussed in the next chapter. The first type of hysteresis is the Takeda hysteresis model with a bilinear primary curve. The Takeda hysteresis rules are modified in the Type Two model to include a pinch effect and a strength decay.

It should be mentioned again that four different finite element models are incorporated in the computer program. They are different only in the way that nonlinearity is taken into account. Therefore, it is possible that more than one analytical model of a test structure is produced and analyzed by the computer program. In each case, it is just that particular model is being analyzed. The degree to which the response of the analytical model corresponds to the response of the test structure relys not only on the way that nonlinearity is taken into account but also on the numerical techniques employed for solving nonlinear equations of motion as well as on the approximations of material properties.

CHAPTER 4

HYSTERESIS MODELS

4.1 Introductory Remarks

The hysteresis models and definition of ductility used in this study are discussed in this chapter. Two types of hysteresis rules, which are available in the program, are explained in the first part of this chapter which is then followed by the definition of ductility. The first hysteresis model, which is referred to as the Hysteresis-1 is the Takeda type hysteresis model with a bilinear primary curve (Takeda, et al., 1970). In Hysteresis-2, the Takeda hysteresis model is modified 1---to include a pinching effect between unloading and reloading in order to represent bond deterioration and bar slippage; 2---to include a strength decay due to changes in the shear resisting machanism.

4.2 Hysteresis-1

To have a successful analytical solution to a nonlinear problem, a realistic hysteresis model is essential. Simplifications to the hysteresis model can be made depending on the load range of primary interest in the analysis. Because the study emphasis is on the post-yielding behavior, a simplified Takeda type hysteresis model with a bilinear curve, as illustrated in Fig. 4.1, is adopted for the force-deformation relationship of all analytical models. The basic relationship is in the form of a bilinear curve with an initial elastic stiffness and a subsequent strain-hardening stiffness. Also shown in Fig. 4.1 are branches for large and small deformations. Hysteresis-1 consists of eleven possible branches.

The first branch represents the linearly elastic relationship of the force-deformation curve. Branches with even numbers represent loading, while the remaining five branches, odd numbers, are unloading conditions. The unloading stiffness depends on the previous maximum deformation. It is controlled by an input parameter α as expressed in Eq. 4.1.

$$k_u = k_o \left(\frac{D_y}{D_{Max}}\right)^{\alpha} \qquad 0 \leq \alpha \leq 0.5 \qquad (4.1)$$

where

k_o : Elastic stiffness of force-deformation;

D_{Max} : Maximum deformation;

D_y : Yield deformation;

α : Unloading power.

For the one-component and the general two-component models, the force-deformation curve relates end moment to end rotation for a unit length cantilever beam. For the proposed model, the force-deformation curve represents the moment-curvature relationship at the critical section, while it relates the moment-curvature curve at the center of each segment in a multiple spring model.

4.3 Hysteresis-2

Two modifications have been made to the simplified Takeda type hysteresis model, Hysteresis-1, in order to include the pinching effect and a strength decay which are usually observed in typical reinforced concrete elements when those elements are loaded deeply into their inelastic zones. The first modification is the pinch action that results from bond deterioration and bar slippage between unloading and reloading (Lybas and Sozen, 1977; Paulay and Santhakumar, 1976). The other modification is the

loss of strength due to change in the shear resisting mechanism (Abrams, 1976; Saatcioglu, et al., 1980). These two modifications are introduced in the Hysteresis-1 after the force has exceeded the force at the yield point.

The Hysteresis-2 model incorporates the pinch action by adding additional flexibility to the hysteresis model whenever the force and deformation do not have the same sign. In other words, the force-deformation relationship during reloading is presented by two straight lines, Fig. 4.2. The slopes of these two lines are determined from Eqs. 4.2, and 4.3, respectively.

$$k_{r1} = \left(\frac{1}{k_p} + \frac{1}{k_1}\right)^{-1} \tag{4.2}$$

$$k_{r2} = 2\left(\frac{1}{k_2} + \frac{1}{k_1}\right)^{-1} \tag{4.3}$$

where

k_1 : Slope of the line connecting the point at zero force level to the maximum deformation point that is of the same sign as the current force, line AB;

k_2 : Slope of the line connecting point at zero deformation, i.e. assumed cracked closing point, to the maximum deformation point at corresponding end, line CB;

k_{r1} : First slope of the reloading range;

k_{r2} : Second slope or stiffening slope of the reloading range;

$1/k_p$: Additional flexibility.

The first slope, k_{r1}, represents the range when the crack in the compression zone stays open, mainly due to residual plastic strain in steel, and the compression force is then resisted solely by the reinforcement. After the closing of such cracks, assumed at point C, the compression caused

by force (moment) is resisted by both the compression steel and the concrete. This causes a significant increase in the reloading slope, k_{r2}. The value k_p can be evaluated based on the reinforcement resistance.

In order to include the loss of strength due to changes in the shear resisting mechanism, a guide-line is introduced in Hysteresis-2, Fig. 4.3. After the deformation has exceeded an assumed value of ductility, μ_o, the strength of the section is reduced on subsequent cycles according to the guide-line. For simplicity, the rate of the strength decay is assumed to depend only on the maximum deformation in the corresponding direction as expressed in Eqs. 4.4.

$$C_1 = C_{Max} - (\mu - \mu_o)\, k_g \geq C_{Min} \tag{4.4a}$$

$$\mu = \frac{D_{Max}}{D_y} \tag{4.4b}$$

$$\Delta F_D = F_{Max} - F_y * C_1 \tag{4.4c}$$

where

F_{Max}, D_{Max} : Maximum force and deformation which model has experienced at this end and at the same sign as current force;

F_y, D_y : Yield force and deformation;

μ_o : Ductility value which indicates starting point of strength decay;

C_1 : Reduction coefficient;

C_{Max}, C_{Min} : Maximum and minimum values of coefficient C_1;

k_g : Slope of strength decay guide-line, absolute value;

ΔF_D : Total amount of loss in strength due to strength decay and pinch action.

4.4 Definition of Ductility

As a measure of the relative amount of inelastic deformation of a member, the concept of ductility ratio is widely used. There are many definitions of ductility which are suitable for a limited type of hysteresis model, (Giberson, 1967; Shibata and Sozen, 1974; Aziz and Roesset, 1976; Saatcioglu, et al., 1980). The most widely used definition of the ductility is based on the ratio of maximum rotation to yield rotation. In order to estimate yield rotation, an anti-symmetrical deformed shape is normally assumed.

When considering a typical structure subjected to horizontal components of earthquake, the anti-symmetric distribution of bending moment is seldom developed in any columns and in general in beams. It is apparent that the yield rotation of a typical member is a function of its yield moment, stiffness properties, deformed shape or the position of inflection point, etc. The yield rotation has a minimum value based on an anti-symmetric deformed shape.

Rotation ductility computed in this study is defined as the ratio of maximum rotation to yield rotation. Maximum rotation is calculated from the hysteresis model. Anti-symmetric deformed shape is used to calculate yield rotation. Although this definition may be questionable in a general case, it will be used in this study only for the beams to compare the results from using different parameters or element models, but without claiming a true representation of a real situation. It must be regarded as no more than it is: an estimation of ductility based on rotation or as a normalized maximum rotation.

CHAPTER 5

COMPUTED RESULTS

5.1 Introductory Remarks

The objectives of this chapter are 1---to evaluate the goodness of the model proposed in chapter 2 when it is used for predicting the nonlinear behavior of R/C column members. This has been accomplished by analyzing one column member and two coupled shear wall systems for which experimental results are available; 2---to compare the results from different element models such as the one-component model, the general two-component model, the multiple spring model, and the proposed model with each other and against test results recorded during experiments to emphasize any shortcomings that maybe present in any of these models. Objective 2 has been achieved by analyzing one cantilever element and one small-scale 10-Story wall-frame system.

5.2 Experiment by Gilbertsen & Moehle (1980)

The purpose of these tests was to investigate experimentally the inelastic response of small-scale R/C column specimens. One of the variables in these tests was the rate of change in axial load with changes in the lateral load. A total of 8 specimens were tested in that study. Four columns were tested with constant axial force. For the remaining four columns, axial load varied in direct proportion with column shear. Only two specimens (4B, and 4C) are considered here. These two cantilever columns had a length of 254 mm, a cross-sectional area of 38x51 mm, and a reinforcing ratio of 1.75 %, Fig. 5.1.

The following table summarizes the relationship between specimens and test variables.

Specimen	Initial Axial Load, kN	Change in Axial Load / Change in Lateral load
4B	5.36	0.0
4C	3.25	4.0

In order to analyze the response of these two simple R/C cantilever columns, a small computer program has been written. Three of the element models described in chapter 2 are incorporated in this program. the program can analyze the response of a R/C cantilever column for a prescribed displacement history at the end. Hysteresis-1 is used in this program. This hysteresis is a simplified Takeda hysteresis model which does not consider either strength decay and pinch action.

The values for the various model parameters used in the analysis are given in Table 5.1. The loading history of two specimens was a prescribed displacement history as shown in Fig. 5.2. This history consisted of 11 cycles. Gilbertsen and Moehle (1980) describe the test setup and test procedures in more detail.

Experimental tip load-deflection curves and base moment-tip deflection curves of these two specimens appear in Figs. 5.3, and 5.4. Also shown in these figures are the computed results obtained by using the extended one-component model, the multiple spring model, and the proposed model. Base moment included the effect of axial forces acting through lateral displacements (P-Delta effect). Decrease in the post-yield slope of the tip load-deflection curves in the compression zone, which can be seen in Fig. 5.3, is due to the P-Delta effects. The computed axial force in specimen 4C

changed from approximately -1.2 kN tension to +10. kN compression. The bounds of measured axial force in this specimen ranged from -0.5 kN to +10. kN.

It is seen that the agreement between the various analytical models and experimental curves is quite good. In the proposed model, the discrepancies due to the average approximation in the evaluation of the section stiffness in the reloading range can be seen in these figures. The model is stiffer in one direction and more flexible in the other direction as compared to the multiple spring model in the reloading range. This is mainly due to the fact that a single average effective section stiffness was assumed to represent the section stiffness of the entire inelastic zone in the reloading range.

Comparison of the results from the multiple spring model and the one-component model shows a good agreement in this cantilever beam in which the I.P. is fixed and the inelastic length is less than 20 % of the length of the element. This indicates that the assumption of the concentrated equivalent nonlinear rotational spring at the end of the cantilever beam in order to account for inelastic deformations which leads to a constant post-yield stiffness coefficient is adequate.

5.3 Experiment by Lybas & Sozen (1977)

These sets of tests were designed to study the effect of the strength and stiffness of the coupling beams on the behavior of a R/C coupled shear wall structure. A total of six small-scale structures were built and tested for this purpose. The principal variable in the series was the strength and stiffness of the connecting beams. Each test structure consisted of two frames and each frame contained two walls connected by coupling beams at six

levels, Fig. 5.5. Five structures were subjected to the scaled North-South component of the base motion measured at El Centro, (specimens 1 to 5). Only one structure, S1, was subjected to statically applied lateral loads. Specimen S1 which was tested under cyclic static loading and specimen D2 which had almost the same material properties as specimen S1 are investigated in this study. In further discussion they are referred to as Structure-1.

This experimental work is selected to test the proposed model because the strength and stiffness of the coupling beams reflect the maximum axial force as well as the fluctuation of axial force in the walls. Structure D2 from these series is chosen because the flexural stiffness of the coupling beams is neither too small to obtain insufficient coupling action between the two walls nor too large to induce large changes in the wall axial forces.

Each wall had a 1 by 7 in. cross section and a height of 54 in. The reinforcing steel was uniformly distributed over the cross section for a steel ratio of one percent. The coupling beam had a cross section of 1 by 1.5 in. and a steel ratio of approximately 1.5 percent, Fig. 5.5. Weights of 2000 lb were placed at the levels of the second, fourth, and sixth story. This provided a total of 6000 lb of weight on a test structure or 3000 lb on each single frame.

Material properties assumed for the model are listed in Table 5.2. The stiffness properties of the coupling beams and walls are calculated by the procedure described in chapter 2. These calculated stiffness properties are listed in Table 5.3.

It should be mentioned that because the reinforcing steel in the wall is uniformly distributed throughout the depth of the section, yielding will

occur in a gradual sequence starting at the outer layer of the tension reinforcement and proceed layer by layer to the layer closest to the neutral axis of the section. Consequently the slope of the moment-curvature curve gradually decreases with increasing moment after yielding of the outer layer, therefore, there is no well-defined yield point. The moment at the break point of the idealized moment-curvature curve is defined as the yield moment in the wall, Fig. 2.3.

5.3.1 Static Analysis of Structure-1

As mentioned earlier, structure S1 was tested under statically applied lateral loads. The loads were applied to the test structure by three hydraulic rams, one at the level of each test weight. The hydraulic rams were programmed to maintain a predetermined ratio among the three lateral loads. The load ratio used corresponds to the calculated first mode shape of the test structure, Fig. 5.6. The test was conducted by applying certain predetermined increments of top level deflection. The low and middle rams simultaneously forced loads in the appropriate ratio to the load in the top ram. The schedule of top level deflections is shown in Fig. 5.6. Lybas and Sozen (1977) describe the test setup and test procedures in more detail.

The results of this static analysis are used not only to obtain some information about individual elements which can not be determined from only stress-strain relationships of steel and concrete under monotonically increasing loads, but also to justify the "Reduced" model which will be discussed in the next section. This 6-Story coupled shear wall structure was also investigated by Lybas (1977) under five different hysteresis models applied to the coupling beams.

5.3.2 "Reduced" Model

Because of the lack of mass at levels 1, 3, and 5, it is considered essential to reduce the number of horizontal DOFs. Such a reduction in the number of stories is essential not only because of possible numerical error caused by this type of diagonal mass matrix in a dynamic analysis, but also because of the large number of analyses to be run. This means a reduction in the number of beams and wall elements and consequently in the computer time required for the analysis.

To achieve this objective, the following criteria are considered, (Saatcioglu, et al., 1980):

1--- Overall geometry of the structure is maintained. The lever arm is especially preserved since the fluctuation of axial force is considered in the determination of the wall's stiffness.

2--- Fundamental periods and mode shapes, shear force envelope, bending moment envelope for the model and "Reduced" model should be in close agreement.

Reduction of the 6-Story to a 3-Story structure is usually based on the requirement of preserving relative stiffnesses of beams and walls meeting at a joint. However, when the contribution of wall stiffness to overall structural stiffness is far more significant than the contribution of beam stiffness, overall structural stiffness is dominated by the walls. Therefore, the beams can be lumped at every other floor without changing the stiffnesses of the walls. This results in a structure with the same beam stiffness but a smaller wall stiffness (due to increased height between coupling beams), and consequently smaller overall structural stiffness.

5.3.3 Effect of "Reduced" Model

To verify equivalence between the 6-Story test model and the 3-Story reduced model under cyclic static loading, a comparison is made between these two models.

The models used for analysis are depicted in Fig. 5.5. The line elements representing the beams and walls are connected by rigid links. Beams are idealized as elastic line elements with inelastic rotational springs located at member ends, i.e. one-component model. The inflection point is assumed to be fixed at mid length of the beam. This should result in negligible error for the beams. For walls, line elements are also considered to be acceptable. The "proposed model" is used to model the walls. The effect of changing axial force in the wall is only considered in the "Reduced" model Case-1.

The fundamental frequencies and mode shapes of the two models are listed in Table 5.4. All three periods and mode shapes of the "Reduced" model are quite consistent with those of the full model. This indicates that the reduction in the number of stories in the way discussed in the previous section has no significant effect on the fundamental periods.

It has to be mentioned that these fundamental frequencies are evaluated based on the reduced axial rigidity with almost fully cracked section stiffness properties and should not be considered as the initial frequencies of the test structure.

Comparison of base overturning moment and coupling moment vs. top level displacement, beam ductilities, bending moment at maximum displacements, and yielding sequence for the two models all show good agreement as indicated in Figs. 5.7 through 5.10.

5.3.4 Effect of Changing Axial Force on Wall Stiffness

To study the effect of changing axial force on the wall stiffness, the relationships of base overturning moment and base coupling moment to top level displacement and also force distributions between the two walls for different assumed stiffnesses of the wall are compared in this section.

Overturning moment at the base of the structure is calculated as the algebraic sum of the products of lateral forces and corresponding heights from the base. The moment due to the P-Delta effect is not included in the base overturning moment (Lybas and Sozen, 1979). This moment should be resisted by the bending moments at the base of the first story walls and the coupling moment due to the change in the axial forces in those walls.

The curve of Case-1 is obtained by considering the effect of fluctuations in the axial force in the wall on the wall's stiffness while the constant initial axial force is used to evaluate the wall stiffness in Case-2. All other assumed conditions are the same for both cases.

The order of yielding of the elements under the cyclic loading is presented in Fig. 5.10. Yielding of the beams start at about the same loading levels for the two cases. However, yielding of the wall occurs at the base of the tension wall at a base moment of roughly 44 Kip-in followed by the yielding of the compression wall at a base moment of about 57.5 Kip-in in Case-1. While in Case-2, whose wall element stiffnesses are calculated from constant initial axial force, the two walls are yielded at the same loading level which is equal to 55.8 Kip-in.

As shown in Fig. 5.7, there are no significant differences in the overturning moment vs. top level displacement curves between the two cases and also test result. This indicates that the yielding of the tension wall

in the early stages of Case-1 does not change markedly the structure's gross lateral stiffness as long as the compression wall remains elastic. However, yielding of tension wall does change the distribution of shear and moment between the two walls as shown in Fig. 5.7. In early stages of loading the walls possessed nearly identical properties, however, variation in axial load between the walls causes the stiffness of one wall to be different from that of the other, leading to the difference of shears in two walls. The shifting of the base shear from the tension wall to the compression wall continues to increase up to the point at which the compression wall also starts to yield. At this point up to 75 % of the total shear is being carried by the compression wall while only the remaining 25 % is carried by the tension wall. Such a large value of shear in the compression wall may cause shear failure in that wall although its shear strength also increases with the increasing axial force.

No appreciable difference exists between the coupling moment curves of the two cases. This means that the behavior of the connecting beams does not change with the shifting of the shear force from one wall to another in this structure.

Moment distribution patterns in the walls when the base shear equals +1.32 Kips, and when it is -1.31 Kips are shown in Fig. 5.11. The concentration of flexural moment on the compression wall at the base is clearly observed in this figure. These results indicate that maximum flexural forces in the walls can be affected significantly by the axial force-flexural interaction. The analysis which ignored the effect of axial force on flexural strength and stiffness underestimates maximum shear and moment at the base by as much as 50 %. However the average of the base moments of the two walls in Case-1 at any step is roughly equal to the base

moment of the Case-2, as also obtained by Suharwardy and Pecknold (1978).

The undershooting problem which was mentioned in Section 3.10, can be seen at maximum positive and negative displacements, Fig. 5.7. The problem arises because of using an updated structural stiffness matrix at the end of the loading step for the first step in the unloading stage. In other words, a very flexible structural stiffness matrix is used for the first step in the unloading. Such an undershooting problem can be avoided by using an iteration procedure during the step in which unloading occurs or the problem can be minimized by decreasing the loading step.

5.3.5 Preliminary Remarks of Dynamic Analysis

A series of dynamic analyses are carried out to answer several questions related to modeling techniques. The original waveforms of input base motion for the experimental tests were the acceleration signals of the El Centro (1940) NS component. The original time axis was compressed by a factor of 5 and the amplitude of acceleration was modified depending on the purpose of the experimental work. Only the first 3 seconds of the recorded based motion from the model test with run one is used in the calculations. Run one is considered only because the analysis is based on the assumption of no damage (yielding) prior to loading.

The damping matrix is assumed to be proportional to the stiffness matrix with the damping factor of 2 % for the first mode shape. The damping matrix is calculated from the current structural stiffness matrix based on a variable scalar multiplier, damping matrix type II.

Numerical integration of the equations of motion is carried out with a time step of 0.001 sec. This time step, which is roughly 4 % of the third period of the analytical model, requires 3000 steps for the calculation of

the response history of the structure to the 3 sec. of input base motion. For the integration scheme, the acceleration is assumed to be linear during the time step, Beta= 1/6. The structural stiffness matrix is updated at the end of every step. No iterations are carried out on the element states either during or subsequent to a time step, resulting in equilibrium residual forces or imbalances due to any nonlinearities that develop in the structure during a time step. These residual forces are ignored in this study.

To check on the accuracy achieved using this time step, an analysis with a time step of 0.0005 sec. is made. The results of this second analysis are compared with the 0.001 sec. time step analysis. The short trial analysis, i.e. with the time step of 0.0005, indicates very little difference in terms of displacements, but does show slightly different forces and element ductilities when compared to those obtained with the 0.001 sec. step. Hence, the 0.001 sec. time step is selected for use throughout this investigation of Structure-1. It is important to note that in any case, an exact match of forces should not be expected because any residual forces that develop are neglected.

Basic properties of the structure are listed in Tables 5.2, and 5.3. These are used unless otherwise noted.

5.3.6 Linear Dynamic Analysis of Structure-1

Linear analyses are carried out to obtain the elastic response characteristics of the structure to form a basis for understanding the inelastic action effects. Linearly elastic analysis is obtained by using essentialy the same conditions as in the inelastic analysis. However, this time, Run-0, the initial structural stiffness matrix is used throughout the

response. Therefore, linear elastic response of the test structure to the base motion is calculated based on stiffnesses almost equal to the cracked section stiffnesses of the members by a step-by-step numerical method. The results of this run are presented in Fig. 5.12.

The linear analysis is useful in showing that extensive inelasticity should be anticipated in the case of nonlinear analysis of this structure. The 33 % larger maximum top displacement (compare to measured one) observed during this elastic analysis should be expected as the structure is subjected to the base overturning moment that is approximately three times higher than the measured one. Although the total overturning moments resisted by the elastic model is 3 times larger than those of the inelastic model or measured, more than 66 % of the maximum overturning moment in the elastic model is provided by the coupling moment produced by changing of axial forces in the walls. The maximum overstress ratios (maximum moment / yield moment) of the beams and the walls in this run are 6 and 2, respectively.

5.3.7 Dynamic Analysis of Structure-1

The computed response histories of the structure subjected to the base motion are shown in Figs. 5.13 through 5.16. The influence of geometric nonlinearities (P-Delta effect), inelastic shear rigidities, and axial force-moment interaction when calculating wall stiffness are included in this computed response, which is referred to as Run-1. The measured response histories of the top level displacement, the base overturning moment, the base shear, and the top level acceleration are also plotted on the same axes to make a close comparison of the response possible.

The response waveforms are quite similar to those recorded for the test results. The analytical model successfully simulates the response waveforms except for the elongation of the fundamental period after 1.5 sec. Up to 1.5 sec., where the largest oscillation occurred in the test, the computed responses are similar to the observed responses. The test structure oscillated in a period longer than the model after 1.5 sec. In other words, the analytical model remains stiffer than the test structure. This might be due to 1--the usage of the bilinear moment-curvature relationship even for this wall with its uniform reinforcement distribution; 2--the usage of the assumed free parameters in Hysteresis-2 model. Also the way that pinch action is considered may contribute. Such a difference is also present in the comparison of the computed results around the origin and the test result under cyclic static loading.

The overall shape of the base overturning moment is very similar to that of the top level displacement: smooth and almost dominated by the first mode shape except at time 0.47 sec. where some contributing influence of the second mode in the computed results is evident. The double peaks of the computed displacement time history support this observation. The base shear response contains more higher frequency components than does the overturning moment. It should be mentioned that the measured base overturning moment as well as base shear time histories contain more higher mode effects than those corresponding to the computed responses. This is maybe partially due to the effect of the "Reduced" model.

The response waveforms of internal forces such as shear force and axial force at the base of the left wall, the total flexural moment at the base of the two walls, and the flexural moments of the beam rotational springs at three levels as recorded in Run-1 are also shown in Fig. 5.13. The axial

force waveform contains the same frequency and shape as the top level displacement. The distribution of the base shear between two walls is clearly observed in the base shear of left wall time history. During the first and second response peaks at 0.7 sec. and 1.2 sec., the left wall which is subjected to a tensile force does not resist as much shear at the base as the right wall.

The values of computed base overturning moment and top level displacement are plotted against each other in Fig. 5.14 in order to see overall structural response history during the dynamic motion. The effect of higher mode shape at time 0.47 sec. in the computed results can be seen. The measured base overturning moment vs. top level displacement is not as smooth as the computed one. That is because the measured base overturning moment contains more higher mode effects than does the computed base overturning moment.

To provide an assessment of the effect of changing axial force on the behavior of the individual walls, the moment-axial force relations and moment-curvature curves at the base of the walls as recorded during Run-1 are presented in Figs. 5.15-16. Also shown in Fig. 5.16, is the assumed moment-axial force interaction diagram for the wall section. The maximum quantities of compressive and tensile forces obtained at the base of the walls were +4.0 Kips and -1.0 Kip, respectively. This maximum compressive force is roughly 1/4 of the balanced axial force. The yielding of the walls at the base, the strain-hardening effect of walls, the overshooting problem, the pinch action and yielding of coupling beams (only in Fig. 5.16) are clearly observed in these figures. Another observation from these figures is the effect of axial force in the hysteresis loops of tension and compression walls. Increase (decrease) in strength, yield moment, and

stiffness during loading and reloading of compression (tension) wall can be seen in these figures.

As mention earlier, yielding of one wall, usually the tensile wall, at the base does not mean that the structural system loses it resistance to further load. At the time when yielding of the tension wall occurs the compression wall is still capable of carrying the additional forces applied to the structural system with increased section stiffness due to large value of compression force.

5.3.8 Effect of Pinch Action and Strength Decay of Coupling Beam

The existence of a pinch action and strength decay in the connecting beams of a coupled shear wall was shown by Abrams (1976) in his experimental study and in the P.C.A. report (Saatcioglu, et al., 1980). To examine the consequences of these two phenomena when present in the coupling beams on overall dynamic response of Structure-1, two analyses are carried out. The response of Run-2 is obtained by using a simplified Takeda hysteresis model (Hysteresis-1), which does not consider either pinch action or strength decay, for all coupling beams. Hysteresis-2 is used for the moment-rotation curve of all coupling beams in Run-1. In other words, the only difference between these two runs is that the effects of pinch action and strength decay are considered in Run-1 by using a modified Takeda hysteresis loops, Hysteresis-2, for all coupling beams.

The maximum responses of both runs are listed in Table 5.5. The response time histories, the beam ductilities, and the moment-rotation curve of the left-end mid-level beam rotational spring for both runs are shown in Figs. 5.13, 5.17, 5.18, and 5.19. Although maximum shear force and bending moment are only slighly altered, maximum horizontal displacements,

rotational ductilities of the beams, and period of the structure are increased as a result of pinch action and strength decay as observed by comparing these figures.

The response time histories of Run-2 are fairly consistent with those of Run-1 up to 0.8 sec. The maximum rotation of the coupling beams before the first negative peak at time 0.7 sec. is less than 4 times the yield rotation. This indicates the level of deformation at which strength decay starts. After the first negative peak at 0.7 sec., the period of the structure of Run-2 is shorter than those of Run-1 and those of the test results.

The above comparisons indicate that the effects of strength loss and pinch action in the coupling beams are most noticeable in increased horizontal displacements, elongation in the period of structure, and increased coupling beam ductility requirements.

5.3.9 Effect of Changing Axial Force

To study the effect of axial force-flexure interaction on dynamic response, the structure is analyzed first by neglecting this effect, Run-3, and then a second time with the effect of axial force-flexure interaction in evaluating wall stiffness matrix, Run-1. Because the fluctuations of axial force are not considered in Run-3, the structural response to loads is antisymmetric with respect to the centerline of the frame. For this run, the yield moments in the walls are assumed to be independent of axial load and equal to values corresponding to the initial axial force. The results of these two runs are presented in Figs. 5.13 for Run-1 and 5.20 for Run-3. Comparisons of these results indicate that there is no significant difference between these two runs as far as overall structural response is concerned.

5.3.10 Comparison of One- and Two-Component Models

To examine the effect of coupling beam modeling in the response of Structure-1, another analysis is made using essentially the same conditions as in Run-3. This time, Run-4, the coupling beams are modeled by means of the general two-component model. The strain-hardening ratio in the moment-rotation relationship of the general two-component model is assumed to be the same as the strain-hardening ratio of the moment-rotation curve used in the one-component model, Section 2.5.2.

The maximum responses of Run-3 and Run-4 are listed in Table 5.5. All the maximum responses of Run-4 are quite consistent with those of Run-3. The response waveforms of Run-4 are also quite similar to those of Run-3 in this analytical model in which beams are subjected to exact antisymmetric bending moment as observed by comparing Figs. 5.20 and 5.21.

5.3.11 Effect of Damping Matrix

There are several ways by which a convenient damping matrix can be selected. Most of these ways are based on an elastic analysis approach and they are justified in the inelastic range because they lead to a mathematical simplification. Therefore, it is desired to investigate the effect of stiffness proportional damping based on the initial elastic or tangent stiffness matrix.

The effects of damping on dynamic response of this structure is investigated by analyzing it three times: In the first analysis, Run-3, the damping matrix is calculated from a tangent stiffness matrix based on the damping factor of 2 % for the current first frequency. The current first frequency of the structure is evaluated based on the constant first mode

shape of the structure, damping matrix type II. In the second analysis, Run-5, the constant damping matrix which is based on the initial elastic stiffness matrix with the damping factor of 2 % for the initial first frequency is used, damping matrix type I. In the third analysis, Run-6, the damping matrix is based on the tangent stiffness matrix. In this analysis the constant scalar multiplier is calculated from a damping factor of 2 % for the initial first frequency.

The maximum responses of three analyses are listed in Table 5.5. The response time histories and the beam ductilities are presented in Figs. 5.20, 5.22, 5.23, and 5.18. Comparison of the responses of the three analyses are quite similar to each other in this structure, except that the model which is based on the initial stiffness proportional damping is slighly stiffer than the other two.

5.4 Experiment by Aristizabal-Ochoa & Sozen (1976)

The second coupled shear wall structure selected to evaluate the goodness of the proposed model is the small-scale, 10-Story, one-bay structure, figure 5.24, which has been tested by Aristizabal-Ochoa and Sozen (1976). Each test structure consisted of two frames and each frame contained two walls connected by coupling beams at 10 levels. Cross sectional dimensions of the walls and the beams were 1 by 7 in. and 1 by 1.5 in. , respectively. Structure weight was simulated by placing a 0.50 Kips weight at each floor level. The material properties as well as the stiffness properties of the coupling beams and walls, which are listed in Tables 5.6, and 5.7, are the same as those used by Takayanagi and Schnobrich (1976) for roughly a cracked section. Aristizabal-Ochoa (1976) describes the test setup and test procedures in more detail. In the subsequent

discussion, this structure is referred to as Structure-2.

Other investigators have also studied this structure (Takayanagi and Schnobrich, 1977; Takayanagi and Schnobrich, 1976; Saatcioglu, et al., 1980). In fact, Takayanagi (1976) has analyzed this structure in great detail, far more than is intended in this study. Influences of many assumed conditions such as effects of elastic, inelastic, and reduced axial rigidity, effects of the M-P interaction, effects of the pinch action and the strength decay, etc., were studied in the dynamic response of this structure by Takayanagi.

The objectives of restudying this structure here are: 1---to test the analytical model proposed in section 2.5.4 on another coupled shear wall which has a stronger coupling effect than Structure-1; 2---to assess the influence of axial force on the overall response of Structure-2; and, 3---to examine the suitability of the response of this structure if it is modeled as a 5-Story coupled shear wall.

5.4.1 Dynamic Analysis of Structure-2

The models used for the dynamic analyses are depicted in Fig. 5.24. The one-component model and the proposed model are used to represent the coupling beams and the walls, respectively.

A type II damping matrix with a damping factor of 2 % for the computed first mode shape is assumed. Numerical integration of the equations of motion is carried out with the time step of 0.0004 sec. The structural stiffness matrix is updated every 2 steps, i.e. every 0.0008 sec. This time step, which is roughly 2.5 % of the third period of the analytical model, requires updating the structural stiffness matrix 3750 times during the calculation of the response time history of the structure for 3 sec. of

input base motion. The equations of motion are solved by using the step-by-step application of Newmark's Beta method based on Beta= 1/6. Hysteresis-2 is used to model the end moment-end rotation relationships of the coupling beams. The free parameters of the hysteresis, which are listed in Table 5.7, are the same as those used by Takayanagi (1976).

The computed response time histories of Structure-2 subjected to 3 sec. of recorded (initial) base motion under three different analytical conditions as well as elastic analysis are shown in Fig. 5.25 through Fig. 5.28. The response time history of Run-1 includes the effect of a changing axial force on the flexural rigidity of the walls. For the response time history of Run-2, the yield moment as well as the section stiffness of the walls are assumed to be independent of the axial force and equal to values corresponding to the average axial load developed in Run-1. In Run-3, the structure is modeled in the same manner as the second analysis, however, in this run the structure is reduced to a 5-Story coupled shear wall, Fig. 5.24. Finally in the elastic analysis, Run-0, the structural stiffness matrix is not updated throughout the response.

Although the results from Run-2 were obtained earlier by Takayanagi (1976, Run-3 in this report), they are re-computed in this study so that results for the three models are obtained from an identical computational procedure to eliminate any modeling or numerical differences. Careful comparison of these two analytical studies reveals that the main differences are in 1---the use of slightly different base motions, Fig. 5.34, and, 2---ignoring the initial cracking moments in the beams and walls for this study.

In spite of the fact that all three analytical models fail to simulate the maximum responses, their predictions of the elongations of the

fundamental period are fairly consistent with those observed in the test. The maximum responses from these three runs are compared with the corresponding test values in Table 5.8. All three runs predict the maximum displacements at the same time as the time recorded in the test. However, the computed maximum displacements and overturning moments are considerably smaller than those of the test results, on the order of 20 % lower. The smaller maximum moments observed during the inelastic analysis should be expected when the maximum moment from the elastic analysis is almost the same as the measured one. In addition, all analytical models in this study not only fail to predict the maximum responses properly, but also are unsuccessful in simulating all the maximum relative displacements, overturning moments, and base shear after 1.5 sec. of the response. However, the elongations of the fundamental period of all three runs are the same as those of the test showing that all three runs seem to predict the structural damage properly.

In order to assess the structural damage during the base motion, the yielding sequences of the structural elements and ductility requirements for the beams are shown in Fig. 5.33 and Fig. 5.32. Also shown in Fig. 5.32 is the beam ductilities which were reported by Takayanagi (1976). In Run-2 and Run-3, the maximum moment in the walls is roughly 32 Kip-in which is less than the yield moment. This indicates that the walls remain fully elastic for those cases. In addition, in those two runs the moments in the walls above the third level never exceed one half of the corresponding yield moment.

Although the analytical models in this study and the analytical model in the second study by Takayanagi (1976) predict the change of the period for the structure properly, the response of the coupling beams computed in this

study corresponds to less damage than was observed in the earlier study, Fig. 5.32. That might be due to the fact that in this study a constant section stiffness slightly stiffer than that for a cracked section is assumed in the walls before yielding. The force-deformation relations of the wall elements are not idealized as a bilinear curve over an expected range of forces, but rather an identical primary force-deformation relation is assumed for the wall elements from the sixth level to bottom for a constant axial force, Table 5.7. This may have some effects on the response of this structure. On the other hand, it should be mentioned that even when the analytical model in the first study by Takayanagi and Schnobrich (1977) failed to simulate the elongations of the fundamental period, the maximum top level displacement and base overturning moment obtained in that report were quite consistent with those of the test results.

From the results obtained in Run-1 and Run-0, the following observations can be made:

1---Based on the stiffness properties of the elements, the fact that the maximum moment obtained in Run-1 is smaller than that of the test is understandable from the elastic analysis. In view of the maximum displacements, however, it is not apparent as to why the analytical model in Run-1 predicts the change of the fundamental period of the structure, but fails to simulate the maximum displacements. It is believed that ignoring the cracking moment in the walls is not the main reason that the analytical model fails to simulate the maximum responses properly.

2---The measured base moment vs. top level displacement displays a pronounced pinching on the hysteresis loop, Fig. 5.29. A significant portion of this reduction in the structural stiffness around the origin after 1.2 sec. of the response is believed to be caused by the pinching in

the coupling beams. Although a pinch action in the coupling beams is considered in the analytical model, Fig. 5.30, the computed response history of the base moment vs. top level displacement does not show any pronounced pinching.

The hysteresis properties of beams used to couple structural walls can have a significant influence on overall response of the structure. The stiffness of the coupling beams can dictate the extent to which each wall will act independently or as a coupled unit. The way that pinch action and strength decay are modeled in this study does not accurately represent the behavior of a coupling beam (Abrams, 1976). The force-deformation relationship obtained from the testing of a small-scale coupling beam-wall subassemblage under cyclic loading shows a very large pinching on the hysteresis loop (Abrams, 1976). The large cracks which open up during application of loads producing tension in one side of the section (top or bottom) do not close up immediately at zero deformation (Abrams, 1976). What this means in terms of the analytical model, is that the energy dissipative properties of the coupling beams have been over-estimated. This is clearly seen in Fig. 5.29.

It is interesting to note that the time step for updating the structural stiffness matrix must be small, if a very small value is assumed for the stiffness of the nonlinear rotational spring around origin. This is necessary mainly because no iterations are carried out to eliminate the residual forces.

5.4.2 Effect of Axial Force-Flexural Interaction

Comparison of results from Run-1 against those of Run-2 indicates that there is no difference between these two runs in so far as the horizontal

displacement, overturning moment, and shear time histories are concerned. In Run-1 where axial force-flexural interaction is considered, both walls yielded when they were in the tension zone, Fig. 5.31. However, in Run-2 both walls remain fully elastic. Increase (decrease) in strength and stiffness during loading and reloading of the compression (tension) wall due to considering the effect of changing axial force is clearly seen in Fig. 5.31.

The above comparison indicates that the fluctuations of axial force change the shear and the corresponding bending moment distribution between two walls, but with no change in total shear as compare to total shear in Run-2. In other words, it can be concluded that the M-P interaction does not have significant effects in overall structural stiffness, and maximum rotations in the coupling beams.

5.4.3 Effect of "Reduced" Model

The effect of using the "Reduced" model for this structure can be observed by comparing the results obtained from Run-2 and Run-3, Fig. 5.27, and Fig. 5.28. In Run-3, the 10-Story coupled shear wall was modeled as a 5-Story structure. The mass at each horizontal DOF in this run is calculated based on the constant acceleration.

Although the initial frequencies and mode shapes of two models are almost identical, the analytical model in Run-3 remains stiffer than that of Run-2. This is believed to be due to the way that mass matrix was calculated for Run-3.

5.5 Experiment by Abrams & Sozen (1979)

The third structure which is studied here is a small-scale 10-Story wall-frame system which was tested by Abrams (FW2, a structure with the "weak" wall). The test structure was composed of two frames in parallel surrounding one centrally-located "slender" wall. The frames and wall were coupled at each level by a 465 kg mass so that the lateral displacements of each element at each story would be equal. Story weight at each level was carried vertically only by the two frames. Thus no dead load was supported by the wall. Abrams and Sozen (1979) describe the test setup and test procedures in more detail.

The properties of the beams, columns, and wall are summarized in Table 5.9. The stiffness properties of the members which are calculated based on the procedures described in Chapter 2 are listed in Table 5.10. It is worth mentioning again that the force-deformation relationships of all elements are bilinearized over an expected range of forces.

The model used for analysis (both static and dynamic) is depicted in Fig. 5.35. The model consists of a frame and a wall connected in parallel through rigid links at each story level. The dashed lines between frame and wall indicate that the lateral displacements of the two systems are identical. Members are represented by line elements which include flexural, shear, and axial deformations with the exception of the beams which are axially rigid. The one-component model is used to model all beams and columns of the frame. The wall is modeled by using the proposed model for all levels except over the first story. First, the multiple spring model is used to model the wall in Case-1. In Case-2 and Case-3, the proposed model and the one-component model are used in the modeling of the first story wall

element, respectively. To account approximately for the effect of reinforcement pullout at the base of the wall, a nonlinear rotational spring is provided at the base of the wall. The flexibility of this additional rotational spring, which is listed in Table 5.10, is calculated from Eqs. 2.26 with the aid of some static wall tests (Abrams and Sozen, 1979; Moehle and Sozen, 1980).

The term "elastic" when used in describing behavior of an element is not according to standard usage and thus requires definition. Because the uncracked section stiffness is not considered explicitly in this study, the "elastic" element means that the moment of the element at any section has not exceeded the yield moment obtained at the corresponding axial force.

5.5.1 Static Analysis of Structure-3

The behavior of Structure-3 as subjected to a monotonically increasing upper triangular "first mode" lateral load is discussed in this section. Such a static analysis will be used as background information when the response of the structure to dynamic loading is presented. Furthermore, the static analysis also serves as a check on the dynamic analysis. Any strange phenomenon that seems to occur in the dynamic analysis while that same behavior does not occur in the static analysis may lead to a source of problems which may develop during the dynamic analysis.

The response of Structure-3 to the triangular load is illustrated by the force-displacement curves of Fig. 5.36. The overall response of the structure is nearly linear up until the time that some of the beams at the second through fifth levels yield. The slight nonlinearity evident earlier in the response is due to yielding of the shear wall at the base. The fact that the stiffness of the structure does not change dramatically after

yielding of the wall at the base, even in the one-component model, can be explained through the use of the first frequency of the structure computed with and without the shear wall. A reduction of only 20 % in the fundamental frequency of the structure when the shear wall is completely ignored supports the observation that the wall provides only a modest increase in lateral stiffness.

The shear wall, which is 150 times stiffer and 15 times stronger than any other individual element in the structure (Table 5.10) completely dominates the elastic response of the structure due to its stiffness. However, the response of the structure after yielding of the wall is not controlled by rigid body rotation of the wall but rather by the behavior of the frame. After the shear wall yields at its base, the frame which is still fully elastic is capable of resisting increased lateral loads.

As expected, the frame picks up a larger percentage of the total force after yielding of the wall. This percentage even increases as more and more plastic hinges form in the beams of the frame. Transfering shear force from the wall to the frame continues until the base of columns yield. At this point which is called "collapse mechanism" 80 % of the shear is carried by frame, Fig. 5.36. The load corresponding to this collapse mechanism is called the "ultimate load". The ultimate base shear and base overturning moment are roughly equal to 14 kN and 23 kN-m, respectively. The corresponding compression axial force at the base of exterior column and top level displacement are equal to +14.7 kN and 28 mm (1.2 percent of height). Beyond this top level displacement of 28 mm, calculated responses become questionable because of 1---yielding of columns with large values of axial force; 2---assumption of an Inflection Point (I.P.) fixed at mid-height of the first story columns; and 3---excessively high forces assumed to be

resisted by beams. After ultimate load, however, the structural model maintains its resisting system against further load increase due to the hardening effects present in the members.

5.5.2 Effect of M-P Interaction

The effect of moment-axial force (M-P) interaction of columns on the overall response of Structure-3 is studied here. Emori and Schnobrich (1978) has also examined this effect on the response of this structure by using a layered model. The structure in his study was, however, a distorted model of the actual test structure for considering M-P effects. The discrepancy stems from the fact that the lever arm of the coupling moment was not preserved. In that study, the layered model was applied to the first story exterior column members of the structure. The element stiffness matrices of these two columns were calculated based on a constant inelastic length. The effect of changing axial force on section stiffness was only considered in this constant inelastic length. It was concluded that moment-axial force interaction does not have a significant effect on the overall response of that structure.

In order to restudy this effect, Structure-3 is analyzed by using the extended one-component model in which the effect of axial force-flexure interaction is considered in evaluating the stiffness matrices and yield moments of all columns. These results are presented in Fig. 5.37. Also shown in this figure are the results obtained while neglecting this effect. When M-P interaction is considered, yielding of columns at the base started at a base shear of 13.6 kN followed by the yielding of the interior columns and the compression column at base shears 14.0 kN and 14.4 kN. On the other hand, when the column stiffness matrices were calculated from a constant

averaged axial force, the interior columns and exterior columns yielded at base shears 13.8 kN and 14.2 kN, respectively.

As shown in Fig. 5.37, the fluctuations of axial force do not have an effect on the overall response of Structure-3. However, it does have significant effect on the distribution of forces between columns especially exterior columns at the base as shown in Fig. 5.38.

5.5.3 Comparisons of Responses Predicted by Different Element Models

The purpose of this section and section 5.5.6 is to study the significant shortcomings of these 4 element models, namely, the one-component model, the general two-component model, the multiple spring model, and the proposed model, when they are used to model the wall element in this structure. Special modeling of the wall element is considered only because wall members are exposed to a more general moment distribution than are the beams and columns of a normal frame. In addition, due to the significant shift of Inflection Point (I.P.), the inelastic flexural behavior in the wall can be expected to expand along the length of the member.

In studies (Hsu, 1974; Takayanagi and Schnobrich, 1976; Emori and Schnobrich, 1978; Koike, et al., 1980), the multiple spring model was used to model wall members. The disadvantage of this model is that it requires each wall element of the structure to be subdivided into several segments for analysis, and hence that the computational costs and storage requirements are increased. However, the procedure has the advantages that a) it can accept almost any form of moment distribution; b) each segment can be subjected to a different stage of inelastic action; and, c) the inelastic flexural behavior can be allowed to expand along the length.

The one-component model and two-component model (non-degrading) have also been used for the modeling of a shear wall by some investigators (Fintel and Ghosh, 1979; Saatcioglu, et al., 1980; Aktan, et al., 1982; Charney and Bertero, 1982). The simplicity is the main advantage of these two models. However, these two models have several weaknesses which are discussed in chapter 2. It was judged by Otani (1981) that the representation of inelastic deformations of a member by that member's end springs, i.e. one-component model, to be insufficient.

Because the multiple spring model is believed the most realistic model against the three others, the calculated results using the other analytical models are studied in this section in relation to the results based on that model.

Three cases in which different analytical models are used for the modeling of the shear wall at the first story of Structure-3 are considered. In Case-1, the wall element at the first story is modeled by means of the multiple spring model. The proposed model and the one-component model are used for representing the first story wall element in Cases-2 and -3, respectively. In Case-3, the I.P. of the one-component model is assumed to be fixed at a distance 0.76 m from the base. All other assumed conditions are the same for these three cases.

The results of the analyses are shown in Fig. 5.36. From the results presented in this figure, the following observations can be made.

1---The proposed model produces results similar to the multiple spring model. It is worth mentioning that under monotonically increasing loading, the results of these two models should be identical, if a large number of subelements are used for multiple spring model.

2---The fact of constant post-yield stiffness coefficients in the one-component model can be observed in this figure. The stiffness of the

wall at the base is suddenly decreased after yielding in the one-component model. However, in the proposed model and the multiple spring model, the stiffness of the wall, which is function of loading history and inelastic length, is gradually decreased after yielding.

3---The fact that the shear wall at the second story in Case-3 was close to yield at the structure's ultimate load is understandable from the independence of the two nonlinear rotational springs at both ends of the first story wall, Eqs. 2.8 (Fig. 5.40). In the other two analytical models, yielding of the element at one end has some effects (depending on the inelastic length) on the stiffness of the element at the other end, Eqs. 2.18, and Eqs. 2.23. It has to be mentioned that the inelastic length of wall at ultimate load is larger than 50 % of the height of the wall in the first story.

To provide an assessment of the effects of the position of the I.P. in the one-component model on the response of Structure-3, two more cases are compared with Case-3. In these two cases, the one-component model with an I.P. at the distance 229 mm (height of the first story) from the base and at the distance 115 mm from the base are used to model the shear wall over the first story. As mentioned in chapter 2, the one-component model based on the I.P. fixed at one end is very similar to the general two-component model, if the end at which the I.P. resides, remains elastic.

Figure 5.39 indicates the relative importance of this effect. The position of I.P. affects the analysis in two ways which are clearly observed in this figure and in Fig. 5.40.

1---Evaluation of the wall stiffness matrix based on an I.P. fixed at mid-height will result in a stiffer wall, and consequently stiffer structure, when the wall is not subjected to an anti-symmetric bending moment.

2---Evaluation of the maximum moment at the base of the wall based on fixing the I.P. at mid-height will result in a larger value than for the two other assumptions. In other words, the maximum moments at the base of the wall obtained from the one-component model based on an I.P. fixed at the mid-height as well as the two-component model overestimate the maximum value of the moment as compared with Case-3 as well as Case-1. It is interesting to note that increase in the base overturning moments and base shears in the cases of the I.P. at 115 mm and at 229 mm are mostly due to the increase in the base moment and base shear of the shear wall.

5.5.4 Preliminary Remarks of Dynamic Analysis

Nonlinear response time histories of Structure-3 are calculated for the measured base motion from the first run used in the experimental series. Only the first 3 seconds of this recorded base motion is used in the calculation. The first three seconds of the recorded base motion is used because the maximum responses and most of the damage to the structure are expected to take place within these 3 seconds. The maximum acceleration of the recorded base motion is 0.49g.

A type II damping matrix with a damping factor of 2 % for the first mode shape is assumed. Numerical integration of the equations of motion is carried out with the time step of 0.0005 sec. This time step, which is roughly 2 % of the third period of the analytical model, requires solving the equations of motion 6000 times for the calculation of the response time history of the structure to the 3 sec. of input base motion.

The structural stiffness matrix is updated every 4 steps, i.e. every 0.002 sec. In order to save computer costs, the structural stiffness matrix is not updated for the first 0.82 sec. of the response. This decision is based on the knowledge that the structure remains elastic during that period

(Emori and Schnobrich, 1978). For the integration scheme, the acceleration is assumed to be linear during the time step (Beta=1/6). No effort has been made to redistribute or eliminate the residual forces that grow out of any overshoot in the force-deformation relationships. This structure was also investigated by Emori and Schnobrich (1978) and Saiidi and Sozen (1979).

5.5.5 Dynamic Analysis of Structure-3

The computed response time histories of Structure-3 subjected to the 3 sec. of recorded base motion are shown in Fig. 5.41. This computed response is referred to as Run-1. The shear wall at the first story in this run is modeled by means of the proposed model. Several of the waveforms such as, top level displacement and acceleation as well as base shear and base overturning moment are compared with the corresponding waveforms from the test. The measured base shear and base overturning moment in this structure are calculated from the measured acceleration and the value of the mass at each level.

Linear elastic analysis of this structure is also carried out to obtain a better understanding of the effects of inelastic action. The linearly elastic analysis is pertormed while using the same input conditions as with the inelastic analysis. However, this time, Run-0, the structural stiffness matrix is not updated throughout the response. The linear analysis of Structure-3, Fig. 5.42, shows that large inelasticity should be expected for the case of a nonlinear analysis. The period of the test structure elongated after one second of the response. It is interesting to note that in the case of elastic analysis, the times when the maximum response of the top level displacement, the base shear, and the base overturning moment occur are comparable to the times recorded for the maximum negative top

level displacement, the maximum base shear, and the maximum negative base overturning moment in the test. These occur at about 1.3 seconds in elastic analysis, Run-0, and 1.4 seconds in recorded one.

The overall features of the response time histories of Run-1 are similar to those of the test. The elongations of the fundamental period which are observed in the response time histories of this run are fairly consistent with those of the test except in the first 0.85 seconds of the response in which the period of the computed response is longer than the test result.

In order to assess the damage experienced by the structure during the base motion, the yielding sequences of the structural elements and ductility requirements calculated for the beams are shown in Fig. 5.43, and Fig. 5.44. This hinging pattern is very similar to that observed in the static analysis. The structure remains linearly elastic up to 0.84 sec. at which time the yielding moment is first reached at the base of the shear wall. It is observed that the structure has developed a sufficient number of plastic hinges to form a "collapse mechanism" at times 1.4 sec. and 2.0 sec. which correspond to the maximum negative (also maximum base shear) and maximum positive displacements. At these two times, the stiffness provided by the strain-hardening of the plastic hinges provides the only additional force capacity of the structure. Although the shear wall is extensively damaged in flexure at its base after 2 seconds of the response , with its inelastic length being larger than 75 % of the height of the first story, the frame is still effective in resisting lateral forces.

Figure 5.44 indicates that the beams are also severely damaged at the maximum positive displacement at time 2 sec. The ductility requirements of most beams are increased at this maximum point as shown in Fig. 5.44. The maximum normalized rotation of the first story columns based on an

anti-symmetric bending moment is 1.3, indicating that those columns are just slightly yielded.

As mentioned earlier, the computed responses up to 0.84 sec. during which the structure has remained elastic are of somewhat low quality. This indicates that when the base motion is not severe, evaluation of the element stiffness based on a constant elastic section stiffness is insufficient. Furthermore, because the moments in columns at the first story have not exceeded 1/3 of the yield moment capacity of those columns before yielding starts in the shear wall at the base, the use of the constant elastic section stiffness before yielding also has some effects on the shear distribution between the frame and the wall after yielding of the wall. It is important to realize, however, that the one-component model based on a trilinear primary curve also does not represent the damage distribution in R/C members when the inelastic action is small. This is because flexural cracking, a major source of member stiffness reduction before yielding, is not concentrated at a member end, but rather spread well into the member (Otani, 1981). It should be mentioned that although the majority of the columns did not yield as a result of the base motion, they were loaded well above their cracking load before completion of one second of the response.

The response waveforms of the base overturning moment and the top level displacement are smooth and governed almost totally by the first mode shape. The response waveforms of the base shear and top level acceleration contain some higher mode components. Furthermore, it is observed that none of yielding beams have larger number of cycles than the shear wall or structure.

Another observation from Fig. 5.41 regards the relative story displacement of the top floor during the response. This relative story

displacement is slightly smaller than the average relative story displacement (1/10 of the top level displacement) at times 1.2 sec., 1.4 sec. and 1.8 sec., indicating larger story relative displacements at the other levels at these times.

The maximum responses from Run-0 and Run-1 are compared with the corresponding test values in Table 5.11. Also the maximum responses of Run-1 and those of the test are presented in Fig. 5.47. The maximum responses for Run-1 are fairly consistent with the test results. The times when the maximum response of the top level displacement (2.0 sec.), the base moment (1.4 sec. and 2.0 sec.) and the base shear (1.4 sec.) occur are comparable to the times recorded for the test.

In order to get a more clear picture of the response, the time variable has been eliminated by plotting the base overturning moment versus the top story displacement as shown in Fig. 5.46. The dominance of the first mode component in the makeup of the structural response and also the severely damage of the structure at time 2 sec. are clearly seen in this figure. This figure also showns the summations of the energy which was dissipated by all of the inelastic hinges in all of the elements.

5.5.6 Comparison of Responses Calculated by Different Element Models

The objectives of this section are 1---to determine if the widely used one-component model and two-component model as well as the proposed model can simulate the dynamic response of a R/C wall-frame structure when they are used to represent the shear wall; 2---to investigate the effect of shifting I.P. and other assumptions in the one-component model on calculated response time histories of Structure-3.

It should be mentioned here that because the relative importance of each element model or nonlinear effect is dependent on the type of structure,

some conclusions drawn from these results might not be easily generalized nor applied directly to other structures. Therefore, the objective here is only to demonstrate the relative importance of different analytical models of Structure-3 with regards to numerical technique in solving the equations of motion.

The effect of different modelings of the wall on the computed dynamic response of Structure-3 is investigated by analyzing this structure three times: In the first analysis, Run-2, the wall at the first story is modeled by means of the multiple spring model. In the second analysis, Run-3, the one-component model based on the I.P. at a distance 0.76 m from the base is used to model the wall at the base. In the third analysis, Run-4, the shear wall at the first story is modeled in the same manner as the second analysis, however, in this run, the I.P. is assumed at distance 0.115 m (mid-height of the first story) from the base. All other assumed conditions are the same and identical to those of Run-1.

The response time histories of three analyses are shown in Figs. 5.48 through 5.50. Comparison of the responses of the three models to the base motion indicates that the response charactristics of the three analyses are more similar to each other than was true during the static analyses. The main difference between the responses of the these three runs appears to be in the maximum moment in the wall at the base. Figs. 5.51 show the force-deformation relationships of the wall at the base obtained from Run-3 and Run-4.

From the results presented in Fig. 5.41, Fig. 5.45 and Fig. 5.48 through Fig. 5.51, the following conclusions are made.

1---The maximum moment at the base of the shear wall obtained from Run-4 is larger than that of Run-3. Furthermore, the maximum hardening moment

(increase in the yield moment due to the strain-hardening effect) at the base of the wall obtained in Run-4 is the largest among these four runs. It should be mentioned that on an element basis, it is the increase in moment beyond the yield moment that determines inelastic length, strength, and ductility demands of a particular critical zone. Thus, the strain-hardening ratio of the force-deformation relationship of an element is an important factor in obtaining these variables.

2---Evaluation of the maximum flexural rotation at the base of the wall computed in Run-4 results in a smaller value than that value for Run-3. In other words, in spite of a larger maximum moment in Run-4, the maximum flexural rotation at the base of the wall in Run-4 is a smaller than that of Run-3. This result is mainly the consequence of the maximum flexural rotations at the base of the shear wall in Runs 3 and 4 being obtained based on an assumed fixed I.P. at distances 0.76 m and 0.115 m up from the base, respectively. However, the maximum fixed-end rotation at the base of the wall (rotation only due to the bond slip) obtained in Run-4 is larger (two times) than that of Run-3. This is because the fixed-end rotation is directly related to the moment and the maximum moment at the base of the wall in Run-4 is larger than that of Run-3. In Run-3, while the energy which was dissipated by flexural rotation of the wall at the base is larger than that of the Run-4, the fixed-end rotation at the base of the wall (rotation only due to the pull out of the reinforcement from the base) dissipated more energy in Run-4 than in Run-3. This is maybe one of the reasons that the results of Run-3 are similar to the results of Run-4.

3---The overall responses of the four runs are similar to each other and also to the observed test results for this structure, except the analytical model in Run-4 remains slightly stiffer after the maximum positive peak.

This indicates that almost identical overall responses will be obtained by using any of the four elements to model the shear wall. However, this conclusion can not be generalized, since the sensitivity of the response of this structure to the behavior of the wall after yielding with regard to the residual forces is not known.

5.5.7 Effect of Time Step and Residual Force

Although a detailed study of the effects of numerical errors (numerical errors due to ignoring residual forces and deformations) on the computed responses of R/C structures are beyond the scope of this study, it is essential to study this effect in Structure-3 since a small time step is not possible, because of the computer cost and number of analyses.

By choosing a large time step for updating structural stiffness matrix, it is obvious that some of the response characteristics which are influenced by the higher modes may not be incorporated in the analyses. Furthermore, the errors arising from overshooting and undershooting may be significant enough to affect the post-yield responses. In addition, large time step causes different force-deformation characteristics in some members, especially in the shear wall, and may somewhat affect the overall structural response.

In order to estimate the effects of time step (time step for updating structural stiffness matrix) and the accumulation of the residual forces, two analyses are carried out. The response of Run-1 is obtained by updating structural stiffness matrix every 4 steps (i.e. every 0.002 sec.). The structural stiffness matrix is updated every 8 steps in Run-1b, (i.e. every 0.004 sec.). In the both runs the numerical integration of the equations of motion are carried out with the time step of 0.0005 sec.

The maximum responses of these two runs are listed in Table 5.11. The response time histories, the beam ductilities, and the corrected force-deformation relationships of the wall at the base and beam at the fifth level are shown in Figs. 5.52 vs. 5.41, 5.53, 5.54 vs. 5.45, and 5.55. Also shown in Fig. 5.54 is the force-deformation relationship of the wall at the base as obtained in Run-1b.

As mentioned in section 3.10, the computed incremental nodal displacements which are calculated from the equations of motion are assumed to be correct. The resisting forces corresponding to these displacements are calculated from the state of the structure at the beginning of that time step. These forces are corrected, if necessary, to satisfy the current force-deformation relationships. Therefore, some residual forces are created whenever the force passes one of these four break points, Fig. 3.4. Two forces are preserved at the end of each element. One is the response force. (the response forces at a time step are calculated as the sum of all the increments to that time step). The other is the corrected force which satisfies the force-deformation relationship in the hysteresis rules.

No iterations are carried out on the element states during or subsequent to a time step, resulting in imbalance forces arising from any change in properties that occur in the structure during that time step. These imbalance forces are <u>not</u> applied as residual forces to the structure during the next time step to eliminate the accumulation of these forces. Due to the accumulation of these residual forces the position of the zero force (the position for the changing slope from unloading to reloading) is shifted by as much as 10 % of the yield moment in Run-1b, Fig. 5.54. The irregularities and deviations observed in the moment-curvature relations of the wall at the base as seen in Fig. 5.54 are caused by these residual

forces and numerical errors arising from the magnitude of the time step used in the updating structural stiffness matrix.

The best method to minimize these types of errors is to reduce the time step. Another method, that still may converge to the wrong results but usually has been used in the dynamic analysis (Kanaan and Powell, 1974; Mahin and Bertero, 1975; Luyties, et al., 1976; Emori and Schnobrich, 1978), is to consider the residual forces as external forces in the next time step. Another method which normally used in the static analysis, is the procedure which satisfied equilibrium exactly at the end of each load increment. In this method, if yielding occurs during a load increment, the program backs up that increment and determines the load increment that just produces yielding. In this procedure then the load increment is not constant. As mentioned earlier, the first method is used in this study.

Comparison of the results of these two analyses (Run-1 and Run-1b) indicates that the analytical model in Run-1b was more flexible than the analytical model in Run-1 after 1.2 seconds of the response. This is only because the beams in Run-1b were more damaged than those in Run-1. At times 1.2 sec., 1.6 sec., and 2.0 sec. while most of the beams in Run-1b were in the strain-hardening range, the wall remained in the reloading range. In other words, in the positive displacement direction, the moment in the wall at the base was larger than yield moment only at 0.8 Sec., Fig. 5.54. From these results, it can be said that the energy dissipated through the frame's plastic hinges consists of a significant percentage of the total energy dissipated by the structure. Therefore, if a small portion of the total energy was dissipated through the wall's plastic hinge at the base, different forms of modeling of the shear wall at the base may not lead to significant differences in the dynamic responses of this structure.

CHAPTER 6

SUMMARY AND CONCLUSIONS

6.1 Summary

The purpose of this study is to provide a method of analysis capable of performing an inelastic analysis of plane, rectangular wall-frame and/or coupled shear wall structures under static as well as dynamic loads. Such a method (computer program) is developed to answer two main objectives of this study. The first objective is to develop a procedure for considering axial force-moment interaction in evaluating the stiffness matrix for a column element. This objective is achieved by formulating a relatively simple but refined analytical procedure capable of considering the effect of fluctuation of the axial force on the element stiffness matrix (Chapter 2). The second objective is to discuss the influence of the different modeling of the wall element on the response of a R/C wall-frame structure.

To complete these two tasks, an analytical model is developed and presented in Chapters 2 and 3. The analytical model is based on flexural line elements representing beams, columns and walls. Four different finite element models which take into account inelastic flexural effects are built into the program. The structural elements can be specified to be any of these four element models, namely, the one-component model (Section 2.5.1), the general two-component model (Section 2.5.2), the multiple spring model (Section 2.5.3) or, the model which is presented in this study (Section 2.5.4). In the first two analytical element models, the member is made up of a single line element. Member end moments are related directly to member end rotations. Therefore, the 2 by 2 element stiffness matrix which relates

the end moments to end rotations is calculated directly from the force-deformation relations at each end. In the other two analytical element models, the member is divided longitudinally into subelements. In each of these subelements the local cross-sectional forces and deformations are related. The resulting functions are integrated along the element to give an end moment to end rotation relationship.

The analytical procedure is developed to study the nonlinear behavior of wall-frame and/or coupled shear wall systems subjected to static as well as dynamic loads. This procedure is applied to two coupled shear wall models and one wall-frame model. These model structures are analyzed for both static loads as well as dynamic loads and their computed results are compared with the test results (Chapter 5). The effects of some assumed analytical conditions on the maximum responses and the response waveforms of the model structures are also discussed (Chapter 5).

6.2 Conclusions

Based on the results of this study, the following conclusions may be stated.

1---The computer program as developed in this study can be used to predict static as well as dynamic inelastic behavior of coupled shear wall and/or wall-frame structures in a post-yielding range with a reasonable accuracy. Results of three analyses using the program and the corresponding results established on the basis of experiments are in good agreement. The analytical models for all three structures satisfactorily reproduce the maximum responses and the response waveforms, especially the elongations of the periods due to the change of structural stiffness, that were recorded during the tests. The most significant exception in the high quality of

reproducation of the experimental results by the analytical models is the maximum responses of Structure-2.

2---The accuracy of the column element model is demonstrated by the analyses of a one column element and two coupled shear wall structures. The comparison between experimental and analytical results shows very good agreement, leading to the conclusion that the model is very effective in predicting the nonlinear behavior of R/C column frame and wall members. The analytical column element predicts changes in strength and stiffness due to changing axial force. It is demonstrated that expression 2.6 can incorporate the effect of axial force variation in the moment-curvature relationships. Increase (Decrease) in moment-carrying capacity and stiffness of a section due to increase (decrease) in the axial force is successfully reproduced in the force-deformation curve by expression 2.6.

3---Fluctuation of axial force in a coupled shear wall as well as in frame structures plays a major role in establishing maximum forces and deformations in the individual walls (or individual columns in the frame structures). The analysis which ignored the effect of changing axial force on flexural strength and stiffness underestimated maximum shear and moment (by as much as 50 %, depending on the degree of coupling) in the individual members at the lower levels of the structure.

In the coupled shear wall systems, variation in the axial force between the walls causes not only a shifting of the shear and bending moment from the tension wall (wall which has axial force smaller than initial axial force) to the compression wall, but also a changing of the moment-carrying capacities of the individual walls due to the axial force-moment interaction. Therefore, increasing the shear force of the compression wall

may cause shear failure in that wall although its shear strength also increases with increasing axial force. Furthermore, decreasing the yield moment of the tension wall may cause high deformation demand in that wall although its available ductility increases with decreasing axial force.

4---Comparative studies of the overall responses of the two coupled shear wall structures with and without the effects of the changing axial force on the wall element stiffness matrix reveals that the response waveforms for the two cases are very similar. The displacements, base shear, and base moment waveforms for the two cases are roughly the same. Maximum forces and displacements as well as maximum ductilities of the coupling beams in these two coupled shear wall structures are not sensitive to the axial force effects in the walls. The major effect of changing axial forces in the walls is the reduction in the section stiffness and the yield moment of one wall due to the decrease in axial force with the reverse happening in the other wall. This behavior does not however have significant control on the overall behavior of the coupling beams. In other words, it is demonstrated that although the shear forces and the corresponding bending moments in the individual walls are significantly affected by the changing of axial force, the axial forces in the walls themselves are not greatly affected.

5---The hysteresis relations of the coupling beams exerts a major effect on the overall hysteresis relation of coupled shear wall structures. The coupling between the two walls exerts a considerable influence on the structural stiffness. Pinching action and strength decay of the coupling beams produce larger displacements due to the decrease in the degree of the coupling between the two walls.

6---Comparison of experimental and analytical results show that the one-component model is suitable for modeling inelastic behavior of R/C beam members. The good agreement between experimental and analytical load-deflection curves indicates that when the I.P. (Inflection Point) is fixed, the assumption of a concentrated equivalent nonlinear rotational spring at the end of the cantilever beam in order to account for inelastic deformations is adequate. Shifting of the I.P. in the beams with equal positive and negative yield moment capacities does not have a significant effect on the response of a structure. This is because in the beams with the absence of any gravity load applied to the beams, yielding at one end of the beam shifts the I.P. away from its elastic position. However, yielding at one end is usually quickly followed by beam yielding at the other end thus shifting the I.P. back to nearly its elastic I.P. position. Therefore, in view of the fact that many different nonlinearities such as bond slip, pinch action and strength decay can be incorporated in this model very easily and also with regard to simplicity, the use of one-component model for the beams of frame structures is believed to be appropriate.

7---It is shown that the general two-component model has the same versatility as the one-component model. The results of these two models when they are used to model the coupling beams in the coupled shear wall structures are very similar.

8---The observations related to the different modelings of the wall in Structure-3 under static and dynamic loads are presented in Sections 5.5.3 and 5.5.6. The main conclusion among those observations is that in the multistory wall-frame structures, evaluation of the wall stiffness matrix based on the one-component model with an I.P. fixed at mid-height of the

first story or the two-component model will result in a stiffer wall and consequency stiffer structure. Therefore, the maximum moments at the base of the wall as obtained from the one-component model (I.P. at mid-height) and the two-component model overestimate the maximum value of the moment as compared with the moment obtained from a more accurate element model (multiple spring model). The position of the I.P. directly affect the strain-hardening slope of the nonlinear rotational spring at each end. The strain-hardening ratio (strain-hardening stiffness over (3EI/L)) of the nonlinear rotational springs for the cases of the I.P. at distances 0.115 m, 0.229 m, and 0.760 m up from the base are 6.4 %, 3.2 %, and 1.0 %, respectively.

Comparison of the analytical results of the wall-frame structure obtained from using two different element models, (one-component model with an I.P. fixed at elastic position and multiple spring model), to represent the wall element at the base indicates that the response waveforms for the two analytical models are similar. This means that the shifting of the I.P. due to yielding of the wall at the base as well as propagation of the inelastic zone do not have significant effects on the responses of this structure, a structure with a "weak" wall.

6.3 General Observations

One obvious shortcoming of this study is that a relatively small number of test structures is considered. One cantilever column member and two coupled shear wall structures were used to test the accuracy of the proposed model. Under dynamic loading, these two coupled shear wall structures were not subjected to very severe earthquake motions. In both structures the walls did not yield when they were under compressive forces. When axial

force-moment interaction was not considered, the maximum moment in the walls was less than 95 % of the yield moment in Structure-1 and less than 85 % of the yield moment in Structure-2. Only one structure, Structure-3, was used to study the effects of the different modelings for the wall element on the response of the structure. Therefore, it is believed that this study lays the foundation upon which further research may provide additional insight into the computed behavior of coupled shear wall and wall-frame structures.

TABLES

Table 2.1 Comparison of the Flexural Flexibility Coefficients of the One- and the General Two-Component Models

One-Component Model

	f_{11}	f_{12}	f_{22}
Both Ends Elastic	$\frac{\ell}{3EI}$	$-\frac{\ell}{6EI}$	$\frac{\ell}{3EI}$
Not Both Ends in the Strain-Hardening (S. H.)	f_{A1}	$-\frac{\ell}{6EI}$	f_{B1}
Both Ends in the S. H.	$\frac{\ell}{3p_1EI}$	$-\frac{\ell}{6EI}$	$\frac{\ell}{3p_1EI}$

$$f_{A1} = \frac{\ell}{3EI} + \ell_A\left(f_{AA} - \frac{1}{3EI}\right)$$

$$f_{B1} = \frac{\ell}{3EI} + \ell_B\left(f_{BB} - \frac{1}{3EI}\right)$$

If $\ell_A = \ell_B = \ell/2$

$$\begin{cases} f_{A1} = \frac{\ell}{2}\left(f_{AA} + \frac{1}{3EI}\right) \\ f_{B1} = \frac{\ell}{2}\left(f_{BB} + \frac{1}{3EI}\right) \end{cases}$$

General Two-Component Model

		f_{11}	f_{12}	f_{22}
Both Ends Elastic		$\frac{\ell}{3EI}$	$-\frac{\ell}{6EI}$	$\frac{\ell}{3EI}$
Not Both Ends in the Strain-Hardening	$f_{B2} \leq f_{A2}$	$\frac{3}{4} f_{A2} + \frac{1}{4} f_{B2}$	$-\frac{f_{B2}}{2}$	f_{B2}
	$f_{B2} \geq f_{A2}$	f_{A2}	$-\frac{f_{A2}}{2}$	$\frac{3}{4} f_{B2} + \frac{1}{4} f_{A2}$
Both Ends in the S. H.		$\frac{\ell}{3p_2EI}$	$-\frac{\ell}{6p_2EI}$	$\frac{\ell}{3p_2EI}$

$$\begin{cases} f_{A2} = \frac{\ell}{2}\left(f_{AA} + f_{AA}\right) \\ f_{B2} = \frac{\ell}{2}\left(f_{BB} + f_{BB}\right) \end{cases}$$

f_{AA} (f_{BB}) : Instantaneous end moment-end rotation flexibility of unit length cantilever beam at end A(B).

Table 5.1 Stiffness Properties of Column Elements

A) SPECIMEN 4B		
Axial Force	kN	5.36
Moment-Curvature Relationship		
First Slope	$kN-m^2$	3.54
Second Slope	$kN-m^2$	0.055
Yield Moment	kN-m	0.345
Moment-Rotation Relationship		
First Slope	kN-m	41.81
Second Slope	kN-m	2.05
Yield Moment	kN-m	0.375
B) SPECIMEN 4C		
Axial Force	kN	3.25
Change of Yield Moment/ Change of Axial Force	m	0.019
Moment-Curvature Relationship		
First Slope	$kN-m^2$	3.20
Second Slope	$kN-m^2$	0.055
Yield Moment	kN-m	0.305
Moment-Rotation Relationship		
First Slope	kN-m	37.80
Second Slope	kN-m	2.05
Yield Moment	kN-m	0.325

Table 5.2 Assumed Material Properties for Structure-1

Properties		
CONCRETE		
Compressive Strength, f_c'	ksi	5.3
Tensile Strength, f_t	ksi	0.5
Strain at f_c'		0.0038
STEEL		
Yield Stress	ksi	43.7
Ultimate Stress	ksi	53.1
Young's Modulus	ksi	29000.
Strain at Yield		0.0015
Strain at Ultimate		0.066
Strain at Strain-Hardening		0.025

Table 5.3 Stiffness Properties of Constituent Elements of Structure-1

A) BEAM (1 No. 11 gage wire per face)

Moment-Rotation Relationship, Unit Length

3EI	Kip-in	720.
First Slope	Kip-in	310.
Second Slope	Kip-in	25.
Yield Moment	Kip-in	0.625

B) BEAM (in "Reduced" Model)

Moment-Rotation Relationship, Unit Length

3EI	Kip-in	1440.
First Slope	Kip-in	620.
Second Slope	Kip-in	50.
Yield Moment	Kip-in	1.25

Free Parameters in Hysteresis-2

$\alpha = 0.4$ $\mu_o = 4.5$ $C_{Max} = 1.25$

$C_{Min} = 1.00$ $k_g = 0.1$ $k_p = 100.$

C) WALL (6 No. 11 gage wire, Uniform)

Axial Rigidity	Kip	14000.
Shear Rigidity	Kip	8200.
Axial Force	Kip	1.5
Change of Yield Moment/ Change of Axial Force	in	3.0

Moment-Curvature Relationship

First Slope	Kip-in^2	16875.
Second Slope	Kip-in^2	200.
yield Moment	Kip-in	13.5

Table 5.4 Comparison of the Mode Shapes of the 6-Story and "Reduced" Model of Structure-1

	First Mode		Second Mode		Third Mode	
Level	Whole	Reduced	Whole	Reduced	Whole	Reduced
6	1.28	1.28	-0.36	-0.35	0.08	0.08
5	1.07		-0.06		-0.15	
4	0.83	0.83	0.40	0.39	-0.22	-0.22
3	0.56		0.50		0.05	
2	0.31	0.31	0.41	0.41	0.28	0.28
1	0.10		0.16		0.15	
	Frequency, Hz					
	5.7	5.4	20.7	19.6	41.9	38.6

Table 5.5 Measured and Computed Maximum Responses of Structure-1

Level	Measured	Run-0	Run-1	Run-2	Run-3	Run-4	Run-5	Run-6
1--DISPLACEMENT (in)								
Top	0.46	0.61	0.46	0.42	0.46	0.46	0.44	0.47
Mid	0.30	0.42	0.28	0.26	0.27	0.27	0.27	0.26
Low	0.12	0.16	0.10	0.09	0.09	0.09	0.09	0.09
2--ACCELERATION (g)								
Top	0.89	2.29	1.17	1.16	1.18	1.18	1.13	1.24
Mid	0.82	2.26	1.24	1.29	1.24	1.24	1.23	1.35
Low	1.33	1.54	1.36	1.33	1.36	1.36	1.39	1.44
3--OVERTURNING MOMENT (Kip-in)								
Top	--	41.2	20.2	19.8	20.5	20.5	20.3	21.7
Mid	--	88.2	33.2	33.4	34.2	34.2	33.9	35.4
Low	58.0	151.9	51.4	50.2	53.4	53.4	49.7	52.3
4--BASE SHEAR (Kip)								
Top	--	2.28	1.12	1.09	1.13	1.13	1.12	1.20
Mid	--	3.43	1.28	1.32	1.33	1.33	1.39	1.37
Low	1.54	3.94	1.75	1.68	1.79	1.79	1.70	1.79

Table 5.6 Assumed Material Properties for Structure-2

Properties		
CONCRETE		
Compressive Strength, f'_c	ksi	4.5
Tensile Strength, f_t	ksi	0.4
Strain at f'_c		0.003
Strain at f_t		0.00013
STEEL		
Yield Stress	ksi	72.
Ultimate Stress	ksi	83.
Young's Modulus	ksi	29000.
Strain at Yield		0.0025
Strain at Ultimate		0.08
Strain at Strain-Hardening		0.01

Table 5.7 Stiffness Properties of Constituent Elements of Structure-2

A) BEAM (1 No. 8 gage wire per face)

Moment-Rotation Relationship, Unit Length

3EI	Kip-in	600.
First Slope	Kip-in	270.
Second Slope	Kip-in	27.
Yield Moment	Kip-in	1.55

Free Parameters in Hysteresis-2

$\alpha = 0.5$ $\mu_o = 1.$ $C_{Max} = 0.7$

$C_{Min} = 0.4$ $k_g = 0.1$ $k_p = 54.$

B) Wall (1-st to 6-th level)

Axial Rigidity	Kip	12700.
Shear Rigidity	Kip	7600.
Change of Yield Moment/ Change of Axial Force	in	2.2

Moment-Curvature Relationship

First Slope	$kip\text{-}in^2$	56000.
Second Slope	$kip\text{-}in^2$	1000.
yield Moment	kip-in	39.
Axial Force	Kip	3.

C) Wall (6-th to 10-th level)

Axial Rigidity	Kip	12700.
Shear Rigidity	Kip	7600.
Change of Yield Moment/ Change of Axial Force	in	2.2

Moment-Curvature Relationship

First Slope	kip-in	37000.
Second Slope	kip-in	420.
yield Moment	kip-in	20.
Axial Force	Kip	1.

Table 5.8 Measured and Computed Maximum Responses of Structure-2

Level	Measured	Run-0	Run-1	Run-2	Run-3
1--DISPLACEMENT (in)					
10	1.16	0.76	0.92	0.90	0.87
9	1.00	0.68	0.82	0.80	
8	0.86	0.60	0.71	0.69	0.68
7	0.71	0.51	0.60	0.58	
6	0.58	0.42	0.48	0.47	0.47
5	--	0.33	0.36	0.35	
4	--	0.24	0.25	0.25	0.26
3	--	0.15	0.16	0.15	
2	--	0.08	0.08	0.08	0.08
1	--	0.02	0.02	0.02	
2--ACCELERATION (g)					
10	1.66	1.43	1.33	1.34	1.33
9	1.12	1.05	0.96	0.97	
8	0.75	0.73	0.71	0.71	0.73
7	0.73	0.75	0.65	0.66	
6	0.85	0.78	0.72	0.72	0.73
5	0.86	0.78	0.74	0.74	
4	0.82	0.71	0.67	0.67	0.67
3	0.71	0.60	0.57	0.58	
2	0.57	0.49	0.48	0.48	0.49
1	0.47	0.42	0.42	0.42	
3--OVERTURNING MOMENT (Kip-in)					
9	7.5	6.4	5.8	5.9	
8	19.9	17.5	15.6	15.8	15.9
7	34.6	31.4	28.0	28.3	
6	51.5	46.7	41.7	42.3	42.4
5	69.2	62.2	55.8	56.5	
4	86.0	77.3	69.5	70.5	71.0
3	102.1	92.0	82.7	84.0	
2	118.9	107.4	95.8	97.4	98.7
1	135.4	130.0	110.2	112.4	
Base	151.5	154.8	126.9	129.8	131.9
4--BASE SHEAR (Kip)					
9	0.83	0.71	0.64	0.65	
8	1.37	1.22	1.08	1.10	0.89
7	1.69	1.55	1.39	1.41	
6	1.88	1.72	1.57	1.59	1.50
5	1.91	1.81	1.66	1.69	
4	1.94	2.00	1.76	1.78	1.75
3	2.12	2.30	1.94	1.98	
2	2.15	2.56	2.13	2.17	2.12
1	2.37	2.74	2.36	2.37	
Base	2.54	2.86	2.53	2.55	2.54

Table 5.9 Assumed Material Properties for Structure-3

Properties			
CONCRETE			
Compressive Strength, f'_c	MPa	42.1	
Tensile Strength, f_t	MPa	3.5	
Young's Modulus	MPa	23000.	
Shear Modulus	MPa	13000.	
Strain at f'_c		0.003	
Strain at Ultimate		0.004	
Strain at f_t		0.00011	
STEEL			
		Beams & Columns	Wall
Yield Stress	MPa	352.	338.
Ultimate Stress	MPa	382.	400.
Young's Modulus	MPa	200000.	200000.
Strain at Yield		0.0018	0.0017
Strain at Ultimate		0.07	0.07
Strain at Strain-Hardening		0.01	0.002

Table 5.10 Stiffness Properties of Constituent Elements of Structure-3

A) BEAM (2 No. 13 gage wire per face)

Moment-Rotation Relationship, Unit Length

3EI	kN-m	3.6
First Slope	kN-m	2.0
Second Slope	kN-m	0.07
Yield Moment	kN-m	0.09

B) BEAM (3 No. 13 gage wire per face)

Moment-Rotation Relationship, Unit Length

3EI	kN-m	4.65
First Slope	kN-m	3.00
Second Slope	kN-m	0.09
Yield Moment	kN-m	0.13

C) COLUMN (3 No. 13 gage wire per face)

Axial Rigidity	kN	40000.
Change of Yield Moment/ Change of Axial Force	m	0.02

Moment-Roatation Relationship, Unit Length

First Slope	kN-m	8.0
Second Slope	kN-m	0.25
Yield Moment	kN-m	0.29
Axial Force	kN	5.1

D) COLUMN (2 No. 13 gage wire per face)

Axial Rigidity	kN	40000.

Moment-Rotation Relationship, Unit Length

Axial Force	kN	0.85	2.0	3.5	5.1
First Slope	kN-m	4.5	5.0	6.0	7.0
Second Slope	kN-m	0.2	0.2	0.2	0.2
Yield Moment	kN-m	0.145	0.17	0.20	0.23

Table 5.10 (Continued)

E) WALL (4-th to 10-th level)		
Shear Rigidity	kN	50000.
Moment-Curvature Relationship		
First Slope	$kN-m^2$	600.
Second Slope	$kN-m^2$	2.6
Yield Moment	kN-m	4.25
F) WALL (1-st to 3-rd level)		
Shear Rigidity	kN	50000.
1--Moment-Curvature Relationship		
First Slope	$kN-m^2$	430.
Second Slope	$kN-m^2$	2.6
Yield Moment	kN-m	4.25
2--Moment-Rotation Relationship, Unit Length		
First Slope	kN-m	1290.
Second Slope	kN-m	40.
Yield Moment	kN-m	4.4
3--Moment-Fixed End Rotation Relation (Only at the base)		
First Slope	kN-m	12000.
Second Slope	kN-m	1200.

Table 5.11 Measured and Computed Maximum Responses of Structure-3

Level	Measured	Run-0	Run-1	Run-2	Run-3	Run-4	Run-1b
1--DISPLACEMENT (mm)							
10	28.4	19.5	28.9	30.2	31.3	29.5	35.9
9	25.6	17.4	26.1	27.1	28.2	26.5	32.6
8	23.6	15.4	23.2	24.1	25.0	23.5	29.2
7	20.6	13.4	20.2	21.0	21.8	20.5	25.7
6	17.3	11.3	17.2	17.7	18.4	17.4	22.0
5	14.2	9.1	14.1	14.4	15.0	14.1	18.1
4	10.7	6.8	10.8	11.2	11.6	10.9	14.1
3	8.3	4.5	7.8	8.1	8.2	7.6	10.0
2	5.1	2.4	4.6	5.0	5.0	4.5	5.9
1	2.3	0.7	1.8	2.0	2.1	1.2	1.9
2--ACCELERATION (g)							
10	0.91	1.17	0.84	0.83	0.85	0.90	0.84
9	0.74	0.89	0.66	0.66	0.67	0.67	0.67
8	0.61	0.73	0.56	0.56	0.56	0.56	0.57
7	0.60	0.70	0.51	0.49	0.50	0.53	0.48
6	0.54	0.66	0.48	0.48	0.49	0.50	0.47
5	0.54	0.66	0.46	0.46	0.46	0.48	0.45
4	0.56	0.61	0.42	0.41	0.42	0.44	0.42
3	0.49	0.52	0.37	0.38	0.38	0.38	0.37
2	0.39	0.39	0.41	0.41	0.41	0.41	0.41
1	0.38	0.44	0.44	0.44	0.43	0.44	0.44
3--OVERTURNING MOMENT (kN-m)							
9	--	1.2	0.8	0.8	0.9	0.9	0.8
8	--	3.4	2.3	2.3	2.3	2.4	2.3
7	--	6.1	4.3	4.3	4.4	4.3	4.4
6	--	9.3	6.6	6.6	6.7	6.6	6.7
5	--	13.0	9.2	9.2	9.3	9.2	9.3
4	--	16.9	12.0	12.0	12.0	12.0	12.1
3	--	21.0	14.5	14.4	14.6	14.6	14.8
2	--	25.0	17.3	17.3	17.6	17.9	17.4
1	--	29.1	20.4	20.3	20.6	21.2	20.0
Base	28.2	34.6	23.7	23.1	23.6	24.5	23.4
4--BASE SHEAR (kN)							
9	--	5.3	3.8	3.6	3.8	3.9	3.6
8	--	9.3	6.6	6.6	6.6	6.5	6.7
7	--	12.2	8.8	8.8	8.9	8.8	8.9
6	--	14.5	10.4	10.3	10.4	10.4	10.6
5	--	16.3	11.4	11.4	11.5	11.6	11.6
4	--	17.8	12.8	12.7	12.9	13.3	12.2
3	--	20.0	14.2	14.2	14.3	15.0	13.4
2	--	22.2	15.6	15.4	15.6	16.2	14.6
1	--	23.8	16.0	16.0	16.0	16.5	15.7
Base	18.0	24.7	16.4	16.8	16.5	17.4	17.2

FIGURES

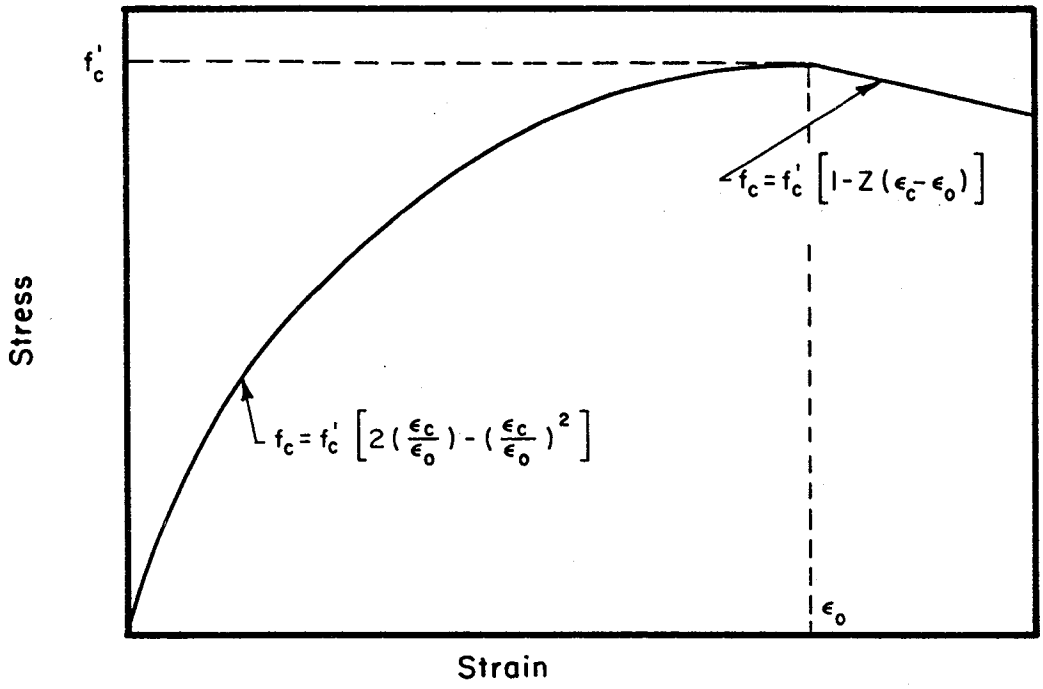

Fig. 2.1 Idealized Stress-Strain Curve for Concrete

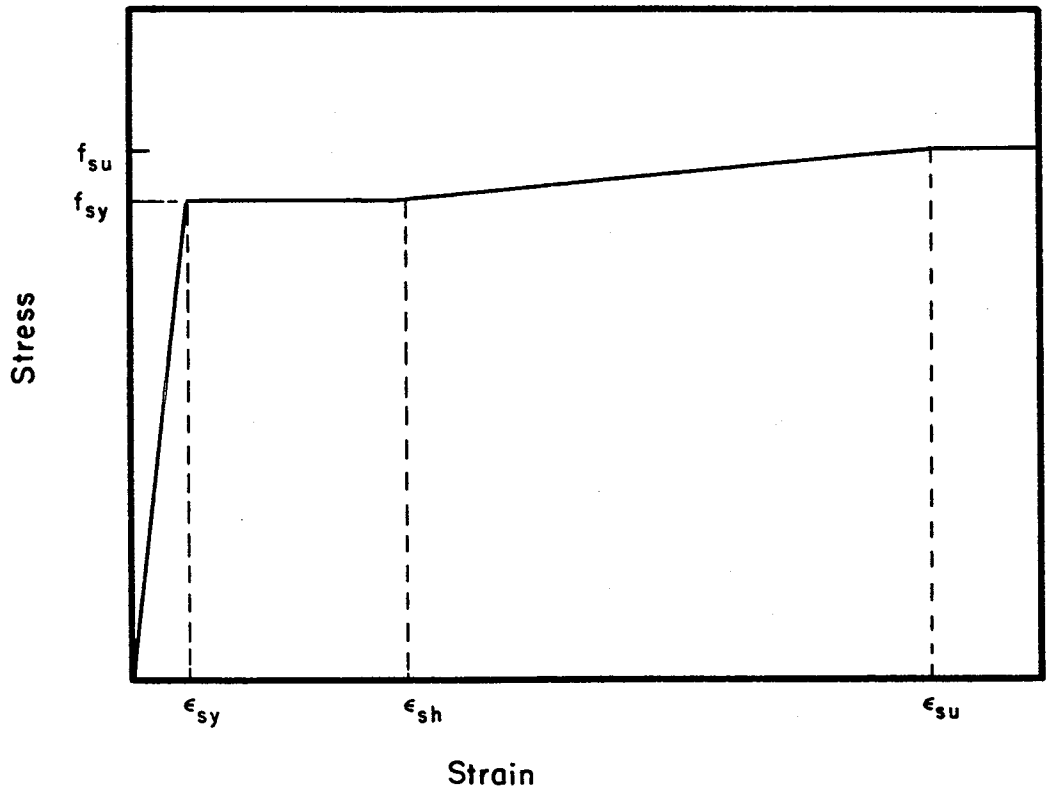

Fig. 2.2 Idealized Stress-Strain Curve for Steel

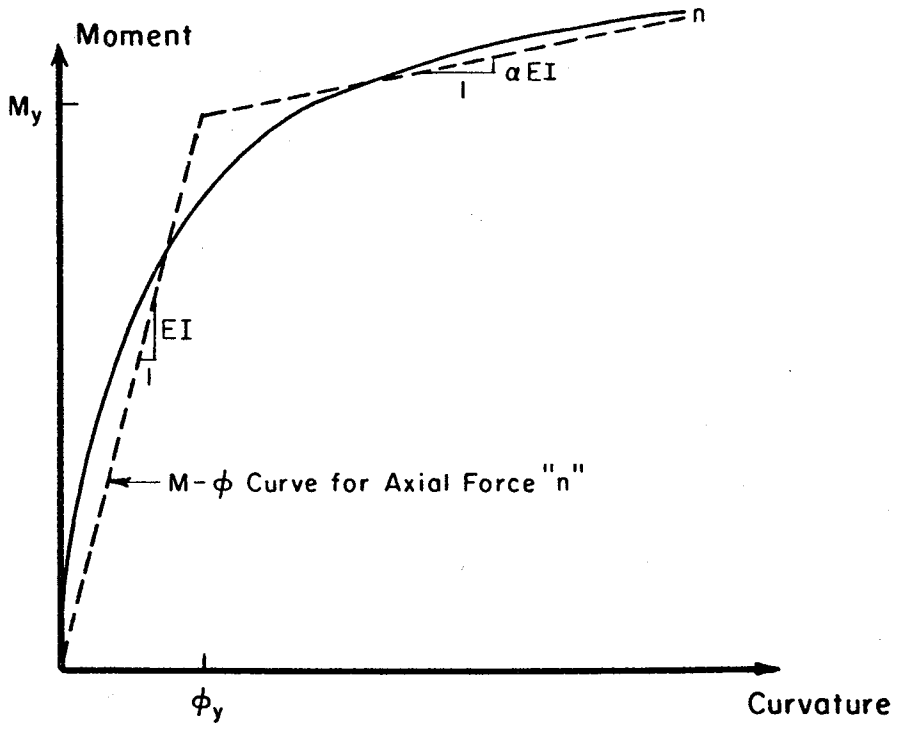

Fig. 2.3 Idealized Moment-Curvature Curve for a Member

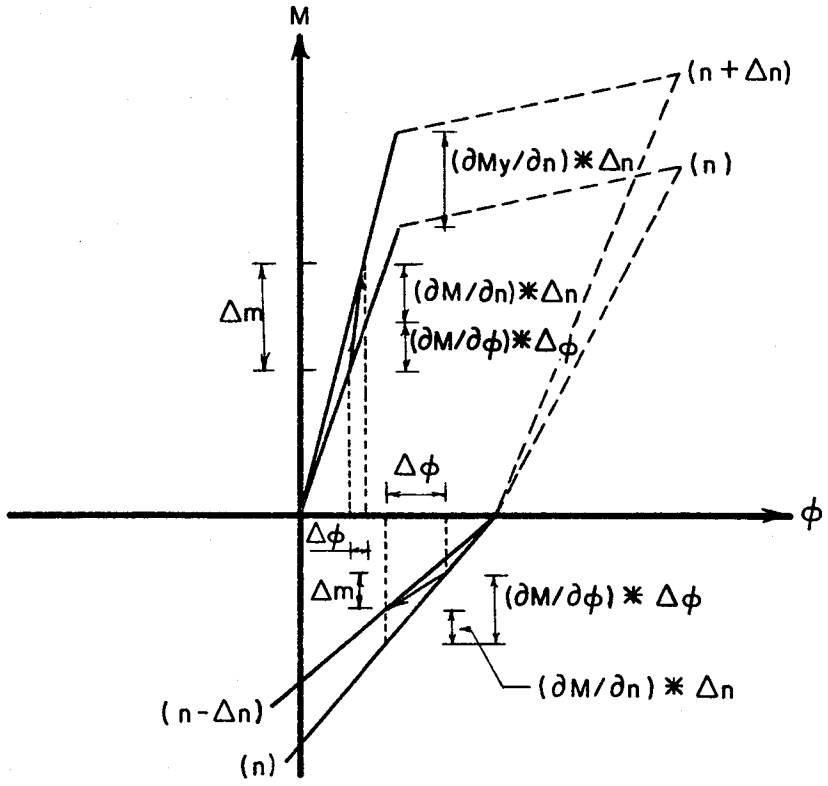

Fig. 2.4 Effect of Axial Force on M-φ Curve

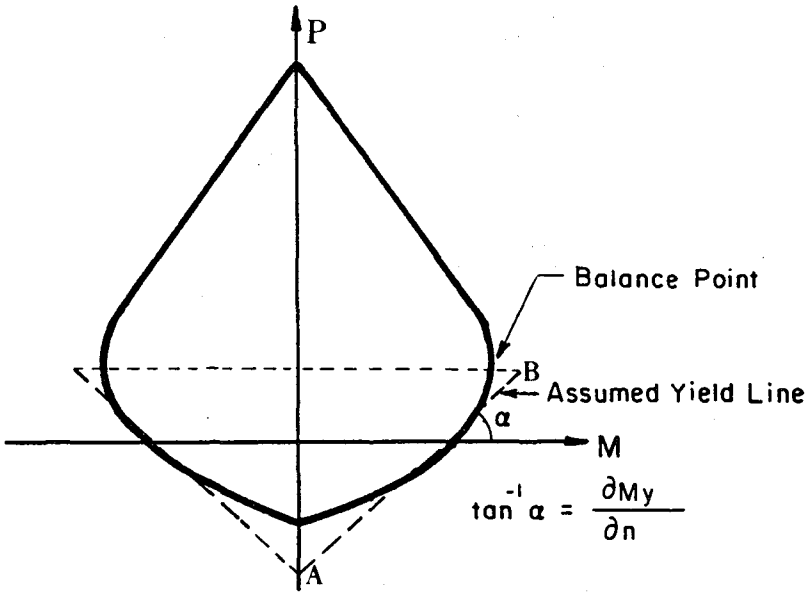

Fig. 2.5 Moment-Axial Force Interaction Diagram

1- End Rotation

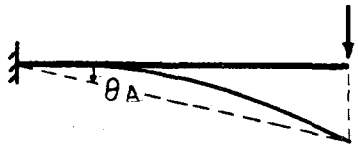

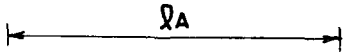

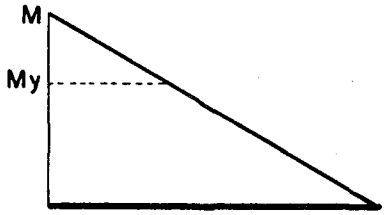

2- Bending Moment Diagram

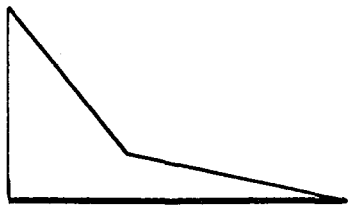

3- Curvature Diagram

Fig. 2.6 Calculation of End Moment-End Rotation Relation for a Cantilever Beam

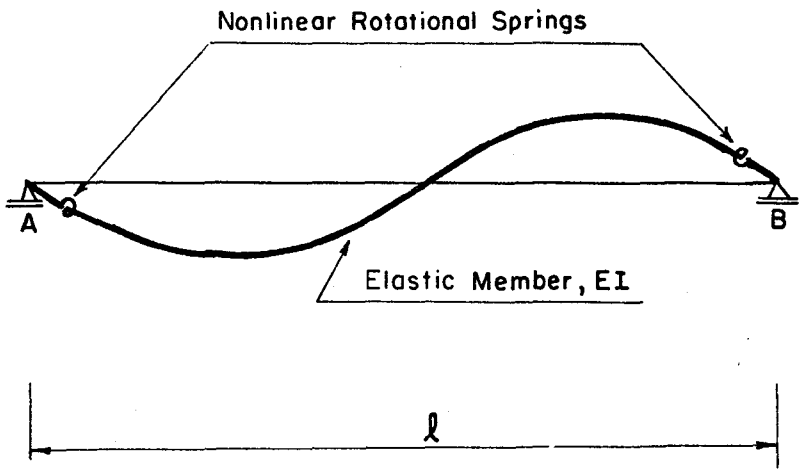

Fig. 2.7 One-Component Model

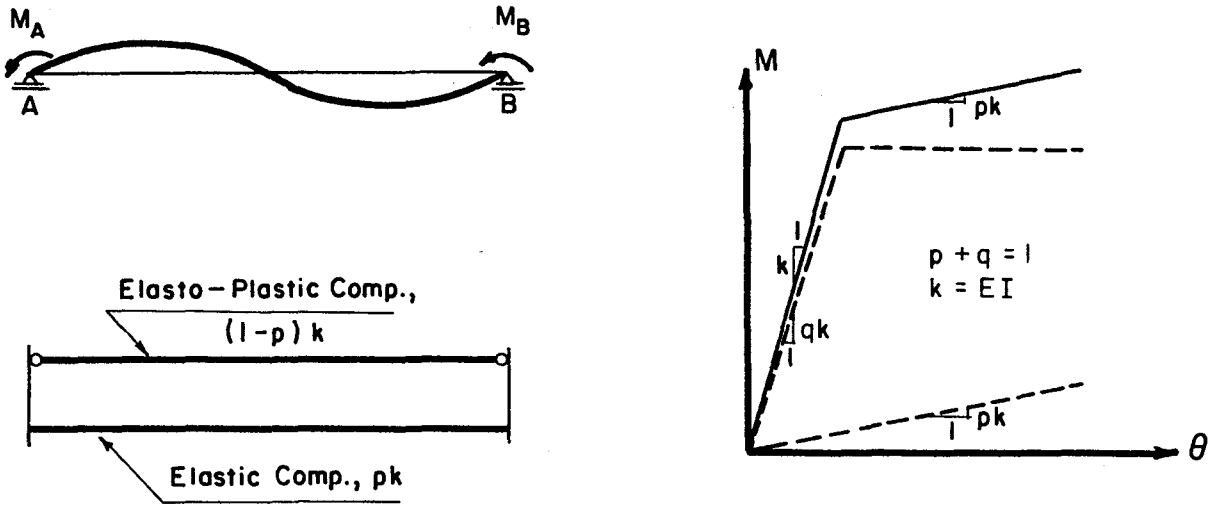

Fig. 2.8 Two-Component Model

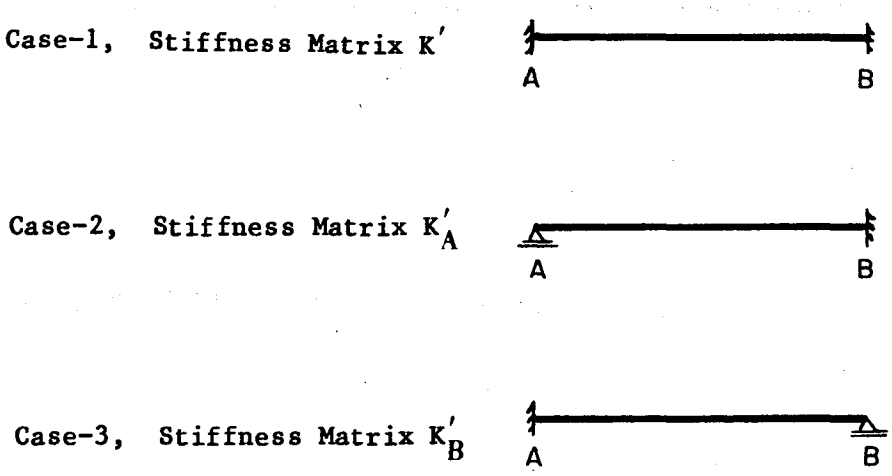

Fig. 2.9 Three Fundamental Cases in Two-Component Model

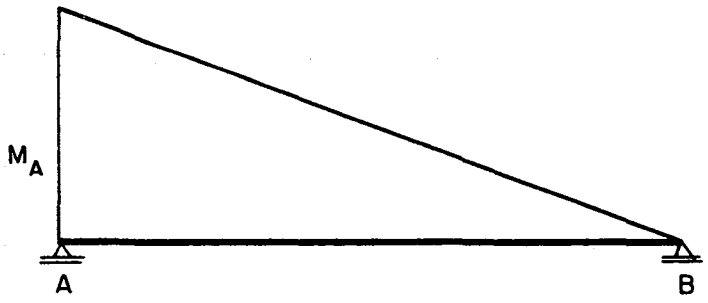

Fig. 2.10 Assumed Loading Condition along a Member

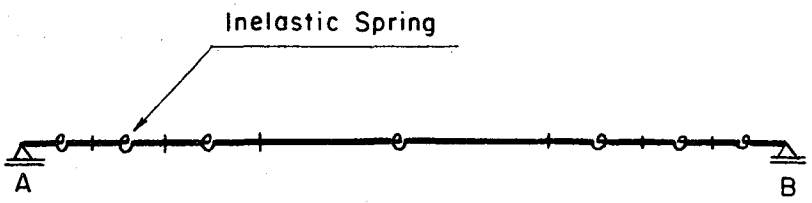

1- Element Model

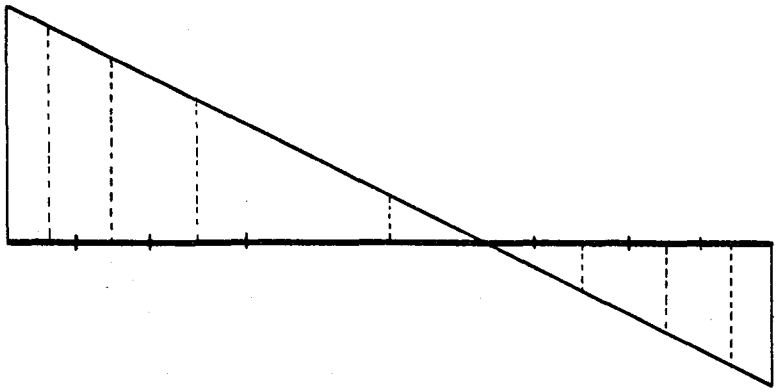

2- Bending Moment Diagram

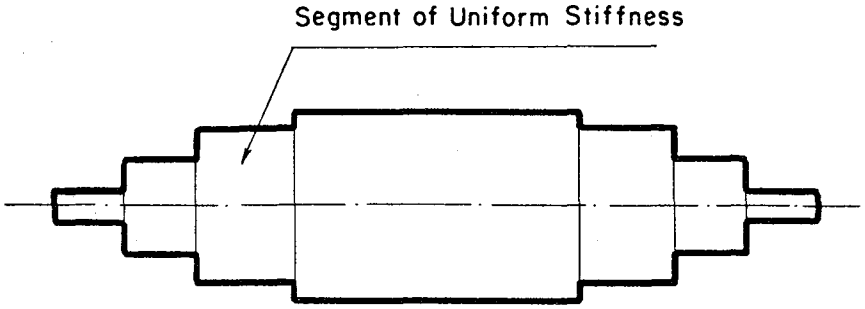

3- Section Stiffness Distribution

Fig. 2.11 Multiple Spring Model

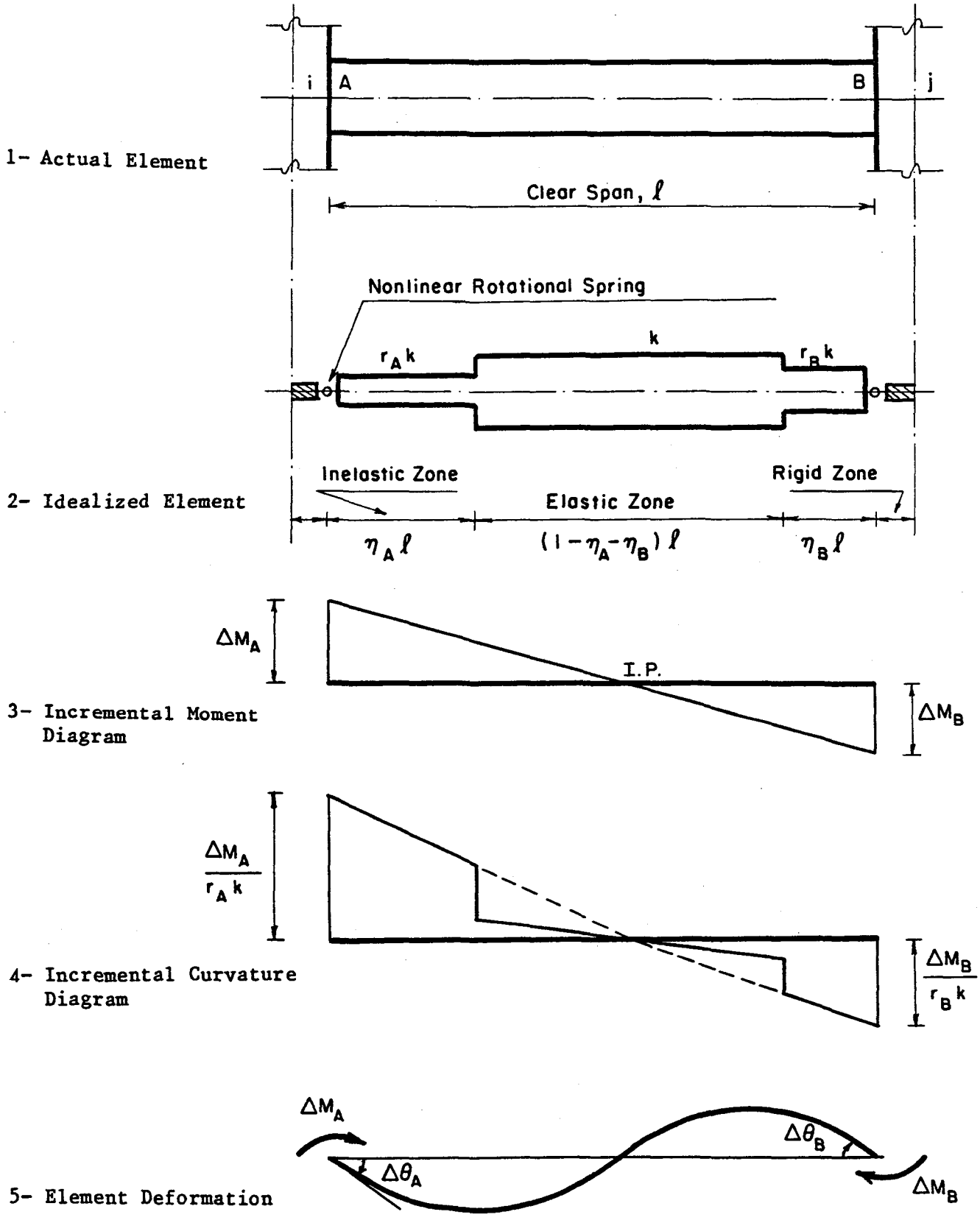

Fig. 2.12 Proposed Model

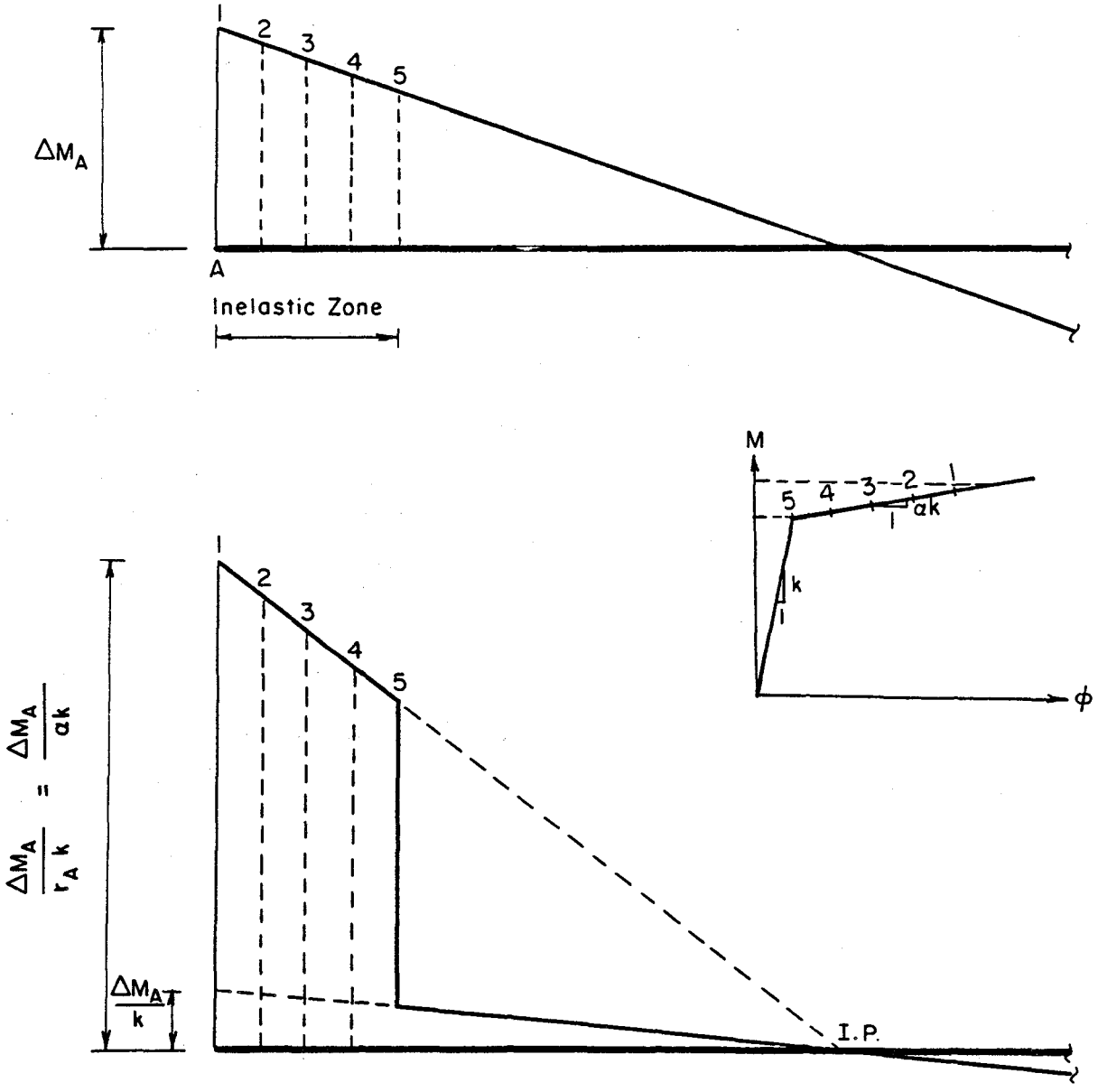

Fig. 2.13 Incremental Curvature Distribution, Strain-Hardening Range

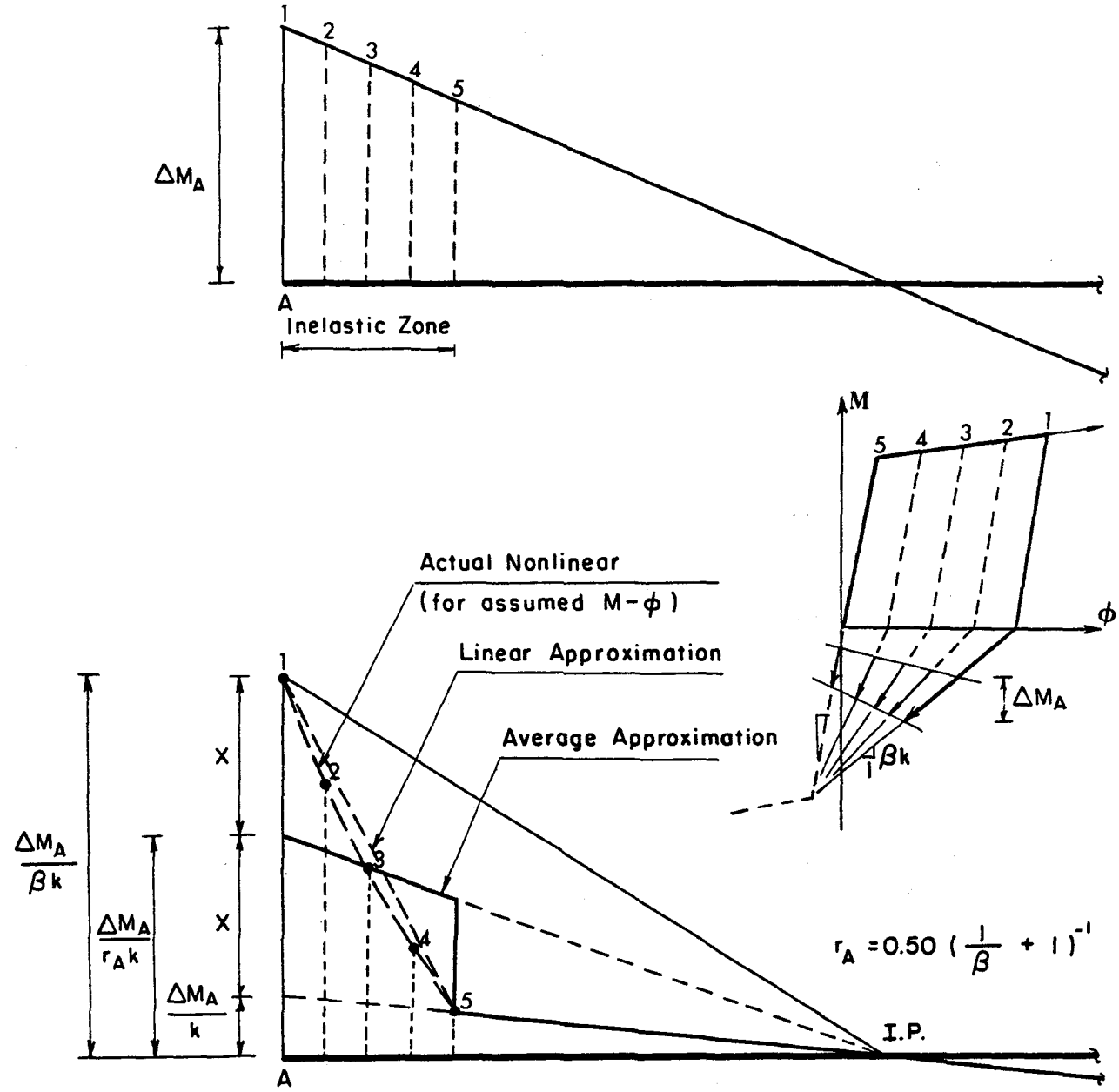

Fig. 2.14 Incremental Curvature Distribution, Reloading Range

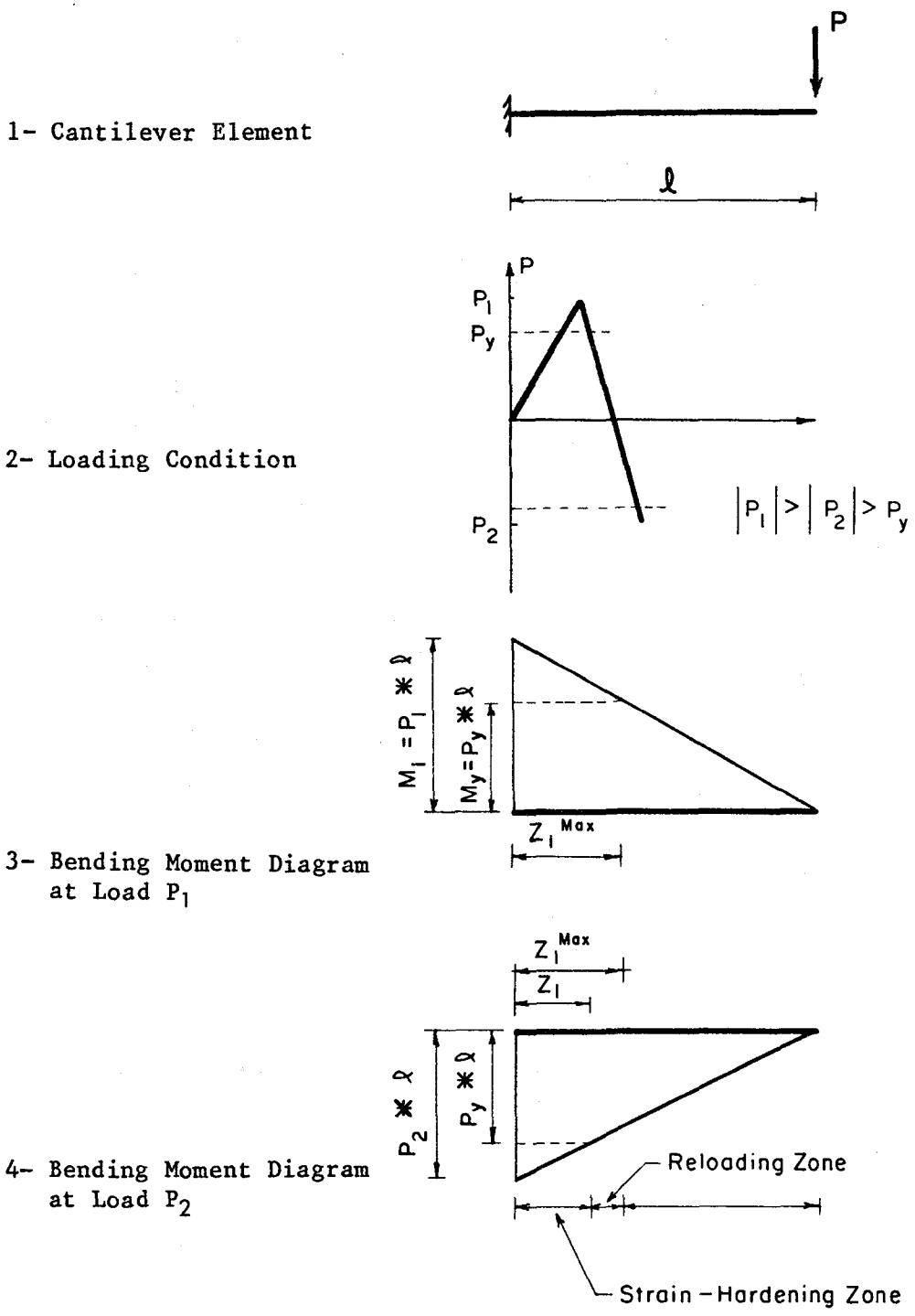

Fig. 2.15 Inelastic Zone Length Discrepancy due to the Different Actions

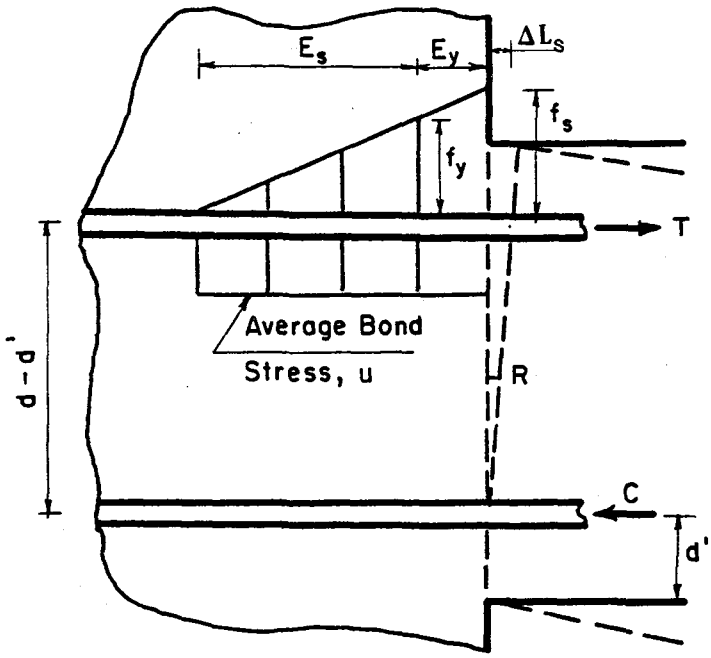

Fig. 2.16 Rotation due to Bond Slip

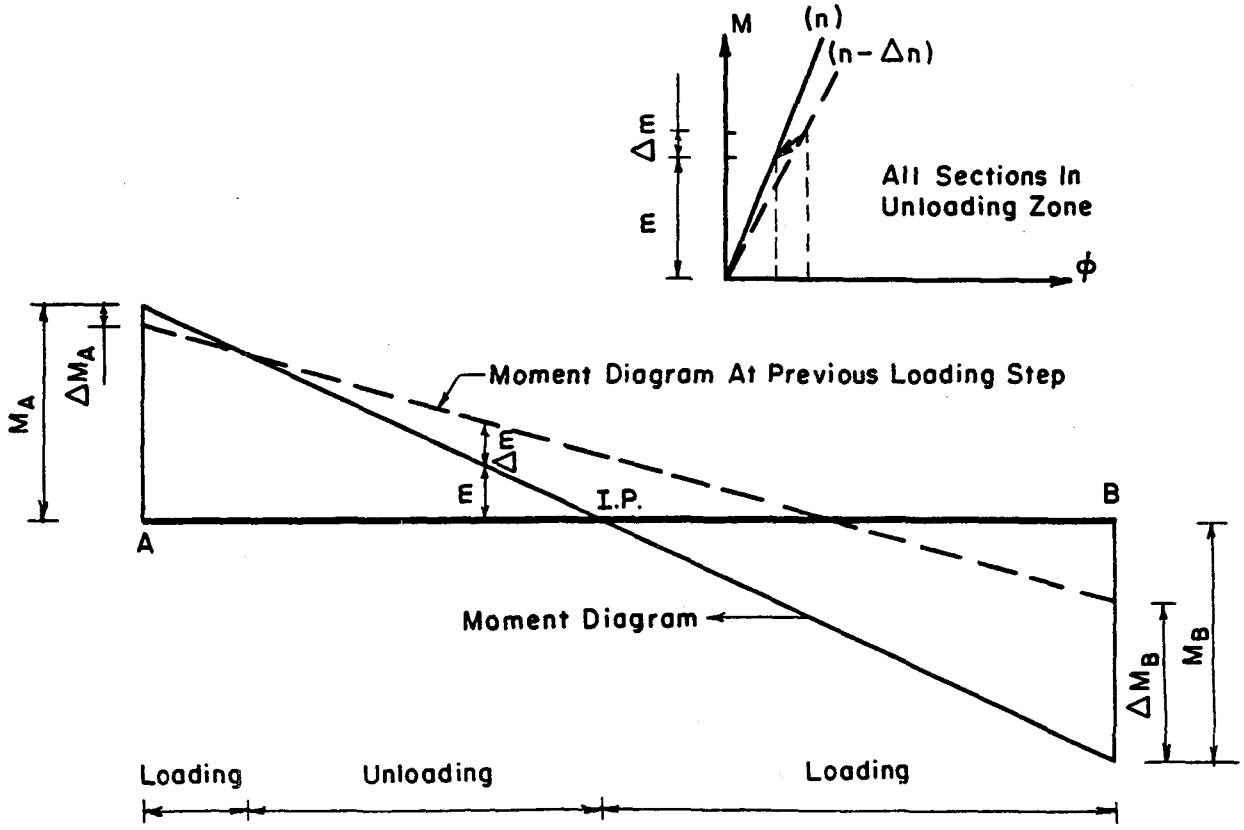

Fig. 2.17 Section Stiffness Discrepancy due to the Shifting of the Inflection Point

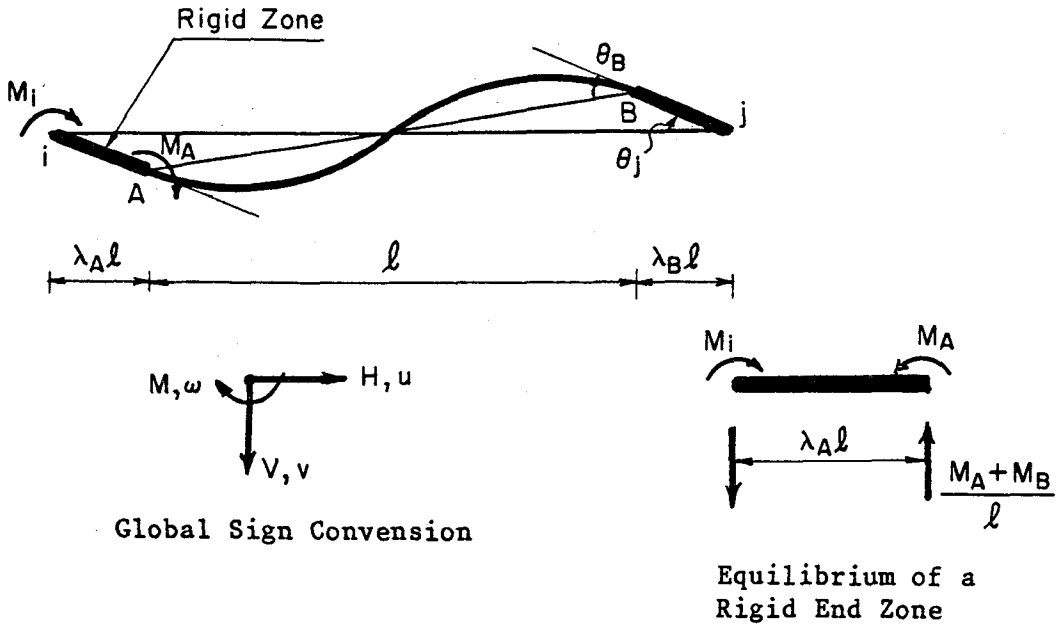

Global Sign Convension

Equilibrium of a Rigid End Zone

Fig. 3.1 Treatment of Rigid End Zone

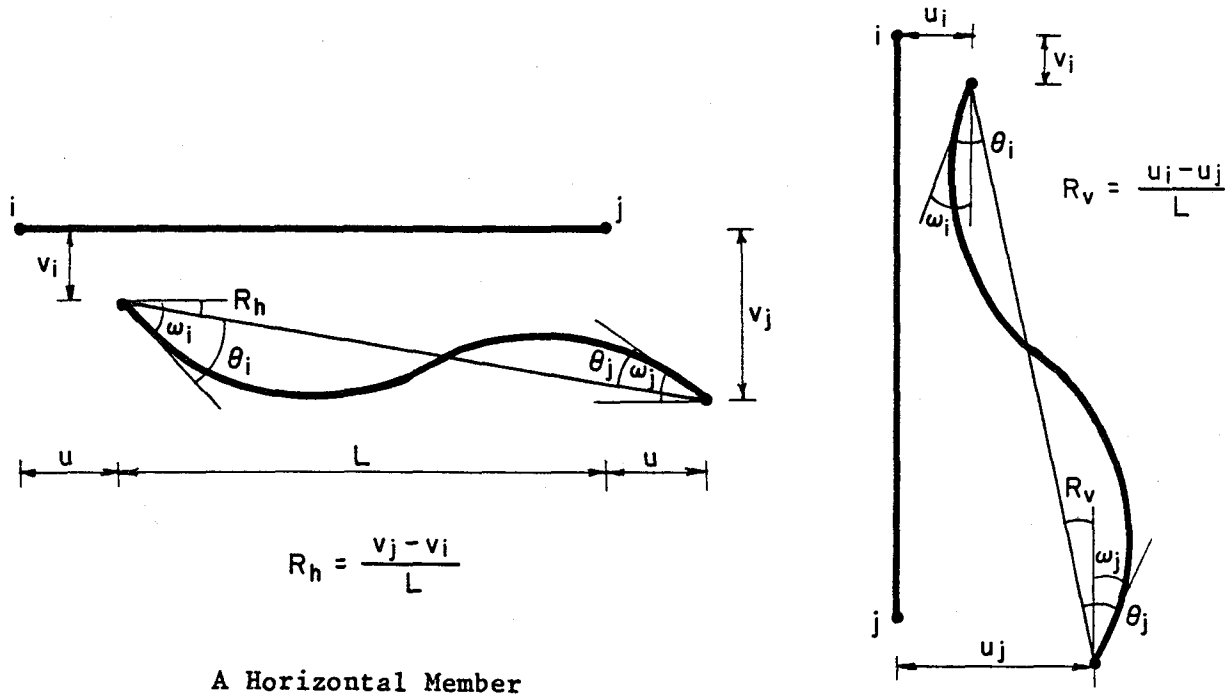

A Horizontal Member

A Vertical Member

Fig. 3.2 Typical Members in Global Coordinates System

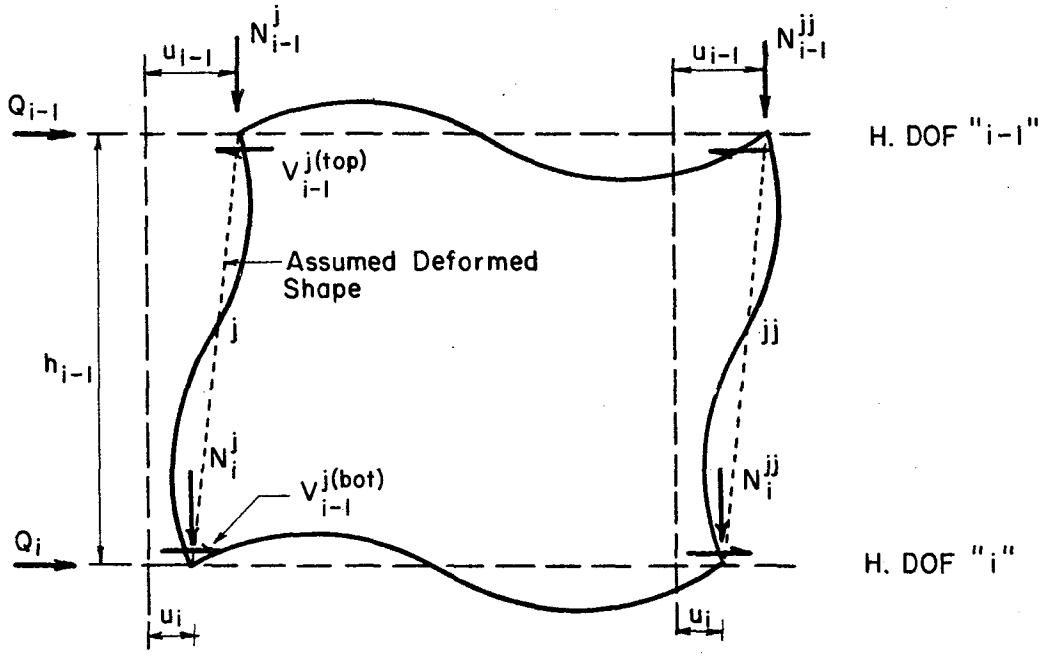

Fig. 3.3 Equivalent Lateral Load to Account for Gravity Effect

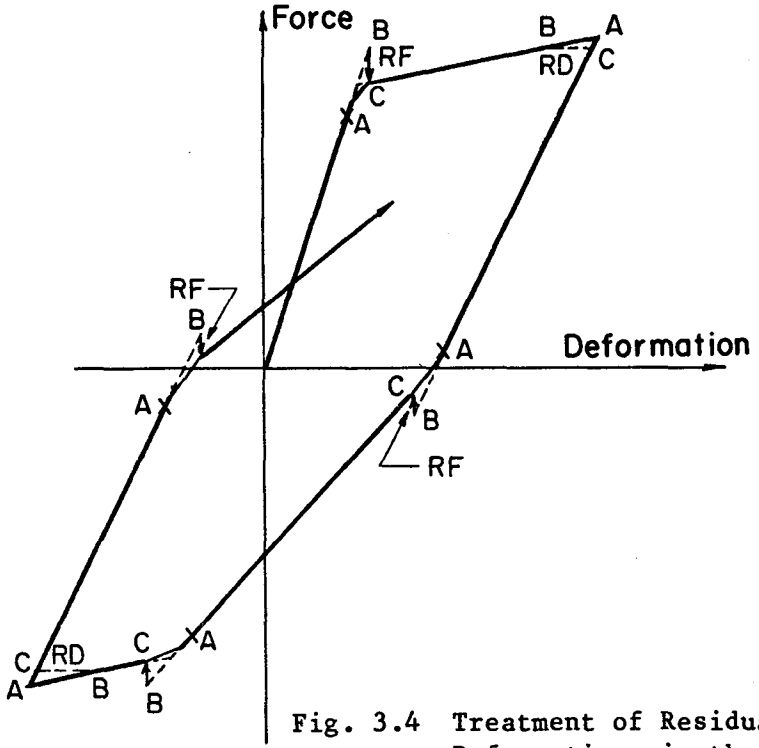

F_A : Force at the Beginning of Loading Step

F_B : Force at the End of Loading Step

F_C : Corrected Force

RF : Residual Force

RD : Residual Deformation

Fig. 3.4 Treatment of Residual Forces and Deformations in the Analysis

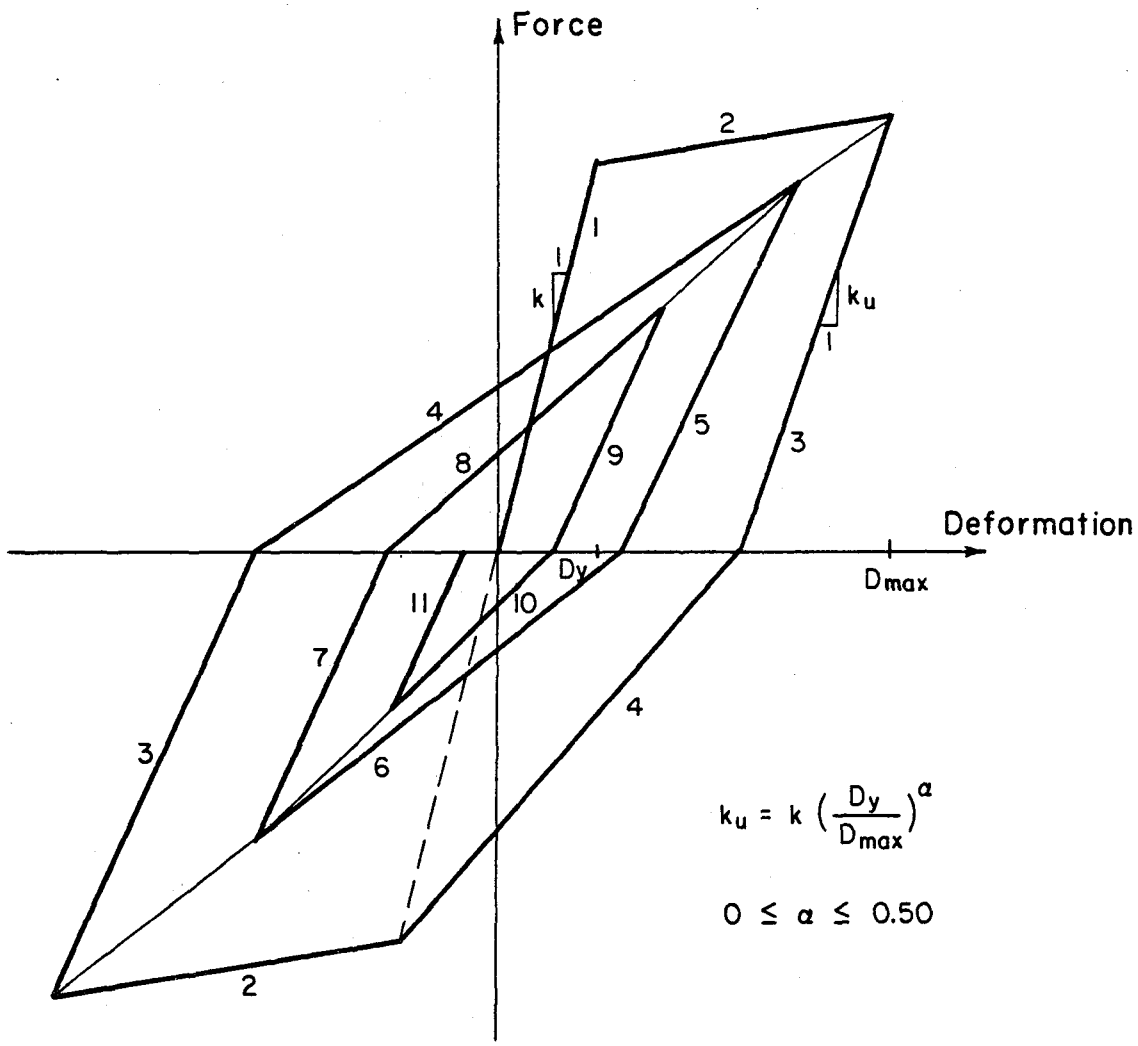

Fig. 4.1 Hysteresis-1, Takeda Hysteresis Model

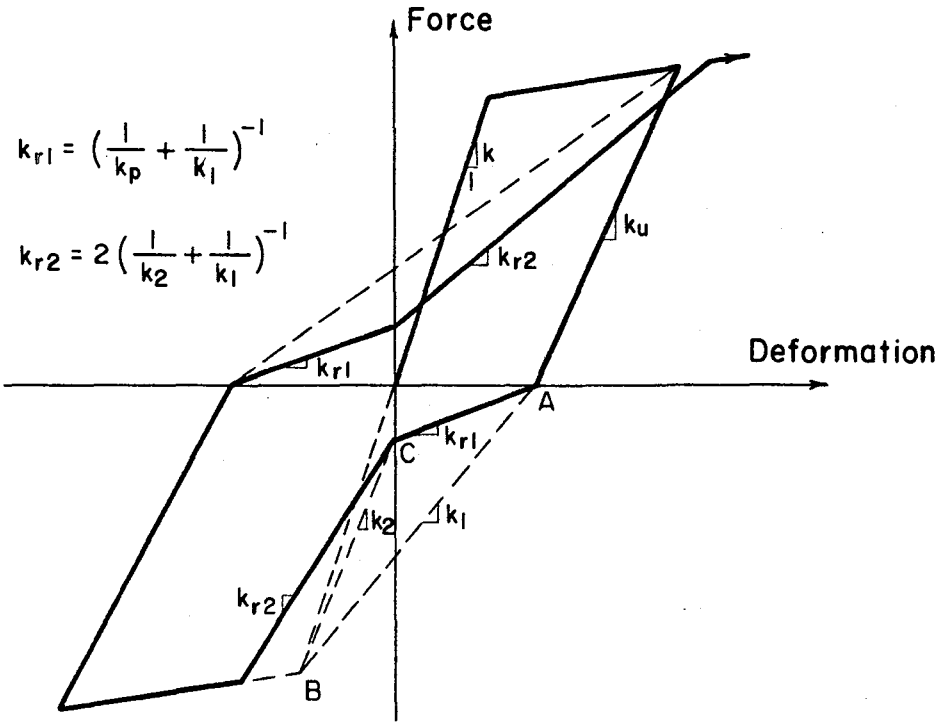

Fig. 4.2 Hysteresis-2, Hysteresis Model with Effects of Pinching Action

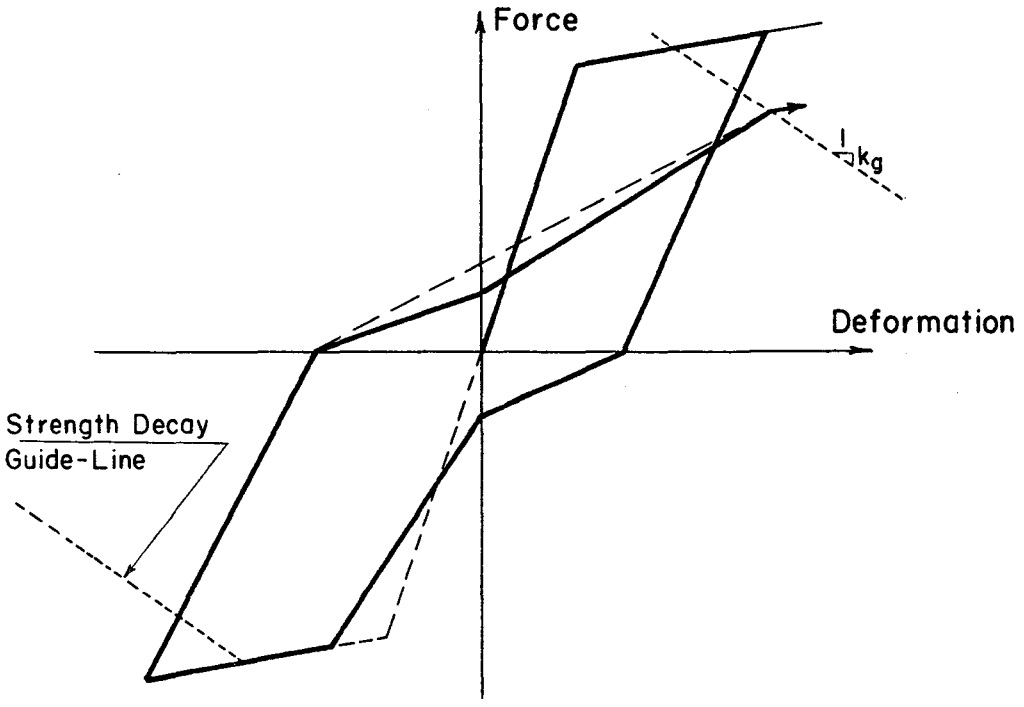

Fig. 4.3 Hysteresis-2, Hysteresis Model with Effects of Pinching Action and Strength Decay

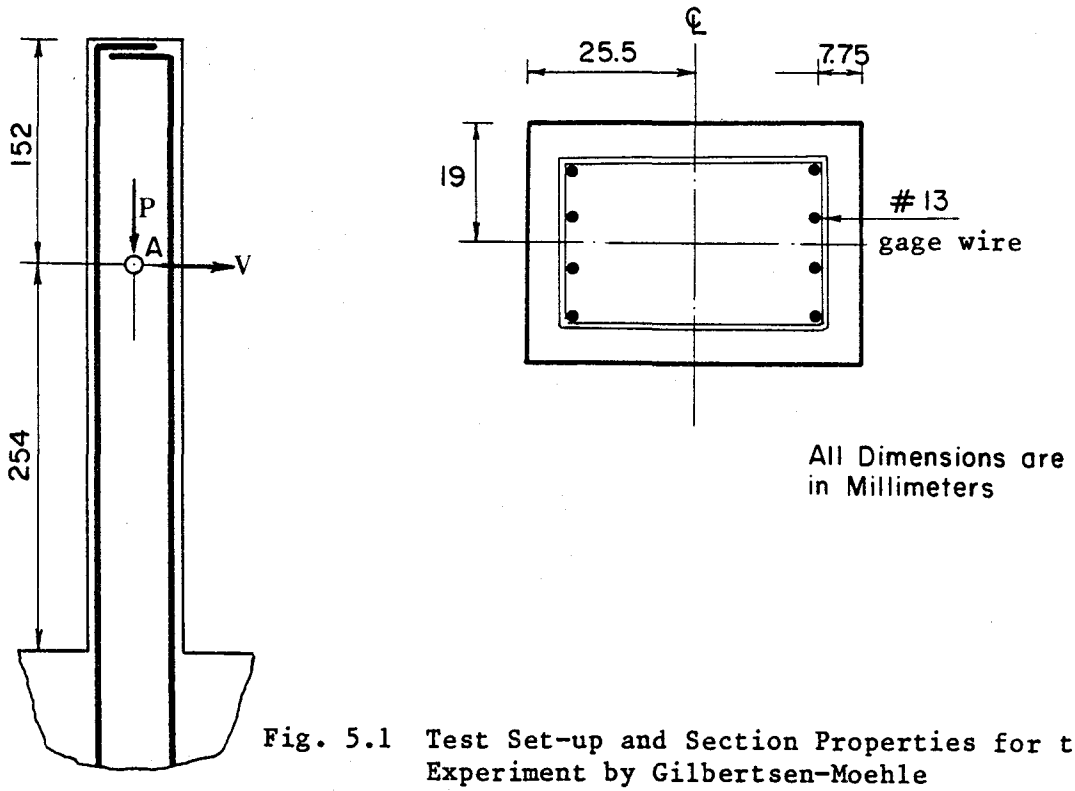

Fig. 5.1 Test Set-up and Section Properties for the Experiment by Gilbertsen-Moehle

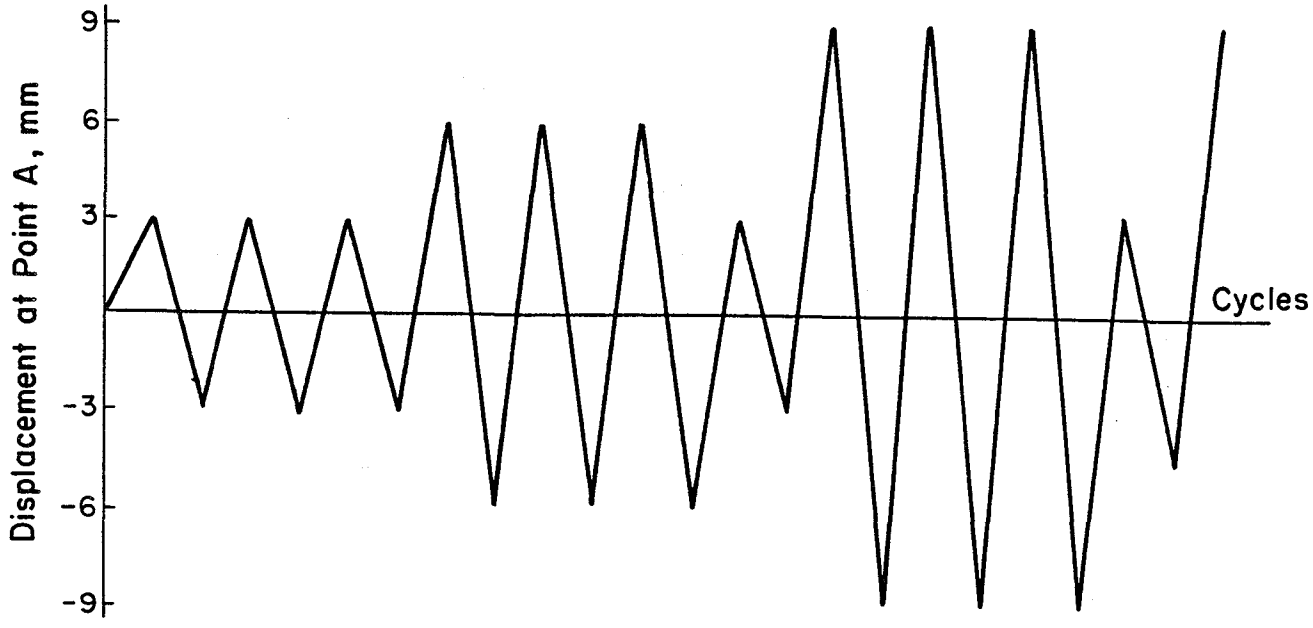

Fig. 5.2 Displacement Pattern for the Experiment by Gilbertsen-Moehle

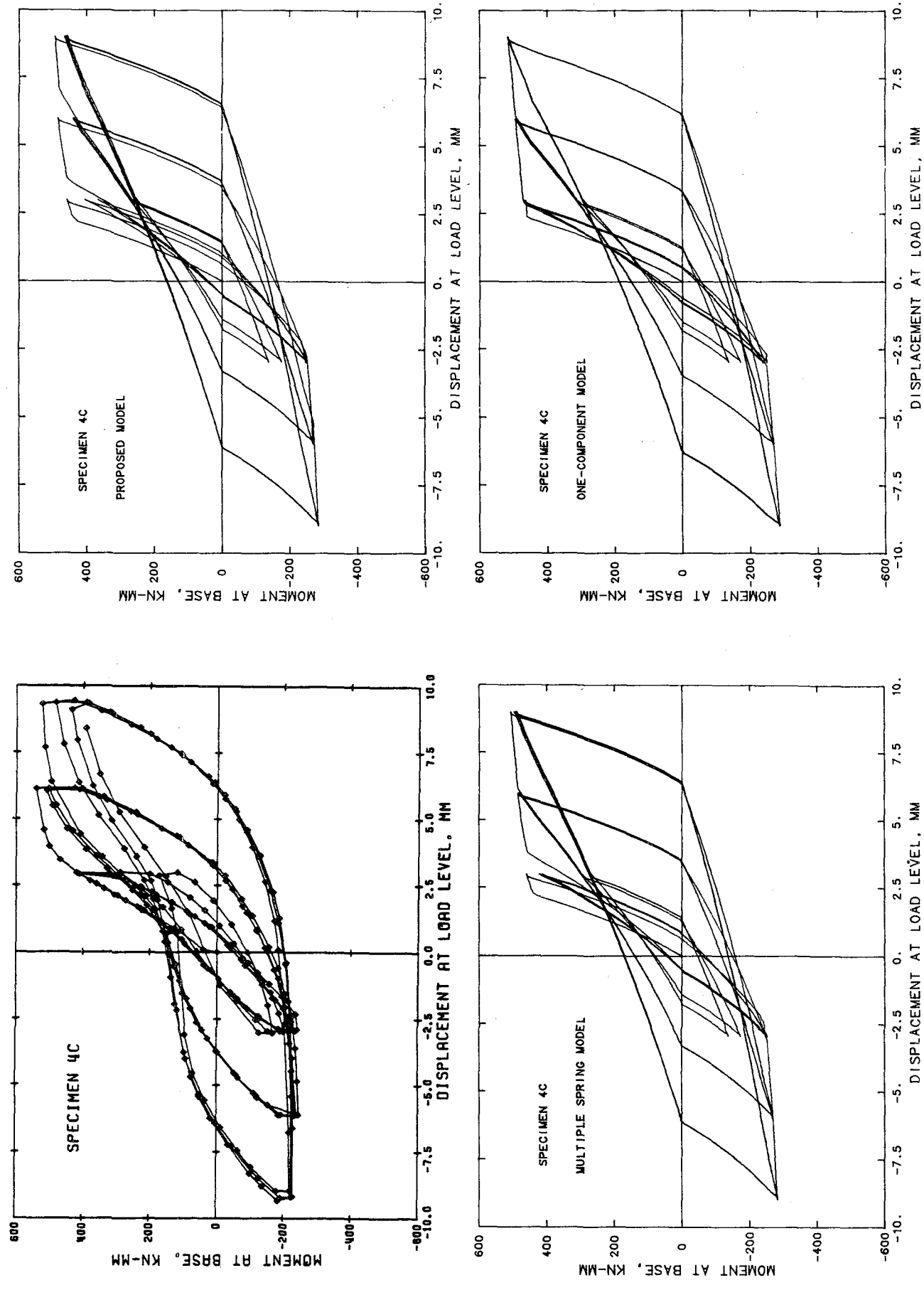

Fig. 5.3 Experimental and Analytical Force-Displacement Curves for Specimen 4C

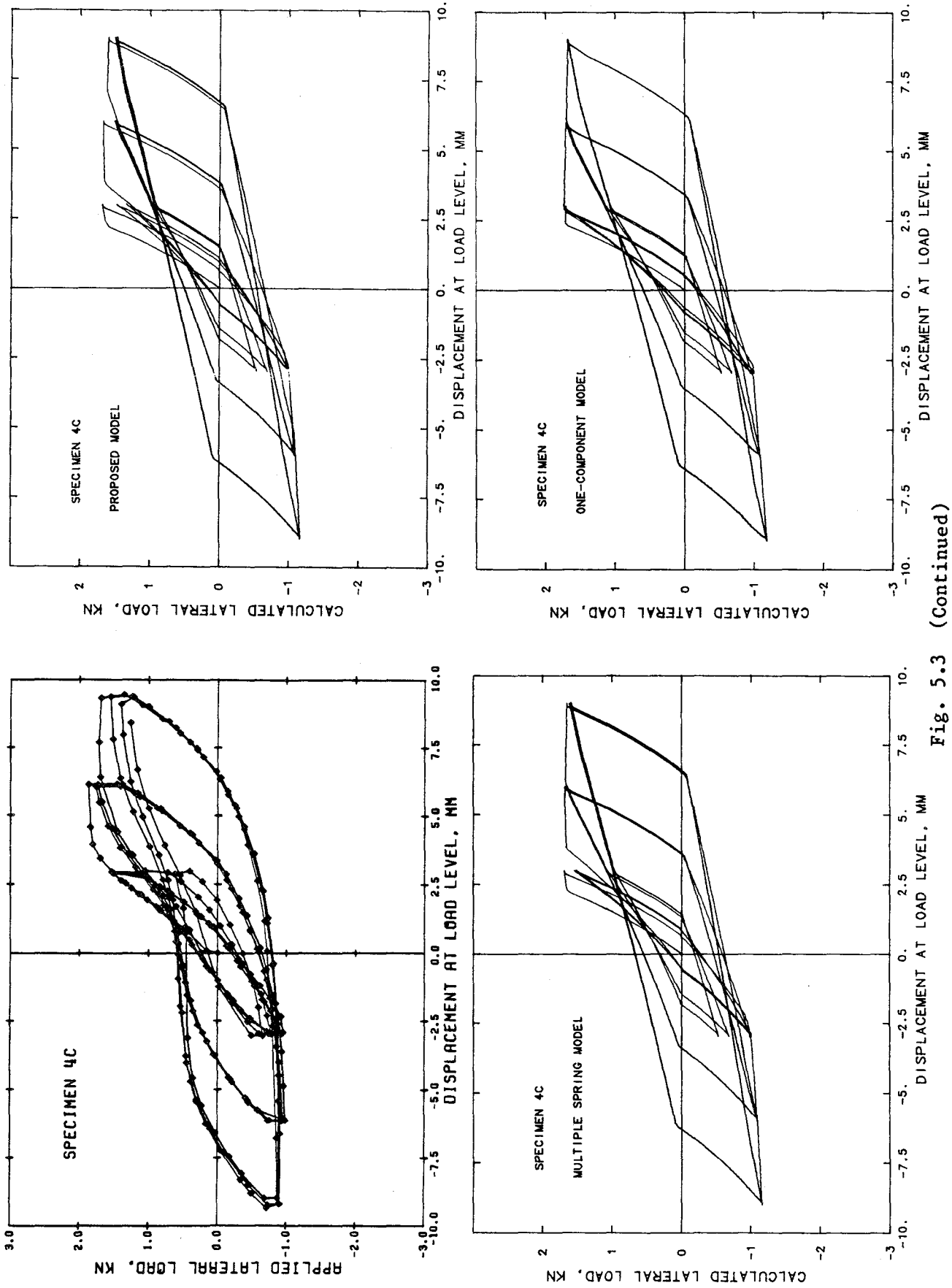

Fig. 5.3 (Continued)

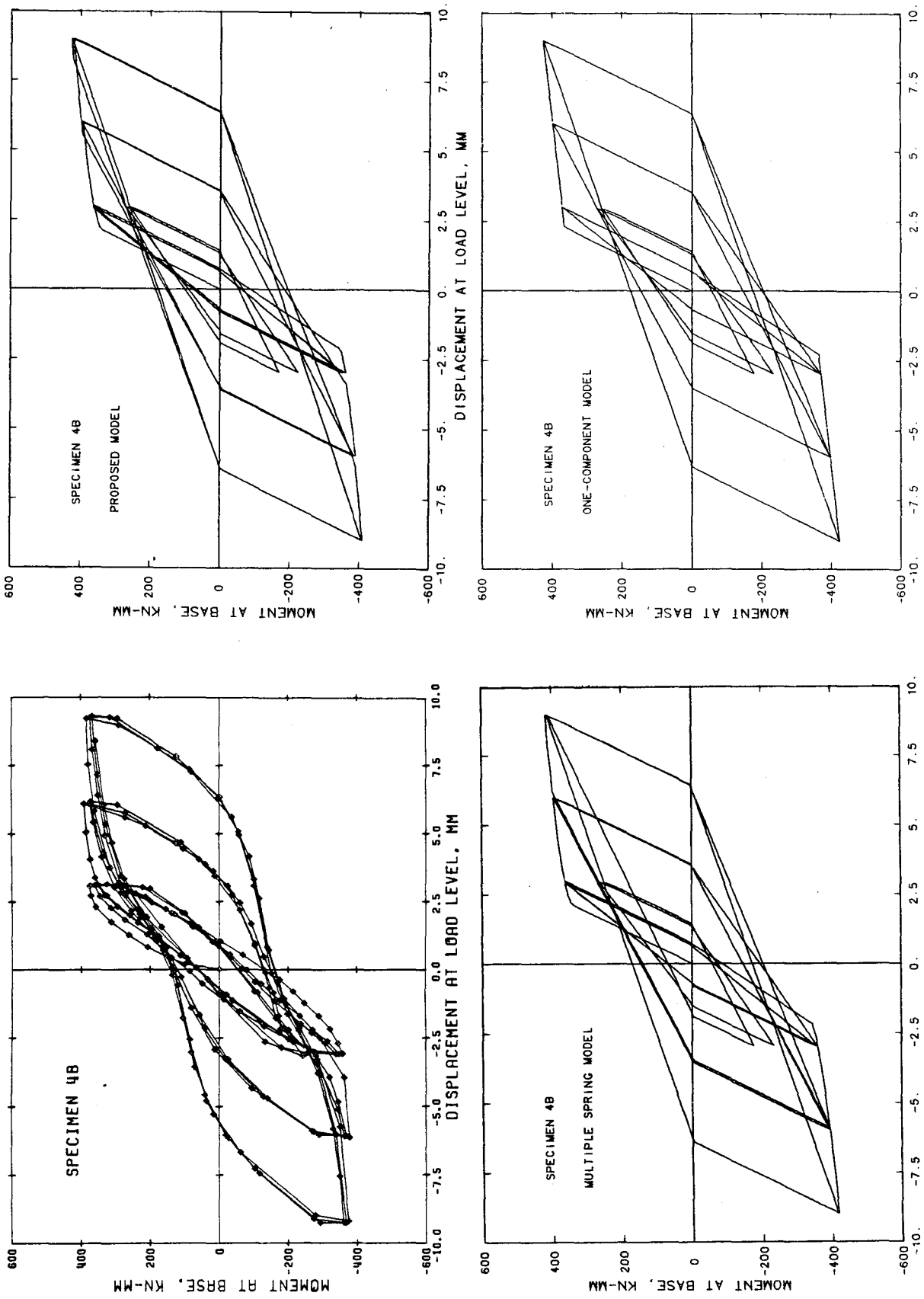

Fig. 5.4 Experimental and Analytical Force-Displacement Curves for Specimen 4B

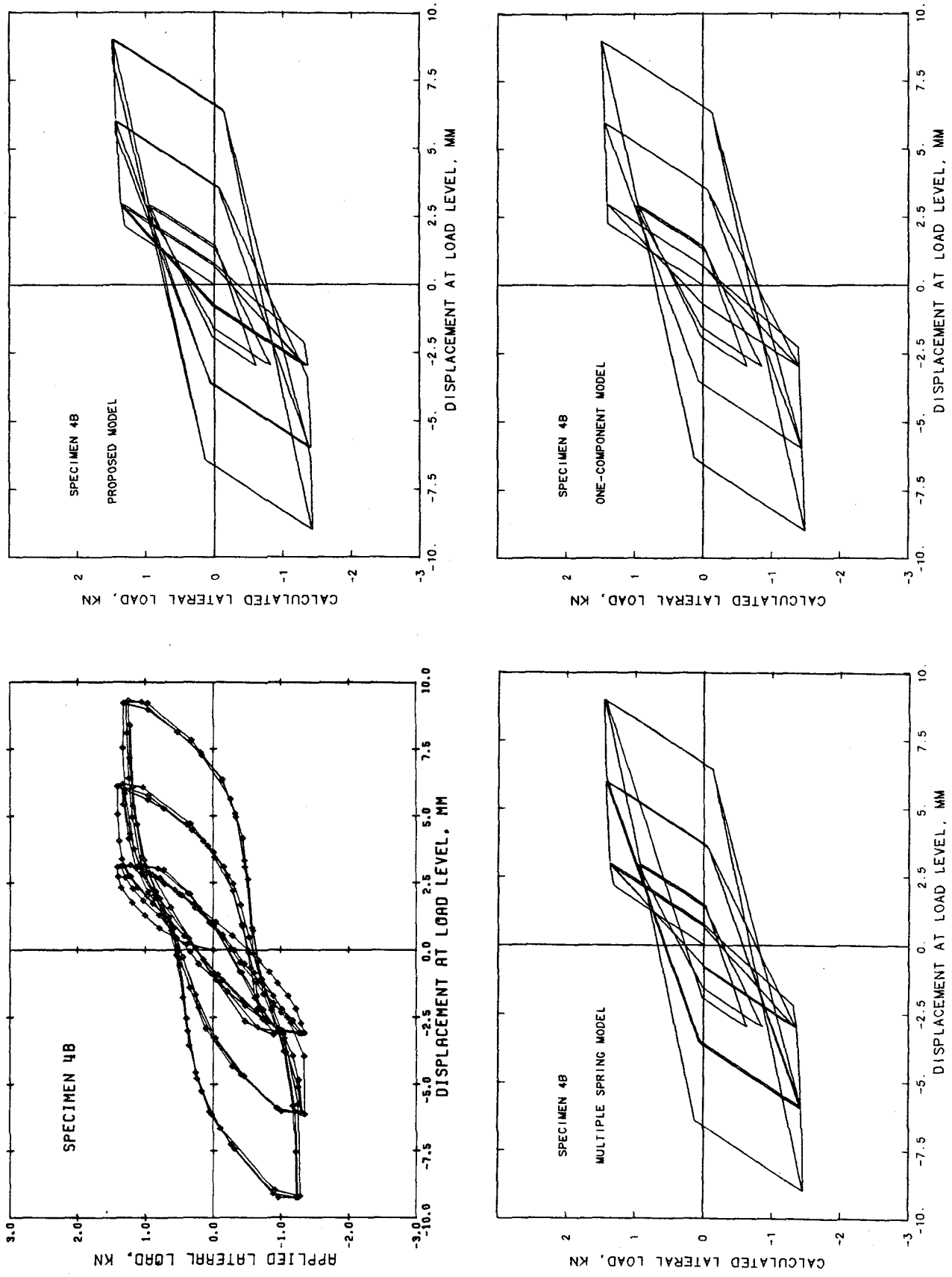

Fig. 5.4 (Continued)

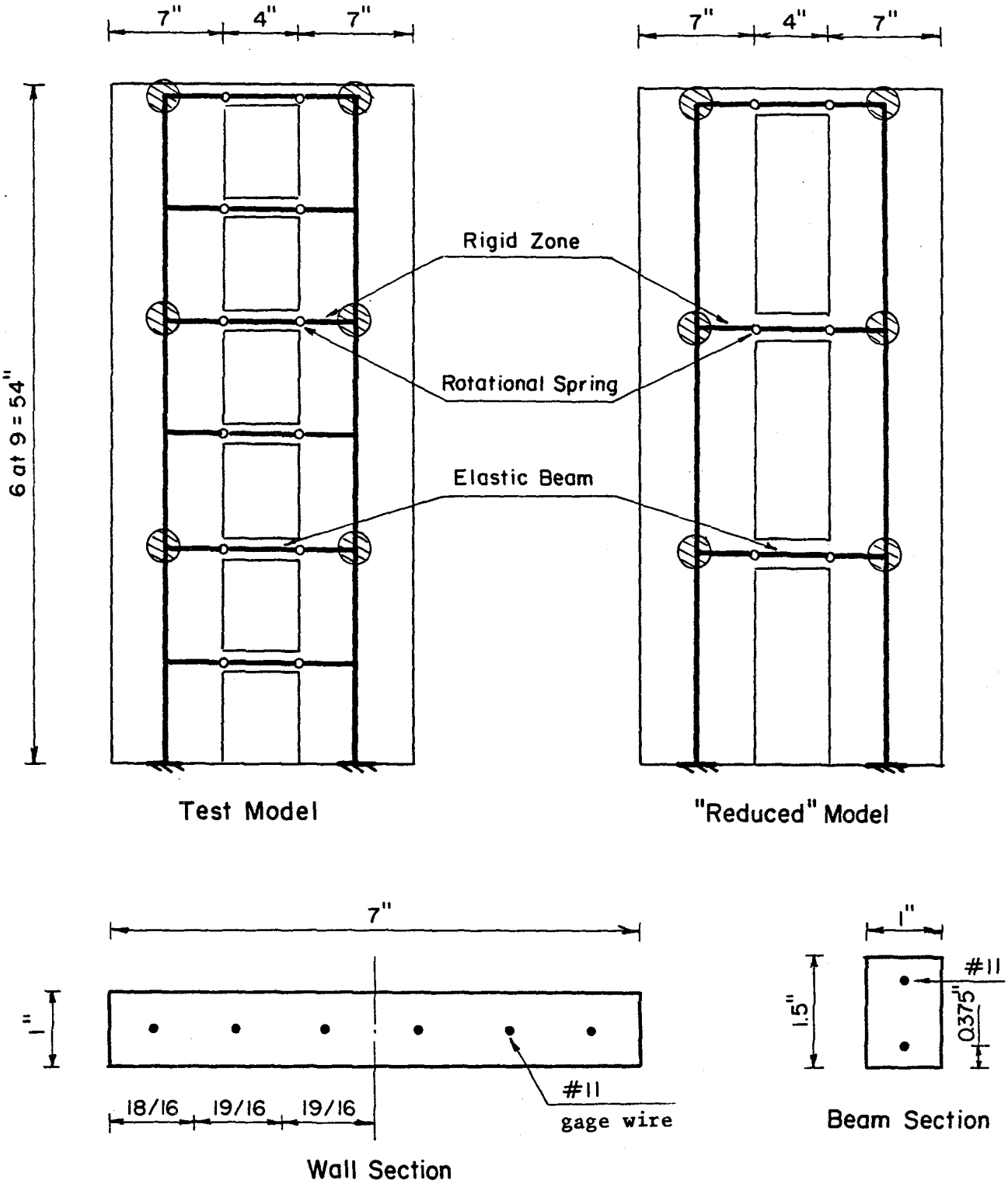

Fig. 5.5 Analytical Models and Section Properties of 6-Story Coupled Shear Wall

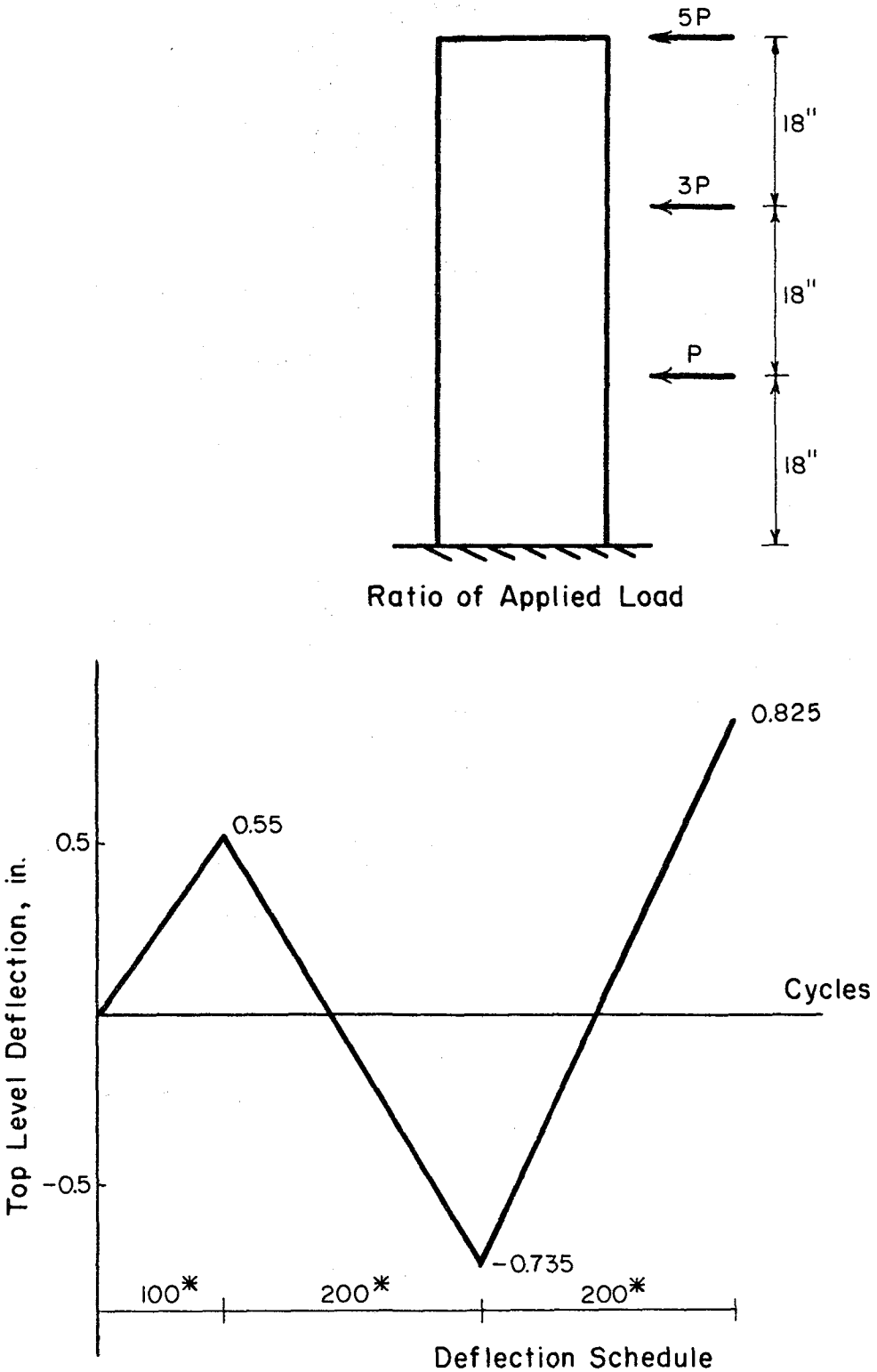

(*) Number Indicating Number of Steps in the Static Analysis

Fig. 5.6 Static Analysis, Loading Information

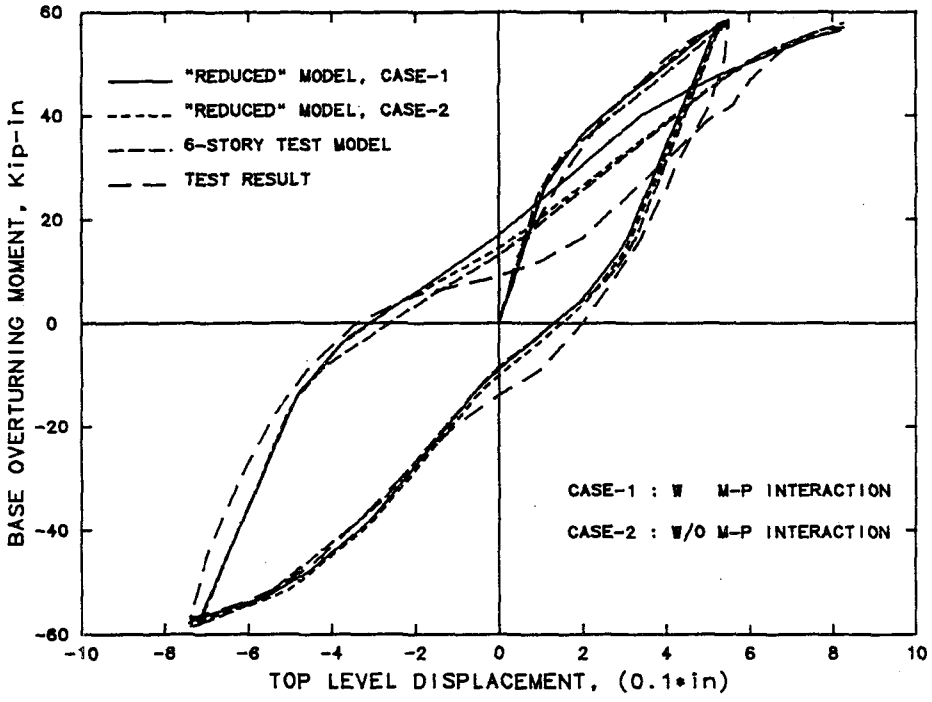

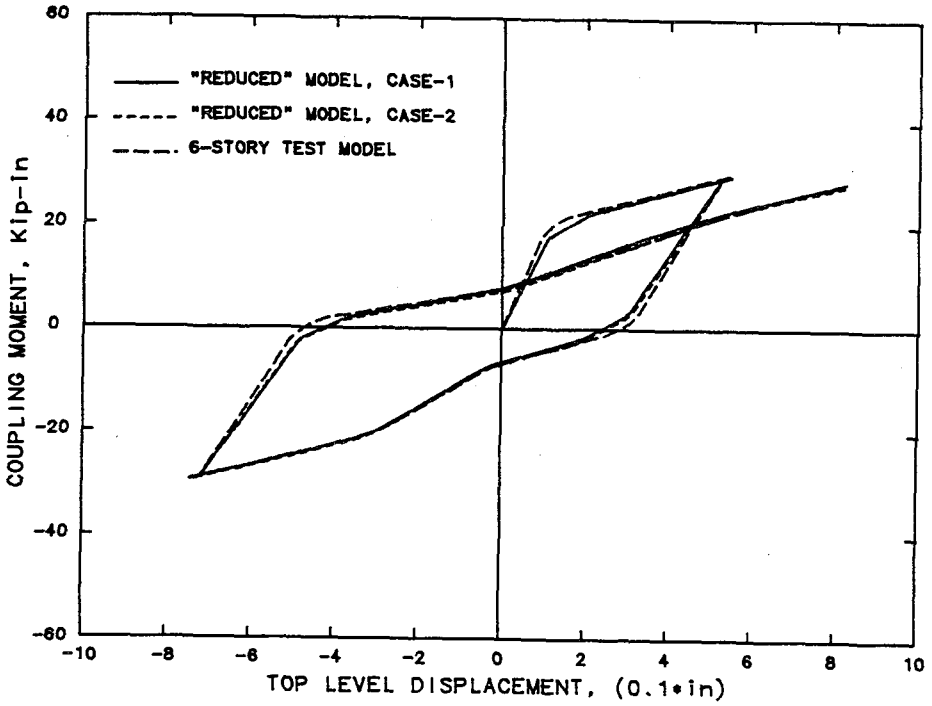

Fig. 5.7 Static Analysis of 6-Story Coupled Shear wall

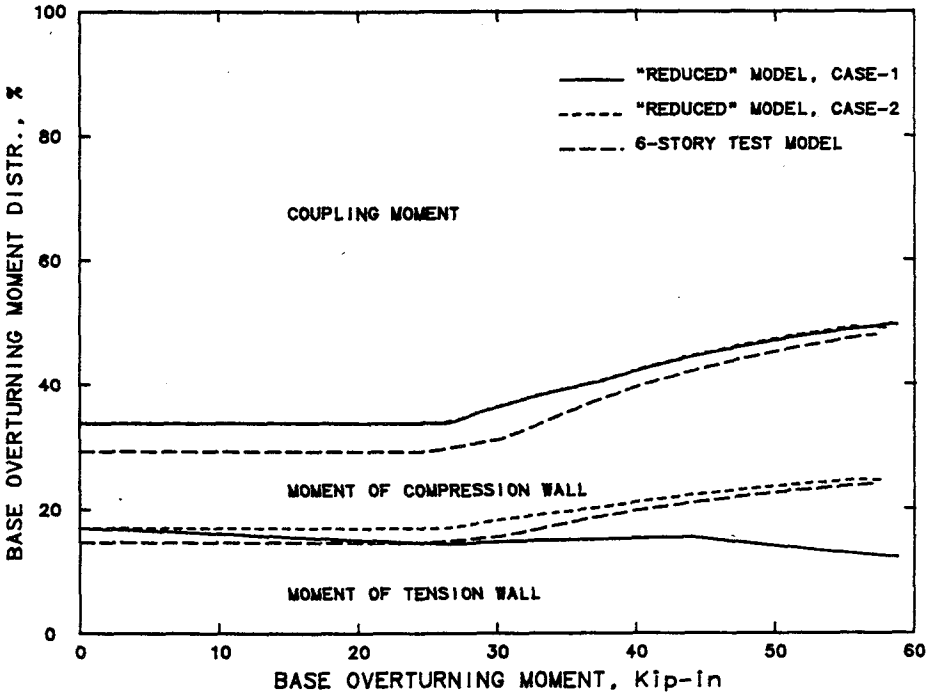

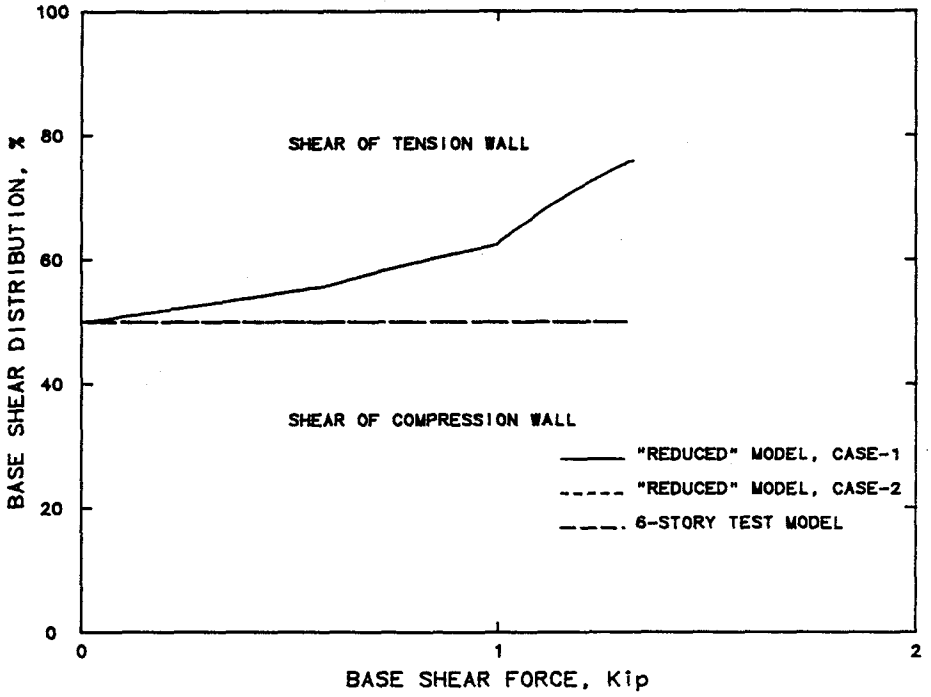

Fig. 5.7 (Continued)

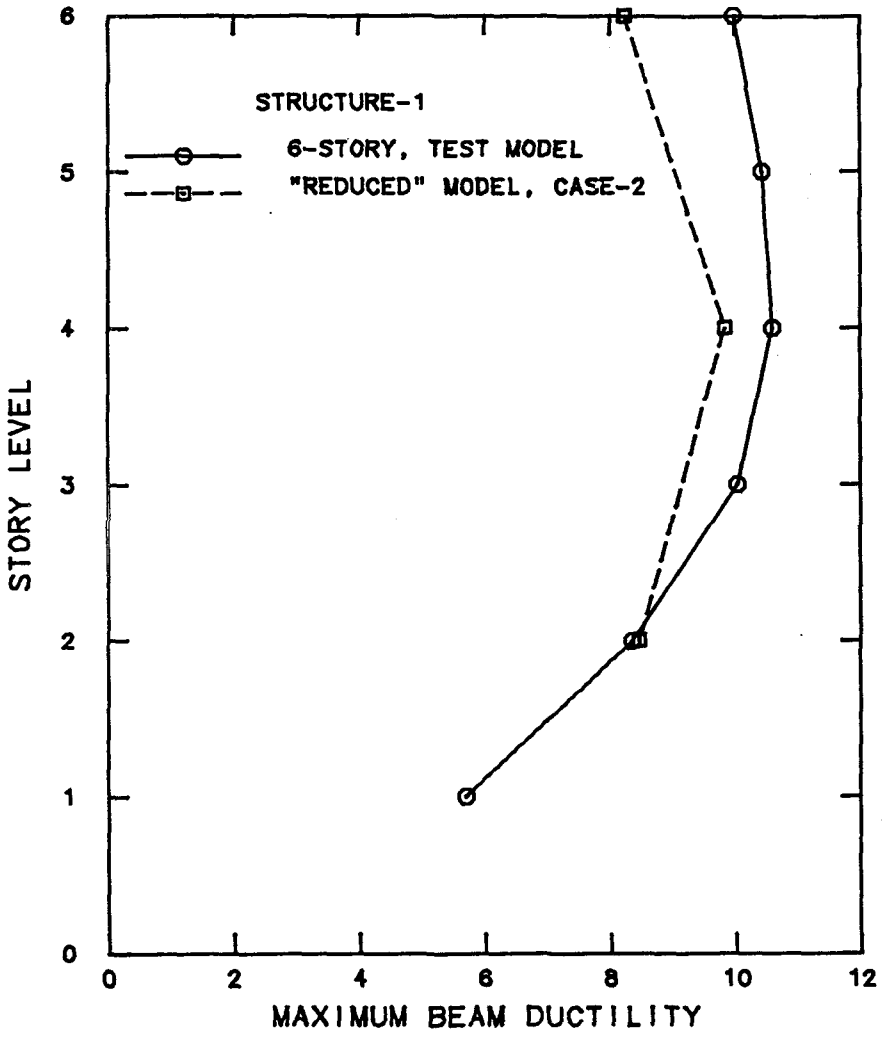

Fig. 5.8 "Reduced" Model Effects, Maximum Beam Ductilities

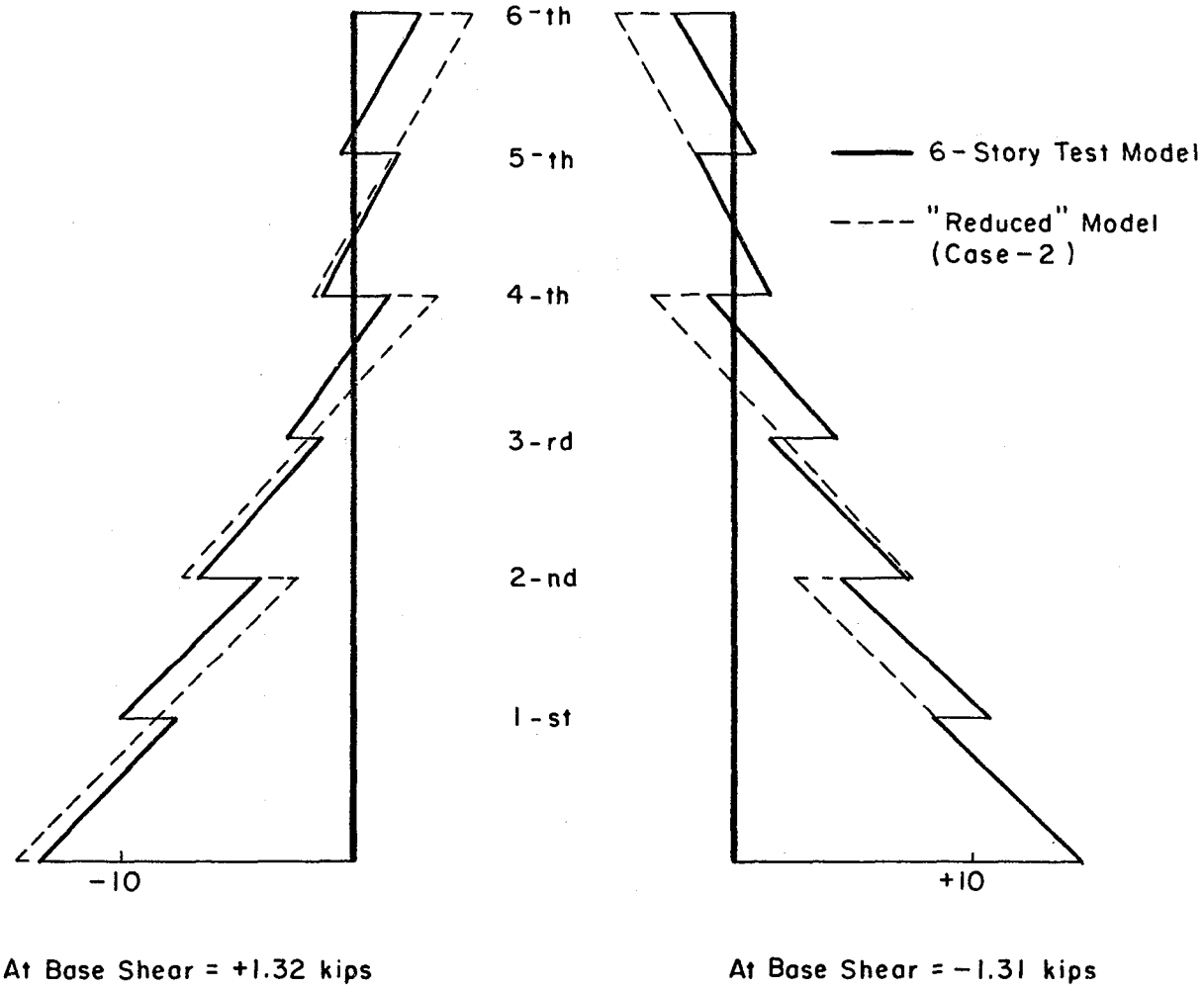

Fig. 5.9 "Reduced" Model Effects, Bending Moments, Kip-in

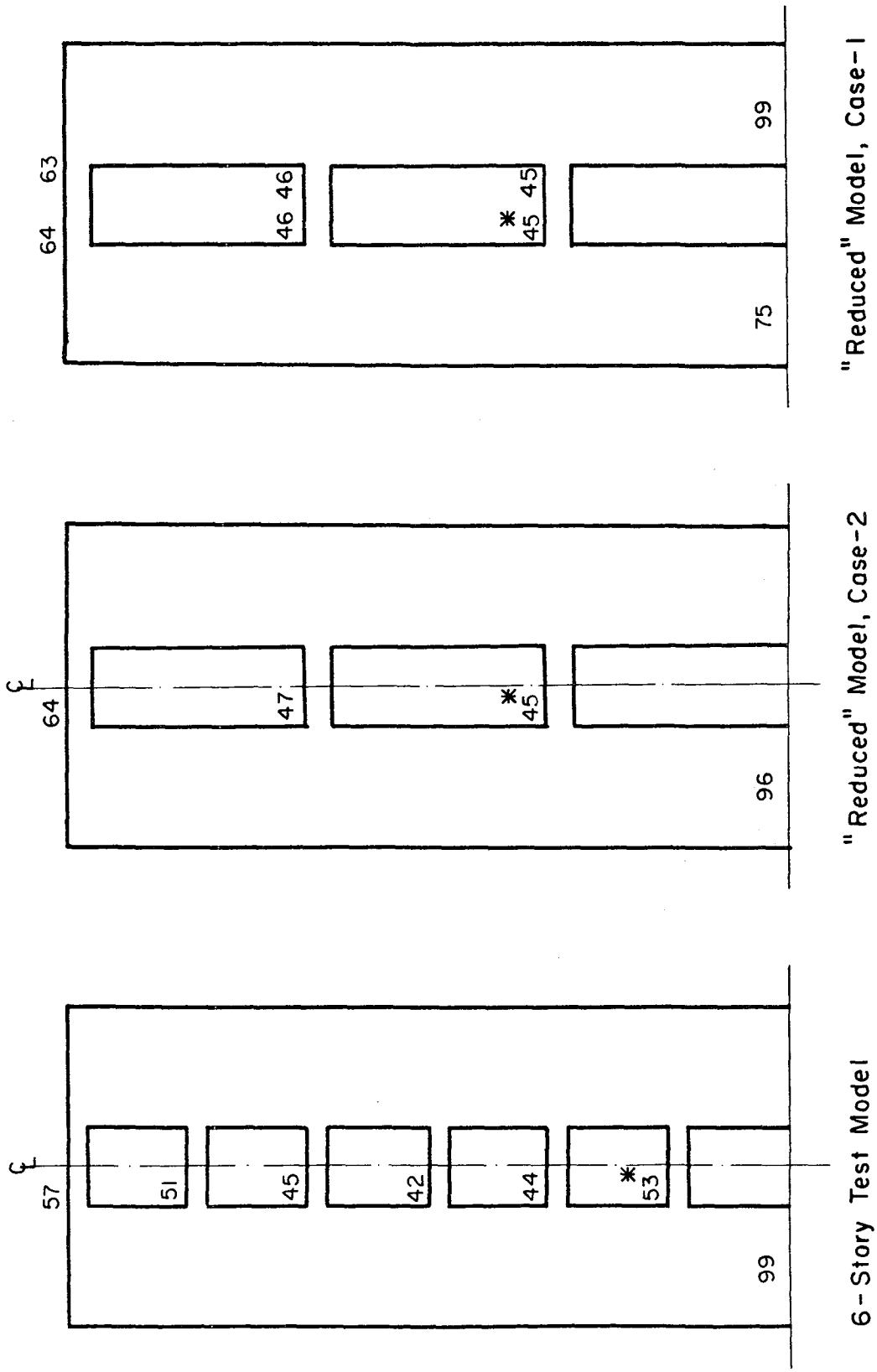

(*) Number Indicating Step Number of Yielding

Fig. 5.10 Order of Yielding of Structure-1 Under Cyclic Loading

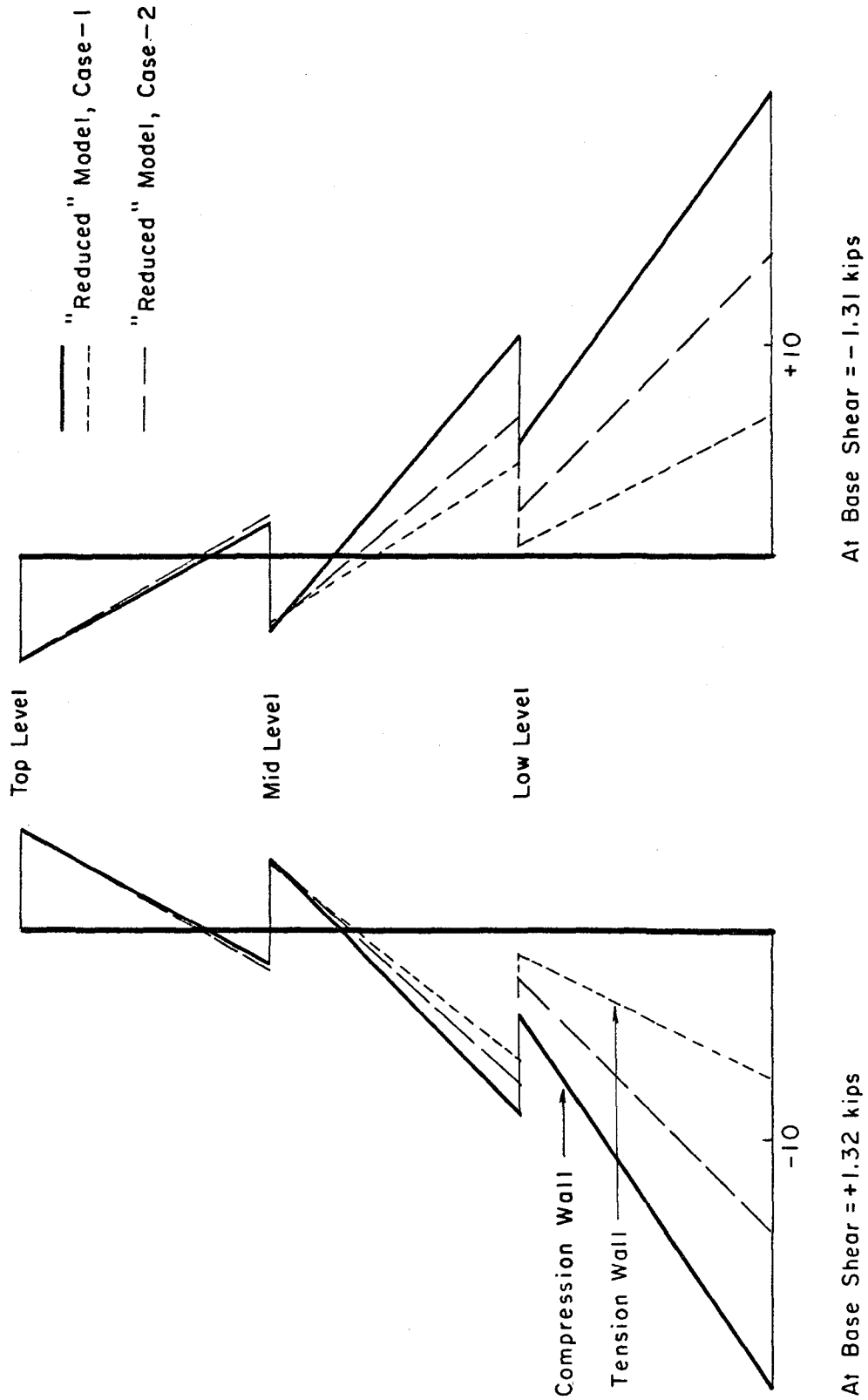

Fig. 5.11 M-P Effects, Bending Moments, Kip-in

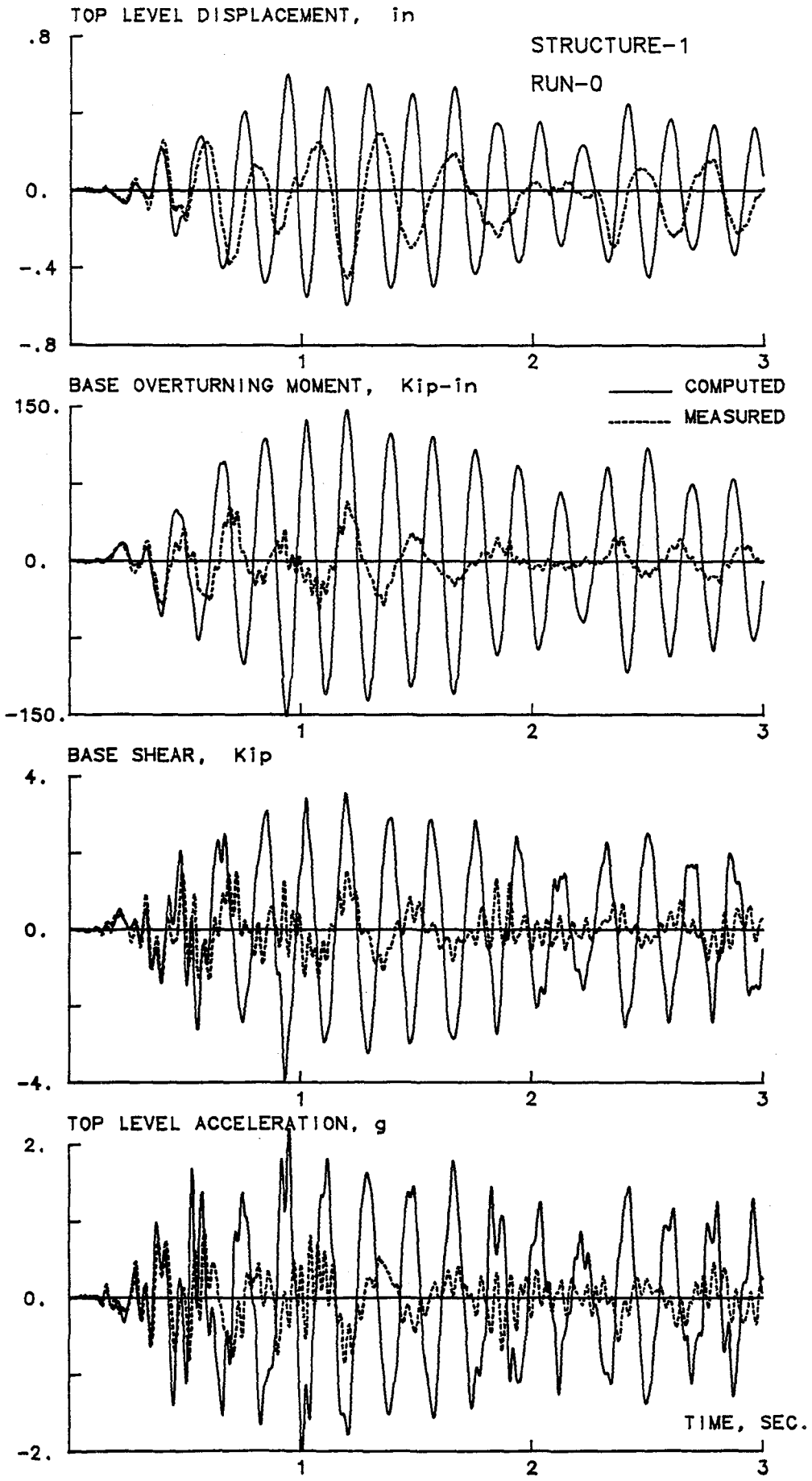

Fig. 5.12 Response Waveforms of Structure-1, Elastic Analysis

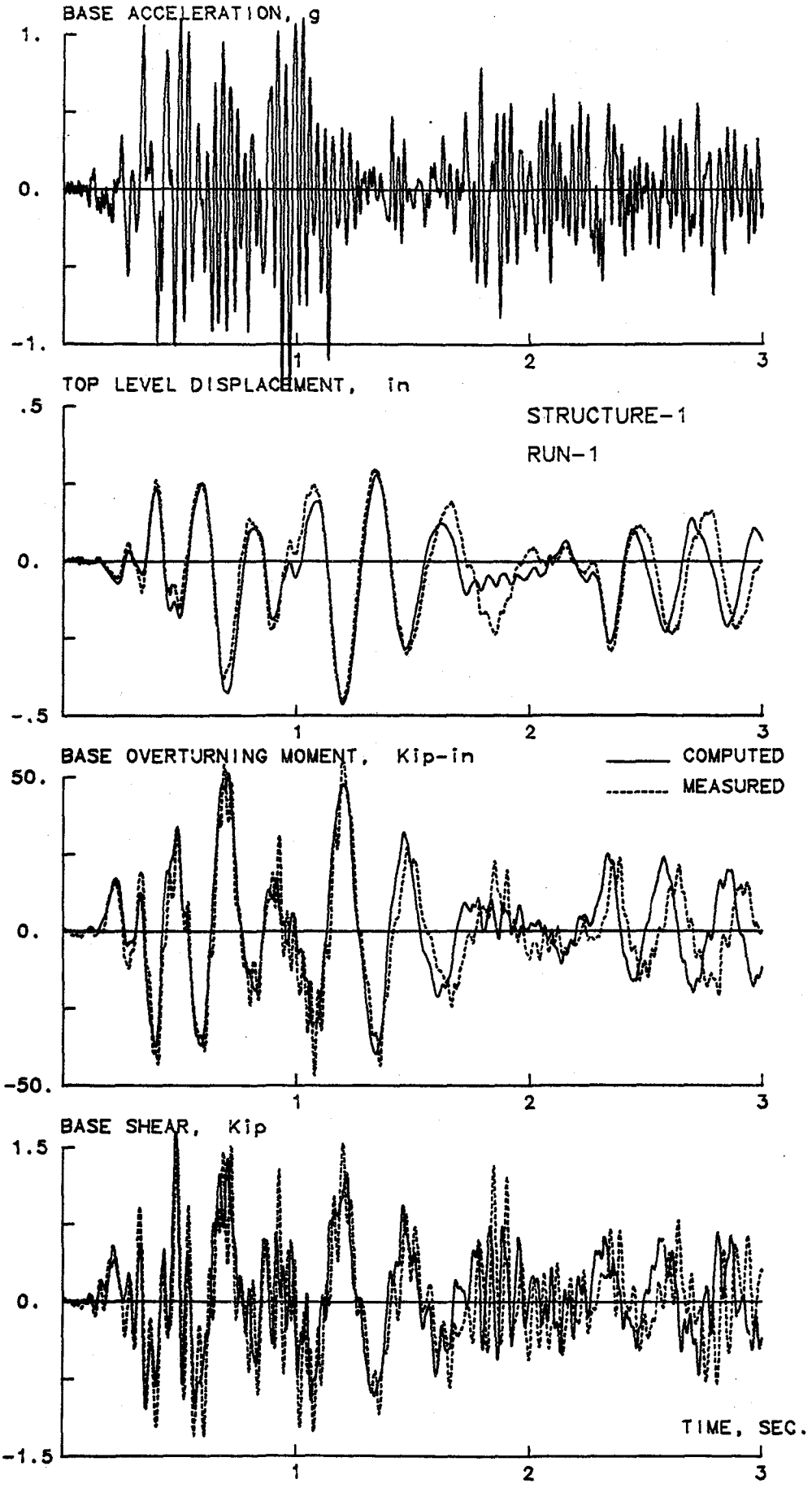

Fig. 5.13 Response Waveforms of Structure-1, Run-1

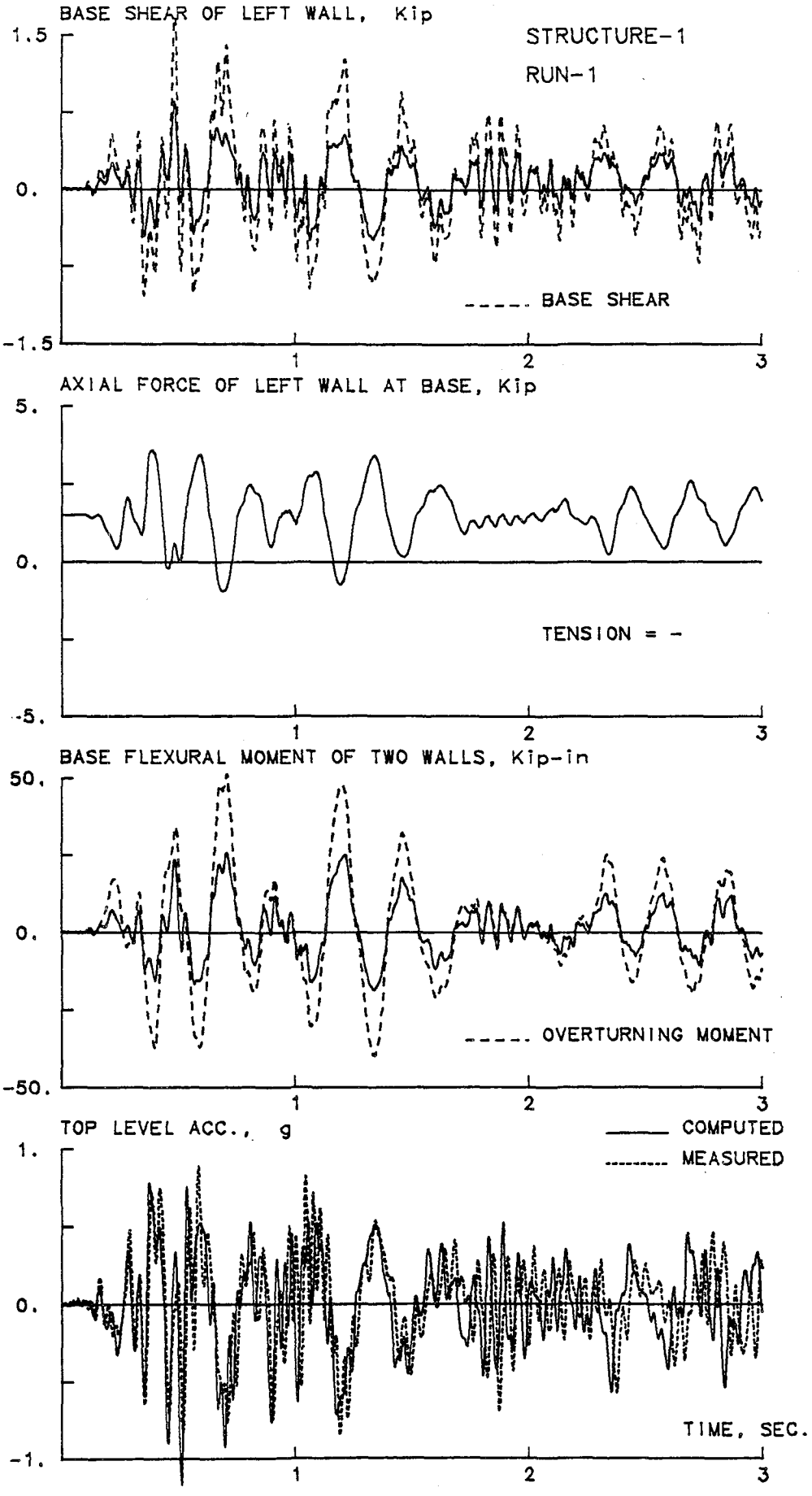

Fig. 5.13 (Continued)

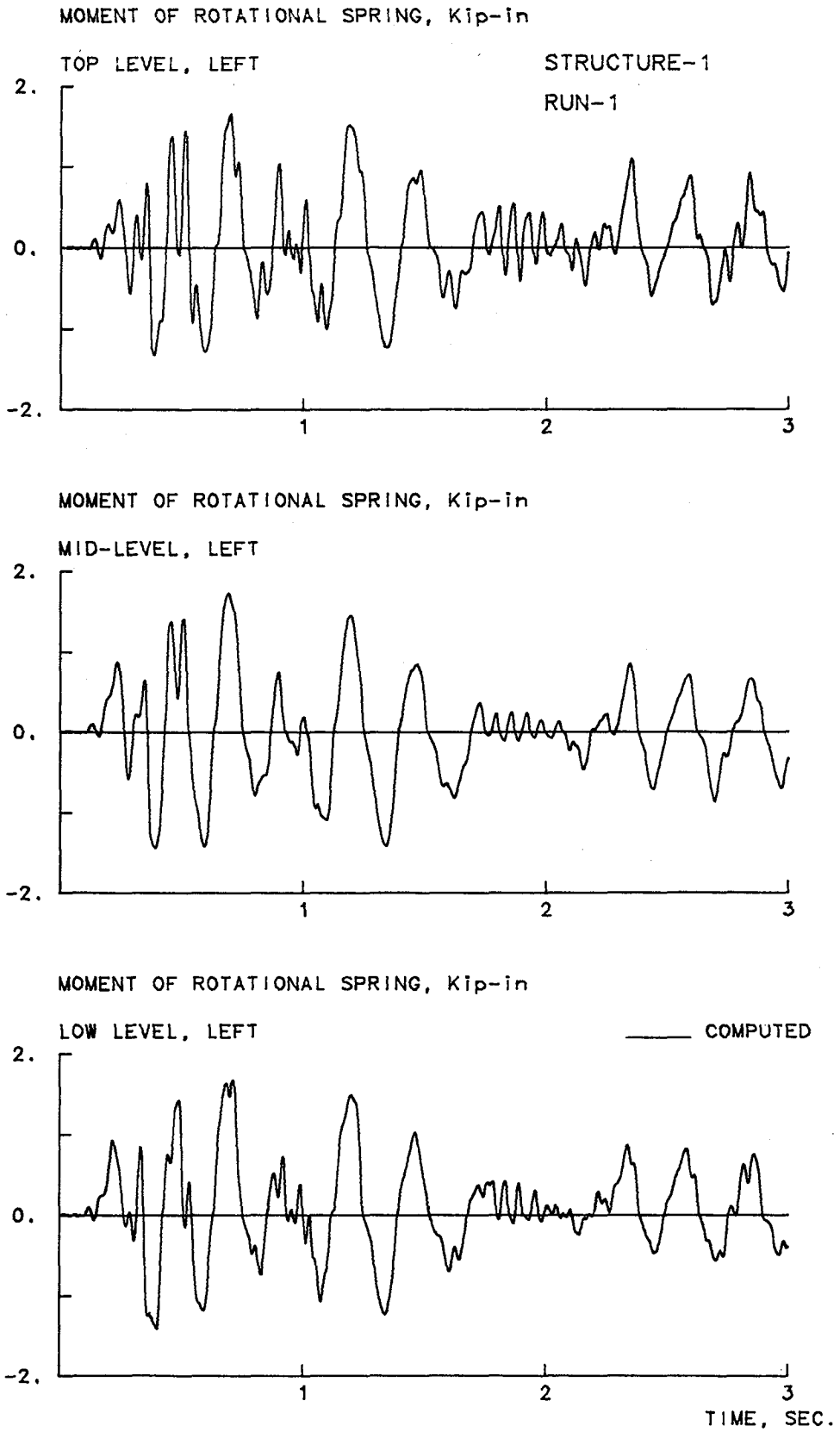

Fig. 5.13 (Continued)

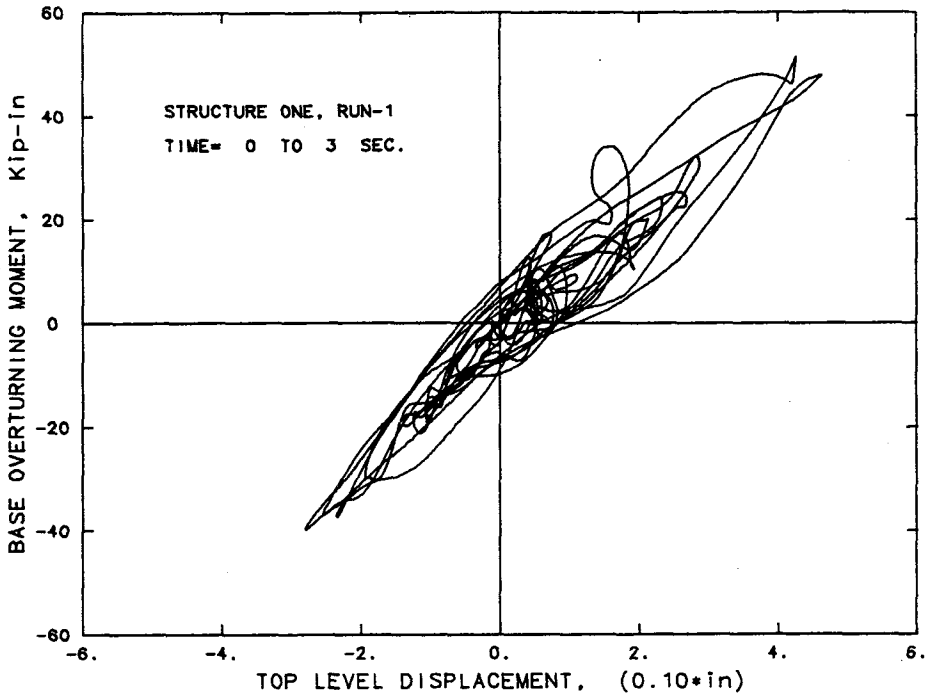

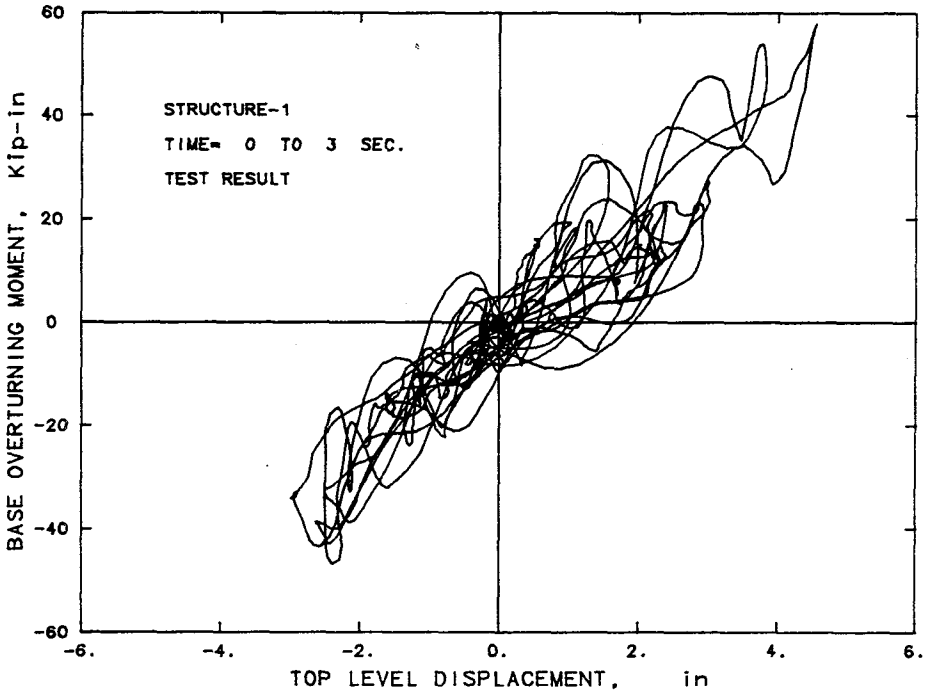

Fig. 5.14 Computed and Measured Response Histories of Base Moment-Top Displacement Relationship of Structure-1

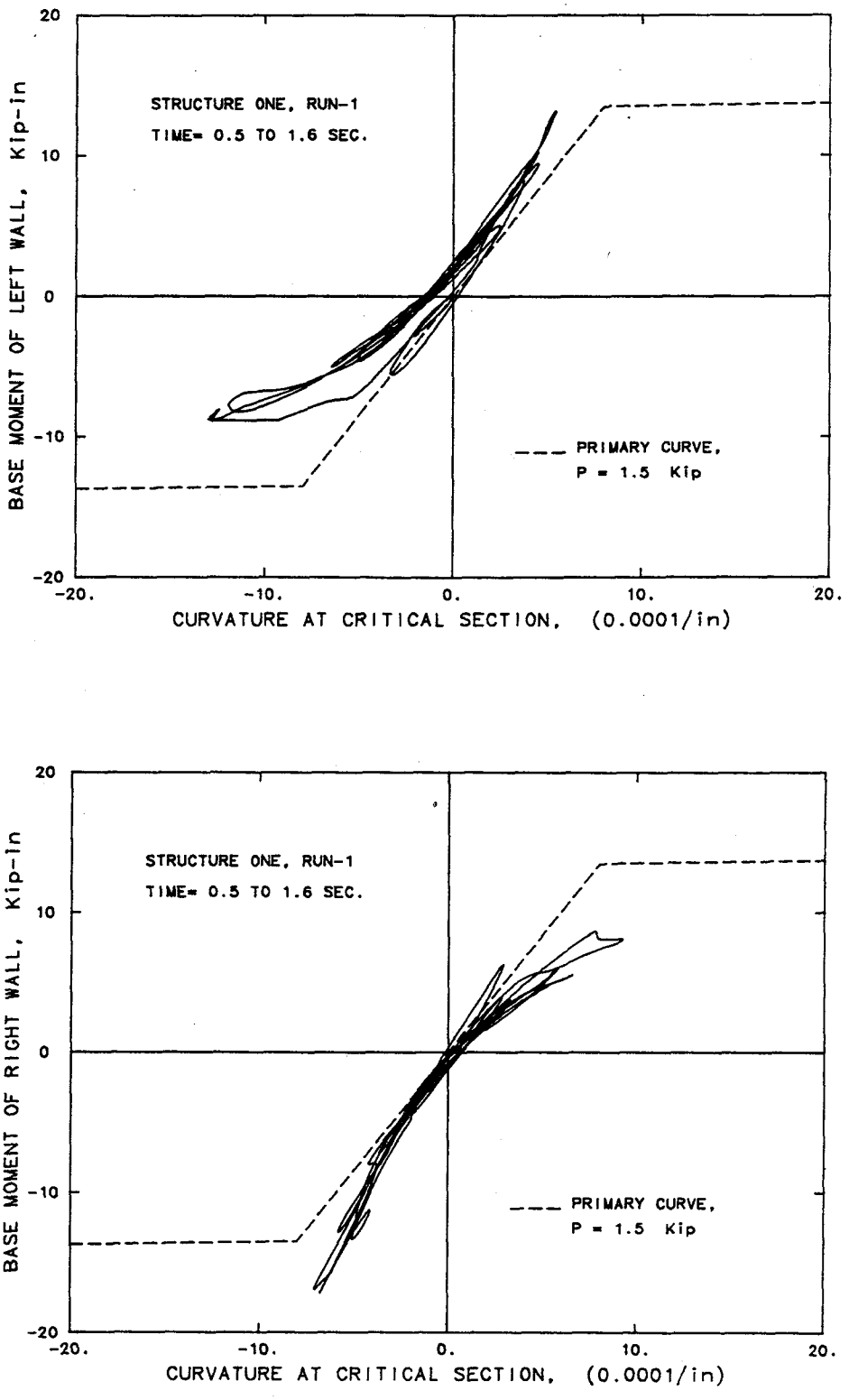

Fig. 5.15 Moment-Curvature Relations at the Bases of Two Walls

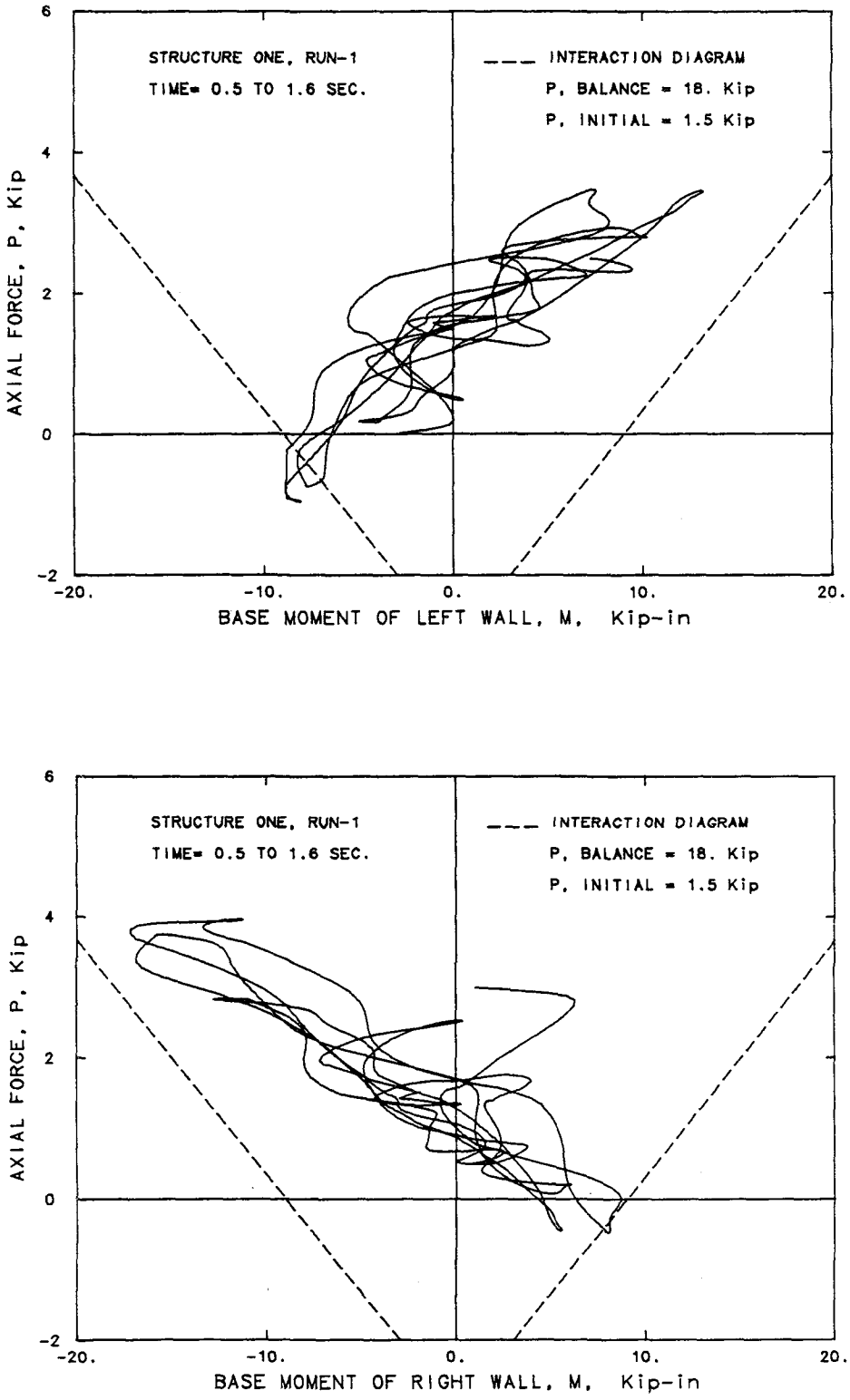

Fig. 5.16 Moment-Axial Force Relations at the Bases of Two Walls

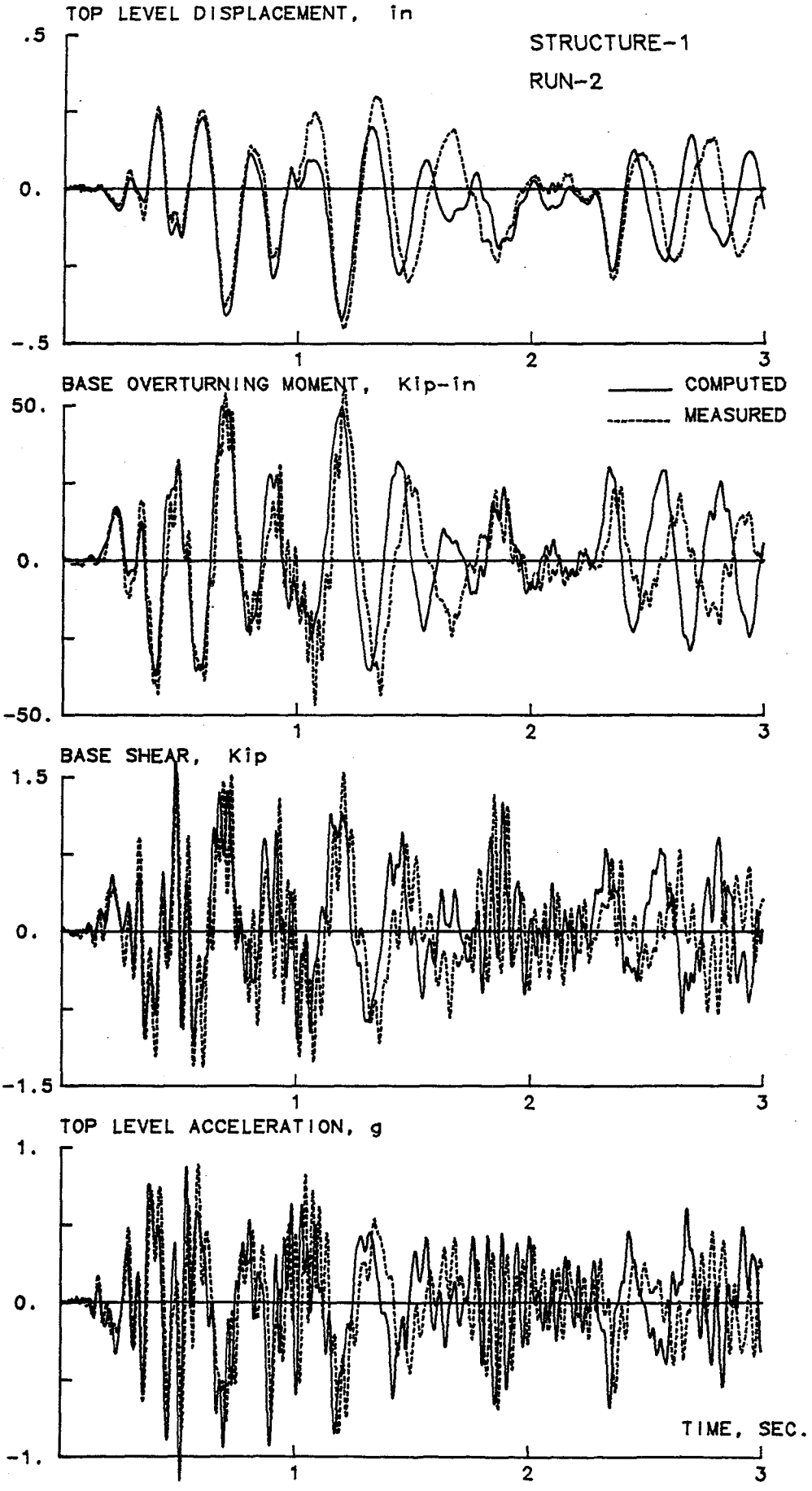

Fig. 5.17 Response Waveforms of Structure-1, Run-2

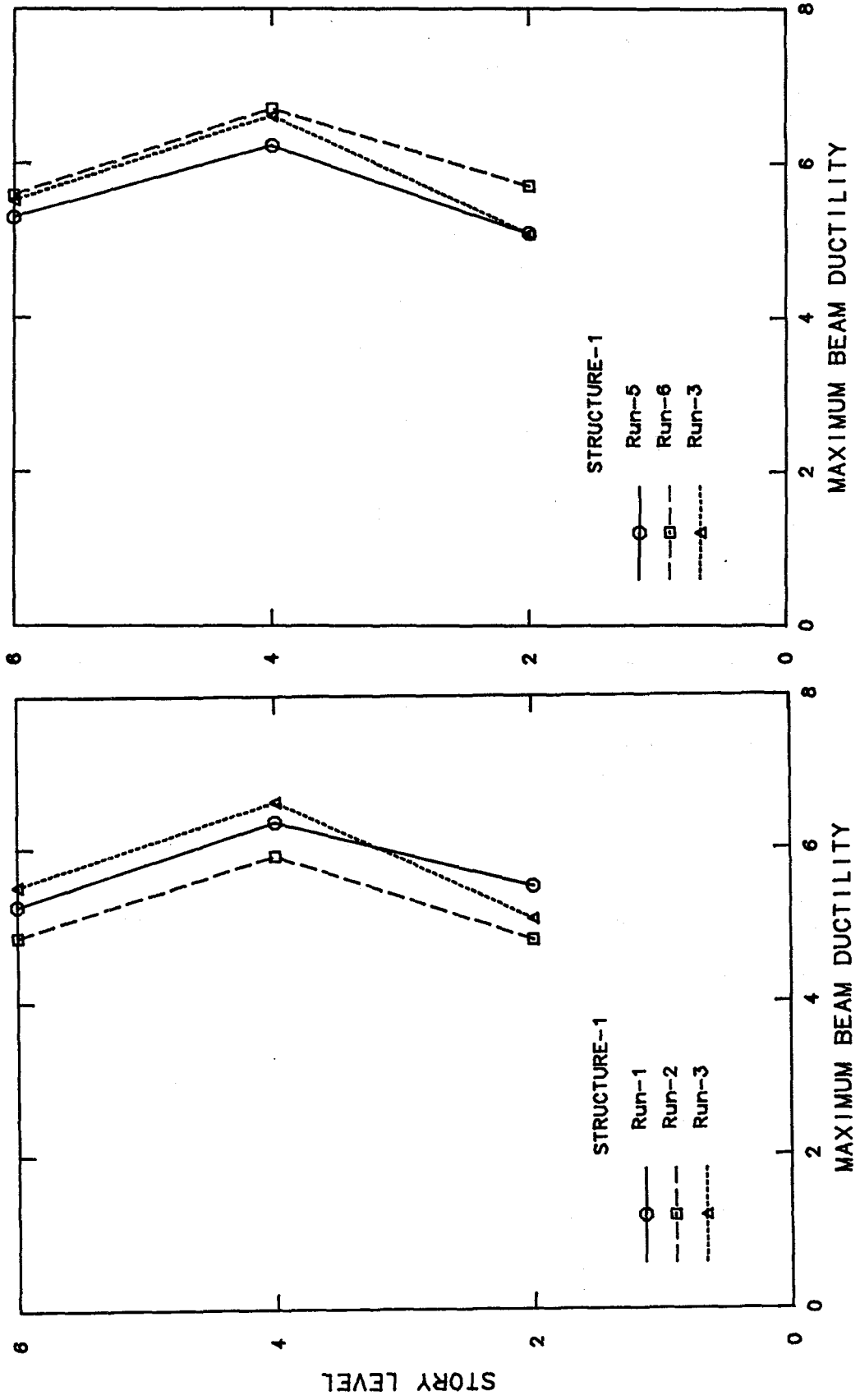

Fig. 5.18 Envelopes of Maximum Rotation Ductility Factors of Coupling Beams for Different Runs

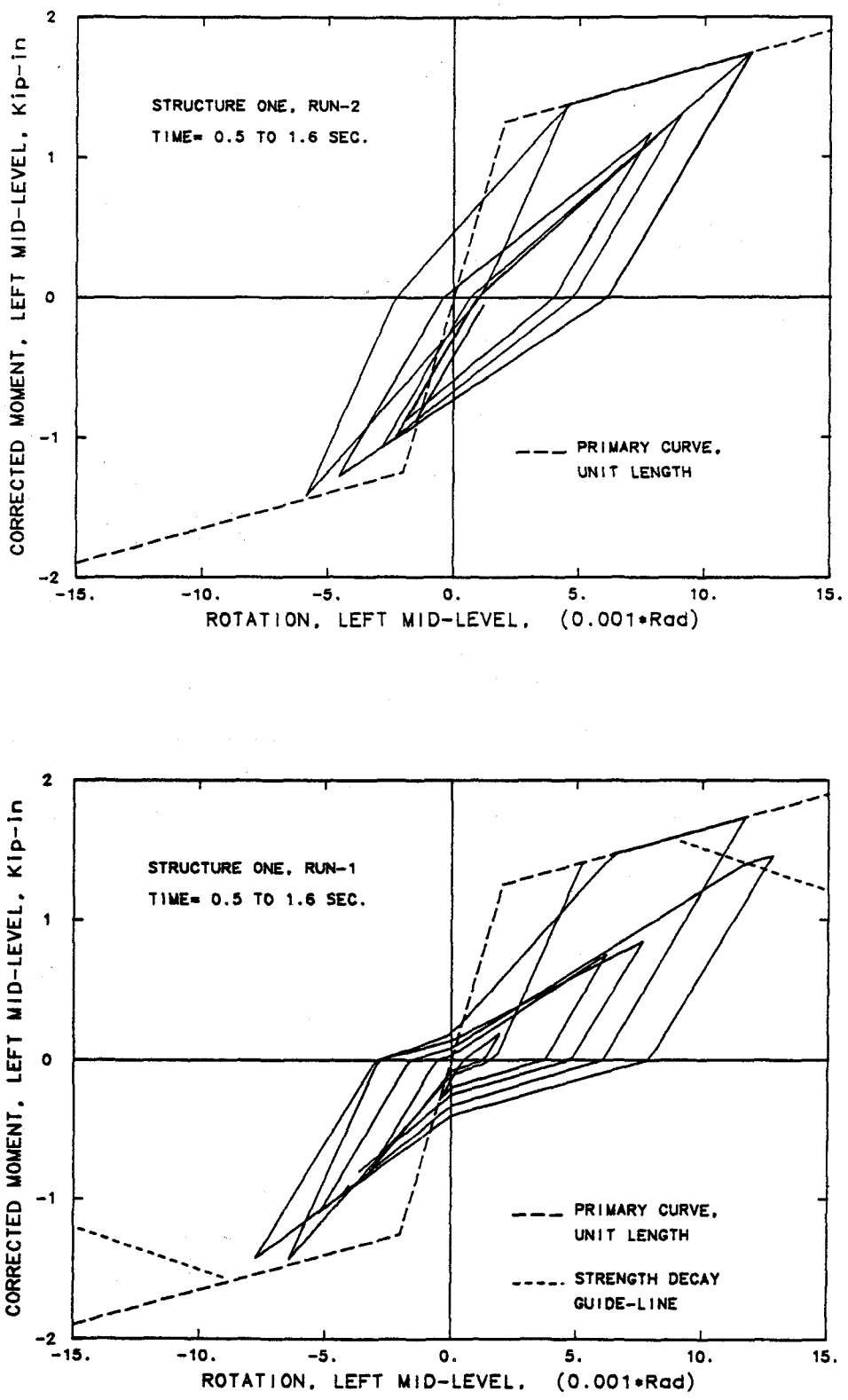

Fig 5.19 Moment-Rotation Relations of the Left-End Mid-Level Beam Rotational Spring of Structure-1

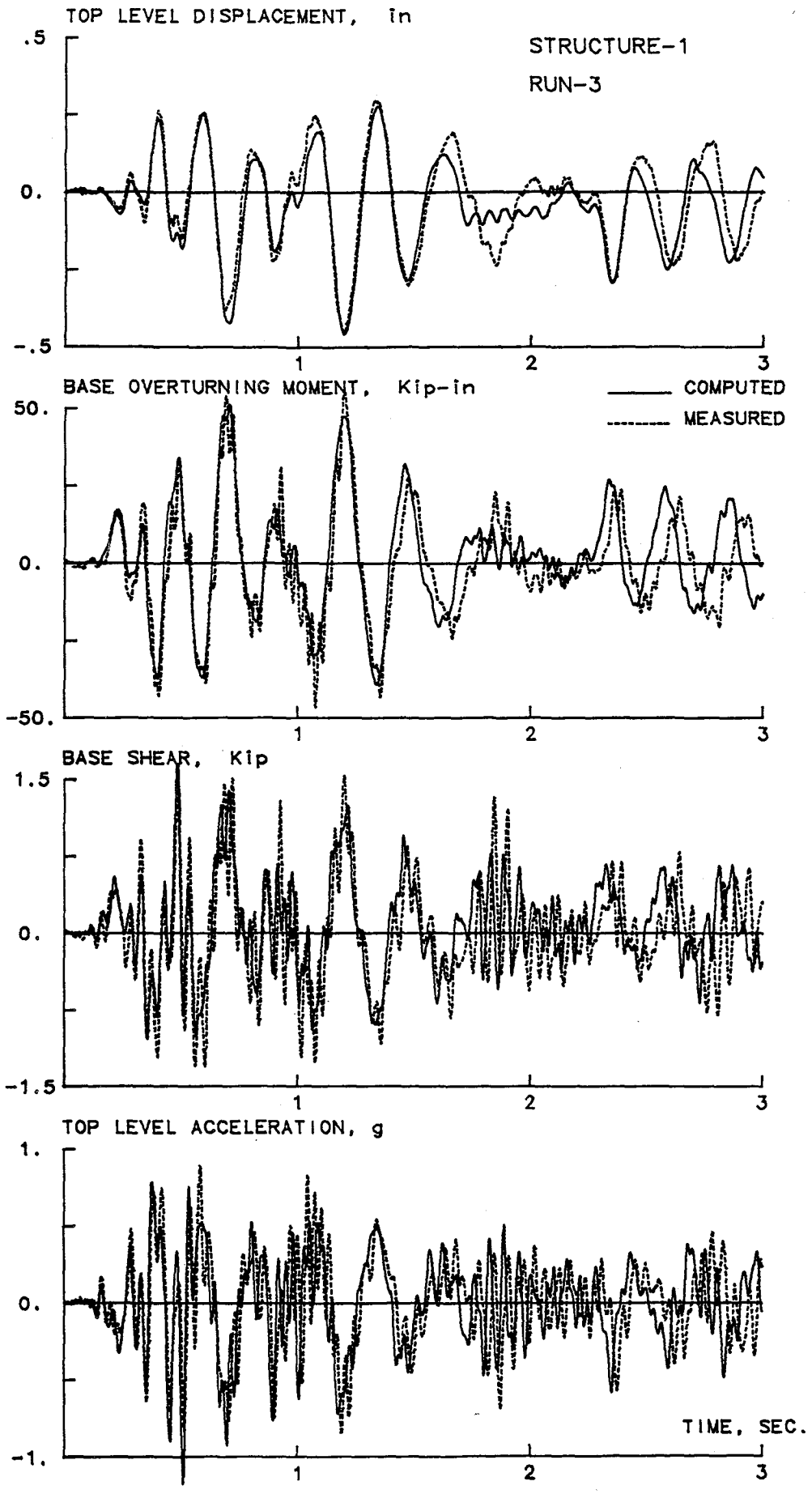

Fig. 5.20 Response Waveforms of Structure-1, Run-3

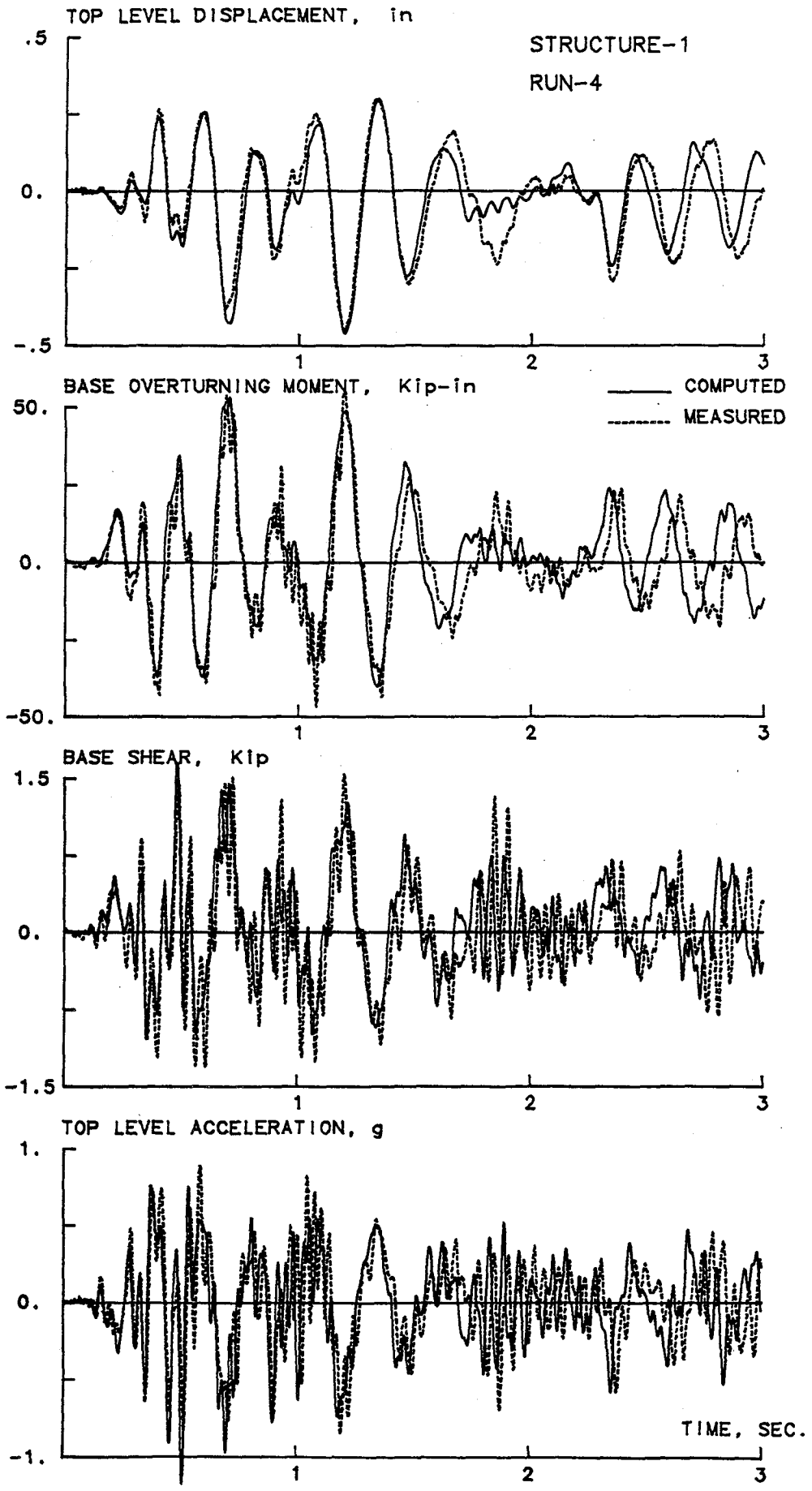

Fig. 5.21 Response Waveforms of Structure-1, Run-4

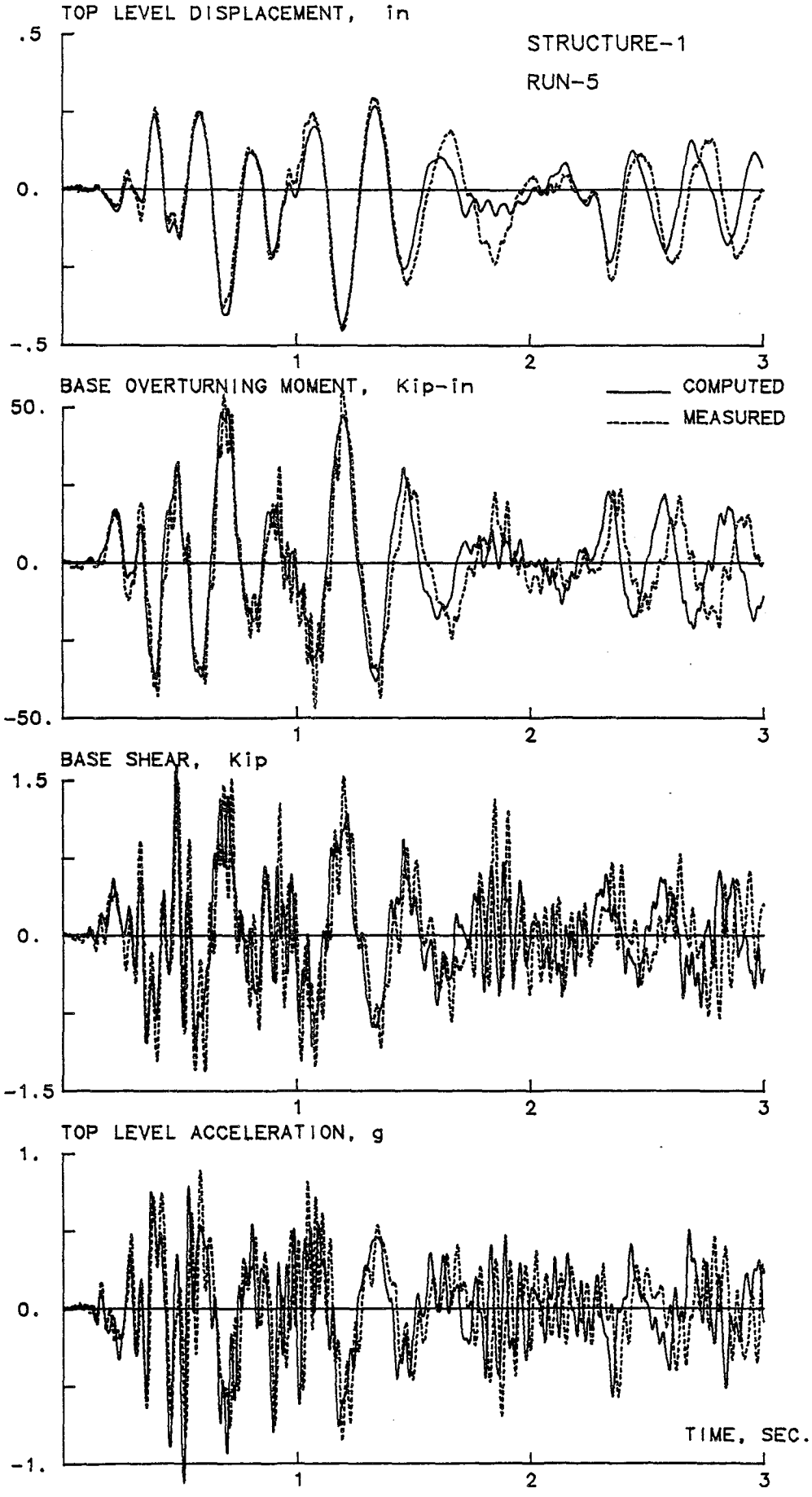

Fig. 5.22 Response Waveforms of Structure-1, Run-5

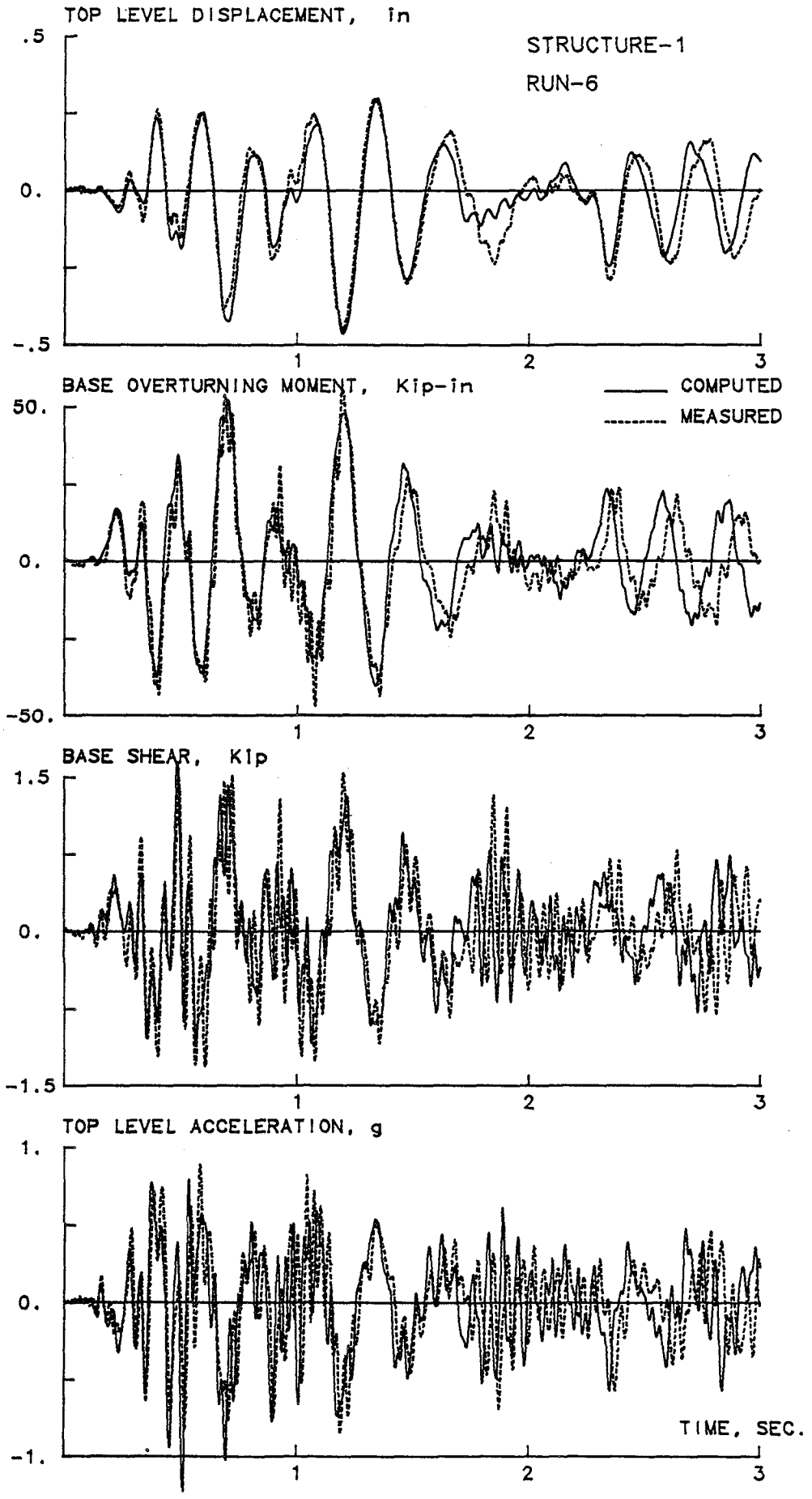

Fig. 5.23 Response Waveforms of Structure-1, Run-6

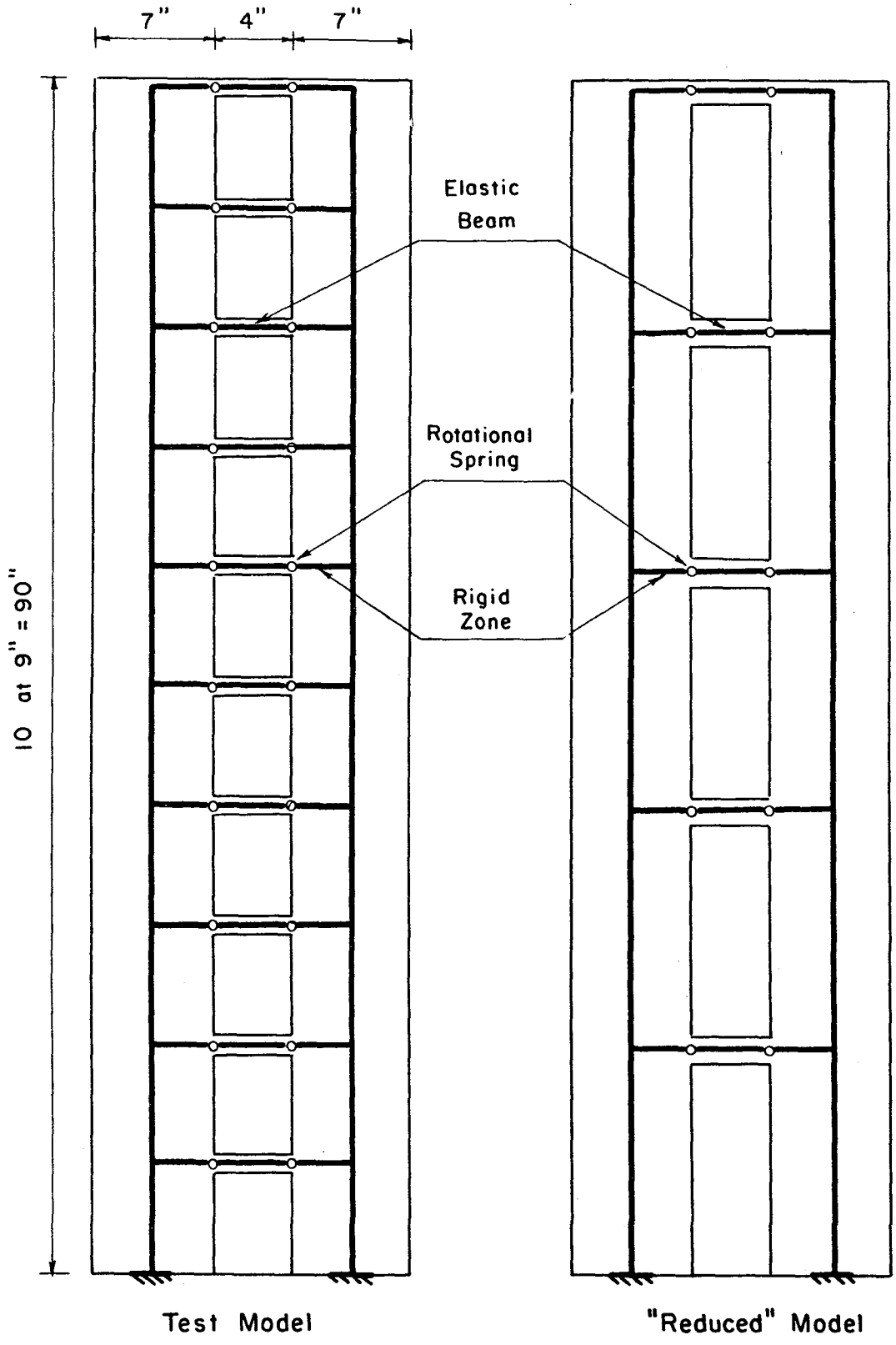

Fig. 5.24 Analytical Models of 10-Story Coupled Shear Wall

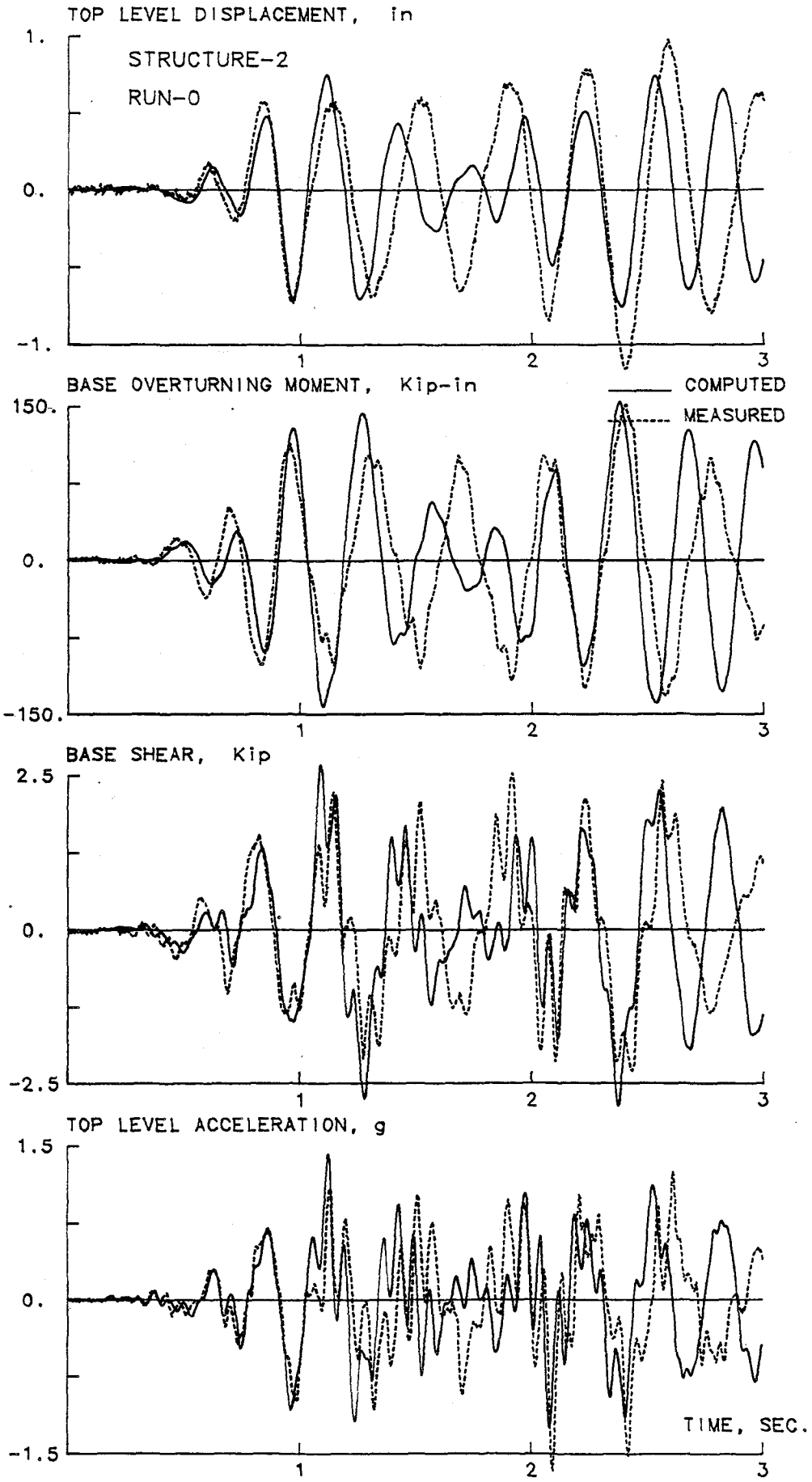

Fig. 5.25 Response Waveforms of Structure-2, Elastic Analysis

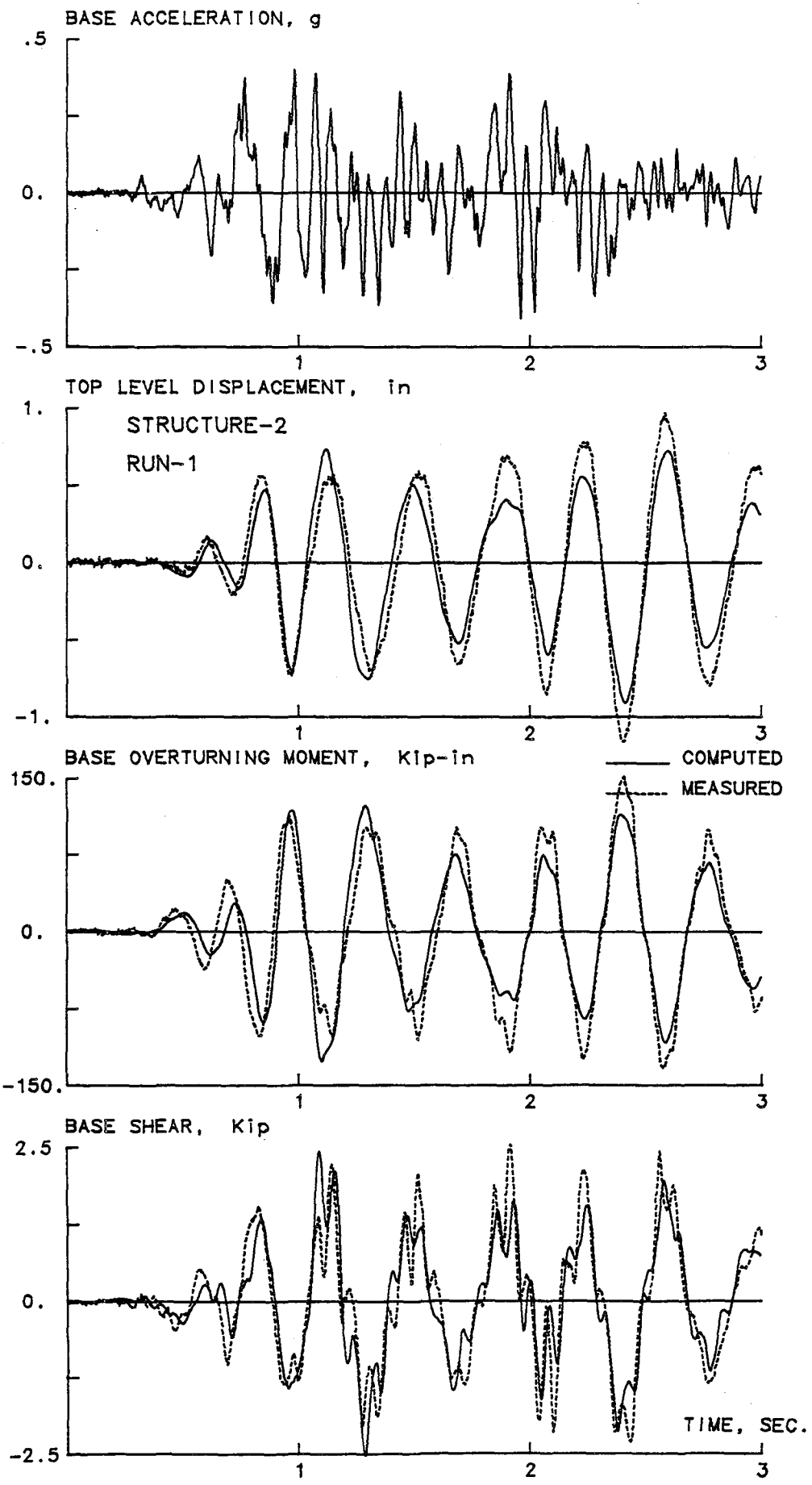

Fig. 5.26 Response Waveforms of Structure-2, Run-1

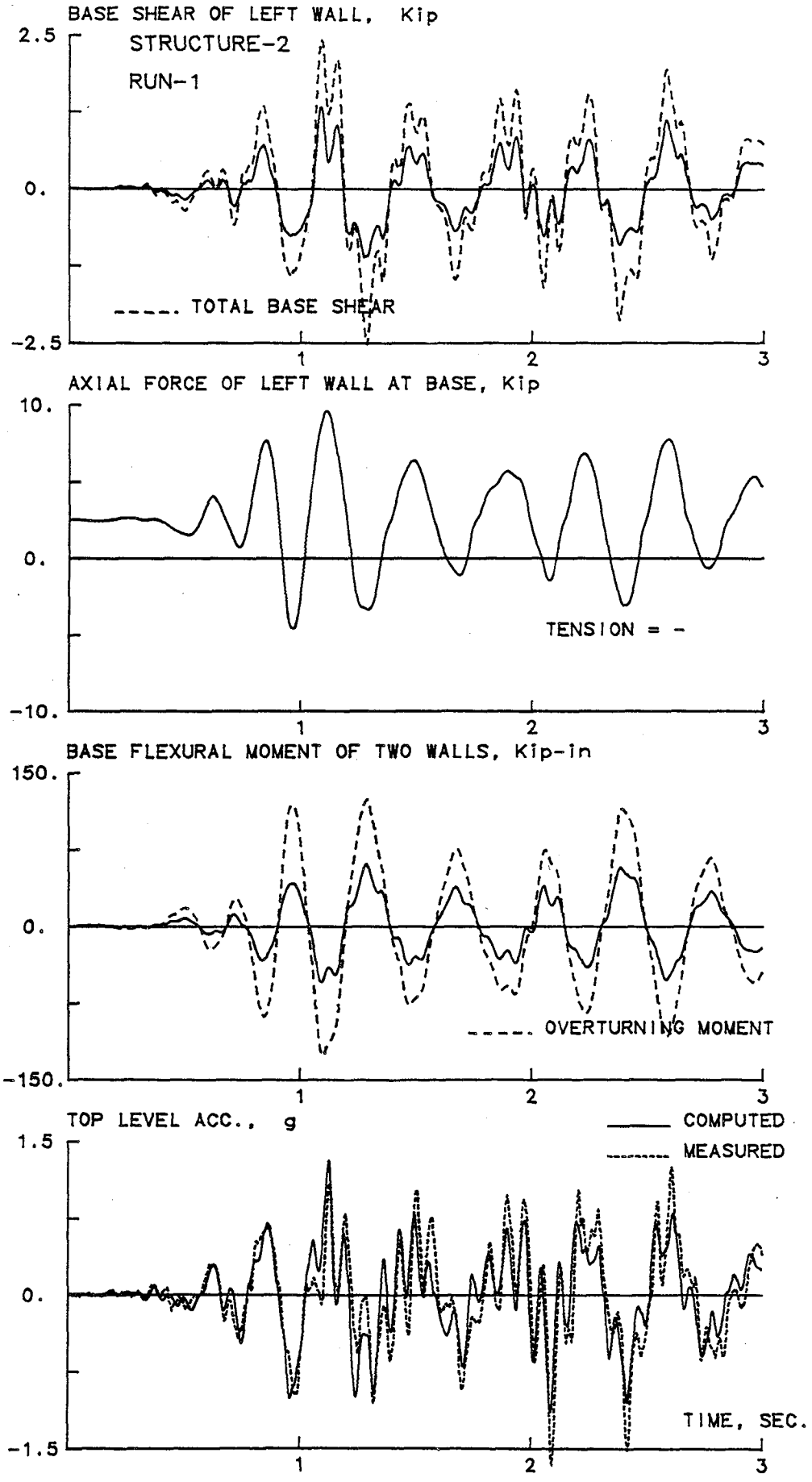

Fig. 5.26 (Continued)

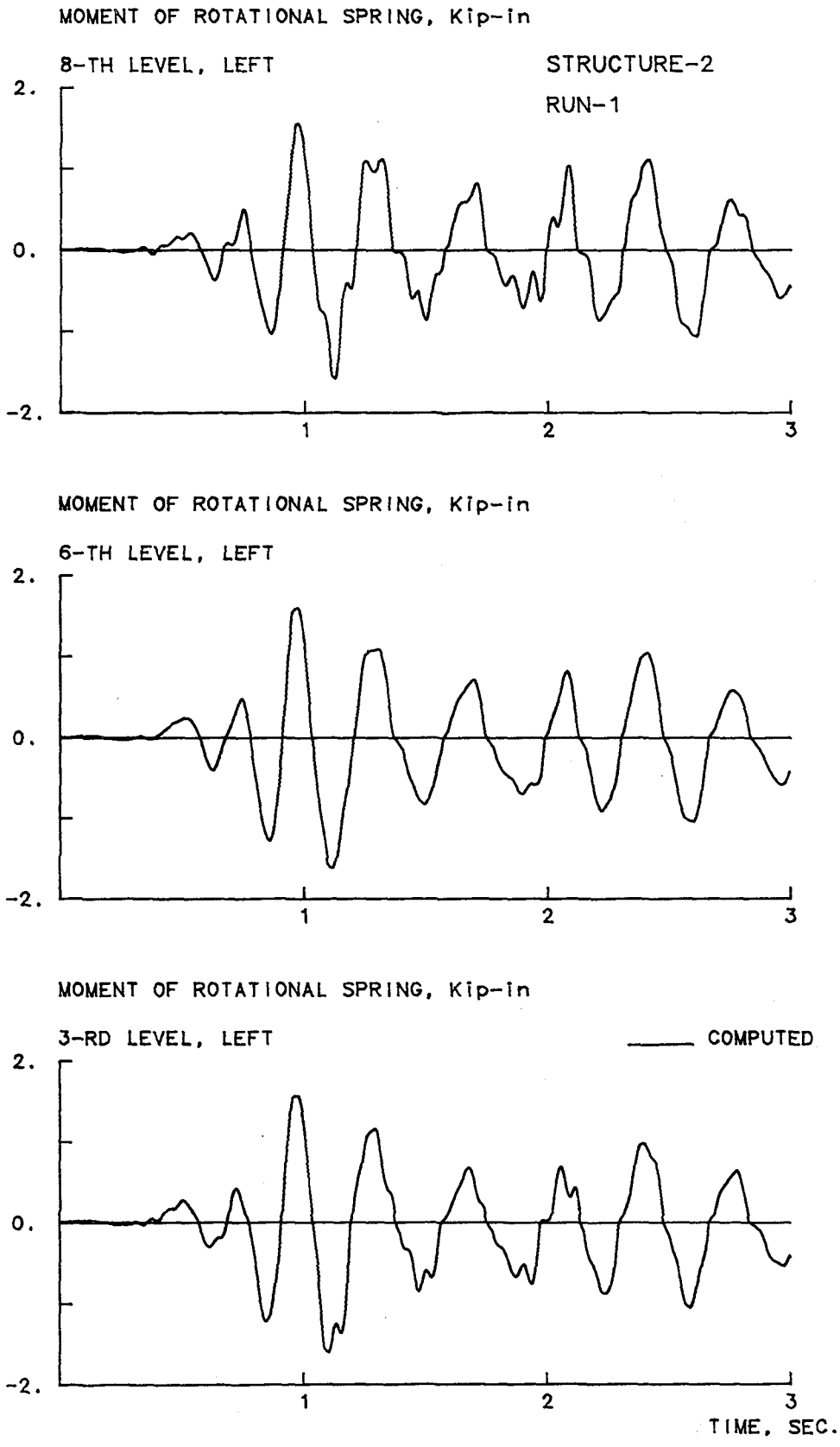

Fig. 5.26 (Continued)

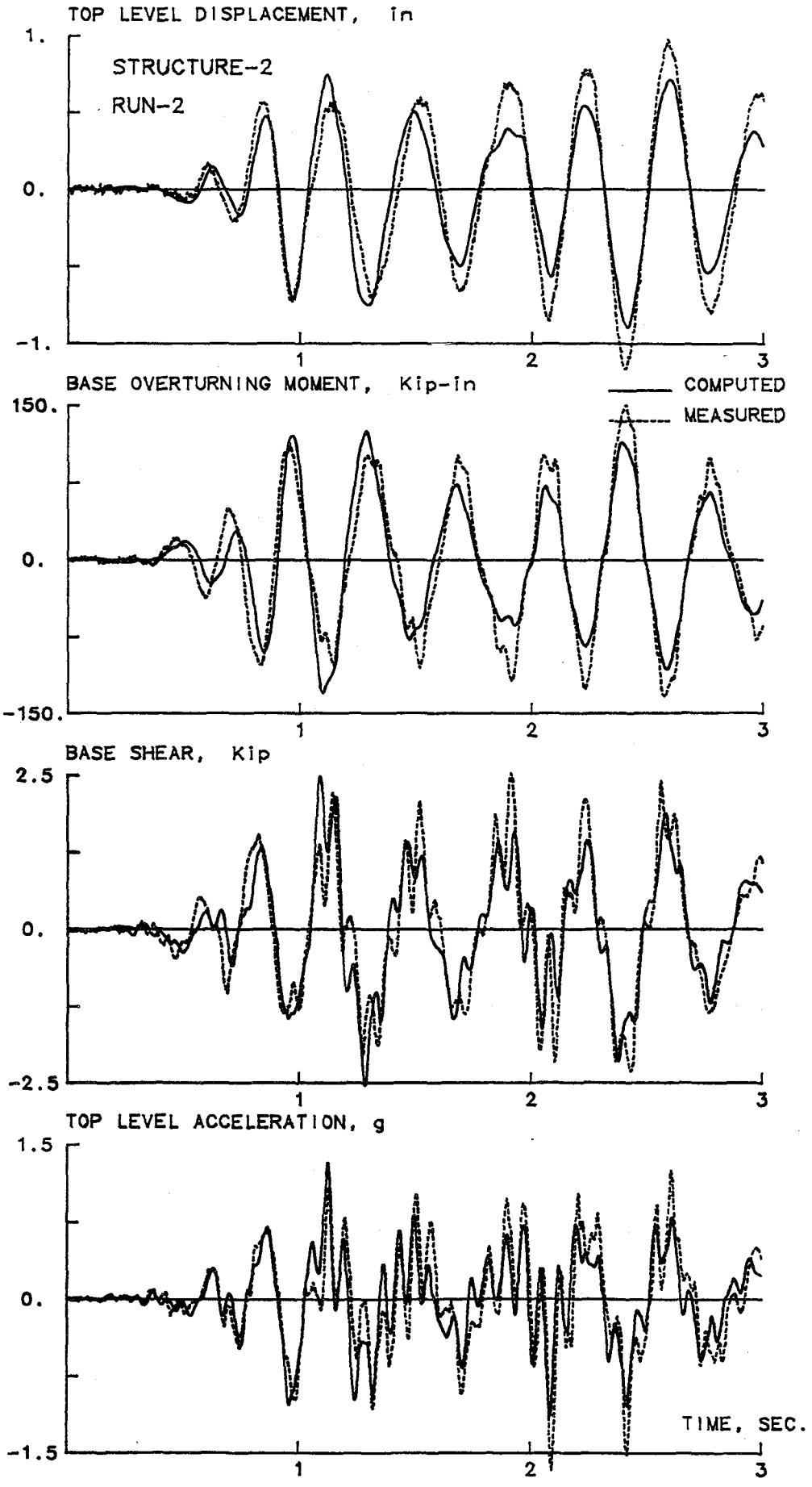

Fig. 5.27 Response Waveforms of Structure-2, Run-2

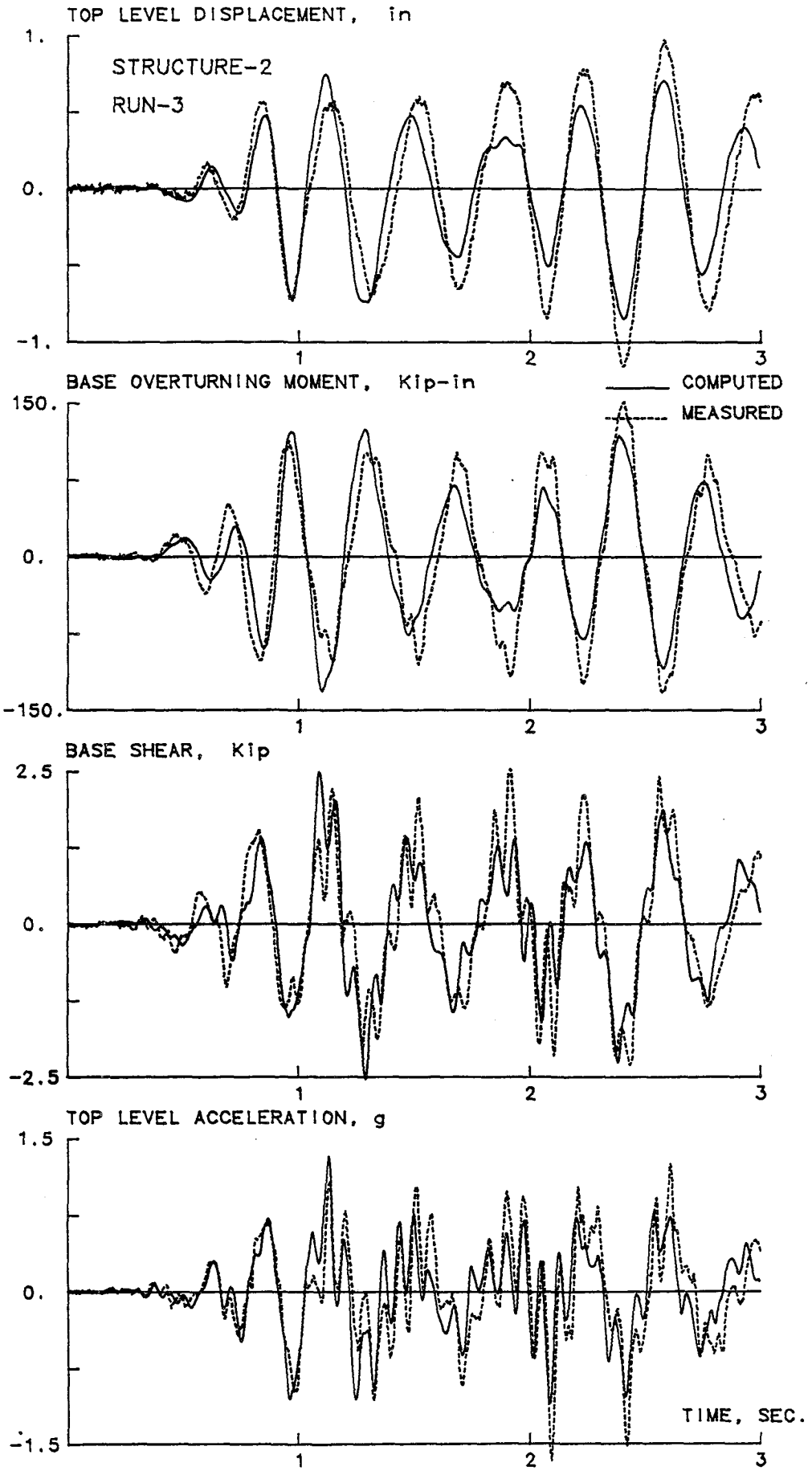

Fig. 5.28 Response Waveforms of Structure-2, Run-3

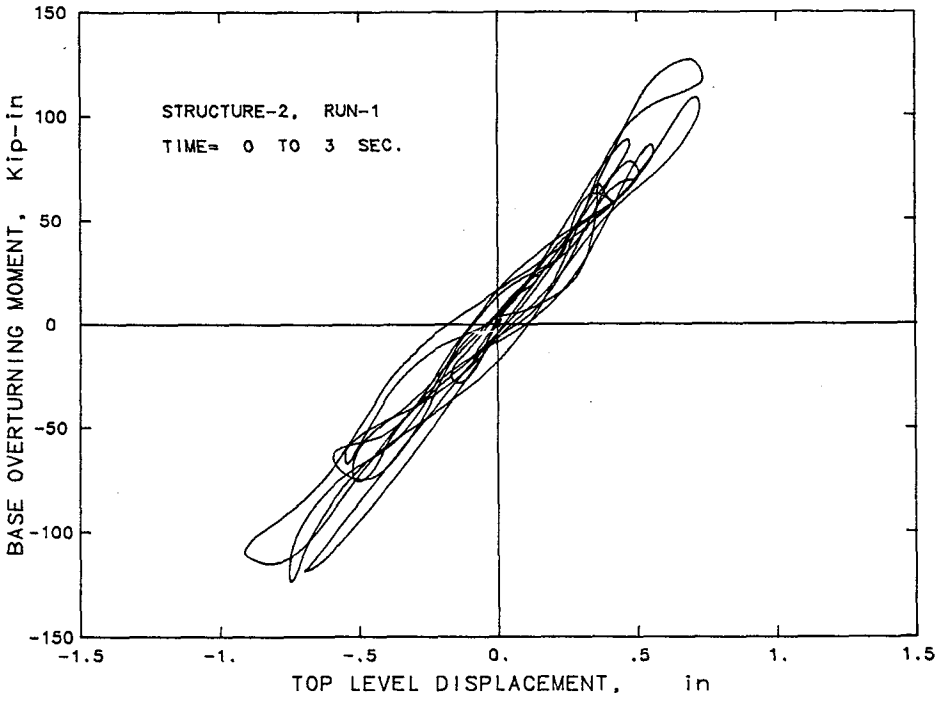

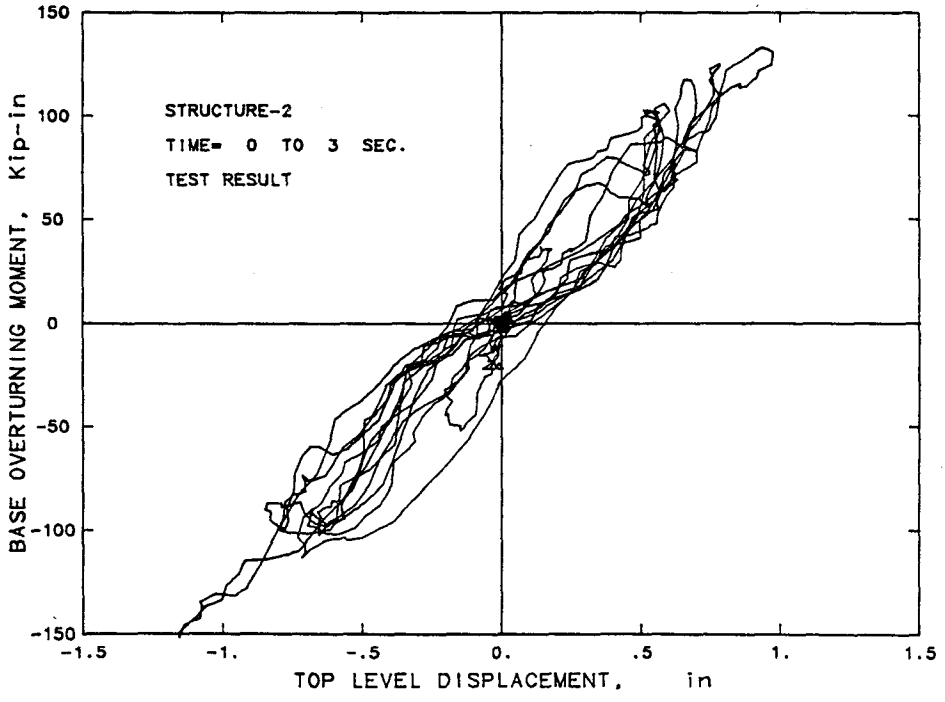

Fig. 5.29 Computed and Measured Response Histories of Base Moment-Top Displacement Relationship of Structure-2

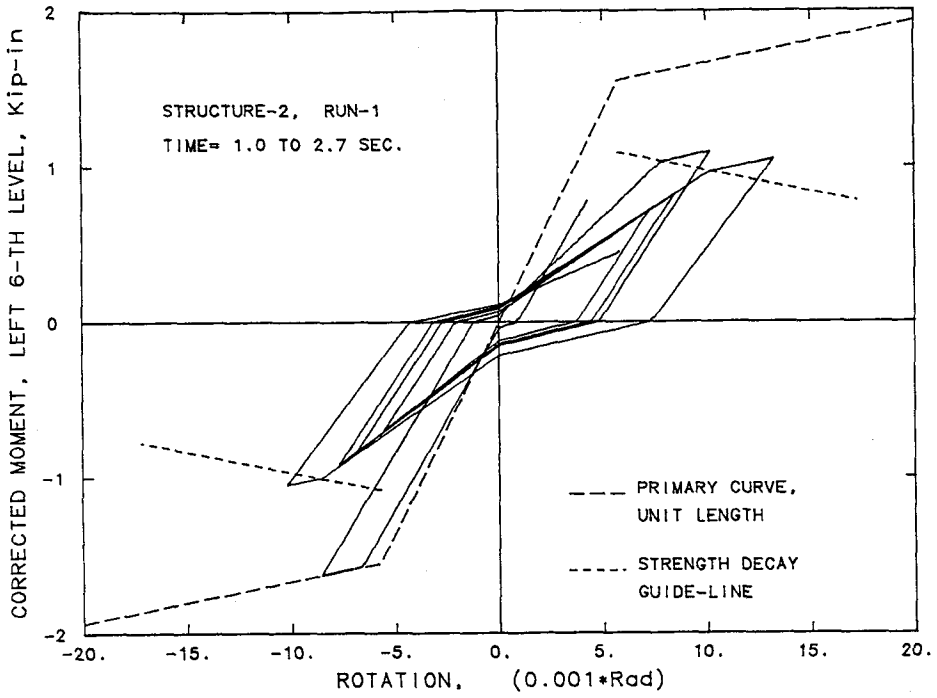

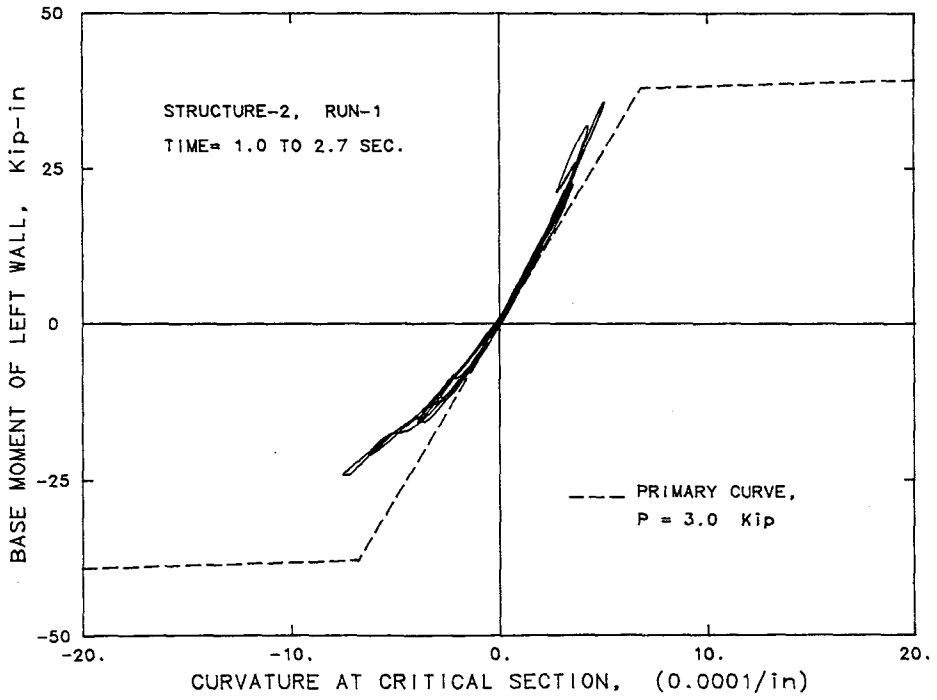

Fig. 5.30 Force-Deformation Relationships of Two Members of Structure-2

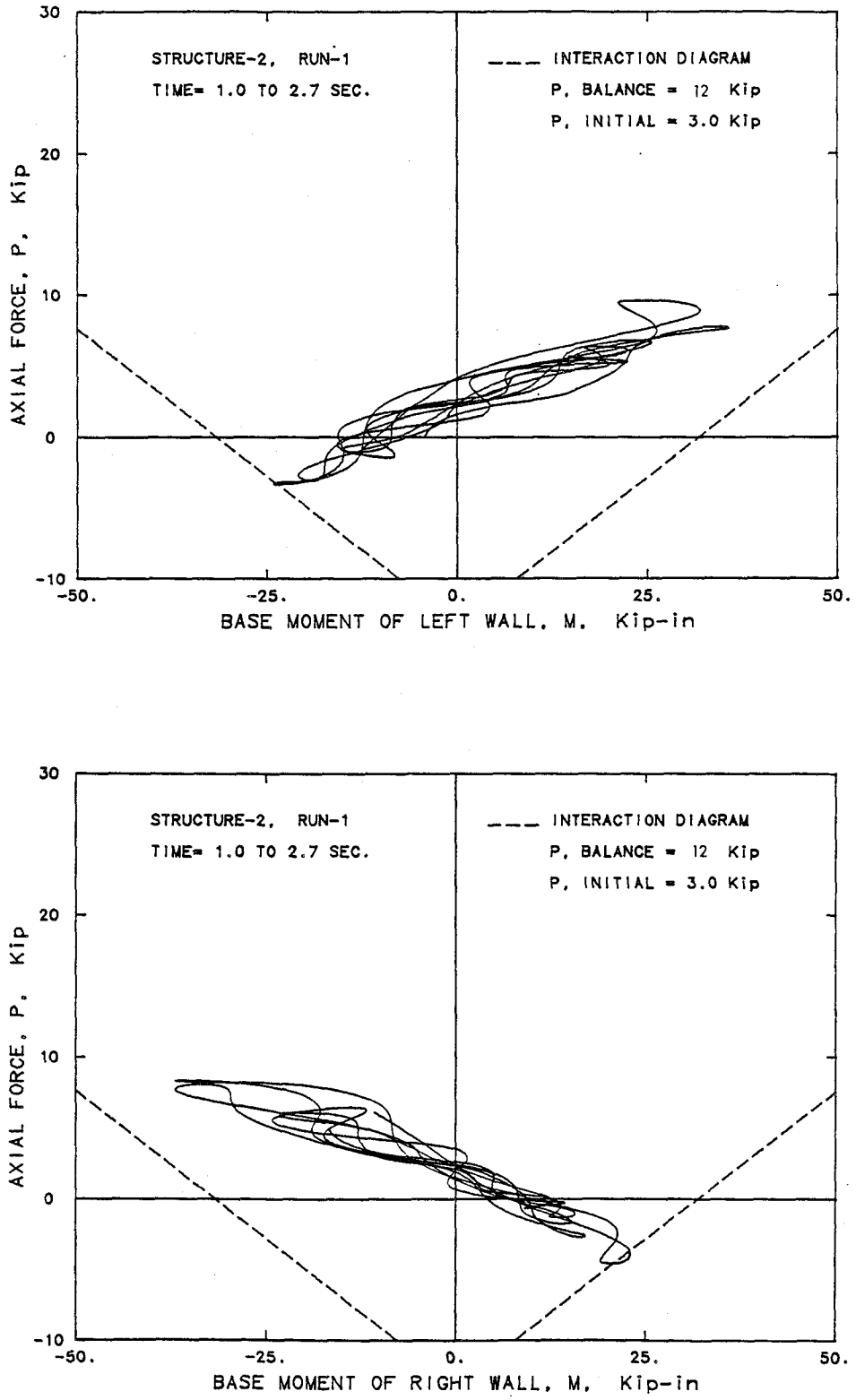

Fig. 5.31 Moment-Axial Force Relations at the Bases of Two Walls

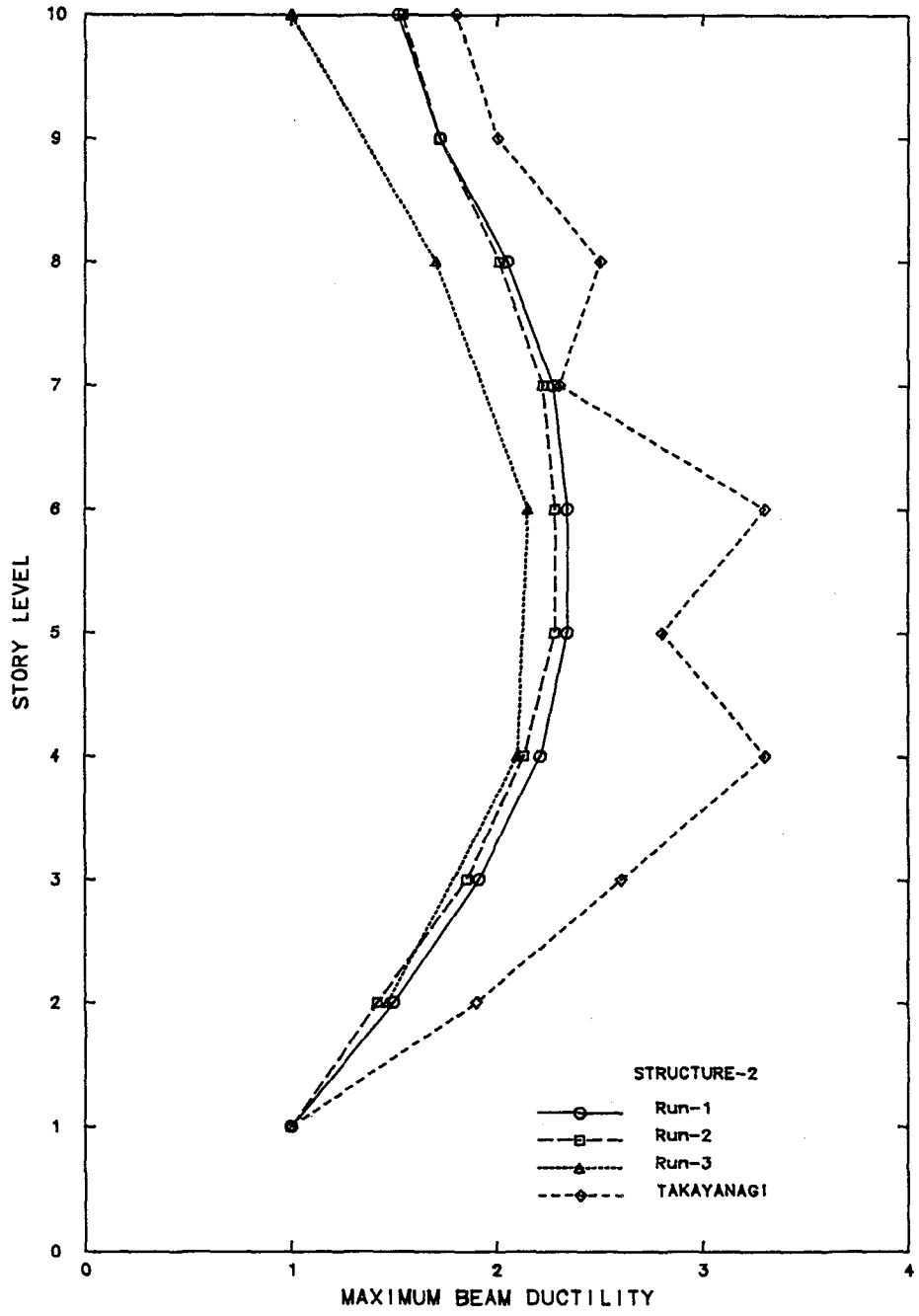

Fig. 5.32 Envelopes of Maximum Rotation Ductility Factors of Coupling Beams for Different Runs

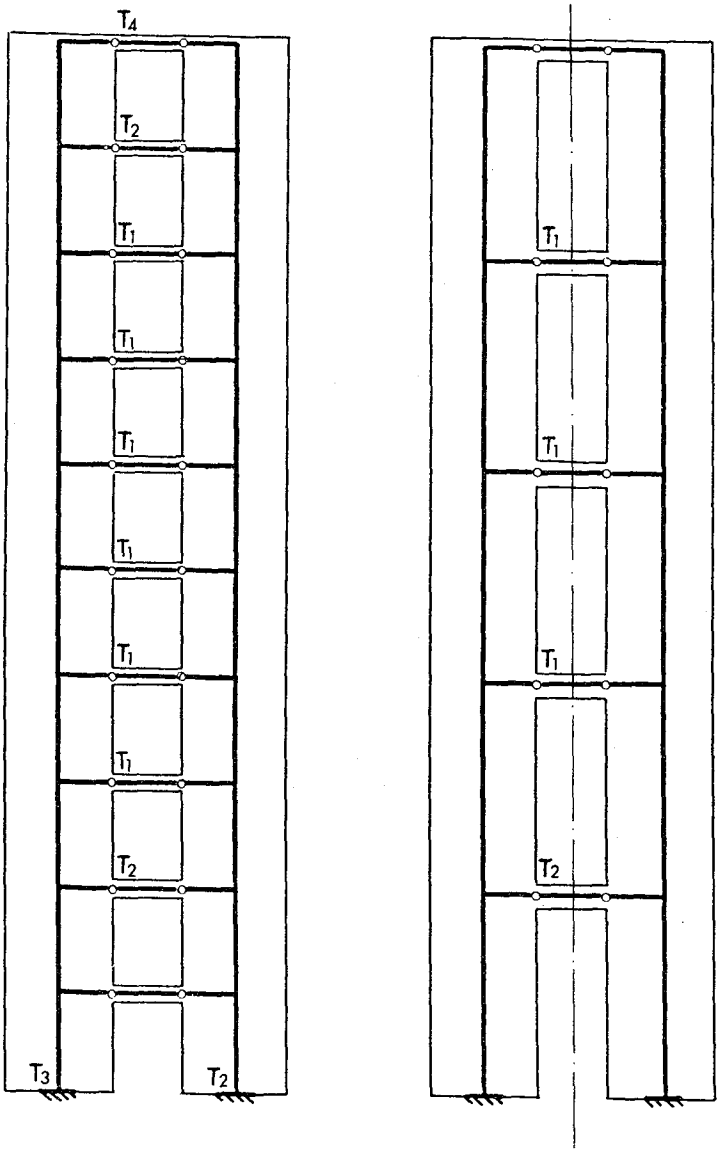

$T_1 = 0.94 - 0.96$ sec.
$T_2 = 1.08 - 1.12$
$T_3 = 1.27$
$T_4 = 2.39$

$T_1 = 0.94 - 0.97$ sec.
$T_2 = 1.08$

Fig. 5.33 Order of Yielding of Structure-2 in Run-1 and Run-3

a) Base Acceleration Used in Ref. 41

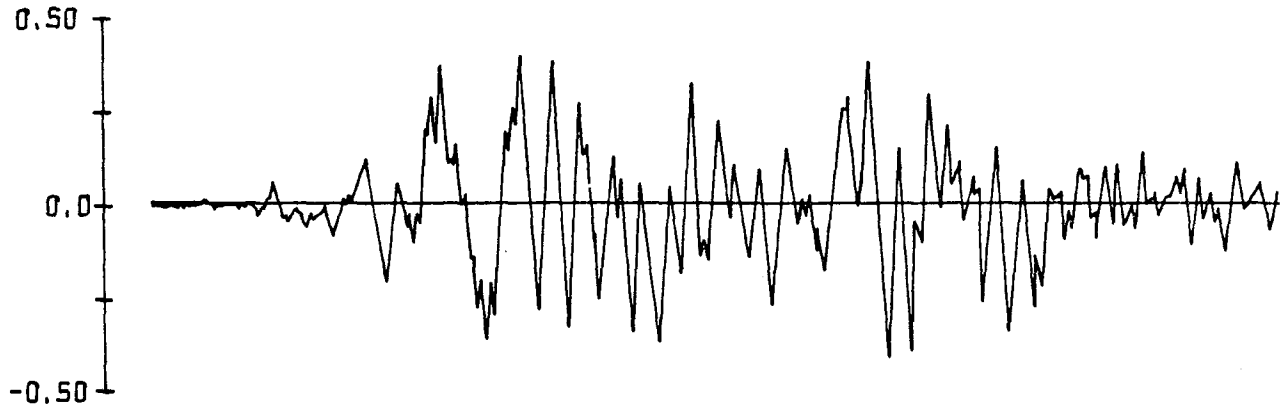

b) Base Acceleration Used in this Study

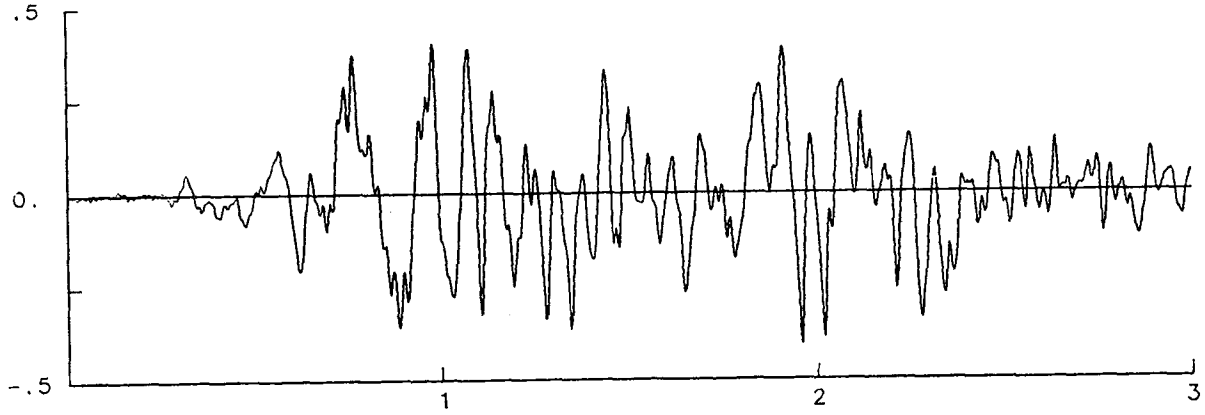

Fig. 5.34 Waveforms of Base Accelerations for Structure-2

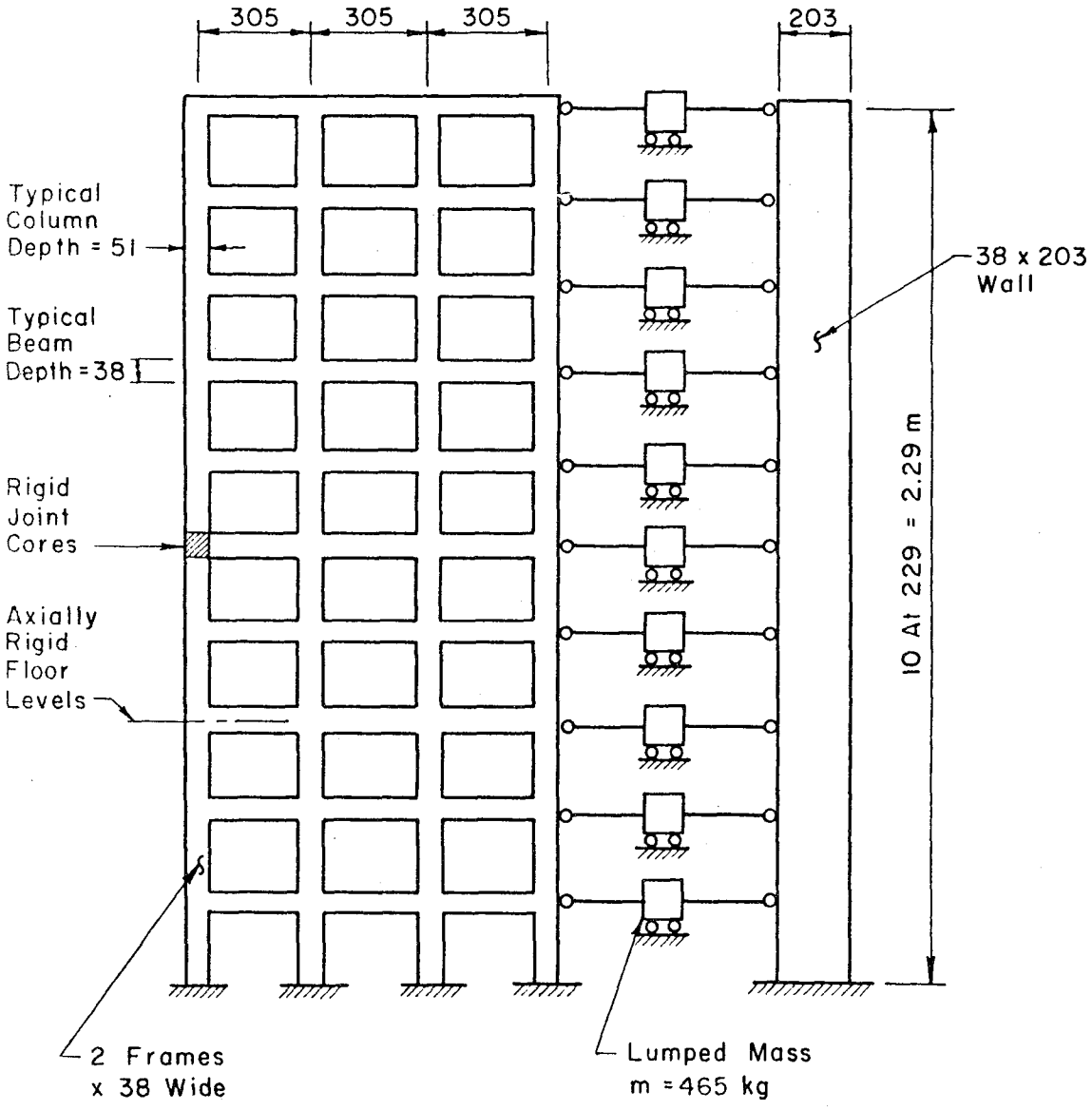

(All Dimensions In Millimeters Unless Noted)

Fig. 5.35 Analytical Models of 10-Story Wall-Frame Structure

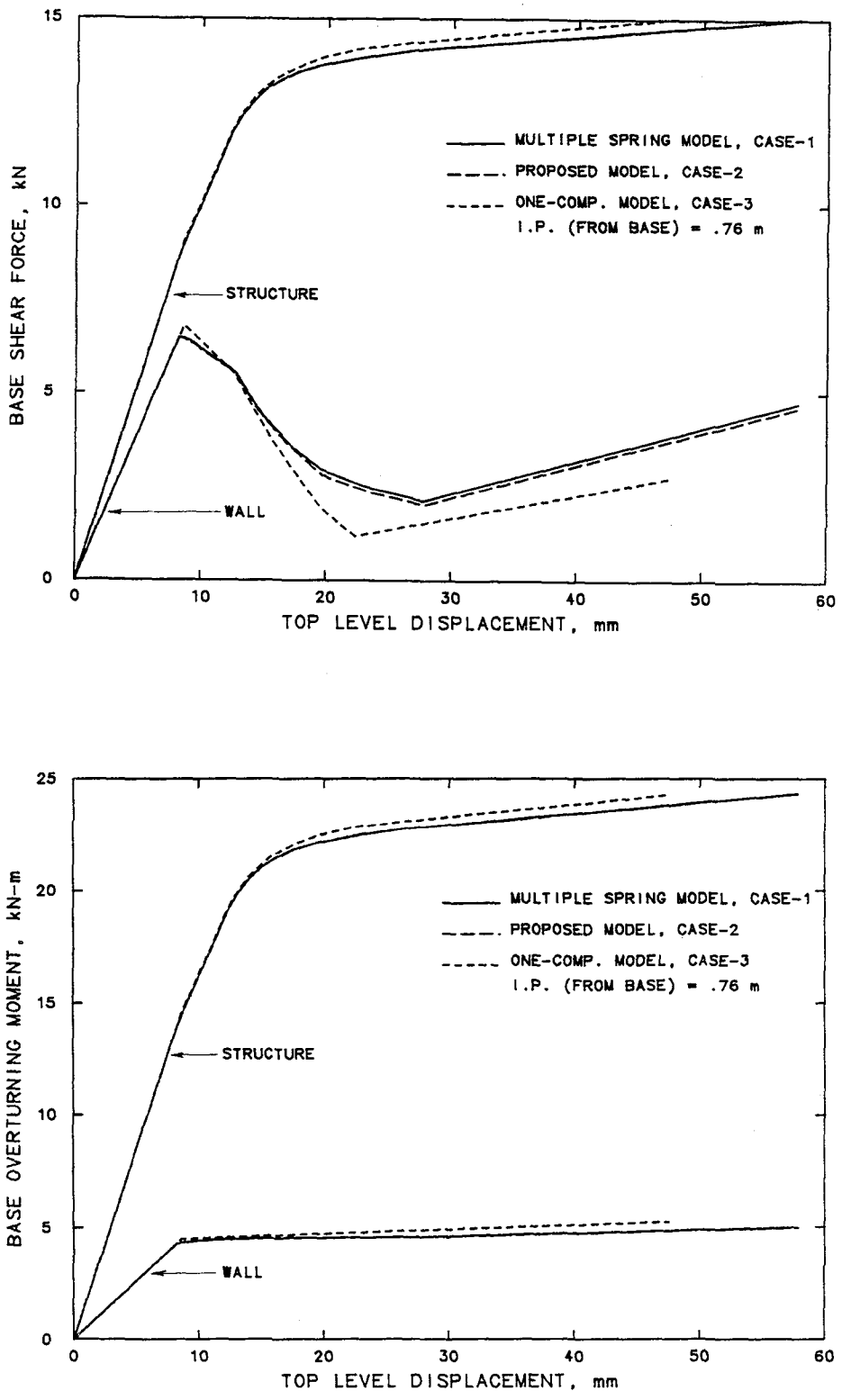

Fig. 5.36 Force-Top Level Displacement Relation of Structure-3 Under Monotonically Increasing Load

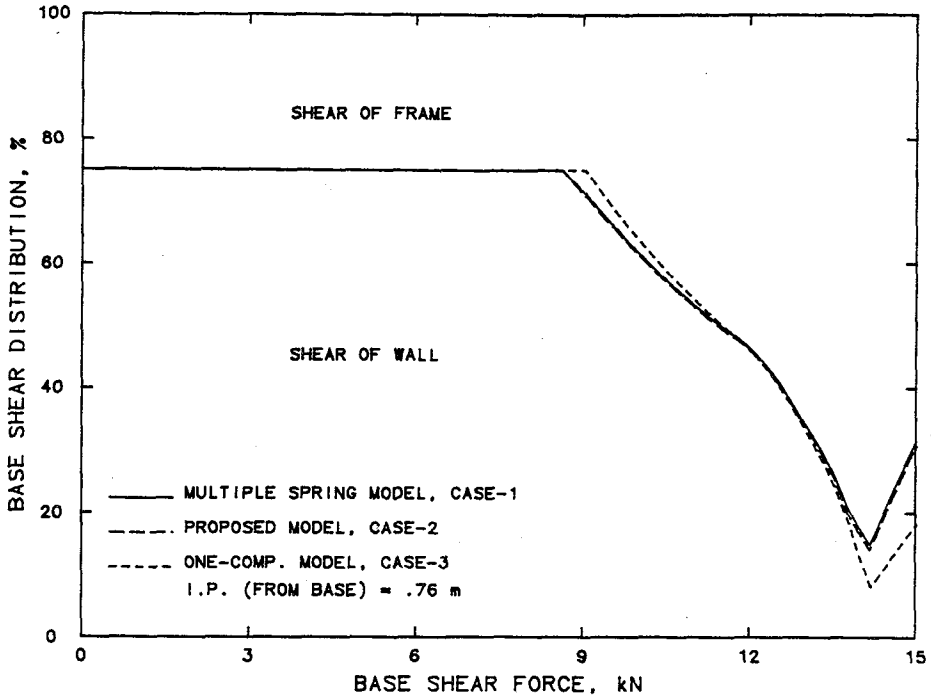

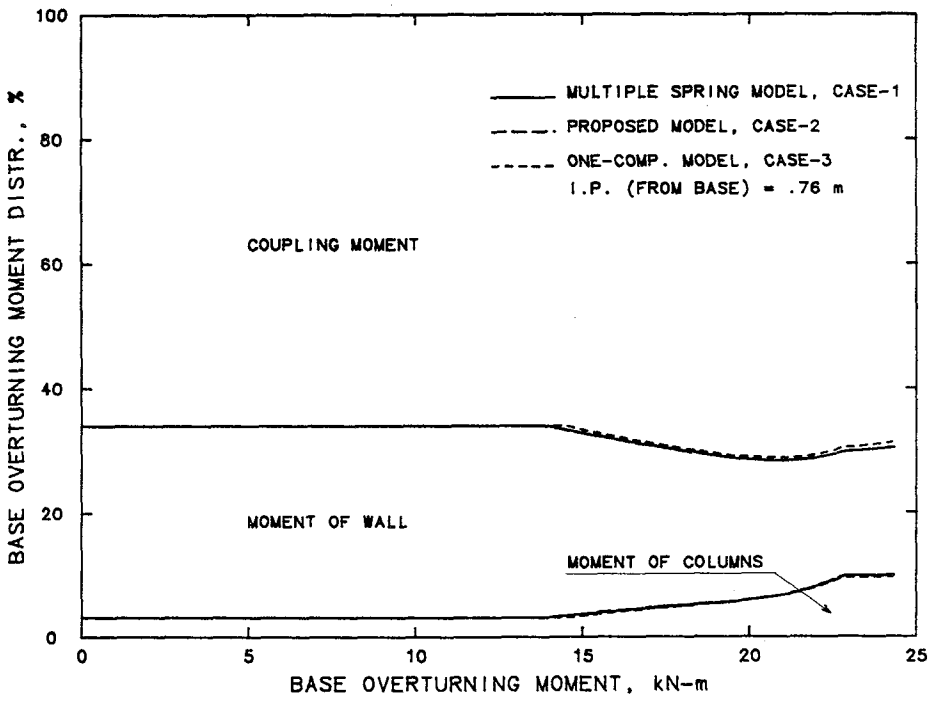

Fig. 5.36 (Continued)

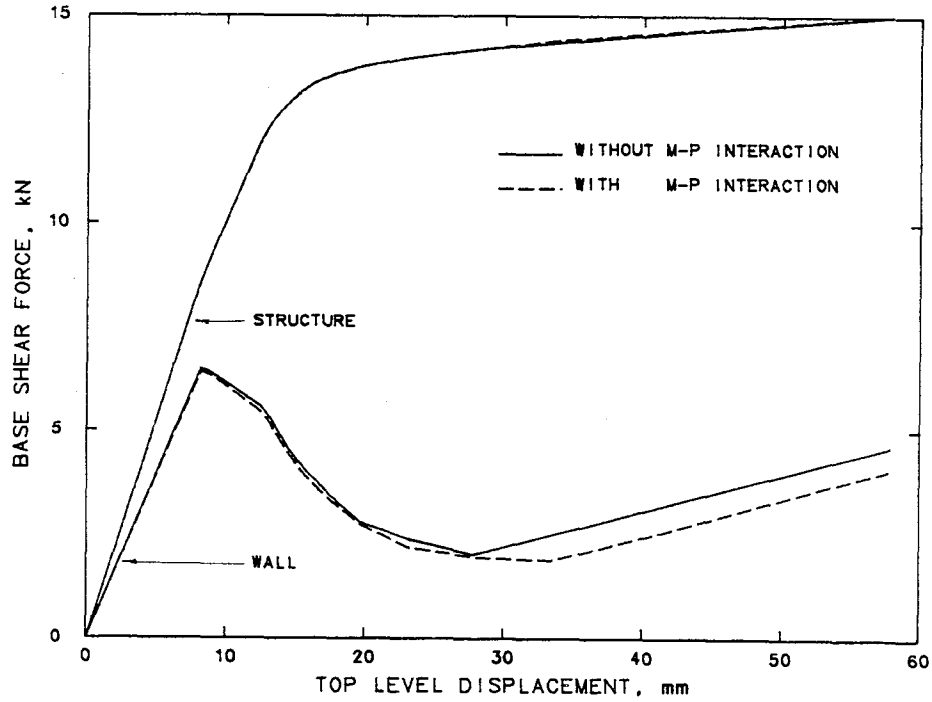

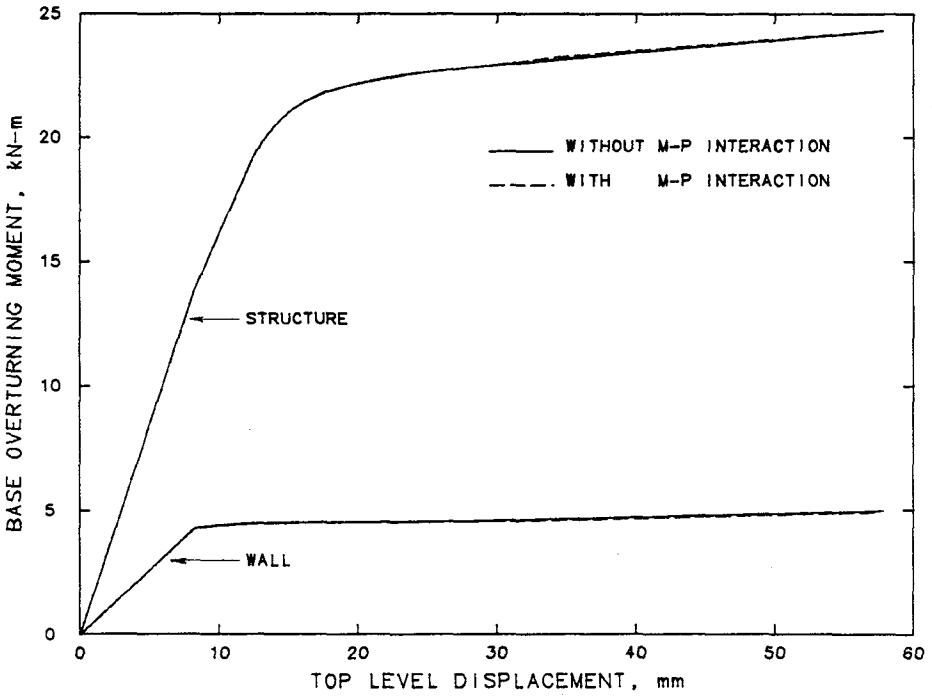

Fig. 5.37 M-P Effects, Force-Top Level Displacement Relations of Structure-3

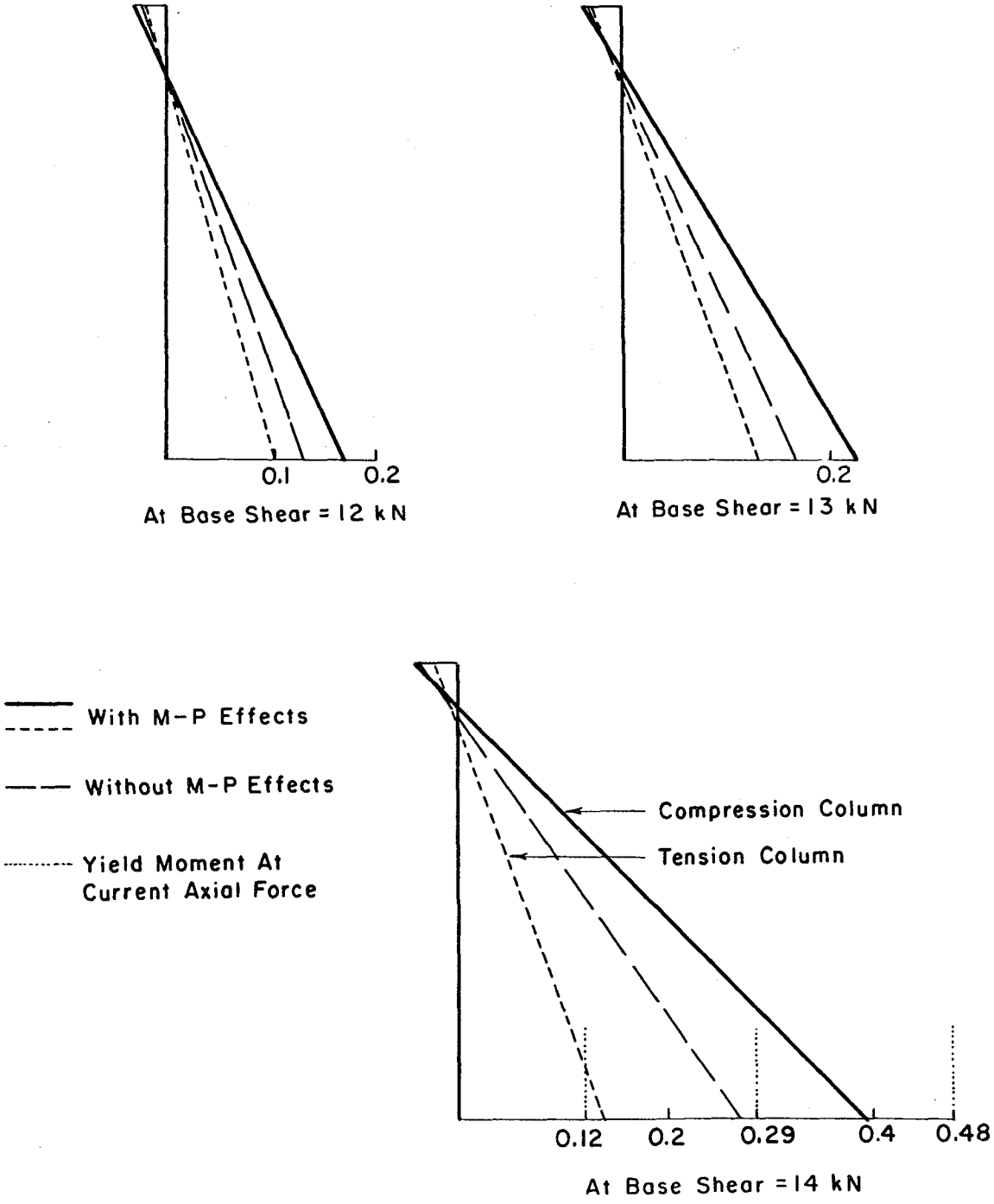

Fig. 5.38 M-P Effects, Bending Moments of the First Story Columns

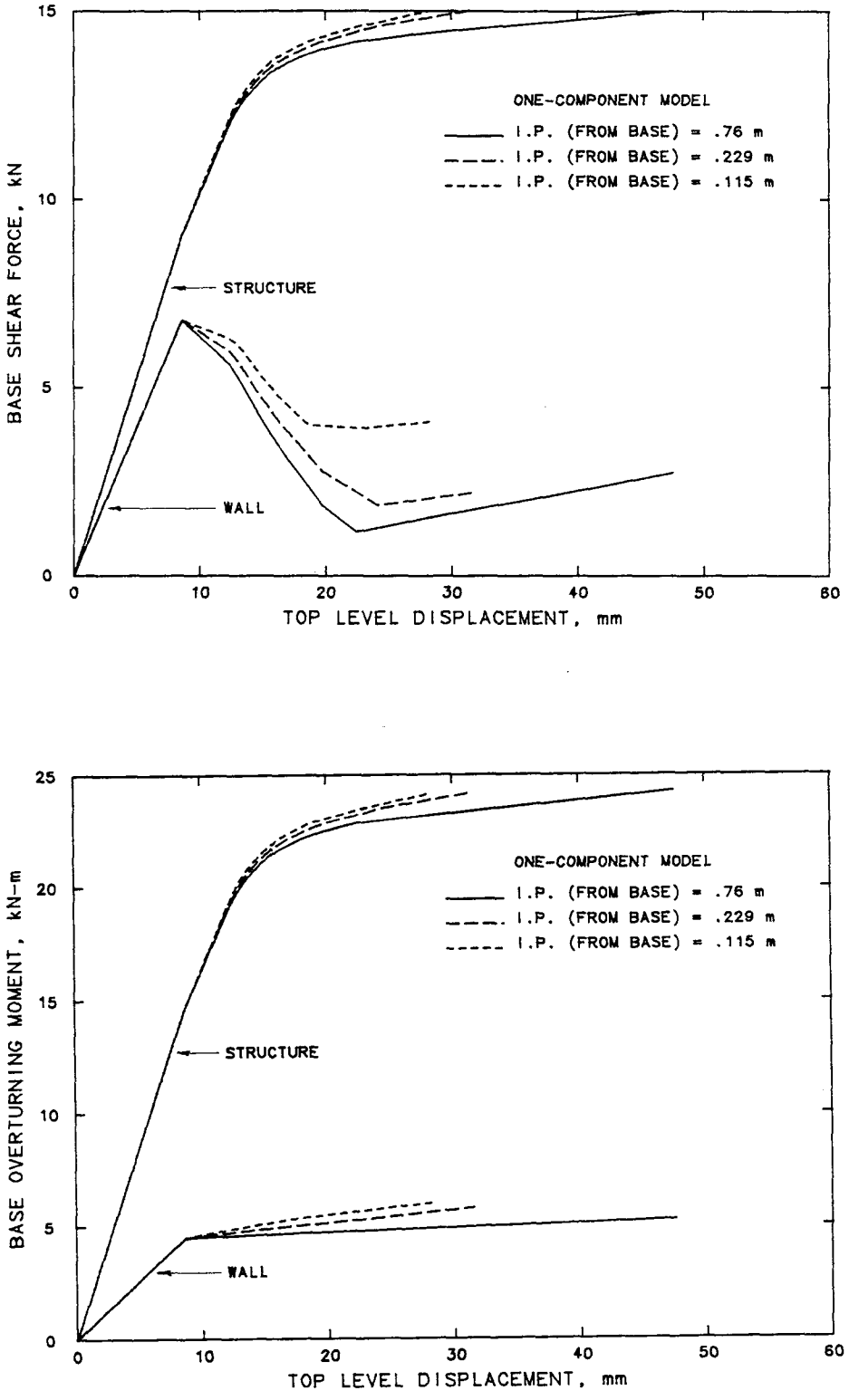

Fig. 5.39 Wall Modeling Effects, Force-Top Level Displacement Relations of Structure-3

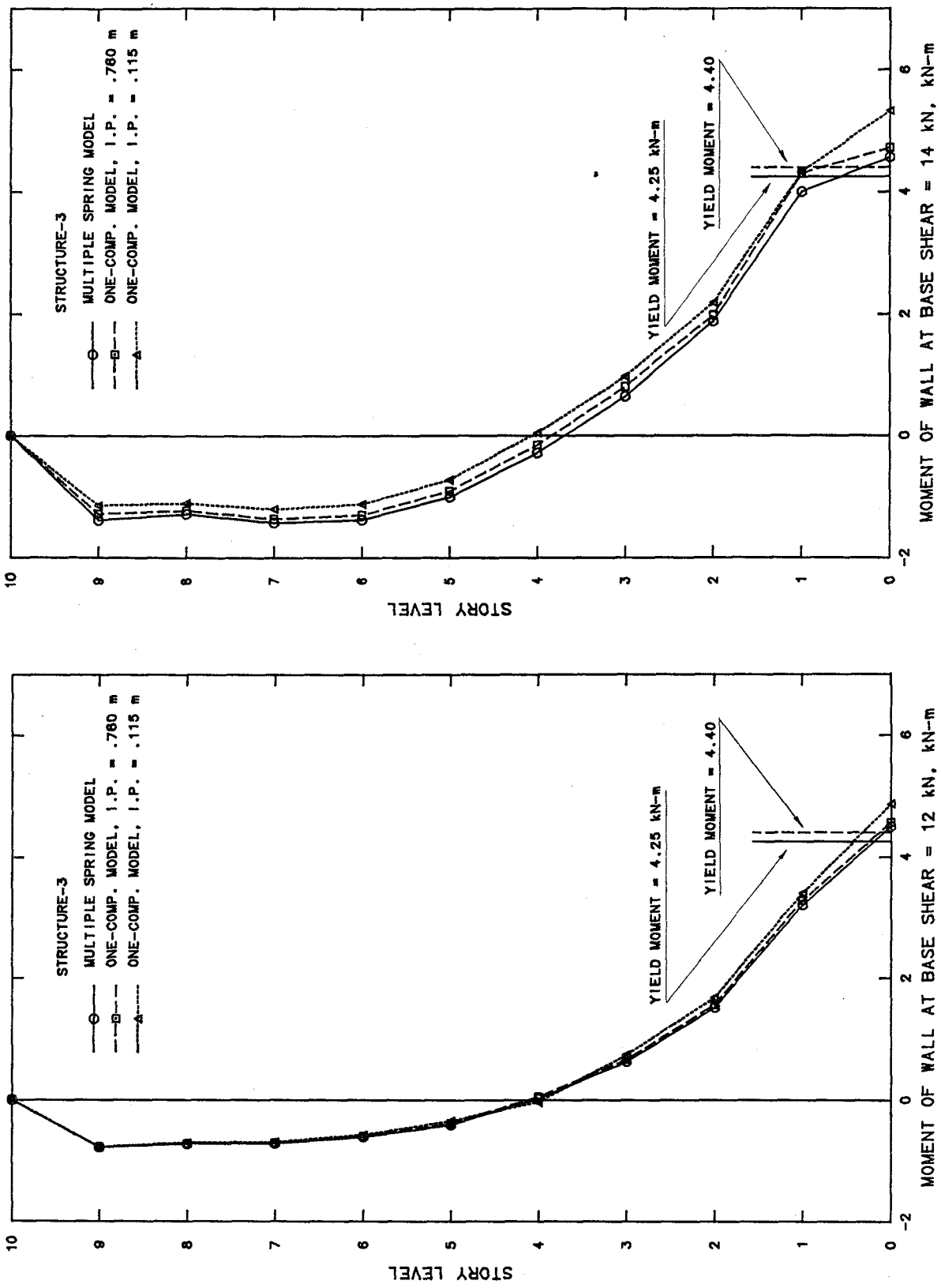

Fig. 5.40 Wall Modeling Effects, Bending Moment of the Shear Wall, kN-m

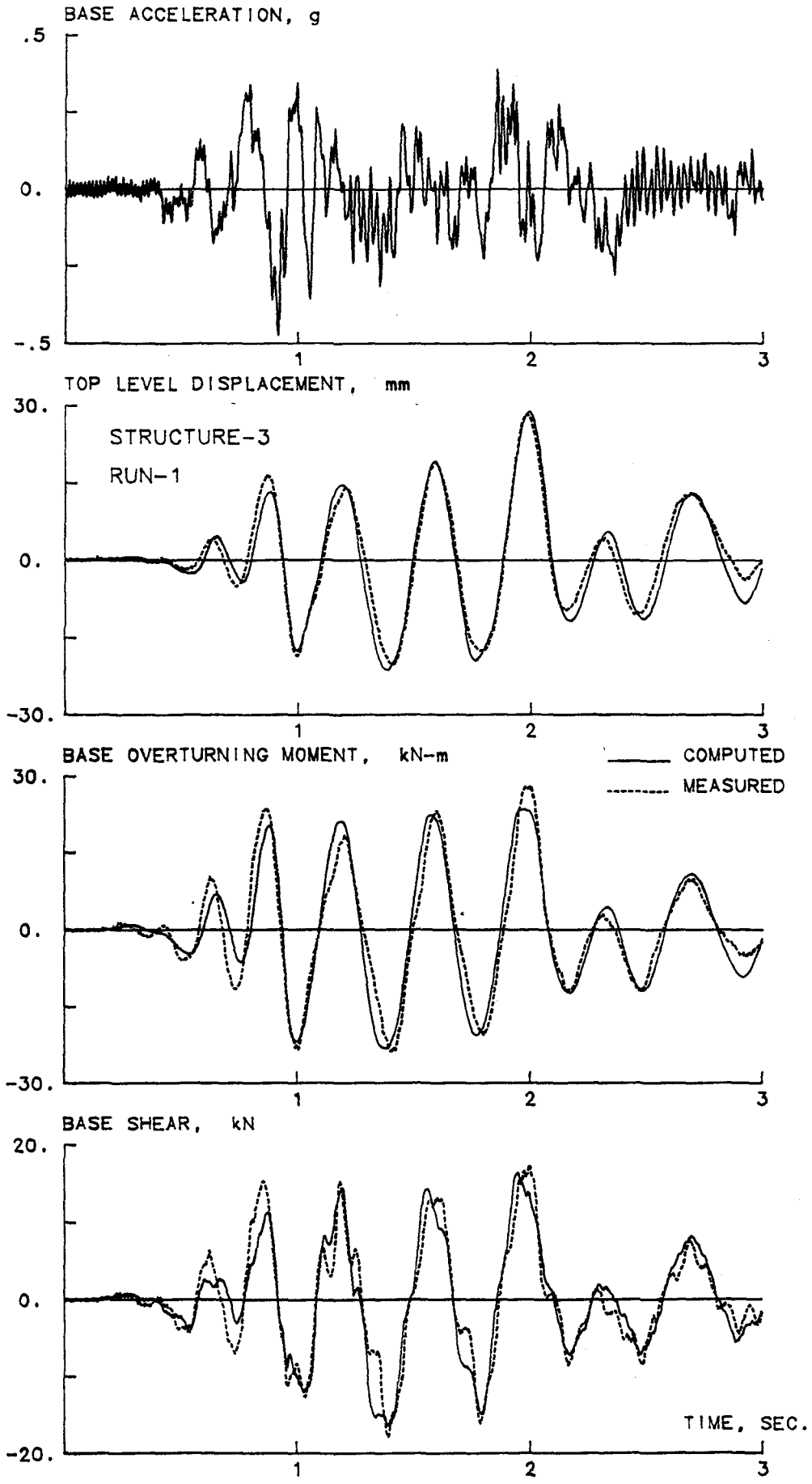

Fig. 5.41 Response Waveforms of Structure-3, Run-1

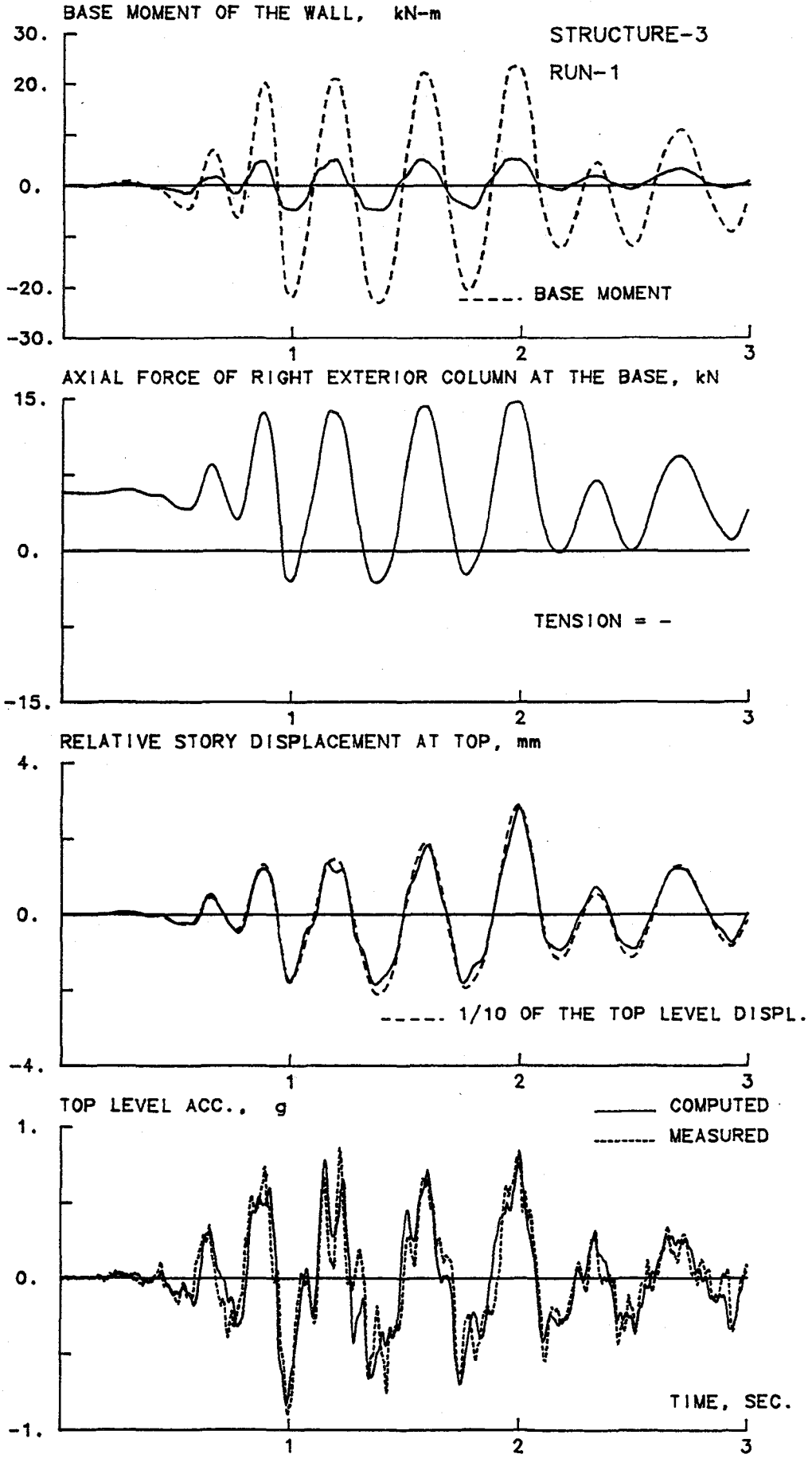

Fig. 5.41 (Continued)

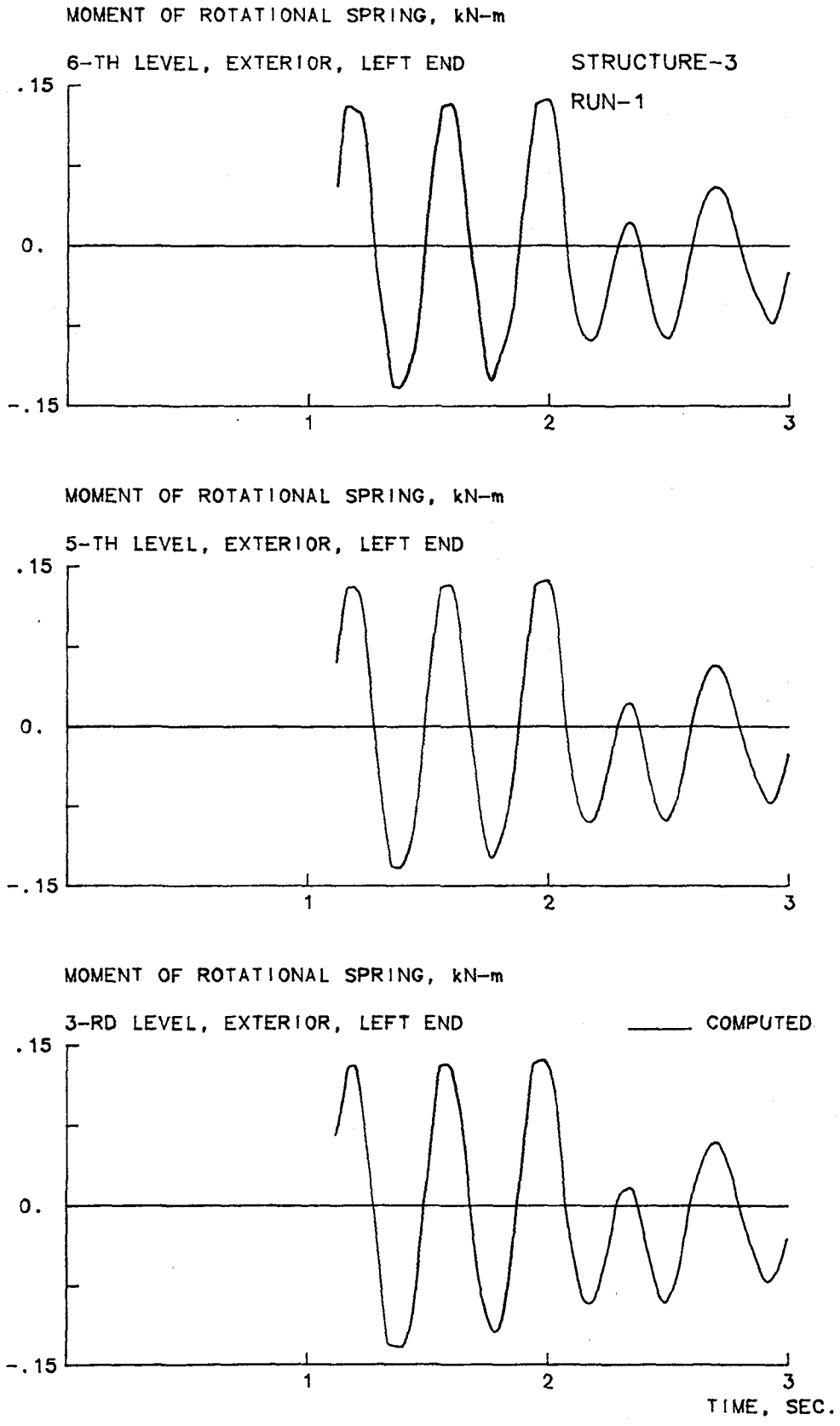

Fig. 5.41 (Continued)

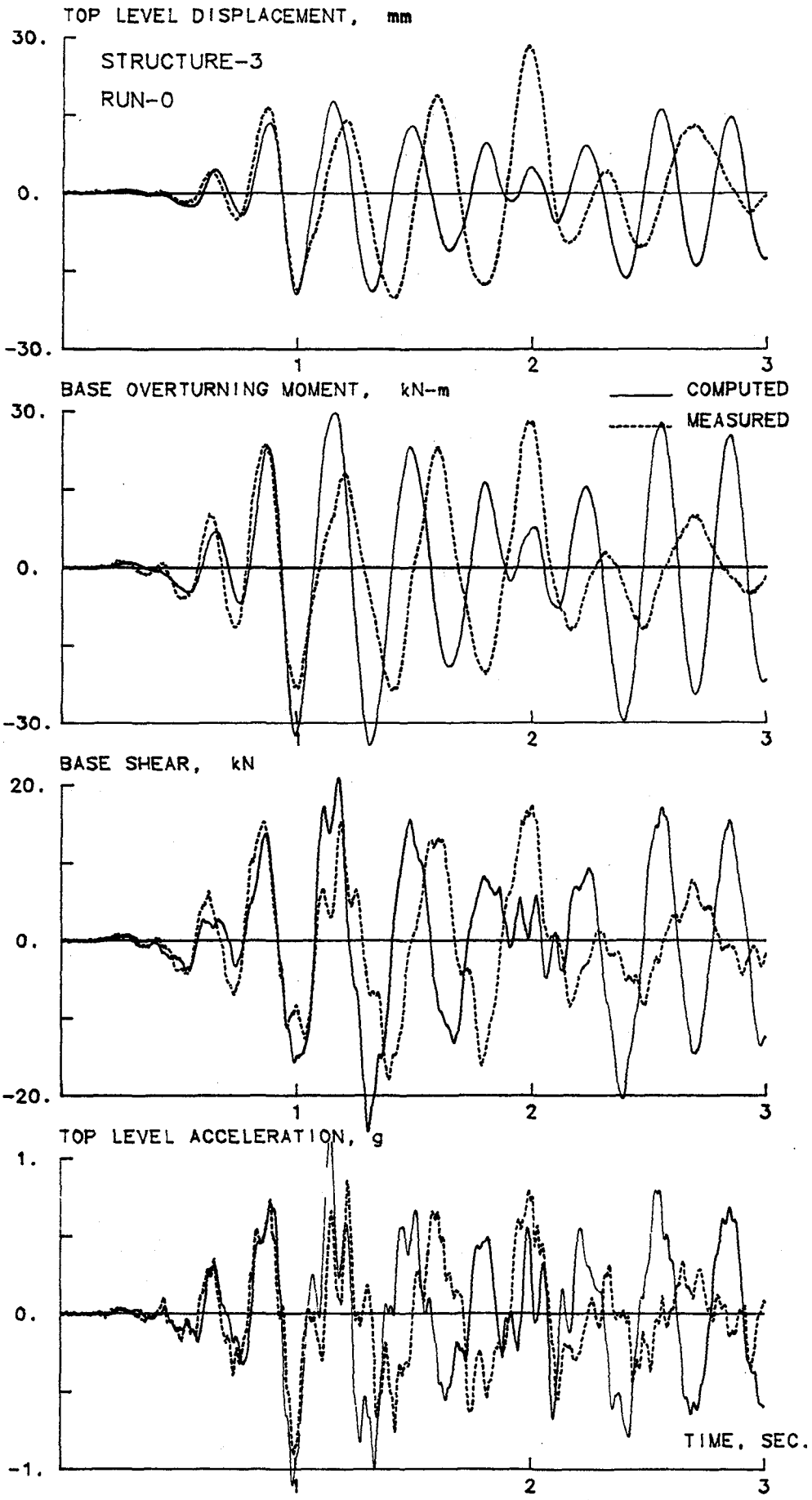

Fig. 5.42 Response Waveforms of Structure-3, Elastic Analysis

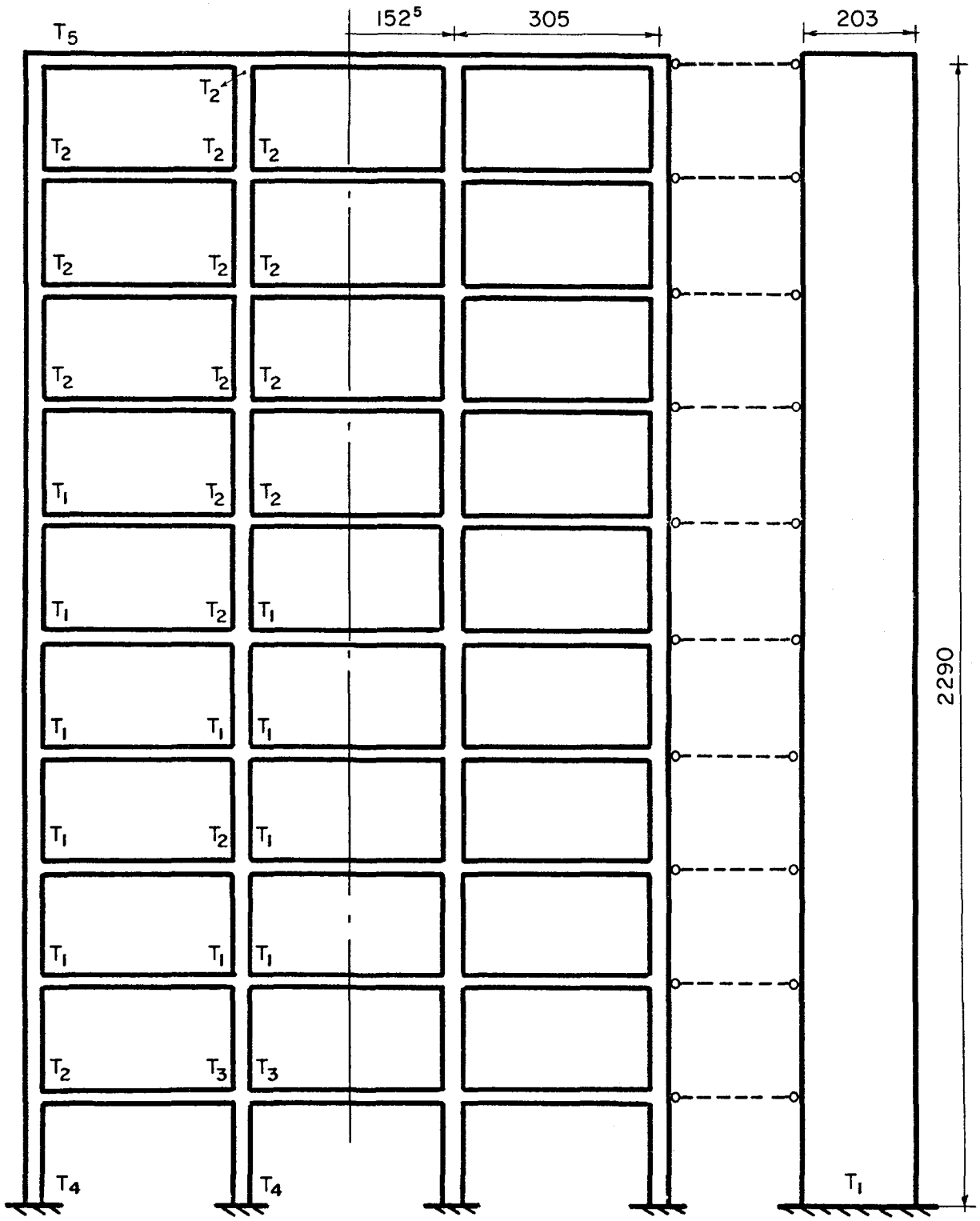

T_1 = 0.84 – 0.88 sec. T_4 = 1.35 - 1.38 sec.

T_2 = 0.97 – 1.00 sec. T_5 = 1.96 sec.

T_3 = 1.18 sec.

Fig. 5.43 Order of Yielding of Structure-3

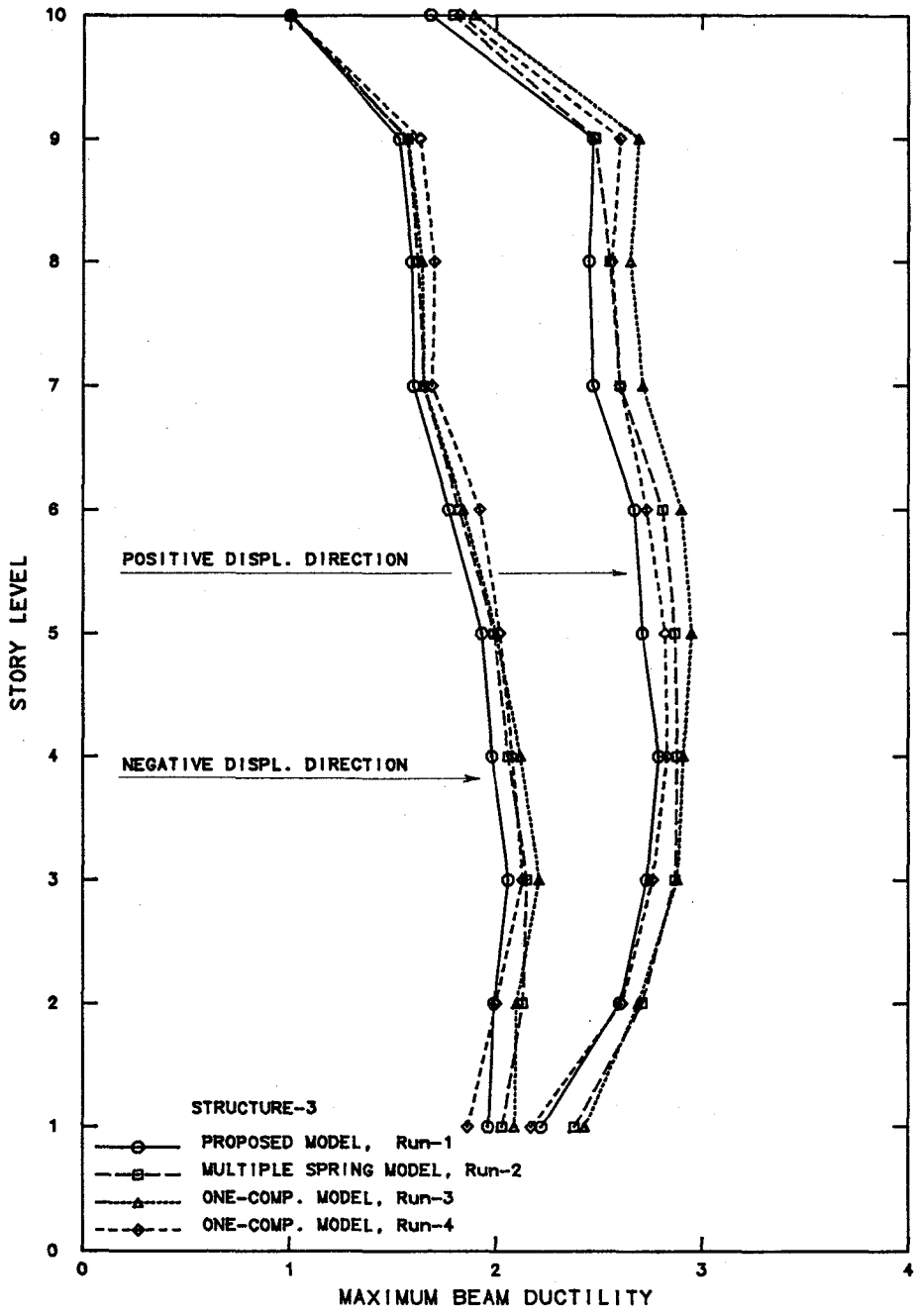

Fig. 5.44 Envelopes of Maximum Rotation Ductility Factors of Beams for Different Runs

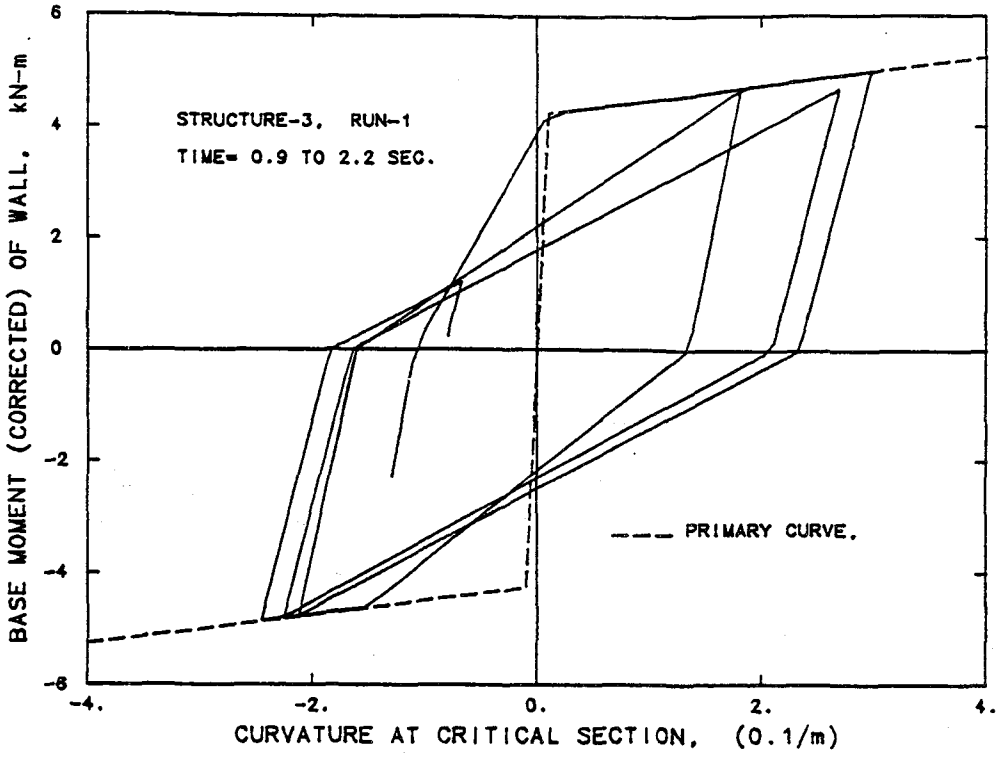

Fig. 5.45 Hysteresis Loops of Wall Element at the Base in Run-1

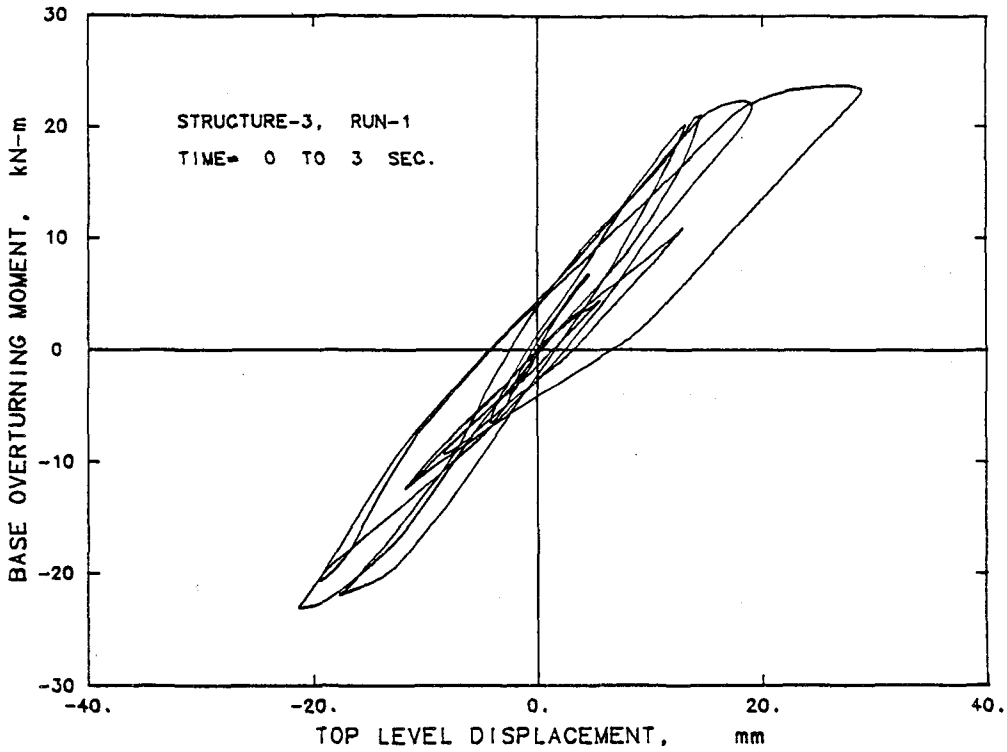

Fig. 5.46 Computed Response History of Base Moment-Top Displacement Relationship of Structure-3

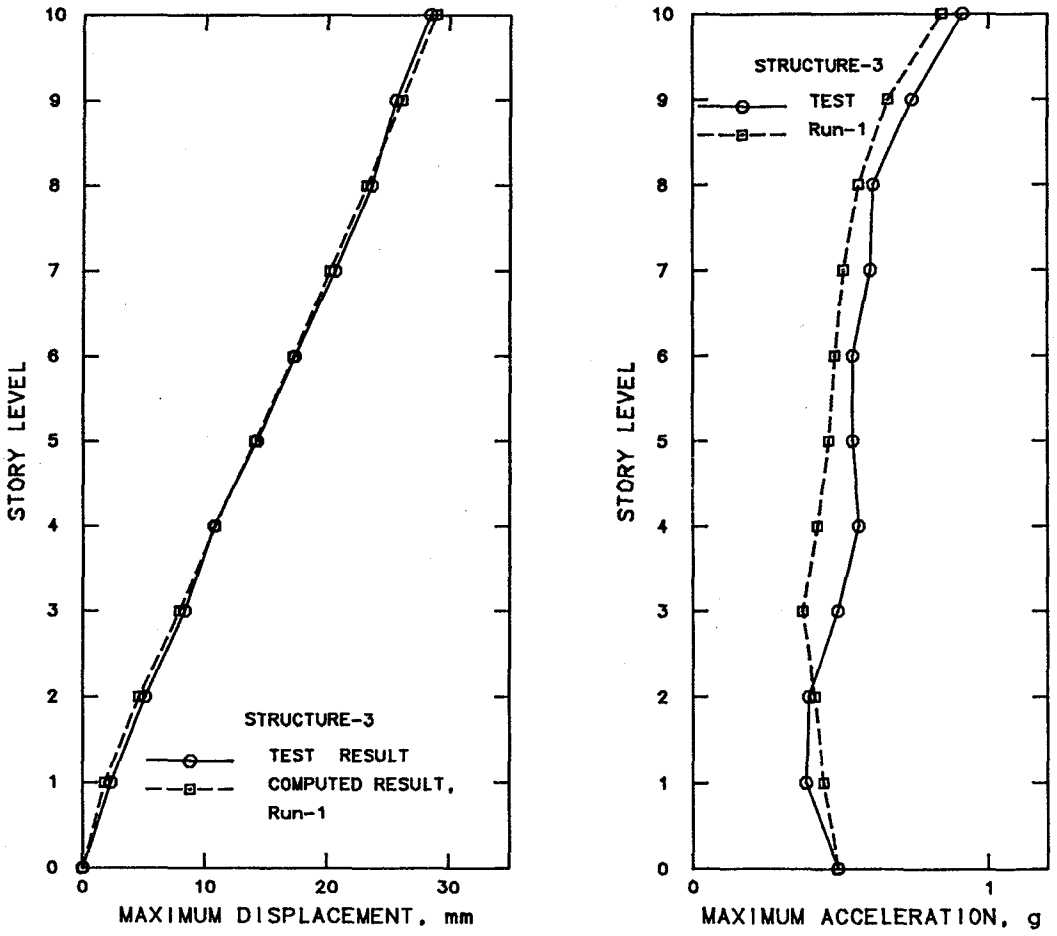

Fig. 5.47 Maximum Responses of Structure-3, Run-1

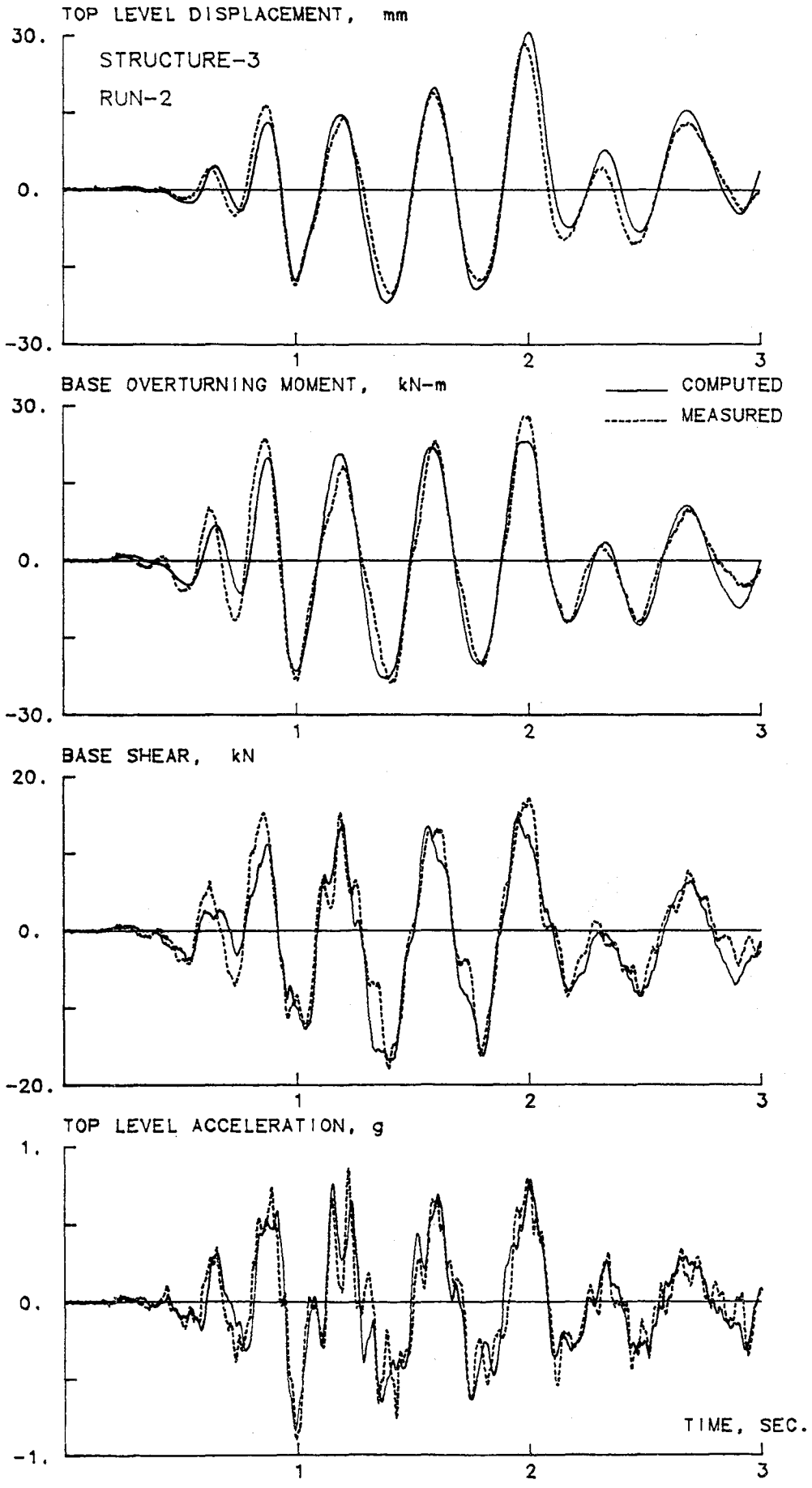

Fig. 5.48 Response Waveforms of Structure-3, Run-2

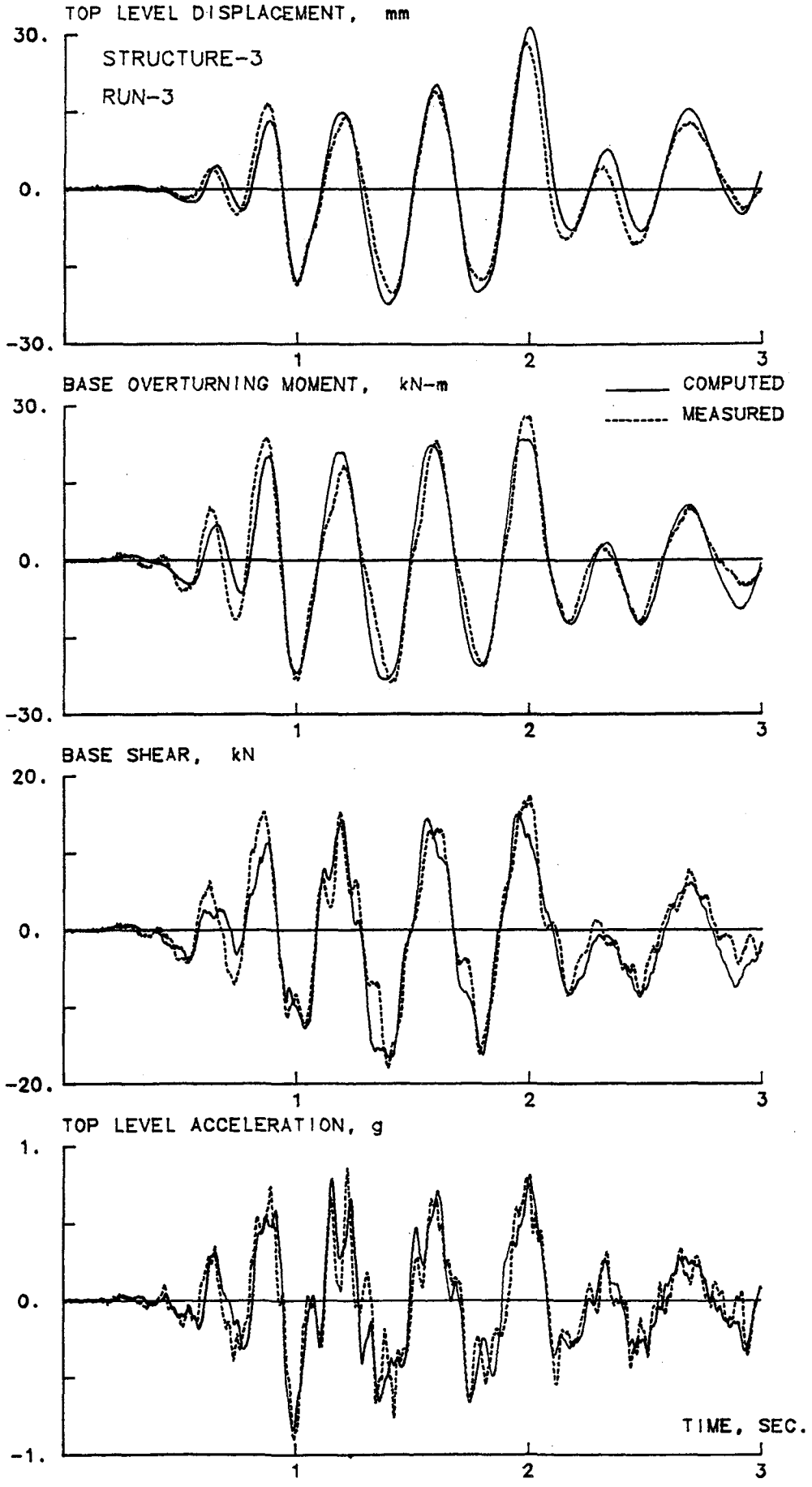

Fig. 5.49 Response Waveforms of Structure-3, Run-3

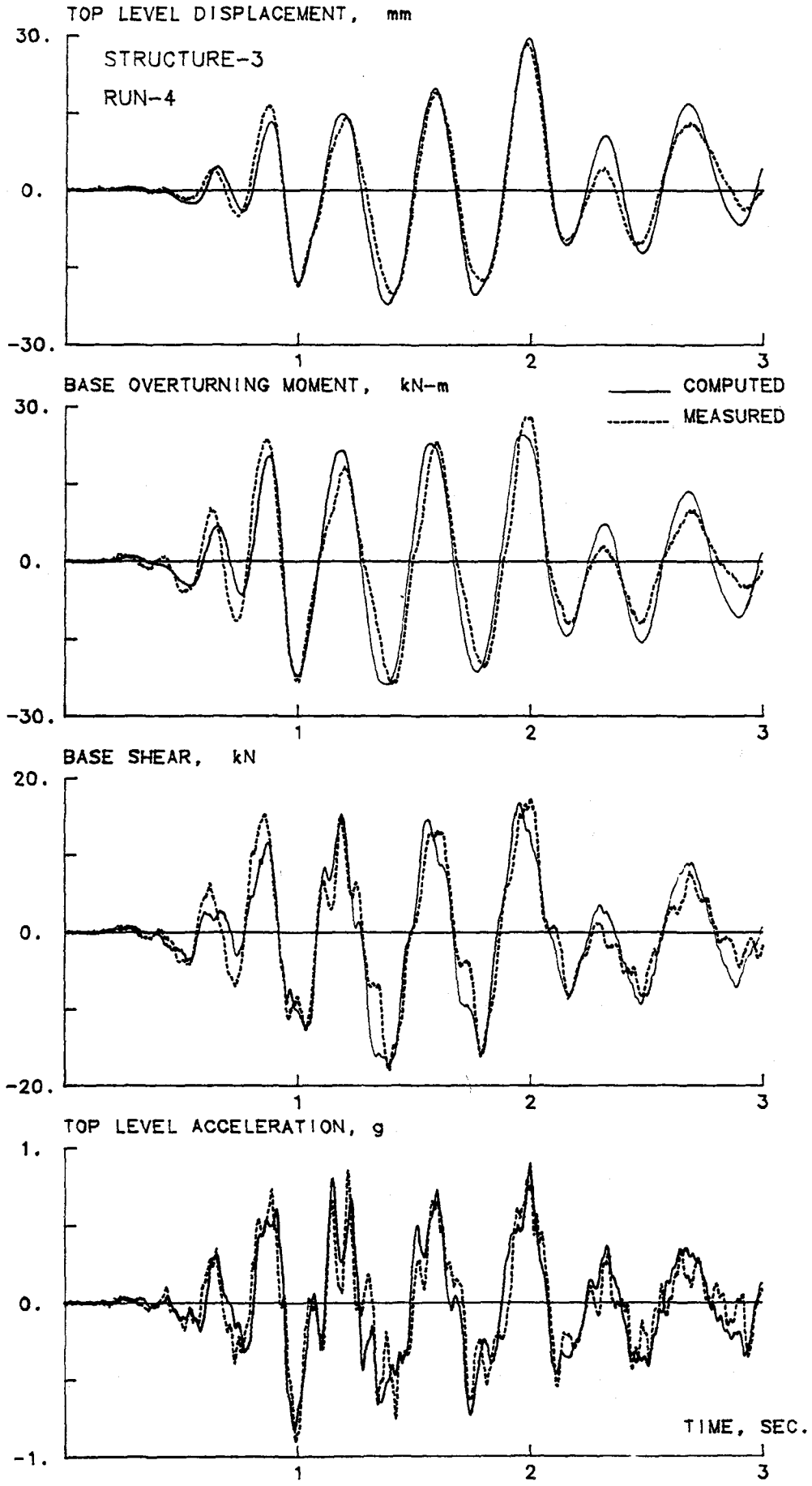

Fig. 5.50 Response Waveforms of Structure-3, Run-4

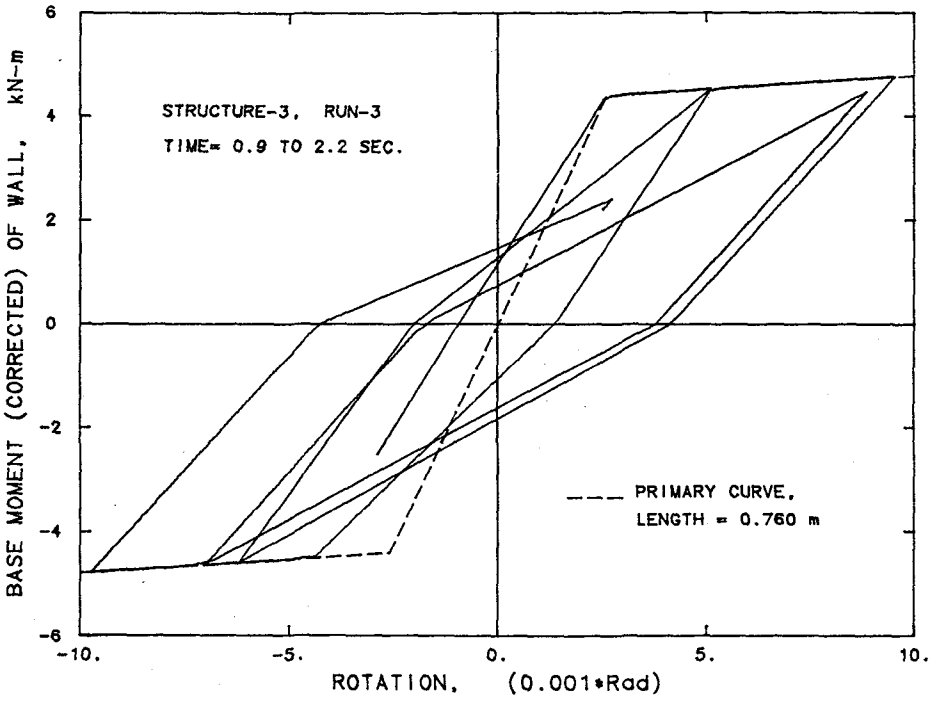

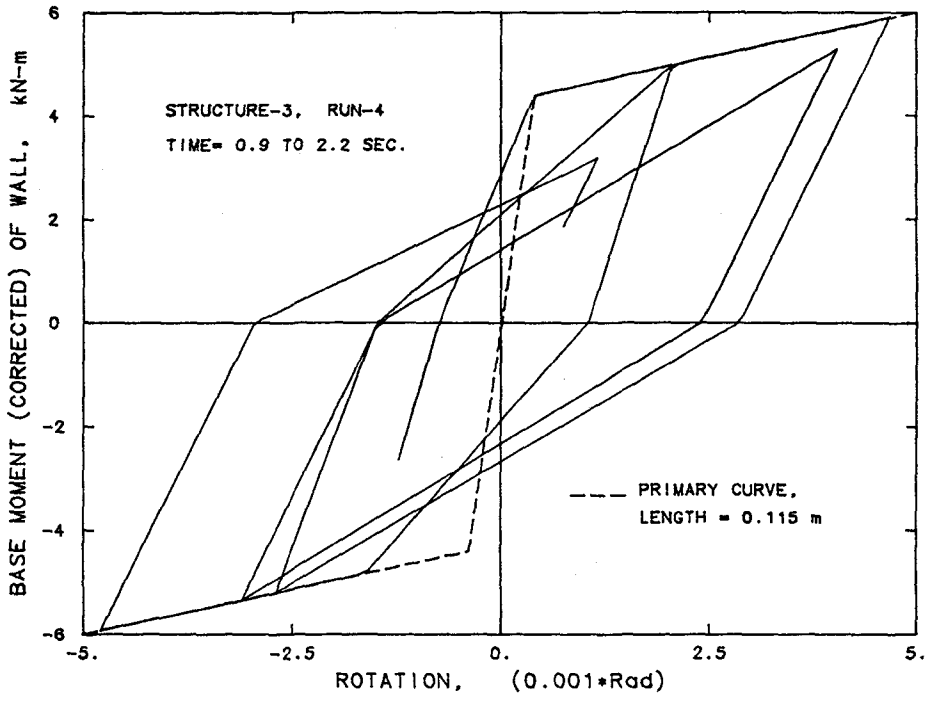

Fig. 5.51 Moment-Flexural Rotation Relations at the Base of the Wall in Run-3 and Run-4

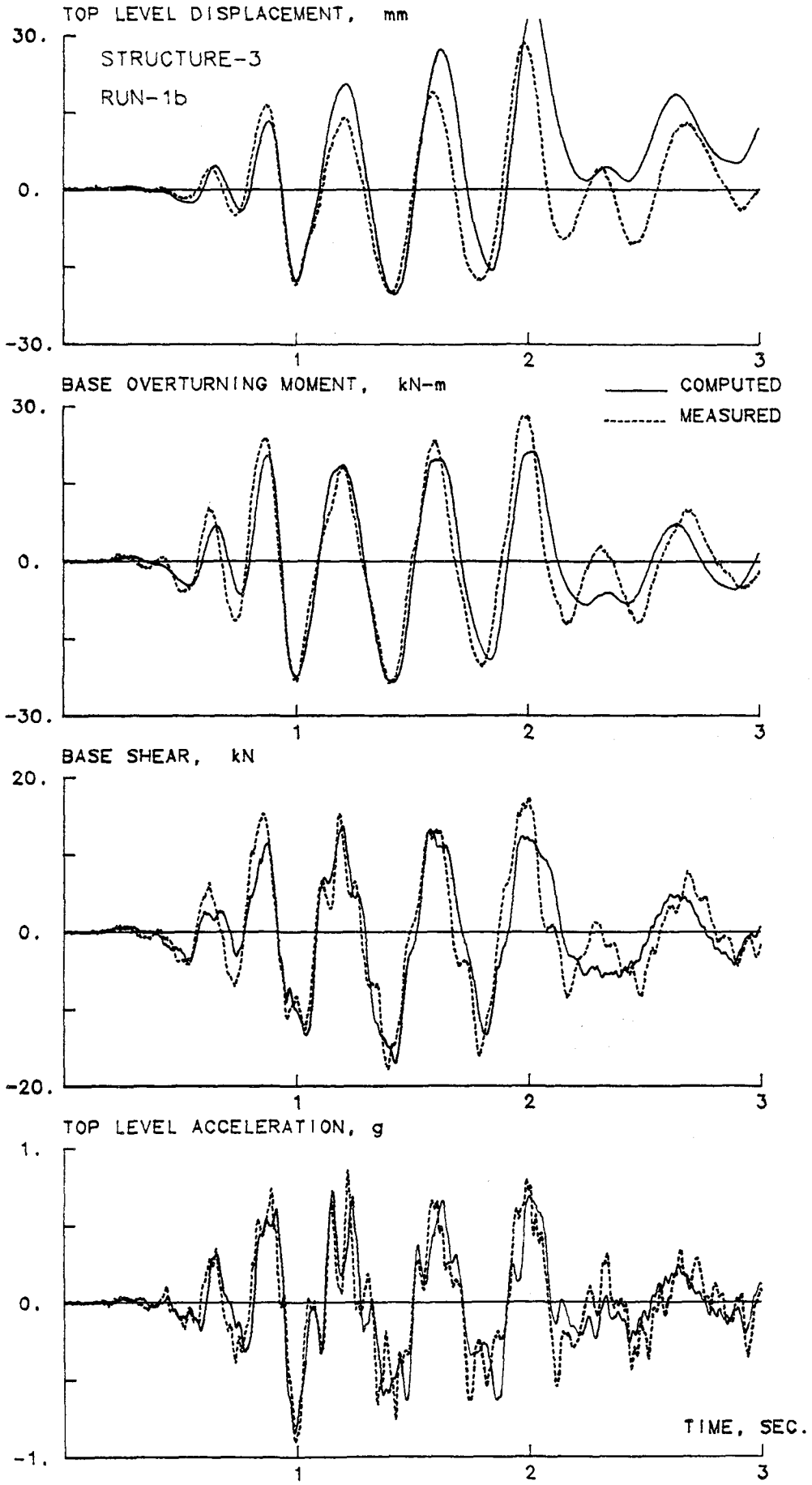

Fig. 5.52 Response Waveforms of Structure-3, Run-1b

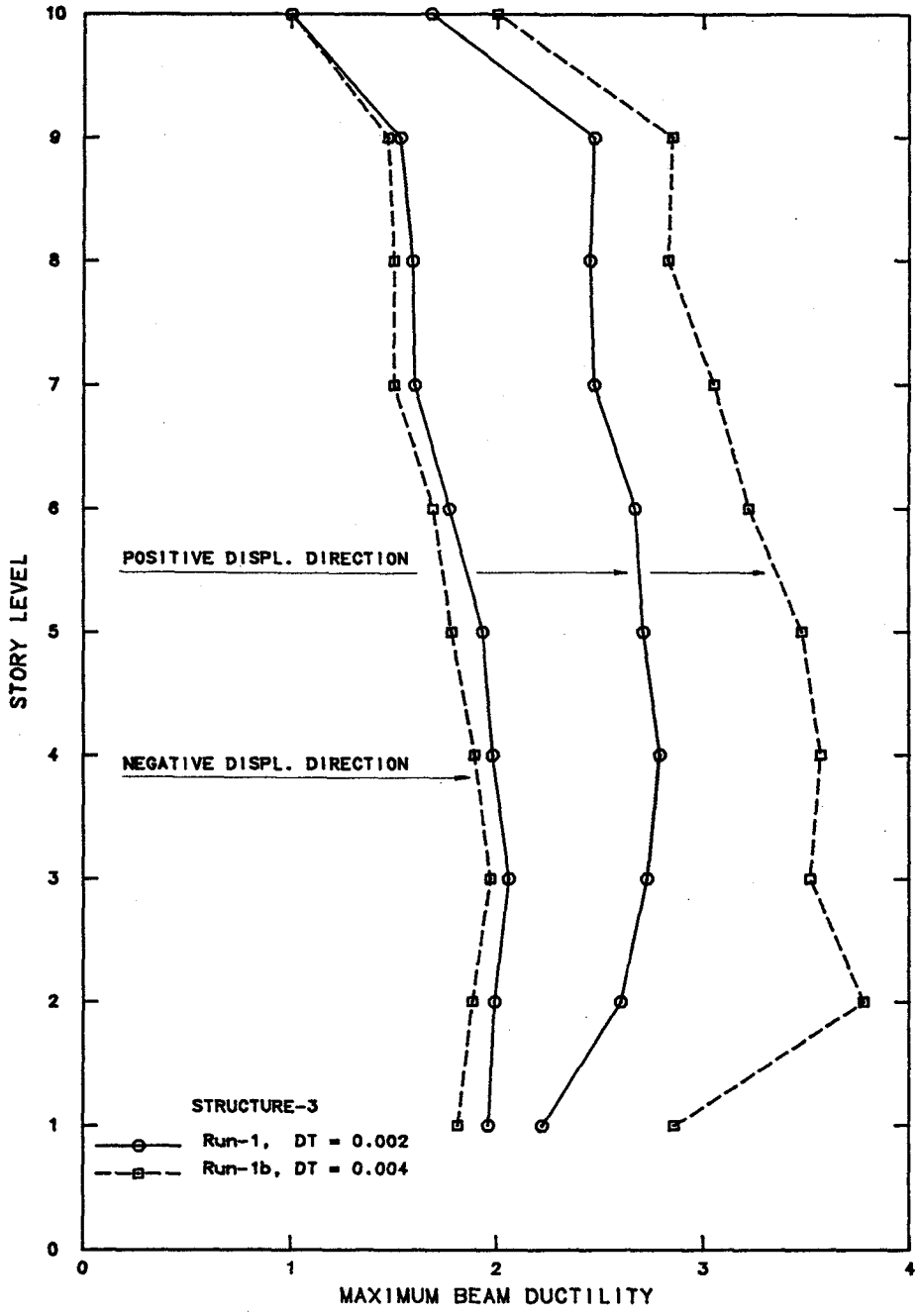

Fig. 5.53 Envelopes of Maximum Rotation Ductility Factors of Beams for Run-1 and Run-1b

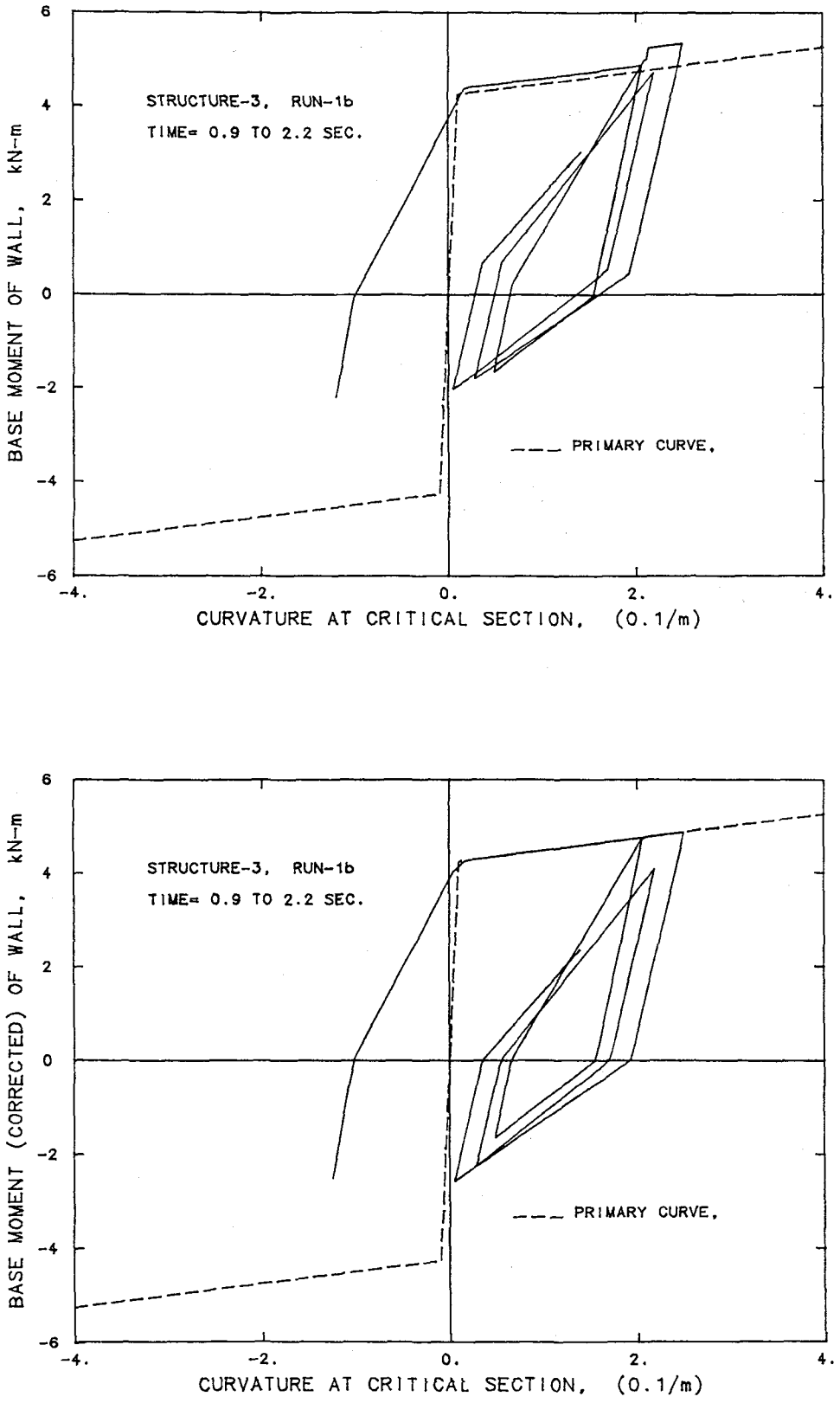

Fig. 5.54 Hysteresis Loops of Wall Element at the Base in Run-1b

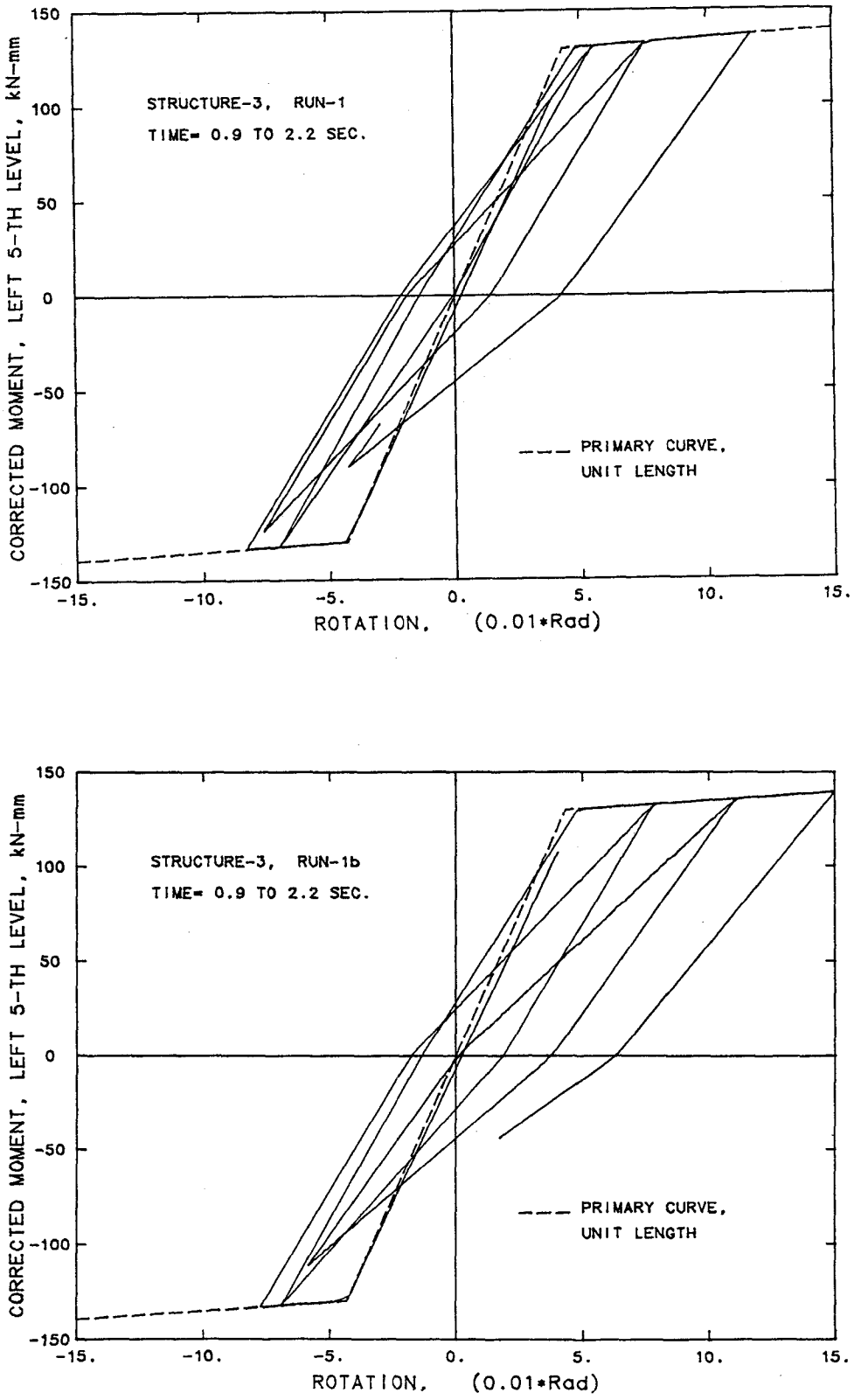

Fig. 5.55 Moment-Rotation Relations of the Left-End Fifth-Level Beam Rotational Spring of Structure-3

APPENDIX A

CALCULATIONS OF COLUMN SECTION STIFFNESS PROPERTIES

The detailed procedures for evaluating the column section stiffness properties are discussed in this Appendix. The values, $\frac{\partial M}{\partial \phi}$ and $\frac{\partial M}{\partial n}$, which are employed in Eq. 2.6 of Section 2.3.1 are calculated here based on several assumptions.

A.1 Value of $\frac{\partial M}{\partial \phi}$

The value of $\frac{\partial M}{\partial \phi}$ is the slope of the moment-curvature curve with a constant axial force acting on the section. Actually the axial force acting on the section of a column element does not remain constant but rather is subjected to change during the loading process. Due to this changing of axial force, the moment-curvature curve can be considered to undergo continual shifts from one moment-curvature curve to another. Therefore, the modified section stiffness, which is a transition slope from one $M-\phi$ curve to another, can not be evaluated from a single hysteresis model. A single primary force-deformation curve is required in the most available hysteresis models.

To overcome this deficiency, a force-deformation curve for a specified axial force is chosen as the basis for the primary curve of the hysteresis loop. The initial axial load, or an assumed average axial force, for the element is considered as the specified axial force around which the primary curve is constructed.

The procedure for calculating the location of a point on the primary curve associated with the present loading level is illustrated in Fig. A.1. Let us assume that at the end of a loading stage, point A is obtained. At point A, the section has specific values of moment, m, axial force, n, and

curvature, ϕ. However, all points on this moment-curvature curve correspond to the axial load n. To be able to develop curvature ϕ, while under a different axial force n_o, the section should be loaded with moment m_o which can be evaluated from the following expression:

$$m_o = m - \frac{\partial M}{\partial n}(n-n_o) \tag{A.1}$$

m_o : Moment on the primary curve, moment-curvature curve with axial force n_o;

m : Moment on the present curve, moment-curvature curve with axial force n;

The value of $\frac{\partial M}{\partial \phi}$ for an arbitrary moment and axial force can be established by modifying the slope of primary moment-curvature curve.

$$\frac{\partial M}{\partial \phi} = \left(\frac{\partial M}{\partial \phi}\right)_o \left[1 + \frac{\Delta\left(\frac{\partial M}{\partial n}\right)(n-n_o)}{\Delta m_o}\right] \tag{A.2}$$

$\left(\frac{\partial M}{\partial \phi}\right)_o$: Slope of primary moment-curvature curve at present loading stage;

$\Delta\left(\frac{\partial M}{\partial n}\right)$: Increment of $\frac{\partial M}{\partial n}$ at present loading stage;

Δm_o : Increment of moment at present loading stage on primary curve.

A.2 Value of $\frac{\partial M}{\partial n}$

The value of $\frac{\partial M}{\partial n}$ is the slope of the moment-axial force (M-P) curve for a section corresponding to a constant curvature. A series of contours of equal curvature of M-P relations for a column section are shown in Fig. A.3, (only a portion of the curves which are around zero axial force are shown in

Fig. A.3). Each curve defines those combinations of moment and axial force which will result in a given curvature. There are an infinite number of such M-P curves corresponding to different values of curvatures.

In order to considerably simplify the task of determining the value of $\frac{\partial M}{\partial n}$, it is assumed that $\frac{\partial M}{\partial n}$ is only a linear function of moment level. Furthermore, it is also assumed that the yielding curvature is constant regardless of the axial force level on the section. Hence, the value of $\frac{\partial M}{\partial n}$ at an arbitrary point on the hysteresis loop can be evaluated by linearly interpolating between the values of $\frac{\partial M}{\partial n}$ at zero moment and at yield moment, Fig. A.2. Because the yielding curvature is assumed to be constant regardless of the axial force level, the value of $\frac{\partial M}{\partial n}$ at the yield moment is equal to the slope of M-P interaction diagram, (slope of line AB in Fig. 2.5). The value of $\frac{\partial M}{\partial n}$ at zero moment is zero. After the yield level, the value of $\frac{\partial M}{\partial n}$ is considered to be constant and equal to the value at the yield moment.

In this procedure, whether the yield point has been exceeded or not can be checked either by referring to the hysteresis loop of the primary curve or by comparing the moment with the current yield moment.

A.3 Summary

Based on the foregoing assumptions, concepts involved in the procedure to evaluate the section properties such as; yield moment, $\frac{\partial M}{\partial \phi}$, and $\frac{\partial M}{\partial n}$ at an arbitrary moment, m, and axial force, n, take the form described below.

As the value of $\frac{\partial M}{\partial n}$ is considered to be a linear function of moment level, the yield moment as well as $\frac{\partial M}{\partial n}$ can be evaluated from Eqs. A.3 and A.4 (or A.5).

$$M_y = M_{yo} + \frac{\partial M_y}{\partial n}(n-n_o) = M_{yo}\,(1+C_4) \qquad (A.3)$$

$$\begin{cases} \dfrac{\partial M}{\partial n} = \dfrac{\partial M_y}{\partial n} * \dfrac{m_o}{M_{yo}} & m_o \leq M_{yo} \quad \text{(A.4.1)} \\ \dfrac{\partial M}{\partial n} = \dfrac{\partial M_y}{\partial n} & m_o \geq M_{yo} \quad \text{(A.4.2)} \end{cases}$$

or

$$\begin{cases} \dfrac{\partial M}{\partial n} = \dfrac{\partial M_y}{\partial n} * \dfrac{m}{M_y} & m \leq M_y \quad \text{(A.5.1)} \\ \dfrac{\partial M}{\partial n} = \dfrac{\partial M_y}{\partial n} & m \geq M_y \quad \text{(A.5.2)} \end{cases}$$

where

$\dfrac{\partial M_y}{\partial n}$: Slope of line AB in the yield moment-axial interaction diagram as shown in Fig. 2.5;

n : Axial force on the section (compression is positive);

n_o : Axial force for which the primary curve is evaluated;

M_{yo} : Yield moment of the primary moment-curvature curve;

M_y : Yield moment of the section at current axial force, n;

m_o : Corresponding moment on the primary moment-curvature curve.

and C_4 is defined as follows:

$$C_4 = \frac{\partial M_y}{\partial n} * \frac{n-n_o}{M_{yo}} \quad \text{(A.6)}$$

The value of moment in the primary moment-curvature curve, m_o can be evaluated from equation A-1 or based on the assumptions in this section from the following Eqs. A.7:

$$\begin{cases} m_o = \dfrac{m}{1+C_4} & m \leq M_y \quad \text{(A.7.1)} \\ m_o = m - C_4 * M_{yo} & m \geq M_y \quad \text{(A.7.2)} \end{cases}$$

Finally, the slope of moment-curvature curve under current axial force, $\frac{\partial M}{\partial \phi}$, is related to the slope of the primary moment-curvature curve, $(\frac{\partial M}{\partial \phi})_o$, by the expression:

$$\begin{cases} \frac{\partial M}{\partial \phi} = (\frac{\partial M}{\partial \phi})_o \ (1+C_4) & m \leq M_y \qquad \text{(A.8.1)} \\ \frac{\partial M}{\partial \phi} = (\frac{\partial M}{\partial \phi})_o & m \geq M_y \qquad \text{(A.8.2)} \end{cases}$$

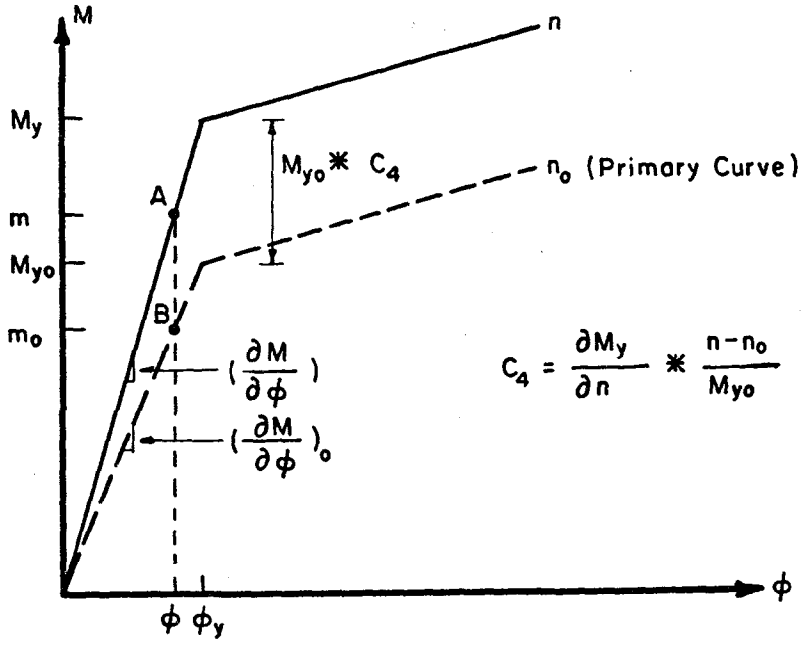

Fig. A.1 Primary Curve for Hysteresis Loops of a Column Member Section

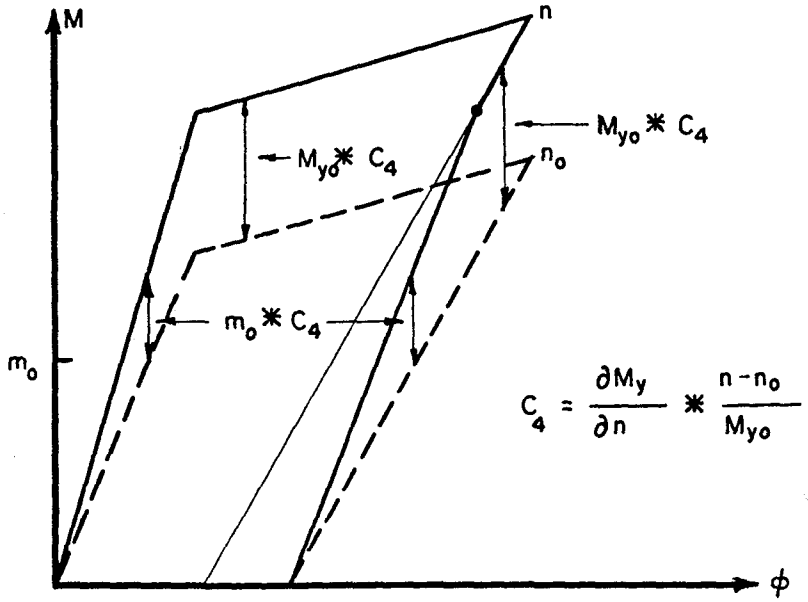

Fig. A.2 Evaluation of $\partial M/\partial n$ for Hysteresis Loops of a Column Member Section

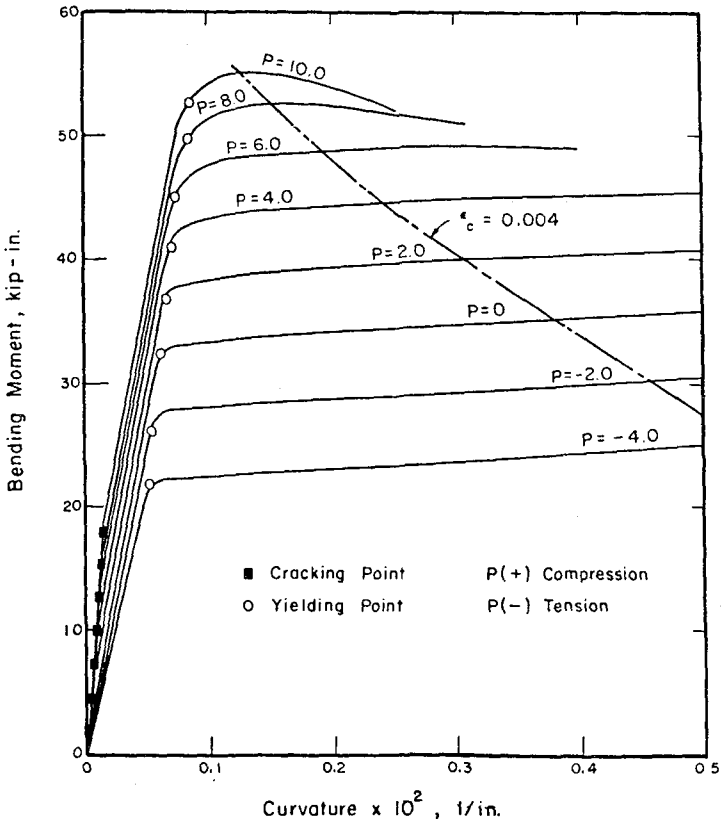

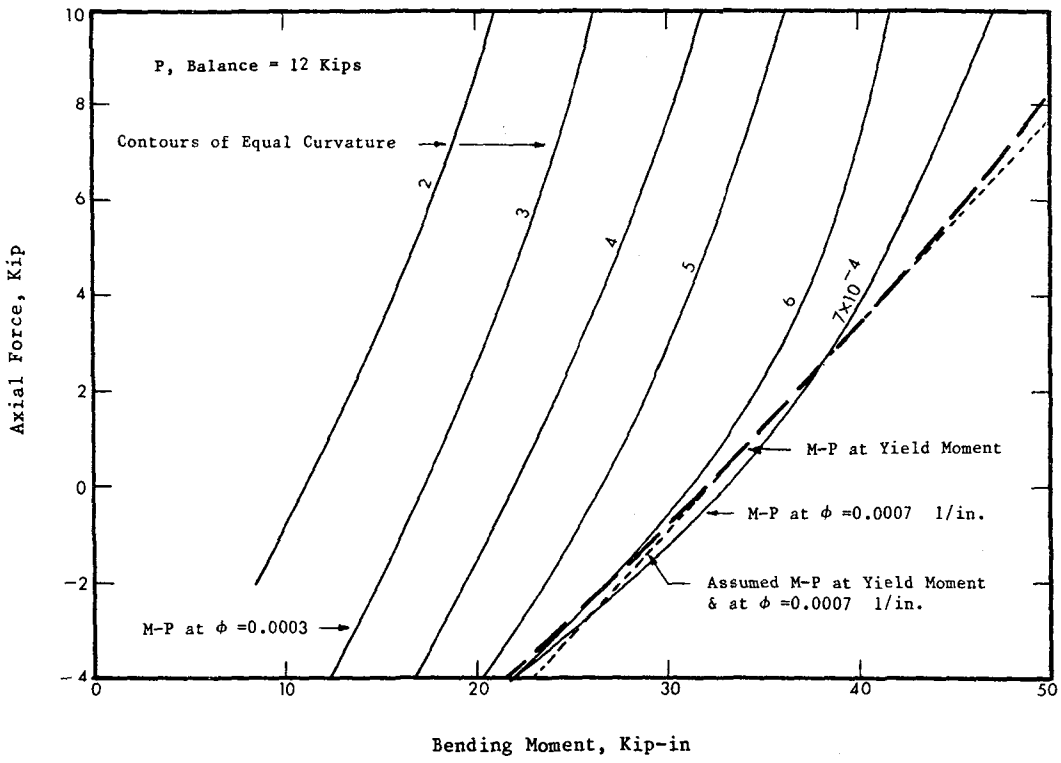

Fig. A.3 Axial Force-Bending Moment-Curvature Relationships of a Column Member Section

APPENDIX B

CALCULATIONS OF COLUMN ELEMENT STIFFNESS MATRIX

The purpose of this Appendix is to logically and systematically review the steps involved in the element stiffness evaluation based on the model which is presented in the section 2.5.4.

At the end of each loading step, the member end moments and axial force are determined from the current member displacements based on the element stiffness matrix at the beginning of that loading step. These new member end moments and axial force as shown in Fig. B.1 are implemented to evaluate the new element stiffness matrix for the succeeding loading step.

Let us assume that at the end of a loading stage, an element of a structure has specific values for its forces, Fig. B.1. Also let us assume that "n_o" is the axial force on which the primary moment-curvature curve is developed, and $\frac{\partial M_y}{\partial n}$ is the slope of the yield moment-axial force interaction diagram of all sections of the element. Based on these assumptions, the procedures to determine five unknowns in Eq. 2.23, (EI_e, r_A, r_B, η_A, η_B), are as follows:

A) Calculation of the yield moment at the current level of axial force from moment-axial force interaction diagram.

$$M_y = M_{yo} \ (1+C_4) \tag{B.1}$$

where the symbols refer to Fig. A.1 with C_4 defined as:

$$C_4 = \frac{\partial M_y}{\partial n} * \frac{n-n_o}{M_{yo}} \tag{B.2}$$

B) Calculation of elastic flexural rigidity, EI_e. The essential steps in the determination of the effective elastic section stiffness are as follows:

STEP 1--Determining the change of moment at mid-length of the element to evaluate the change of curvature, $\Delta\phi_C$.

$$\Delta m_C = \frac{1}{2} (\Delta m_A - \Delta m_B) \tag{B.3}$$

STEP 2--Determining the value of $\frac{\partial M}{\partial n}$ from Eq. A.5.1.

$$\frac{\partial M}{\partial n} = \frac{\partial M_y}{\partial n} * \frac{m_C}{M_y} \tag{B.4}$$

where m_C is the moment at the mid-length of the element.

STEP 3--Determining the slope of $M-\phi$ curve under present axial force from Eq. A.8.1.

$$\frac{\partial M}{\partial \phi} = (\frac{\partial M}{\partial \phi})_o \ (1+C_4) \tag{B.5}$$

STEP 4--Determining the elastic flexural rigidity at current axial force from Eq. 2.6.

$$\Delta\phi_C \neq 0 \qquad \begin{cases} EI_e = \frac{\partial M}{\partial \phi} + \frac{\partial M}{\partial n} * \frac{\Delta n}{\Delta \phi_C} \\ \\ 0.30 * \frac{\partial M}{\partial \phi} \leq EI_e \leq 2.0 * \frac{\partial M}{\partial \phi} \end{cases} \tag{B.6.1}$$

$$\Delta\phi_C = 0 \qquad EI_e = \frac{\partial M}{\partial \phi} \tag{B.6.2}$$

C) Calculation of the current section stiffness at ends A and B. Based on the values of moment at the critical sections , there are two possibilities:

1---The critical section has not been yielded, and the moment at the critical section, m , is smaller than the yield moment ($m \leq M_y$). In this case the current section stiffness is equal to the elastic section stiffness, i.e. r=1.

2---The critical section has yielded. The current section stiffness, $EI_i = rEI_e$, is calculated from the following steps:

STEP 1--Transferring moment to the primary M-ϕ curve, Figs. A.1, and A.2.

$$\begin{cases} m_o = \dfrac{m}{1+C_4} & m \leq M_y \qquad (B.7.1) \\ m_o = m - C_4 * M_{yo} & m \geq M_y \qquad (B.7.2) \end{cases}$$

STEP 2--Based on the value of m_o and loading history, evaluate the slope of the M-ϕ, $(\frac{\partial M}{\partial \phi})_o$, and the change in the curvature, $(\Delta\phi)_o$.

STEP 3--Evaluation of the slope of the M-ϕ curve at current axial force.

$$\begin{cases} \dfrac{\partial M}{\partial \phi} = (\dfrac{\partial M}{\partial \phi})_o \ (1+C_4) & m \leq M_y \qquad (B.8.1) \\ \dfrac{\partial M}{\partial \phi} = (\dfrac{\partial M}{\partial \phi})_o & m \geq M_y \qquad (B.8.2) \end{cases}$$

STEP 4--Evaluating $\dfrac{\partial M}{\partial n}$ at present condition from Eq. A.4.

$$\begin{cases} \dfrac{\partial M}{\partial n} = \dfrac{\partial M_y}{\partial n} * \dfrac{m}{M_y} & m \leq M_y \qquad (B.9.1) \\ \dfrac{\partial M}{\partial n} = \dfrac{\partial M_y}{\partial n} & m \geq M_y \qquad (B.9.2) \end{cases}$$

STEP 5--Evaluating current section stiffness from Eq. 2.6.

$$\begin{cases} EI_i = \dfrac{\partial M}{\partial \phi} + \dfrac{\partial M}{\partial n} * \dfrac{\Delta n}{\Delta \phi} \\ \\ 0.10 * \dfrac{\partial M}{\partial \phi} \leq EI_i \leq 4.0 * \dfrac{\partial M}{\partial \phi} \end{cases} \qquad (B.10.1)$$

$$EI_i = \frac{\partial M}{\partial \phi} \qquad |m| \leq \frac{1}{5} M_y \qquad (B.10.2)$$

These limitations are necessary to prevent any unrealistic values for the current section stiffnesses due to the assumptions which are used in evaluating the variables in Eq. 2.6.

In this study, the axial force is assumed to remain constant when the tension or compression wall is in the strain-hardening zone. This assumption is necessary because the effect of changing axial force is not considered in the strain-hardening ratio. In other words, in establishing the various moment-curvature curves, the yield curvature as well as the strain-hardening ratio for any moment-curvature curve are assumed to be the same regardless of the axial force level.

D) Calculation of the effective section stiffness, EI^*. The effective section stiffness is evaluated from Eq. B.11, if moment at the critical section is in the unloading or reloading range, otherwise from Eq. B.12.

$$EI^* = \frac{1}{2}\left(\frac{1}{EI_e} + \frac{1}{EI_i}\right)^{-1} \tag{B.11}$$

$$EI^* = EI_i \tag{B.12}$$

E) Calculation of the inelastic length at both ends. Based on the values of m_A and m_B, there are two possibilities:

1--If $m_A(m_B) \leq M_y$, and the critical section at this end has not been yielded. then

$$\eta_A(\eta_B) = 0. \tag{B.13}$$

2--When the moment at section A (B) is in the strain-hardening range, the inelastic length at end A (B) is calculated from Eq. B.14.1 (B.14.2), otherwise the maximum value of the inelastic length is used.

$$\eta_A = \frac{m_A - M_y^* (|m_A|/m_A)}{m_A + m_B} \geq 0.02 \qquad \text{(B.14.1)}$$

$$\eta_B = \frac{m_B - M_y^* (|m_B|/m_B)}{m_A + m_B} \geq 0.02 \qquad \text{(B.14.2)}$$

To prevent possible decreases in the inelastic length when the end moment is in the strain-hardening, Fig. B.2, a few restrictions are applied in the value of the inelastic length.

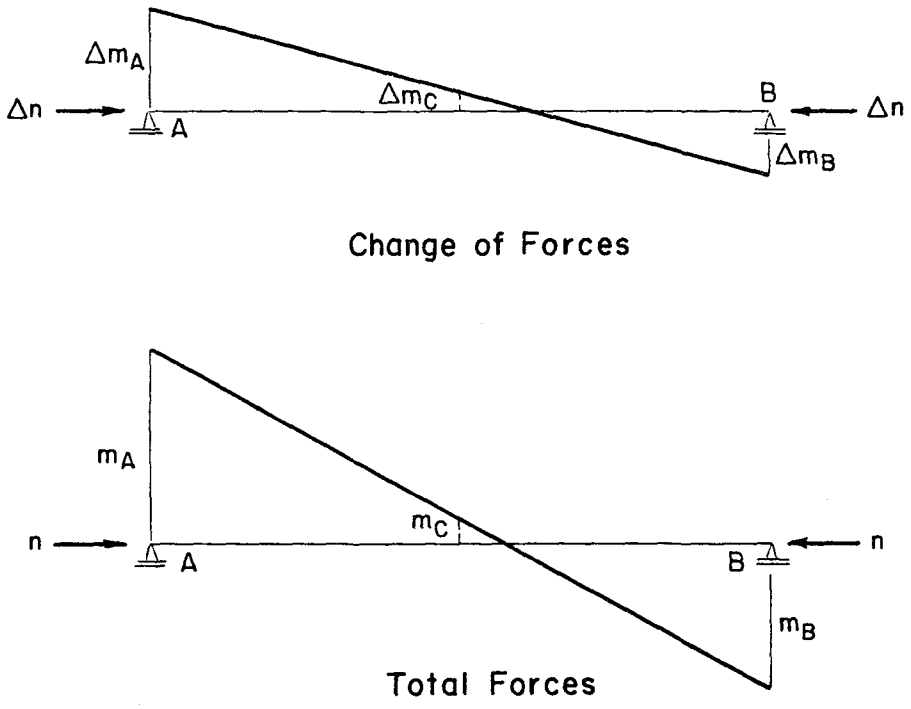

Fig. B.1 Member Forces at the End of a Loading Step

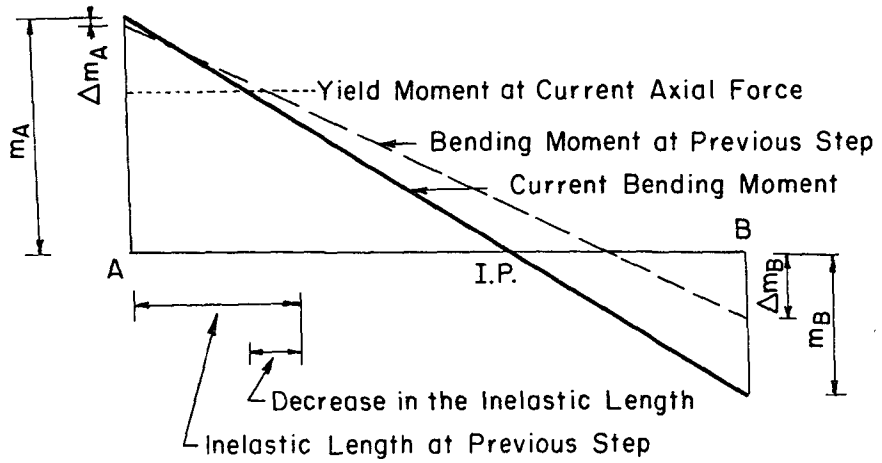

Fig. B.2 Inelastic Zone Length Discrepancy due to the Shifting of Inflection Point

REFERENCES

1. Abrams, D.P., "Measured Hysteresis Relationships for Small-Scaled Beams," Civil Engineering Studies, Structural Research Series No. 432, University of Illinois, Urbana, November 1976.

2. Abrams, D.P., & M.A. Sozen, "Experimental Study of Frame-Wall Interaction in R/C Structures Subjected to Strong Earthquake Motions," Civil Engineering Studies, Structural Research Series No. 460, University of Illinois, Urbana, May 1979.

3. Adeli, H., J.M. Gere, & W. Weaver, "Algorithms for Nonlinear Structural Dynamics," Journal of the Structural Division, ASCE, Vol. 104, No. ST2, February 1978, PP. 263-280.

4. Aktan, A.E., & V.V. Bertero, "The Seismic Resistant Design of R/C Coupled Structural Walls," Earthquake Engineering Research Center, Report No. EERC 81-07, University of California, Berkeley, June 1981.

5. Aktan, A.E., V.V. Bertero, & M. Piazza, "Prediction of the Seismic Responses of R/C Frame-Coupled Wall Structures," Earthquake Engineering Research Center, EERC No. 82-12, University of California, Berkeley, August 1982.

6. Aoyama, H., & T. Sugano, "A Generalized Inelastic Analysis of R/C Structures Based on the Tests of Members," Recent Researches of Structural mechanics, Contributions in Honour of the 60-th Birthday of Prof. Y. Tsuboi, Uno Shoten, Tokyo, Japan, 1968, PP. 15-30

7. Aristizabal-Ochoa, J.D., & M.A. Sozen "Behavior of 10-Story R/C Walls Subjected to Earthquake Motions," Civil Engineering Studies, Structural Research Series No. 431, University of Illinois, Urbana, October 1976.

8. Arzoumanidis, S.G., & C. Meyer, "Modelling R/C Beams Subjected to Cyclic Loads," Technical Report No. NSF-PER-7924695-CU-1, Department of Civil Engineering and Engineering Mechanics, Columbia University in the city of New York, March 1981.

9. Aziz, T.S., & J.M. Roesset, "Inelastic Dynamic Analysis of Building Frames," Report No. R76-37, Department of Civil Engineering, M.I.T., Cambridge, August 1976.

10. Charney, A.F., & V.V. Bertero, "An Evaluation of the Design and Analytical Seismic Response of a 7-Story R/C Frame-Wall Structure," Earthquake Engineering Research Center, EERC No. 82-08, University of California, Berkeley, August 1982.

11. Clough, R.W., & J. Penzien, "Dynamics of Structures," McGraw-Hill Book Company, New York, N.Y., 1975.

12. Clough, R.W., K.L. Benuska, & E.L. Wilson, "Inelastic Earthquake Response of Tall Buildings," Proceedings of the Third World Conference on Earthquake Engineering, Vol. 2, Session 2, New Zealand, 1965, PP. 68-84.

13. Derecho, A.T., S.K. Ghosh, M. Iqbal, & M. Fintel, "Strength, Stiffness, & Ductility Required in R/C Structural Walls for Earthquake Resistance," ACI Journal, August 1979, PP. 875-896.

14. Emori, K., & W.C. Schnobrich, "Analysis of R/C Frame-Wall Structures for Strong Motion Earthquakes, Civil Engineering Studies, Structural Research Series No. 457, University of Illinois, Urbana, December 1978.

15. Fintel, M., & S.K. Ghosh, "Effect of Wall Strength on the Dynamic Inelastic Seismic Response of Yielding Wall-Elastic Frame Interaction Systems," Proceedings of the Third Canadian Conference in Earthquake Engineering, June 4-6, 1979, Montral, PP. 949-968.

16. Giberson, M.F., "The Response of Nonlinear Multistory Structures Subjected to Earthquake Excitation," Earthquake Engineering Research Laboratory, California Institute of Technology, Pasadena, California, May 1967.

17. Gilbertsen, N.D., & J.P. Moehle, "Experimental Study of Small-Scale R/C columns Subjected to Axial and Shear Force Reversals," Civil Engineering Studies, Structural Research Series No. 481, University of Illinois, Urbana, July 1980.

18. Hognestad, E., "A Study of Combined Bending and Axial load in R/C members," University of Illinois, Engineering Experimental Station, Bulletin Series No. 399, November 1951.

19. Hsu, L.W., "Behavior of Multistory R/C Walls during Earthquakes," Ph. D. Dissertation, University of Illinois, Urbana, 1974.

20. Kanaan, A.E., & G.H. Powell, "General Purpose Computer Program for Inelastic Dynamic Response of Plane Structures," Earthquake Engineering Research Center, EERC No. 73-06, University of California, Berkeley, April 1973.

21. Keshavarzian, M., & W.C. Schnobrich, "Analytical Models for the Nonlinear Analysis of R/C Structures," Presented at the 1983 Annual Convention, ACI, Los Angeles, California, March 20-25.

22. Koike, K., Y. Omote, H. Eto, & T. Takeda, "R/C Wall-Frame Structures Subjected to Dynamic and Static Loadings-Model Tests and the Simulations," Proceedings of the 7-th World Conference on Earthquake Engineering, Vol. 6, Istanbul, Turkey, 1980, PP. 419-426.

23. Luyties III, W.H., S.A. Anagnostopoulos, & J.M. Biggs, "Studies on the Inelastic Dynamic Analysis and Design of Multi-Story Frames," Report No. R76-29, Department of Civil Engineering, M.I.T., Cambridge, July 1976.

24. Lybas, J.M., & M.A. Sozen, "Effect of Beam Strength and Stiffness on Dynamic Behavior of R/C Coupled Walls," Civil Engineering Studies, Structural Research Series No. 444, University of Illinois, Urbana, July 1977.

25. Mahin, S.A., & V.V. Bertero, "An Evaluation of some Methods for Predicting Seismic Behavior of R/C Buildings," Earthquake Engineering Research Center, EERC No. 75-05, University of California, Berkeley, February 1975.

26. Meyer, C., M.S.L. Roufaiel, & S.G. Arzoumanidis, "Analysis of Damaged Concrete Frames for Cyclic Loads," Earthquake Engineering and Structural Dynamics, Vol. 11, March 1983, PP. 207-228.

27. Moehle, J.P., & M.A. Sozen, "Experiments to Study Earthquake Response of R/C Structures with Stiffness Interruptions," Civil Engineering Studies, Structural Research Series No. 482, University of Illinois, Urbana, August 1980.

28. Newmark, N.M., "A Method of Computation for Structural Dynamics," Journal of the Engineering Mechanics Division, ASCE, Vol. 85, No. EM3, July 1959, PP. 67-94.

29. Otani, S., "Behavior of Multistory R/C Frames During Earthquakes," Ph. D. Dissertation, University of Illinois, Urbana, December 1972.

30. Otani, S. "Effectiveness of Structural Walls in R/C Buildings during Earthquakes," Civil Engineering Studies, Structural Research Series No. 492, University of Illinois, Urbana, June 1981.

31. Paulay, T., & A.R. Santhakumar, "Ductile Behavior of Coupled Shear Walls," Journal of the Structural Division, ASCE, Vol. 102, No. ST1, January 1976, PP. 93-108.

32. Roufaiel, M.S.L., & C. Meyer, "Nonlinear Analysis of R/C Frames for Dynamic Loading," Technical Report No. NSF-PFR-7924695-CU-3, Department of Civil Engineering and Engineering Mechanics, Columbia University in the city of New York, December 1981.

33. Roufaiel, M.S.L., & C. Meyer, "Analysis of Damaged Concrete Frame Buildings," Technical Report No. NSF-CEE-81-21359-1, Department of Civil Engineering and Engineering Mechanics, Columbia University in the city of New York, May 1983.

34. Saatcioglu, M., A.T. Derecho, & W.G. Corley, "Coupled Walls in Earthquake-Resistant Buildings, Modeling Techniques and Dynamic Analysis," Portland Cement Association, June 1980.

35. Saiidi, M., & M.A. Sozen, "Simple and Complex Models for Nonlinear Seismic Response of R/C Structures," Civil Engineering Studies, Structural Research Series No. 465, University of Illinois, Urbana, August 1979.

36. Shibata, A., & M.A. Sozen, "The Substitute-Structure Method for Earthquake-Resistant Design of R/C Frames," Civil Engineering Studies, Structural Research Series No. 412, University of Illinois, Urbana, October 1974.

37. Soleimani, D., "Reinforced Concrete Ductile Frames under Earthquake Loadings with Stiffness Degradation," Ph. D. Dissertation, University of California, Berkeley, December 1978.

38. Suharwardy, M.I.H., & D.A. Pecknold, "Inelastic Response of R/C Columns Subjected to 2-D Earthquake Motions," Civil Engineering Studies, Structural Research Series No. 455, University of Illinois, Urbana, October 1978.

39. Suko, M., & P.F. Adams, "Dynamic Analysis of Multibay Multistory Frames," Journal of the Structural Division, ASCE, Vol. 97, No. ST10, October 1971, PP. 2519-2533.

40. Takayanagi, T., & W.C. Schnobrich, "Computed Behavior of Coupled Shear Walls," Proceedings of the 6-th World Conference on Earthquake Engineering, New Delhi, India, January 1977, PP. 3069-3074.

41. Takayanagi, T., & W.C. Schnobrich, "Computed Behavior of R/C Coupled Shear Walls," Civil Engineering Studies, Structural Research Series No. 434, University of Illinois, Urbana, December 1976.

42. Takeda, T., M.A. Sozen, & N.N. Nielsen, "R/C response to Simulated Earthquake," Journal of the Structural Division, ASCE, Vol. 96, No. ST12, December 1970, PP. 2557-2573.

43. Takizawa, H., "Notes on Some Basic Problems in Inelastic Analysis of Planar R/C Structures (Part I and II)," Transaction of the Architectural Institute of Japan, No. 240, February 1976, PP. 51-62, No. 241, March 1976, PP. 65-77.